A Steady-State Visual Evoked Potential Brain-Computer Interface System Evaluation as an In-Vehicle Warning Device

by Pouria Riyahi

B.Sc. in Civil Engineering, June 2011, University of Tehran

A Thesis submitted to

The Faculty of
School of Engineering and Applied Sciences
of The George Washington University
in partial fulfillment of the requirements
for the degree of Master of Science

August 31, 2014

Thesis directed by

Azim Eskandarian
Professor of Engineering and Applied Sciences

Dedication

I dedicate this thesis and all of my achievements to my lovely family and all those who helped me to put one step forward during my research.

Acknowledgement

I would like to specially thank my adviser Prof. Azim Eskandarian who his constant support and encouragements during this research despite of many drawbacks helped me to accomplish part of a greater research which seemed far away from my knowledge. I also want to thank Prof. Majid T. Manzari for his encouragements during this research which helped me to reach at this point. I also would like to specially thank my thesis examination committee, Prof. Samer Hamdar and Prof. Muhammad I. Haque, for their time, insightful feedbacks and helpful comments.

I'm so grateful for my family's support during not only the days I was conducting this research but also because of their dedications and wonderful endorsements during my whole life.

Finally, I would like to thank all those in g.TEC bio-medical and medical company who have provided us with their preliminary data and their support for resolving all of issues that happened during this research.

Abstract of Thesis

A Steady-State Visual Evoked Potential Brain-Computer Interface System Evaluation as an In-Vehicle Warning Device

This thesis is part of current research at Center for Intelligence Systems Research (CISR) at The George Washington University for developing new in-vehicle warning systems via Brain-Computer Interfaces (BCIs). The purpose of conducting this research is to contribute to the current gap between BCI and in-vehicle safety studies. It is based on the premise that accurate and timely monitoring of human (driver) brain's signal to external stimuli could significantly aide in detection of driver's intentions and development of effective warning systems. The thesis starts with introducing the concept of BCI and its development history while it provides a literature review on the nature of brain signals. The current advancement and increasing demand for commercial and non-medical BCI products are described. In addition, the recent research attempts in transportation safety to study drivers' behavior or responses through brain signals are reviewed. The safety studies, which are focused on employing a reliable and practical BCI system as an in-vehicle assistive device, are also introduced. A major focus of this thesis research has been on the evaluation and development of the signal processing algorithms which can effectively filter and process brain signals when the human subject is subjected to Visual LED (Light Emitting Diodes) stimuli at different frequencies. The stimulated brain generates a voltage potential, referred to as Steady-State Visual Evoked Potential (SSVEP). Therefore, a newly modified analysis algorithm for detecting the brain visual signals is proposed. These algorithms are designed to reach a satisfactory accuracy rate without preliminary trainings,

hence focusing on eliminating the need for lengthy training of human subjects. Another important concern is the ability of the algorithms to find correlation of brain signals with external visual stimuli in real-time. The developed analysis models are based on algorithms which are capable of generating results for real-time processing of BCI devices. All of these methods are evaluated through two sets of recorded brain signals which were recorded by g.TEC CO. as an external source and recorded brain signals during our car driving simulator experiments. The final discussion is about how the presence of an SSVEP based warning system could affect drivers' performances which is defined by their reaction distance and Time to Collision (TTC). Three different scenarios with and without warning LEDs were planned to measure the subjects' normal driving behavior and their performance while they use a warning system during their driving task. Finally, warning scenarios are divided into short and long warning periods without and with informing the subjects, respectively. The long warning period scenario attempts to determine the level of drivers' distraction or vigilance during driving. The good outcome of warning scenarios can bridge between vehicle safety studies and online BCI system design research. The preliminary results show some promise of the developed methods for in-vehicle safety systems. However, for any decisive conclusion that considers using a BCI system as a helpful in-vehicle assistive device requires far deeper scrutinizing.

Table of Contents

List of Figures

List of Tables

List of Equations

List of Symbols / Nomenclature

1.	x	Input data channels
2.	W	Weighting Matrices and factors
3.	y	Estimated output signal channels or Transformed input data channels
4.	N	Number of EEG signal channels or Input channels
5.	R	Covariance or cross-covariance matrix of input data channels
6.	M	Filters order
7.	S_i/S_J	The estimated brain source signals
8.	t & j	Time or Time steps
9.	i	i^{th} Signal channel
10.	$\varepsilon_i(t)$	Autoregressive White Noise
11.	S_w	Within class scatters
12.	S_B	Between class scatters
13.	m_i	Mean of each class of input data
14.	b	Regression models fitting value
15.	C	ALN functions constant
16.	F(y)	SVM function
17.	α	SVM positive Lagrangian multiplier
18.	ρ	Maximum correlation factor
19.	Q	Orthogonal matrix in QR decomposition
20.	R	Upper Triangular matrix in QR decomposition
21.	T	matrix transpose

22. U Canonical Variant of CCA method

23. V Canonical Variant of CCA method and Bartlett's v-test for Wilks's ratio of CCA Evaluation procedure

24. f_i LED flickering frequency

25. h LED frequency harmonics

26. Λ Wilks's ratio

27. p & q Minimum ranks of input data-sets

28. Cov Cross-covariance matrix of centered data-sets

29. N_p Number of EEG channels

30. N_q Number of LED channels

31. c Minimum rank of input data-sets in Co-inertia method

32. f_t Transformed matrix of input data-sets in Co-inertia method

33. F_t Projected matrix of input data-sets onto featured space in Co-inertia method

34. x_i Estimated brain source signals

35. d Column matrix of LED stimulus signal

36. N Total Number of observation in each data epoch or number of LED channels

37. H Matrix of observed brain signals for an M-order adaptive filter

38. v matrix of noise values

39. λ Forgetting factor

40. u Matrix of observed brain signals

41. Π Positive definite matrix

42. δ Small positive value

43. I Identity matrix

44. U(j) Buffered input signal channels

45. $r_e(j)$ Kalman filter conversion vector

46. $k_{Np,j}$ Vector of Kalman filter gains

47. N_h Total number of frequency harmonics

48. $\hat{S}(f)_{j,i}$ Estimated power spectrum of brain source signals

49. $\hat{\sigma}^2_{j,i}$ Estimated poser of noise signals

50. F_s Sampling rate

51. f desired frequency

52. AR(p) p-order autoregressive model

53. w_0 Transformation matrix for adaptive robust filter

54. γ positive value of encompassing error boundaries

55. $d_{B,n}$ block data of input data-sets

56. B number of data samples collected in each block

57. F Fast Fourier Transform (FFT)

58. $L^c_{i,n}$ Weighting matrix corresponding coefficient in the frequency-domain

59. P SSVEP test sessions average accuracy rate

Chapter 1: Introduction

1.1 Background

Central Nervous System (CNS) functioning system was not recognized clearly until 200 years ago. Before that time, the CNS was considered as an interface and intermediation factor between the human soul and physiological body. Developments in the medical and physiological sciences in the 19th century brought more knowledge about human body and specifically spread out the sensorimotor hypothesis about the CNS. During the past 150 years, the knowledge about CNS and miscellaneous active components of the peripheral nervous system has expanded. In particular, the principles of converting the brains sensory signals to the motor outputs. An intricate complex of neuron's excitations and spinal cord motorneurons reflexes lead to the physical limb function, which is mastered and maintained in the human brain (Wolpaw J. R., 2007). Disruption or deficits in any part of this sequence of functions will lead to the motor disorders. Efforts for restoring the lost motor functions especially by the neuroscientists flourished the idea of connecting the paralyzed people brains sensory neurons as an input commands to the assistive devices. This idea gave birth to the biomedical and bioengineering interdisciplinary area which is called Brain-Computer Interfacing (BCI).

BCI is a pathway between the human brain and any type of targeted device. BCI systems, referred also as Brain-Machine Interfaces (BMI), attempt to interpret the brain signals for communicating with surrounding environment (Alonso N., 2012). This type of research has expanded from just three active research groups since 20 years ago to the six active groups since 10 years ago (Wolpaw J. R., 2007). Nowadays, more than 100 BCI

research groups all around the world are improving different aspects of this research. Advances in technology, engineering and medical sciences are broadening the BCI systems applications to non-medical fields. Currently, different applications in control system design, robotic systems, multimedia, entertainment and motor substitutions (prosthesis) are attracting research groups and companies (Millán J. D. R., 2010).

BCI systems are the combination of a recording device, which collect the brain signals either invasively or non-invasively, and a processing algorithm which convert the recorded signals to the meaningful device commands. Invasive data collection methods need a high level of skill on placing the electrodes in the brain and accompanied by high level of risk. Most of current BCI researches are based on non-invasive methods, which collect the data through different medical devices. Typically, *Electroencephalography (EEG), Magnetoencephalography (MEG), Electrocorticography (ECoG), Functional Magnetic Resonance Imaging (fMRI)* and *Near Infrared Spectroscopy (NIRS)* have been used for the BCI studies (Alonso N., 2012). Non-medical studies have usually benefited from EEG device because of its safety and easy data collection. This device is configured by 16 to 256 electrode channels made of silver chloride (AgCl) and records the electromagnetic fields, perpendicular to the scalp, and potential changes in the cortex.

The EEG device is capable of measuring limited known brain signals which are used for different BCI systems according to their origin in the brain. Significant signals collected from primary and somatosensory motor cortices over frontal and parieto-occipital lobes are delta waves (below 4 Hz), theta waves (4-8 Hz), alpha rhythms (8-12 Hz) and beta rhythms (12-30 Hz). Another important type of brain signals, which are recorded from the Visual

cortex, are called transient Visual Evoked Potentials (tVEPs below 4 Hz) and Steady-State Visual Evoked Potentials (SSVEPs 4-75 Hz) [(Alonso N., 2012), (Elitzur A.C., 2010), (Dobriyal M., 2011)]. Sensory motor cortex signals are mostly employed for developing the control BCI systems to process user brain's cognitive signals. The VEPs are typically used for the goal selection BCI systems in which the process would be triggered by user intention and assistive devices will operate different commands. These two types of brain signals form majority of BCI systems and wide range of applications (Wolpaw J. R., 2007). In the field of motor recovery and motor substitution, different neuroprosthesis devices are partially restoring some of the lost limb functions.

The assistive wheelchairs controlled by brain signals and more recently assistant robots are advances in BCI technologies. Other applications such as entertainment and multimedia for real-time synchronized systems are also burgeoning in BCI technologies for commercial purposes (Millán J. D. R., 2010). Many research institutes within the US, e.g. USA Army (DARPA) and NASA are attempting to develop real-time systems to supersede the human presence in hazardous or challenging conditions (Bakardjiana H., 2009). Developments of BCI systems brought the idea of employing EEG device in other safety fields, such as developing the in-vehicle assistive technologies. The driver behavior and in-vehicle assistive studies have been conducted in the real or simulated environments such as car-simulators. First paces were started with exploring the drowsy drivers' brain signals and vigilance detection [(Matousek M., 1983), (Parikh P., 2004), (Chang C. W., 2010)]. Human safety studies are extended to the modeling of brain signals during the driving task when driver has different psychological statuses [(Lin C. T., 2005), (Lin C. T., 2005),

(Liang S. F., 2005)]. This type of research attempts to estimate the driver's reaction and intention detection in an upcoming emergency situation (Haufe S., 2011). These types of driver behavior research could mainly contribute to development of in-vehicle assistive technologies.

The growth and expansion of the BCI systems applications revealed the necessity for designing the accurate and reliable real-time BCI systems. Traditional BCI processing algorithms are usually based on five steps such as: signal acquisition and artifact rejections, preprocessing step, feature extraction, classification and finally decision detection (Wolpaw J. R., 2007). This prolonged method is usually time consuming and cannot satisfy the quick response detection needed for real-time systems. Typically, BCI system configuration requires long-term training sessions for adapting the system analysis algorithm parameters and user brain signals. Lack of system generality and the subject/subject or even subject/trial performances' variations cause the reduction in the BCI systems accuracy and processing speed. These limitations are caused by two fundamental sources. First, the unknown nature of the brain signals sources and the magnetic field's strength generated by cortical neurons mass for EEG recordings. Second, the brain signals processing algorithms deficiencies. To enhance the efficiency of the BCI systems, research groups are proposing new machine learning and adaptive filtering algorithms to recompense the analyses inefficiencies [(Friman O., 2007), (Vasquez P. M., 2008)]. Some of the researchers are suggesting BCI systems based on analyzing the brain signals which are more stable and detectable (Wolpaw J. R., 2007).

The SSVEP brain signals are recorded from visual cortex over the occipital region, on the back of human scalp. SSVEPs are one of the event related potentials (ERPs) which are evoked by an exogenous stimulus flickering constantly with the frequency of higher than 4 Hz. These Potentials imitate the patterns of their exogenous stimulus signals and remain detectable till person exposed to the stimulus. The analyses algorithms for filtering these signals are less time consuming and provide more accurate and reliable outputs (Elitzur A.C., 2010). Many studies have been conducted to propose accurate and reliable online SSVEP BCI systems and to implement them in a realistic problem [(Friman O., 2007), (Vasquez P. M., 2008), (Guger C., 2012), (Martinez P., 2007)].

1.2 Thesis Objectives

The objectives of this thesis are classified in two categories:

- The first objective is to evaluate and modify different analyses algorithms to detect the SSVEP brain signal responses. By considering the challenge of reliability and accuracy, these algorithms attempt to generate outputs every few hundreds of milliseconds as efficient as possible. To insure the analyses methods proficiency for an online BCI system, for each algorithm, Information Transfer Rate (ITR) is calculated. This criterion determines the amount of information (data bits) which is provided in epochs of data.
- The second objective is to explore the use of an SSVEP based BCI as an in-vehicle driver warning or assistance device. This is evaluated in a driving simulator. To achieve this, different driving scenarios are designed where

subjects face the emergency situations. Meanwhile, SSVEP signals are recorded to evaluate the SSVEP BCI analyses models reliability. The LED warning stimuli's effect on driver's performance in an upcoming emergency situation is evaluated with both a short and long warning periods ahead.

1.3 Summary of Approaches

This thesis attempts to evaluate and modify different analysis algorithms for SSVEP fast response detection (for real-time purposes) and to explore an SSVEP based BCI system for in-vehicle driver assistant system, evaluated in a car driving-simulator. Adaptive filters and multivariate data analysis algorithms, proposed by Martinez et al. and G. Bin et al., are suitable for real-time BCI systems and reach an acceptable accuracy with no training sessions [(Martinez P., 2007), (Bin G., 2009)]. In this thesis, the recursive adaptive filtering algorithms and multivariate data analysis methods' effectiveness for detecting the drivers' brain signals correlation with LED stimuli in a car-simulator is evaluated. These methods are listed below:

- Canonical Correlation Analysis (a multivariate data analysis method).
- Co-Inertia Analysis (a multivariate data analysis method).
- Adaptive Kalman Filter (an adaptive filtering method).
- Adaptive Gauss-Newton Filter (an adaptive filtering method).
- The Constrained Discrete Fourier Transform (DFT) Block Adaptive Filter (an adaptive filtering method).

Two sets of data employed to evaluate the accuracy of these modified algorithms. The first data-set was provided by g.TEC CO. as an external source (collected from 4 subjects' visual cortex). The second data-set is recorded from 30 subjects during a single SSVEP test session at CISR laboratory of The George Washington University. The subjects have not performed a SSVEP based BCI system before participating in our test sessions. The data was collected by 8 EEG channels from visual cortex. The SSVEP test session is described in chapter 4.

In particular, this research considers a SSVEP based BCI system as a collision avoidance warning system and evaluates the drivers' behaviors by measuring their Time to Collisions (TTC) and braking distances (BD). The subjects drove 3 different scenarios in the driving car-simulator. These scenarios are as follows:

- Normal driving scenario with no warning.
- Short warning scenario, LED warning started 3-seconds before emergency situation.
- Long warning scenario, LED warning started 6-seconds before emergency situation.

To measure the LED warning effect on drivers' vigilance or distraction, drivers' performances in scenarios with LED warning activations compared to their normal driving.

Finally, the subjects' intention detection before an emergency situation is evaluated. These can be achieved by detecting subjects' brain signals correlations with LED stimulus signal during the LED warning system activation. The purpose of this correlation detection is to determine whether SSVEP brain signals activities can be detected before subjects'

response to the emergency situations. This can be helpful for the future driving assistive systems which could consider a SSVEP based BCI as an in-vehicle assistive technology.

1.4 Outline of Thesis

This thesis begins with introduction as its 1st chapter and delivers a brief description on the BCI studies background. The topic's significance for providing more reliable and accurate BCI systems is clarified. The importance of applying the BCI system to driver assistance research is also highlighted. The 2nd chapter presents the literature review on the BCI studies and attempts to describe the different BCI system categories. In this chapter, a concise description of the EEG device and the desired brain signals in BCI research will be explained. This chapter finishes by reviewing the traditional signal processing and pattern recognition methods in the earlier BCI research. The 3rd chapter describes the proposed analyses algorithms and formulates all of the filtering and numerical analyses steps. The 4th chapter includes the experimental protocol, instrumentations and test setup configurations. The 5th chapter consists of two parts. The first part presents the SSVEP analyses algorithm results. In second part, drivers' performance is evaluated by calculating the reaction times and reaction distances. Meanwhile, the brain signals correlation with LED stimulus signal is evaluated in various warning scenarios. This chapter ends with the general conclusion and discussions about the effectiveness of the suggested analyses procedures and the feasibility of employing an SSVEP BCI system as an in-vehicle assistive device. The 6th chapter summarizes the contributions of this research and gives suggestions for the future studies.

1.5 Contributions

This thesis evaluates four different signal processing methods to find correlations between human brain signals and external LED stimuli. This thesis proposes the adaptive filtering algorithms and multivariate data analyses methods for detecting the SSVEP brain signals responses. Among the five presented methods; there are methods based on adaptive filtering and multivariate data analysis which have not been used for this purpose previously and one CCA (Canonical Correlation Analysis) is among the most successful multivariate data analysis techniques that have been used in literature for SSVEP response detection. The advantages of proposed modified algorithms are the filtering of brain signals without training sessions and reaching satisfactory level of accuracy. Therefore, the possibility of designing the BCI systems with reliable output commands in an online session is measured. The driver's performances, by calculating time to collisions and reaction distances, during the designated scenarios are assessed. Finally, the effect of the SSVEP stimulation-box (i.e. the visual warning device) presence, on the driver vigilance and performance is also assessed. The driver's performances evaluation with an SSVEP stimulus attempts to evaluate the SSVEP BCI systems for future safety systems. The findings of this research contribute to the brain machine interface with the advanced driver assistance systems of the future, in which enhanced driver monitoring and augmented warning using brain signals correlations may become possible.

Chapter 2: Literature review

This chapter reviews the literature relevant to the focus of this thesis. It starts by reviewing the general Brain-Computer Interface (BCI) systems because they provide foundational information about brain monitoring. Then, after a brief review of physiological origin of electrophysiological measurements in section 2.2, various brain signal measurements using EEG in section 2.3 are reviewed.

The Brain-Computer Interface applications are reviewed, in section 2.4, leading to the driver behavior studies using brain monitoring in section 2.5. Finally, in section 2.6, the various elements of brain signal processing are discussed.

2.1 Brain-Computer Interfaces

During the past two decades there has been a great effort by different psychology, neurology and engineering research groups to improve the life quality of paralyzed, locked-in or spinal injured patients. The idea of creating direct communication and interaction between brain signals and any assistive device resulted in systems which are called Brain-Computer Interfaces. Furthermore, different researches have revealed the important non-medical aspects of these systems. The BCI research efforts on improving the efficiency and reliability still carry on. Any further step toward enhancement of the future BCI research should focus on system's real-time performance practicability and its user friendliness. More reliably developed BCI systems translate the brain signals to desirable system control outputs, more precisely (Millán J. D. R., 2010).

The brain signals employed for BCI systems are measured either by invasive or non-invasive methods, regardless of control device applications. The invasive systems implant

the macro/microelectrodes on brain cortex surface or inside the brain. The non-invasive measurement devices record the brain signals from scalp surface. Non-invasive systems measure the electromagnetic fields which are perpendicular with respect to brain skull. These electromagnetic fields are generated from the synchronized depolarization of large ensemble of fired neurons in the brain cells (Birbaumer, 2006). Among non-invasive devices which collect the electrophysiological/magnetical measurements from brain skull, Electroencephalography (EEG) is more rampant. Researchers prefer this device because of its safety and convenience in usage. However, spatio-temporal resolution of the EEG is limited to hundred milliseconds while brain electrophysiological activities have a high spatiotemporal resolution typically around 20 kHz (Bießmann, 2012).

The EEG comes with different sets of electrodes, either dry or wet. These electrodes are conventionally made of tin, for cheaper devices with acceptable recording resolution, or copper-Au and AgCl electrodes for devices with better resolutions (Millán J. D. R., 2010). The electrodes are placed over head with an electrode cap. Typical electrodes' positioning system which is called 10-20 system is demonstrated in Figure 1. This positioning system is later extended with more channels to 256 electrode locations.

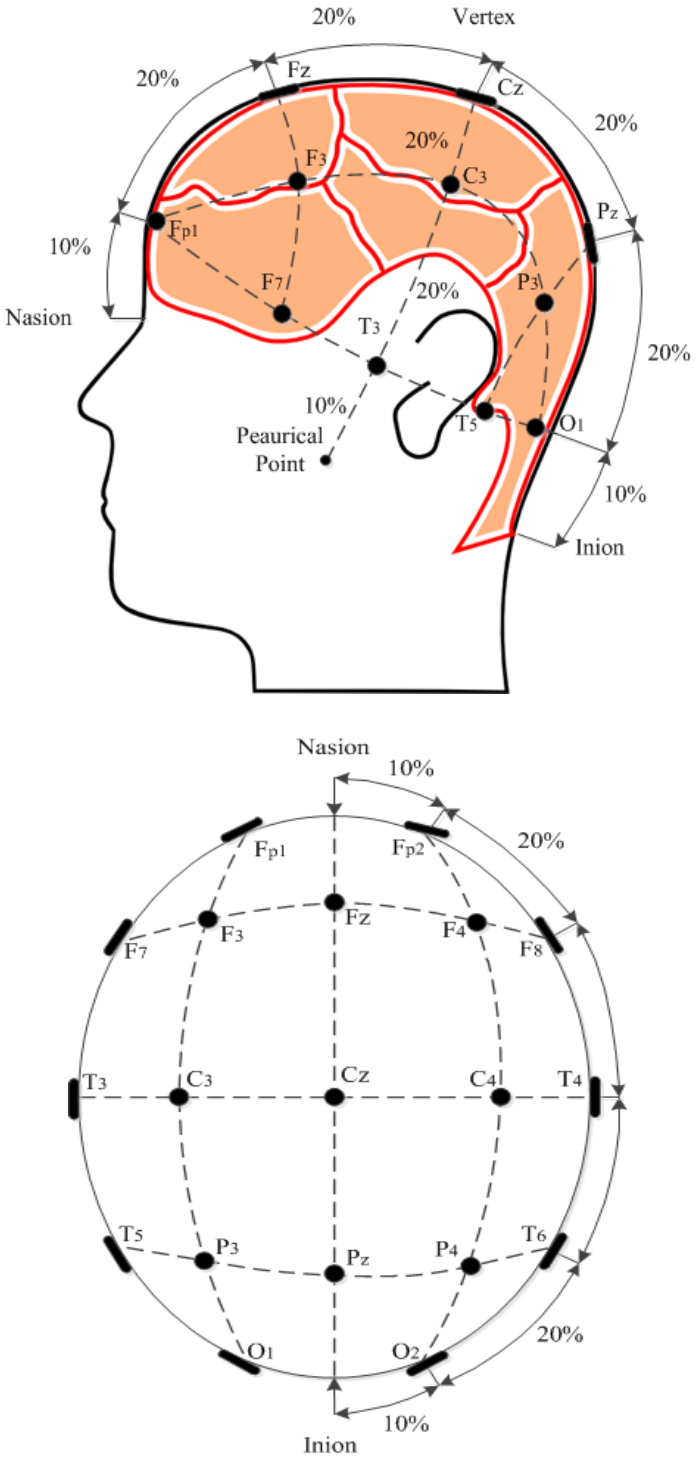

Figure 1. Electrodes' 10-20 positioning system

2.2 Physiological Origin of Electrophysiological Measurements

Electrophysiological measurements are obtained from potential changes in the brain cells due to neurons' dispatches. These electrical fields usually change due to the neurotransmitter chemical ions, firing into the synapses and then reach to the post-synapses chemico-sensitive channels. This transmission opens the post synapses channels and depolarizes the dendritic cell part with respect to its extracellular part. Figure 2 briefly illustrates the schematic procedure of this process. During the rest, intracellular medium is nearly at 70mV with respect to extracellular medium. The depolarized dendritic part of cell with negatively charged soma pole generates an electromagnetic field. This electromagnetic field might be big enough to be measured by EEG. However, only perpendicular fields will be detectable by EEG (Nunez P. L., 2006).

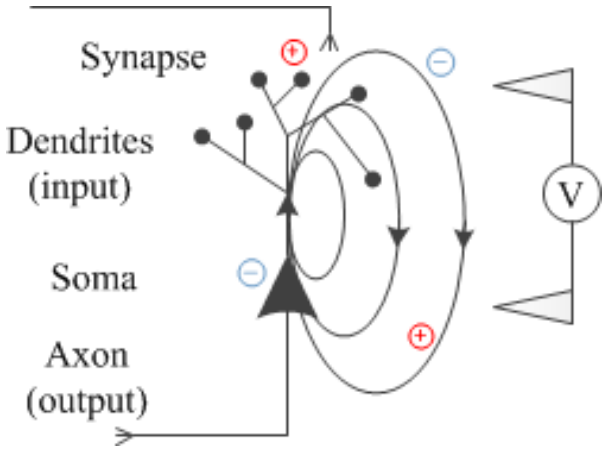

Figure 2. The schematic neural activities taken from (Bießmann, 2012)

2.3 EEG Detectable Brain Signals and Potentials

The human brain masters and controls all types of human physiological activities. All of our muscular movements or imaginary brain activities are resulted from electromagnetic

changes in the human brain. Generally, brain control activities are accomplished in cortex and could be measured by EEG. Figure 3 represents different parts of the human brain and highlights typical cortices used for BCI systems. The Human brain cerebrum is subdivided into 4 different regions including: frontal, parietal, occipital, and temporal lobes. The central sulcus divides the frontal and parietal lobes from each other. The central sulcus also separates the pre-central gyrus (indicated in red) and post-central gyrus (indicated in blue). The most important signals, which are used for BCI systems, are collected from motor areas, somatosensory cortex, posterior parietal cortex, and visual cortex.

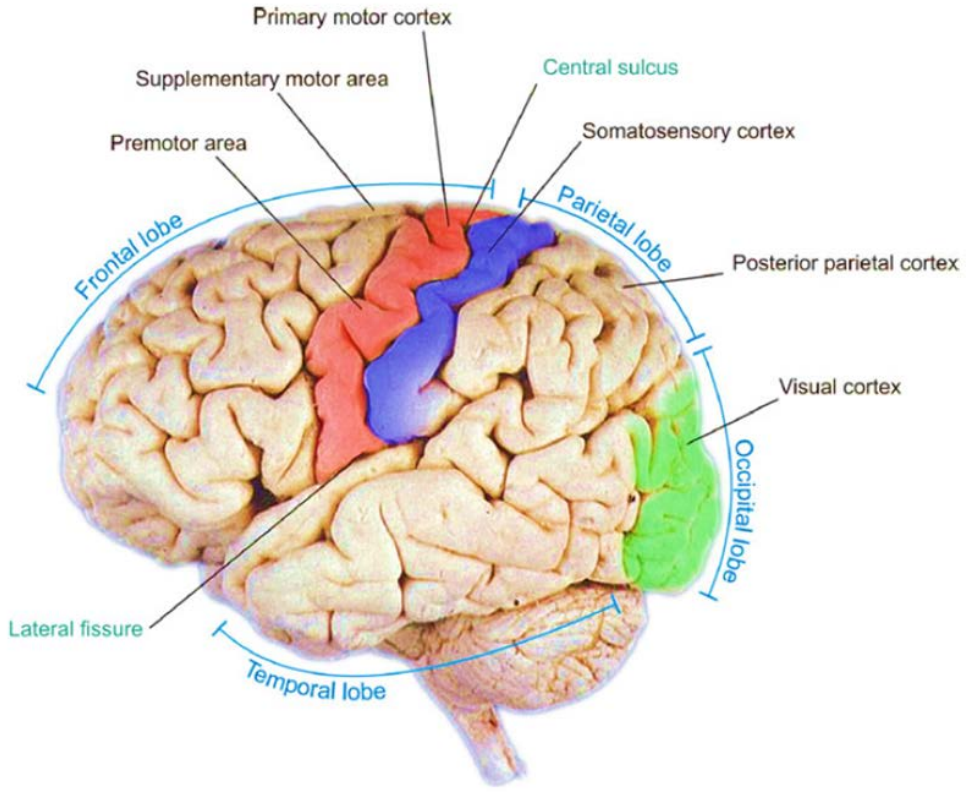

Figure 3. Human brain cerebrum (Elitzur A.C., 2010)

The brain signals which are suitably observable from these cortices by EEG for BCI system design are as follows. These brain signals and potentials usually configure the BCI systems control command's types.

- Event-Related Potentials (ERPs)
- Visual Evoked Potentials (VEPs)
- Sensory Motor Rhythms (SMRs)
- P300 Evoked Potential

Each is described below. The descriptions are taken from references [(Millán J. D. R., 2010), (Elitzur A.C., 2010)].

2.3.1 Event-Related Potentials (ERPs)

The Event-Related potentials are the electrical brain responses to physical stimuli or behavioral activities. These signals are characterized by their voltage amplitude and time of the appearance with respect to stimulus. The earlier components of these signals are originated in primary motor cortex and have latency of less than 100 milliseconds. The components with the latency of 100 to 500 milliseconds are related to more complex cortical activities. The ERPs, detectable up to a few seconds after stimulus, are called Slow Cortical Potentials (SCPs).

2.3.2 Visual-Evoked Potentials (VEPs)

VEPs are generated in response to an exogenous visual stimulus which flickers at specific frequency. These potentials prominently recorded from occipital region and their

characteristics depend on the stimulus signal patterns. The Visual stimuli with constant frequencies over 4 Hz provokes oscillatory brain responses from visual cortex with the same frequency components. These types of responses are called Steady-State Visual Evoked Potentials (SSVEPs). The brain responses to the stimuli with frequencies of less than 4 Hz are called transient VEPs. The VEP responses typically initiate 75 ms after exposure to stimulus in primary visual cortex with negative electromagnetic components. The response is followed by the positive components approximately 100 ms after stimulus initiation. An example of SSVEP stimulation-box is demonstrated in Figure 4.

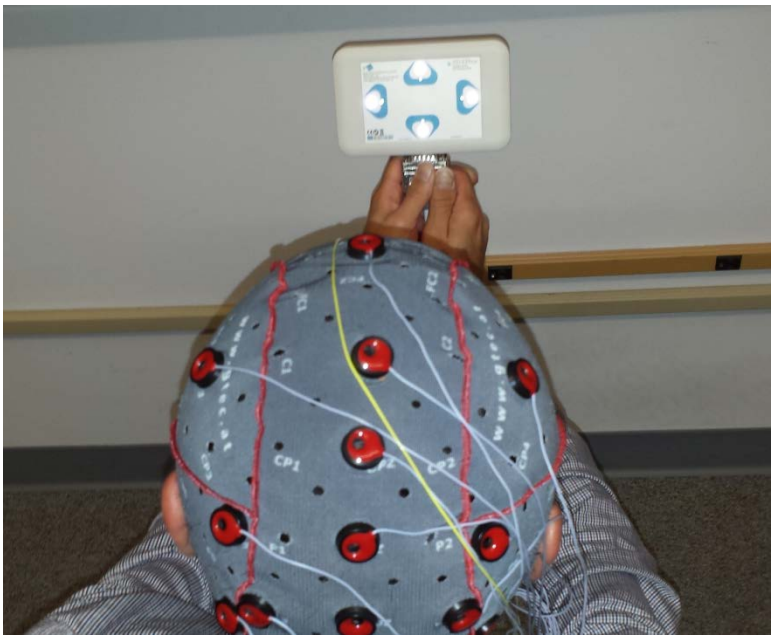

Figure 4. An SSVEP LED stimulation-box (Guger C., 2012)

2.3.3 Sensory Motor Rhythms (SMRs)

Sensory-Motor Rhythms are usually recorded from primary and somatosensory motor cortices. These rhythms are observable at 8-12 Hz or 18-26 Hz frequency ranges and called mu and beta rhythms, respectively. The physiological activities decrease the mu and beta bands amplitudes. This process is called Desynchronization. Desynchronization is called Event-Related Desynchronization (ERD) with respect to other brain's oscillations and activities. After completing any voluntary movement, the power (amplitude) of brain rhythms increases. This phenomenon is called Event-Related Synchronization (ERS). ERS is dominant over contralateral sensorimotor area and the corresponding brain signals maximum amplitudes appear about 600 ms after movement's offset. These brain signals' fluctuations are typically observable at the electrodes C3, C4 and Cz (Alonso N., 2012). Furthermore, some research results indicate that ERD and ERS do not require an actual movement for provocation. This phenomenon also occurs with motor imagery movements. Moreover, some studies' results has shown that people with or without motor disabilities are able to control mu and/or beta rhythm's amplitudes. Generally, performing and imagining the motor action tasks are observable by EEG over motor and sensorimotor cortices (Blankertz B., 2010).

2.3.4 P300 Potentials

An infrequent auditory, visual, or sensory stimulus, when intersperses within a frequent stimulus pattern, evokes a positive amplitude nearly 300 ms at electrode position Pz after subjects' exposure to the stimulus (see the location of Pz on Figure 1). These brain potentials are detectable from parietal cortex. This brain signal peak is called P300

potential. In the P300-based BCI system, the user is exposed to the array of auditory, visual, or somatosensory stimuli, which represent a particular pattern. The desired infrequent stimulus within this pattern elicits the P300 brain potentials and activates the BCI system.

2.4 The Brain Computer Interfaces' Applications

The BCI systems will perform the designated task through appropriate and efficient processing methods. These processing methods and algorithms differ from each other based on BCI systems' applications. In this section, BCI system categories which cover the BCIs applications will be reviewed. The earlier BCI applications were limited to the medical purposes. Recent advances in technology and neural engineering has revealed probable commercial applications of BCI systems. Therefore, demands for real-time operating BCI systems accumulate. The problem of enhancing the performance accuracy and system reliability is challenging. This problem originates from the signal processing and machine learning deficiencies. The BCI systems' applications are classified in four major categories which are motor substitution, motor recovery, entertainment, communication and control (Millán J. D. R., 2010).

2.4.1 Motor Substitutions

Many people are suffering from losing partial or full motor functions of their limbs. Some severe motor action damages are not recoverable with surgery. Usually, the Functional Electrical Simulation (FES) partially restores the lost functions. The Neuroprosthesis are BCI systems which replaces the part of limb lost functions. Some of

these systems are based on non-invasive BCIs, e.g. commercial product NESS-H200 (Bioness Inc., Valencia, USA). Pfurtscheller and his colleagues' research plan have successfully led to a non-invasive BCI system for grasping restoration (Pfurtscheller G., 2003). The notable research has been conducted by Millan's research group in which motor imaginary of hand movements are used for grasping and writing purposes. In this research, a hand orthosis is used for synchronizing the hand movements. This system also applies the user desired forces to the fingers and brings less fatigue in the long term period (Tan D. S., 2010). So far, other research groups also attempted to develop more advanced BCI prosthetic systems through invasive methods.

The assistive mobile devices controlled by brain such as wheelchairs or any other type of telepresence robots are considered as motor substitution BCI system. Some commercial products are available in market e.g. peoplebot (Mobile Robots Inc., Amherst, USA), iRobot (iRobot Corp., Bedford, USA), robotino (Festo AG, Dietikon, Switzerland) (Millán J. D. R., 2010). Finally, the primary challenges for these systems are autonomy level and collaboration between developed smart robots with human brain. The inferior challenges are the BCI systems reliability level and situations where these systems should be trusted to act.

2.4.2 Entertainment

Though, the earlier BCI systems were less seriously considered for entertainment nowadays more BCI devices are designed for these purposes: virtual video gaming, media and music systems, computer related technologies. Producing commercial products with non-medical applications are becoming more important as the BCI technology proliferates.

Enhancing the quality of such systems generally helps other BCI research fields to improve. It has been shown that controlling the games by BCI systems are possible and not dependent on gaming type, even with slightly trained users (Tangermann M. W., 2008). Some research groups developed virtual environments to train and improve the capability of the people who are paralyzed. These research results show better overall BCI performances for those paralyzed people [(Tangermann M. W., 2008), (Nudo, 2006), (Millán J. D. R., 2010), (Elitzur A.C., 2010)].

2.4.3 Motor Recovery

Motor recovery for impaired patients from strokes is critical. Their life quality will be improved by restoring back the lost functions. These days many research labs are seeking the new ways of rehabilitation for spontaneous motor functions recovery through neuroscience and especially with BCI systems [(Nudo, 2006), (Ward N. S., 2004)]. Nevertheless, recovering the lost functions and brain neural activities with the help of BCI systems is controversial. The research review by Lotze discusses examples in which the brain stroke patients have been recovered faster than usual by imagining the mental tasks, when they used BCI systems (Lotze M., 2006).

2.4.4 Communications and Control

The goal of communicating with the surrounding environment for severely disabled people is to improve their life quality and encourages them to pursue their medications. However, neuroscientific labs and research groups have not restricted their research goals to the medical purposes. The BCI studies on control and communication encompass a vast

area and connect the neuroscience, neural engineering and control system design engineering disciplines. The current BCI systems for producing commercial products are also considered for healthy individuals. Different companies, governments and national research institutes are conducting BCI studies. The efforts are on developing the BCI systems for variety of control devices to redeem or reduce the human physical interactions.

Galan et al. and Mason et al. published their results on designing a wheelchair asynchronized with the sensory motor signals [(Galan F., 2008), (Mason S. G., 2000)]. Brouwer et al. developed a P300-based BCI system functioning with vibro-tactile feedback to select the target on screen (Brouwer A. M., 2010). Donchin et al. designed an online BCI system which detects the user intention from evoked brain potentials with randomly flickering frequencies (Donchin E., 2000). The research by Wolpaw et al. has introduced a BCI system which controls the cursor movement in a 2D screen (Wolpaw J. R., 2004). Similar research is proposed by Bell et al. which attempts to navigate a cursor without training the subjects (Bell C. J., 2008). Blankertz et al. conducted research to control the humanoid robot with sensory and somatosensory brain signals (Blankertz B., 2007). They designed the system based on detecting P300 brain potentials and sent feedback to user with cameras mounted on the robot. The research on controlling different devices has continuously improved the BCI systems' accuracy and reliability. All around the world, research groups have tried to develop the faster, more efficient and reliable systems by implementing different brain signals or specific brain temporal pattern. For example, Muller et al. introduced the SSVEP-based BCI system to control a prosthetic arm with different degrees of freedom (Müller G. R., 2008).

The necessity of reducing the training sessions and introducing online BCI systems has dramatically increased during the past decade. Bin et al. proposed the canonical correlation analysis to interpret user intention with SSVEP brain signals without any training session (Bin G., 2009). Other research studies evaluated different analysis methods and contributed in developing the machine learning and signal processing algorithms for online BCI systems' performances [(Friman O., 2007), (Vasquez P. M., 2008), (Martinez P., 2007), (Bin G., 2009)]. Vasquez et al. proposed an SSVEP based BCI system to control a robot (Vasquez P. M., 2008). Their system was configured after short training sessions and reached to an acceptable accuracy level. Bakardjiana et al. implemented an analysis method based on banks of filters and integrated energy classifiers of EEG channels to control a virtual car in the planned route (Bakardjiana H., 2009). Their BCI system performed reasonably in an online session with eight flickering stimuli.

This conclusive effort might be the outcome of unknown nature of the human brain neurons' activities and capability of non-invasive devices for recording brain signals. Recently, more research has been conducted on the real-time processing algorithms with suitable system accuracy and information transfer rate. Friman et al. proposed different SSVEP analysis methods which detect SSVEP responses and estimate the error signals (Friman O., 2007). Other research by Allison et al. suggested combining the imaginary and visual evoked brain signal analyses for improving system operability in a hybrid BCI system (Allison B. Z., 2010). The hybrid BCI system is an effort to improve the accuracy and real-time operability by feeding the system with additional input data collected with other devices or from different brain lobes.

2.5 The Driver Behavior Studies and Brain Signal Processing Research

The importance of in-vehicle assistive systems and driving behavior studies originate from fatality rate and cost of national annual crashes in the US. The National Highway Traffic Safety Administration (NHTSA) has reported 29757 fatalities and an overall of 2,217,000 injured or wounded only during 2011 (DOT Safety Facts, 2011). Among these many accidents, nearly 17 percent occurred by distraction and 31 percent happened because of the drunk drivers [(DOT Safety Facts, 2011), (DOT Driver Distraction Guidelines, 2010)]. This issue attracted the government and many other research institutes and companies to conduct studies and develop systems and manuals for relieving the problem. Since then many driver behavior studies have been conducted because of their importance in saving lives. Moreover, improving the driving safety and traffic efficacy needs more knowledge about human behaviors in different situations or conditions. Correspondingly, the safety studies facilitate a new generation of intelligent transportation safety systems and driver assistive technologies. During the past decade, systems such as adaptive cruise control (ACC), lane keeping assistive system (LKAS), the vehicle navigation systems and collision avoidance system have been developed by the acquired knowledge from drivers' behavior studies. In these studies, the drivers' mental and physical conditions at different situations are observed while driving data are recorded. Various in-vehicle recording devices such as EEG, eye-tracking systems and MEG (magnetoencephalography) are employed to gain the drivers' physical and psychological data. Other driving data such as braking and gas pedal pressures, steering wheel angle and torque, car positioning and its deviation from the lane center are also engaged in transportation safety research [

(Miyajima C., 2007), (Rimini-Doering M., 2001), (Vural E., 2007), (Rau, 2005), (Mulder M., 2004), (Wu Y., 2009)].

The advances in technology and outcomes of the earlier research have led to modeling of more sophisticated systems, which detect the emergency situations and estimate the drivers' behaviors. In particular, using the EEG device in driver behavior and safety studies has dramatically increased with satisfactory achievements from BCI studies, simultaneously. Matousek et al. analyzed the data recorded with 256 Hz by EEG and filtered the time-windows of data samples by the wavelet transformation at different frequencies (Matousek M., 1983). Then, they estimated the linear regression lines for the signals. They suggested that the regression line slope is an indicator, which has a direct relation with drivers' vigilance. Parikh et al. studied alpha waves in frequency range of 8-13 Hz by filtering the recorded brain signals with wavelet transformation. They concluded that increase in drivers' drowsiness level is accompanied by alpha waves' amplitudes increases and could be detectable from the C3-O1 and Cz-Oz electrodes (Parikh P., 2004). Lal et al. conducted the driving simulator experiments on drowsy drivers. The participants were asked to drive 10-15 minutes active driving scenario consisting of curves and different traffic conditions which was followed by 2 hours monotonous driving task. Then, delta, theta, alpha and beta brain waves were band-passed and transformed to frequency-domain by Fast Fourier transformation (FFT). These signals amplitudes were compared via Analysis of Variance (ANOVA). They concluded the increase in drowsiness level was followed by increase in brain waves amplitudes. Their results indicated an average increase of 22 to 26 percent in theta and delta waves amplitudes while this amount was limited to 9

percent for the alpha and beta rhythms (Lal S. K. L., 2002). Other research conducted by Schmidt et al. on drivers' vigilance, consisted of infrequent targeted distractor sounds. The outcome of their research revealed the P300 potential sensitivity to drivers' vigilance. According to this research decreases in drivers' vigilance will result in the P300 amplitude drop (Schmidt E. A., 2007).

The research studies on the driver's brain signals have revealed their meaningfulness and significance for future drivers' behavior estimating models and safety studies. The drivers' behavior estimation modeling and drivers' intention detection using brain signals could contribute to in-vehicle assistive BCI systems for driver safety. However, the type of research connecting the BCI technologies, driving assistant systems and behavior studies is almost remained intact. During the past decade, many researchers' efforts on predicting the drivers' intention via brain cognitive signals have been conducted. However, the reliability issues of the BCI systems and concurrent BCI studies challenges have been problematic in drivers' assistive technologies. Lin and his colleagues in their research proposed an algorithm to predict the drivers' drowsiness and alertness level. Subjects were asked to drive the car-simulator scenarios, two 45 minutes sessions, and keep the car at the road center line. The recorded brain signals band-passed and Independent Component Analysis (ICA) collected the dominant brain signal channels. Then, a 50-order linear regression model of signals' estimated Power Spectral Density (PSD) was calculated. The results of this study present satisfactory fitness between the real brain signals power spectrums and the predicted brain signal power spectrums (Lin C. T., 2005). Chang et al. proposed invasive brain signal acquisition method to improve the observed brain signal quality and

system accuracy. They employed silicon dry electrodes based on micro-electro-mechanical systems (MEMS) to record brain signals from the stratum corneum (SC) which consists of skins' dead cells. The Principle Component Analysis (PCA) collected the prominent EEG channels and reduced the artifacts. The multivariate regression model of brain signals' PSD is estimated. The results show nearly 90 percent accuracy rate in estimation of brain signal amplitudes (Chang C. W., 2010). Haufe et al. conducted the car-simulator study to predict the drivers' intention for braking in an emergency situation. They recorded the data from multiple systems and tried to develop the best estimation algorithm. The EEG brain signals were recorded from the parieto-occipital cortices and the best power spectrum estimation of these signals were calculated. Afterwards, according to the driving outputs data, dominant EEG channels representing the brain source signals were selected (Haufe S., 2011).

Typically, the studies which have been conducted in the field of transportation safety employed the EEG recordings to estimate users' drowsiness level and drivers' vigilance. These studies predict best regressions' models and analysis methods for brain signal power spectrums estimations. The gap between the real-time BCI technologies and driver safety studies still requires more in-depth research. The implementation of the online BCI systems as in-vehicle assistive technologies, and determining system's efficiency and probable effects on drivers' performances necessitate more algorithm development and correlation analysis of brain signals. This thesis attempts to determine the effects of SSVEP-based BCI system presence on the drivers' distraction. Moreover, this research evaluates the accuracy and reliability of analysis methods, which are suitable for future online SSVEP BCI systems design.

2.6 Brain Signals Processing Algorithms

In this section the processing algorithms which are typically used by BCI research groups will be explained, briefly. Algorithms are based on some processing steps to generate meaningful outcomes from noisy recorded brain signals via EEG. Different analysis methods have been employed which have been proposed by the earlier BCI studies (Elitzur A.C., 2010).

The BCI systems are usually closed loop control systems which are initiated from some recorded brain signals and terminated in a control device. These systems' processing algorithms usually take four steps including data acquisition, preprocessing, feature extraction, and feature classification methods. Following paragraphs describe the more commonly used methods in earlier BCI studies [(Elitzur A.C., 2010), (Tan D. S., 2010)].

2.6.1 Data Acquisition

The data acquisition devices which are typically used in BCI studies are as follows: *Electroencephalography (EEG), Magnetoencephalography (MEG), Electrocorticography (ECoG), Functional Magnetic Resonance Imaging (fMRI)* and *Near Infrared Spectroscopy (NIRS)*. The work in this thesis uses EEG sensors, which are further described in other chapters.

2.6.2 Preprocessing and Feature Extraction

Preprocessing is referred to the step where artifacts and noises are detected and removed. The observed brain signals could be accompanied by some artifacts such as user physical activities or psychological loads, power line noises and measurement device

noises. Since the interesting brain signals for BCI systems are usually low-frequency signals, the simplest method to reduce the artifacts and noises is to use band-pass frequency filtering (Elitzur A.C., 2010). Other methods which have been used in BCI research to prepare and extract the brain signals' features are succinctly described as follows.

2.6.2.1 Linear transformations

The linear transformations generally transfer a subset of input data channels (x) with linearly combining them via weight factors (W) to the components of transformation space (y). (Eq. 1) represents the linear transform.

$$y = Wx \qquad \text{(Eq. 1)}$$

Where, in this equation, the transformed signals anticipated to be denoised, which increases Signal to Noise Ratio (SNR). Afterwards, the algorithms such as, temporal filters, Moving Average (MA) filter, or frequency power analysis algorithm are processed on components in transformed space.

2.6.2.2 Common average reference (CAR)

The Common Average Reference (CAR) method adjusts EEG electrode channels by subtracting their values from the overall average of all other selected subset of channels. This can be seen in (Eq. 2)

$$y_i = x_i - \frac{1}{N}(x_1 + ... + x_N) \qquad \text{(Eq. 2)}$$

Where, x_i is selected input channel and N is the number of subset channels and y is the transformed signal channel. The CAR method is decent for removing artifacts which are common among all of electrode's channels and cannot be effective for removing the artifacts which are localized within some EEG channels.

2.6.2.3 The laplacian references

This method adjusts the EEG channel amplitudes by subtracting them from the neighboring channels. Besides, depending on the selected neighboring channels this method is called large or small Laplacian References (LR). Small Laplacian reference method is based on subtracting signal channel's amplitudes from four nearest EEG signal channels' average amplitudes. The large Laplacian method is based on the subtracting from the four secondary closest EEG channels. Figure 5 demonstrates the schema of the laplacian reference derivations.

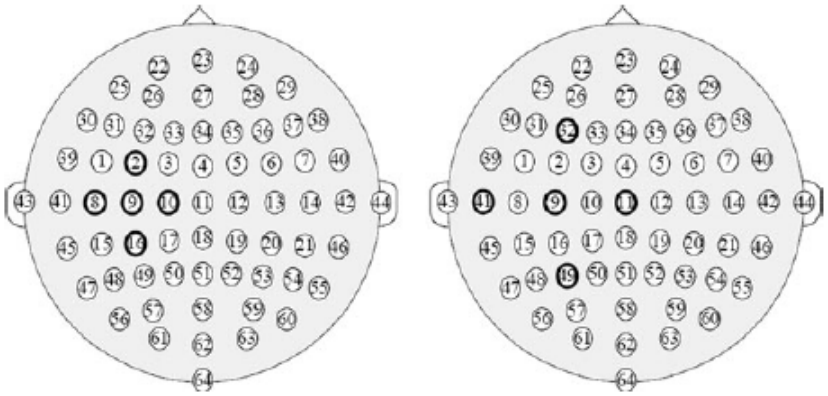

Figure 5. The small laplacian (left) and the large laplacian (right) derivations, figure is taken from (Elitzur A.C., 2010).

2.6.2.4 Principle component analysis (PCA)

This method separates brain source signals' components from observed brain signals. This method will result in distinguishing between desired and noisy (undesirable) brain signals' components. The PCA performs an orthogonal linear transformation and transforms the initial data to the new coordination system. This transformation arranges uncorrelated decomposed components organized according to their variance. The PCA transform is also an effective method for extracting the brain signals' features. The PCA transformation is represented in (Eq. 3):

$$y = W^T x \qquad \text{(Eq. 3)}$$

Where, $W^T = [w^1, \cdots, w^n]^T$ is weighting matrix for n input channels. Each element of this matrix is calculated by solving the eigenvalue decomposition of covariance matrix $R = xx^T$ (Aapo H., 2001)

2.6.2.5 Independent components analysis (ICA)

This method is similar to the PCA method which is effective for removing blind source noises and distinction of unknown brain signal sources. This method's assumption is linear independency between brain signal sources with zero mean value white noises. The ICA attempts to calculate the weighting matrix which is transferring the observed brain signals by EEG to the brain source signals. The ICA method benefits from obtained brain source signals linear independency which considers the acquired brain source signal's different neurophysiological origins. The elements of the weighting matrix are ordered according to their linear independency estimations. This will help to remove the elements with the least relevance and predictability (Aapo H., 2001). This method could be summarized as two consecutive PCA transformations.

2.6.2.6 Autoregressive coefficients modeling (AR)

This method is useful in communication, control and sensory array processing. This method assumes a linear relation between the brain source signals and observed EEG signals and feed the model by an additional white noise signal. This asset could be useful in analyzing SSVEP brain signals because of their origin characteristic in visual cortex. This model is generating a casual signal in which amplitudes are obtained from

data samples up to current time step. The linear formation of M-order autoregressive coefficients model is represented in (Eq. 4):

$$S_i(t) = a_{i1}S_i(t - 1) + \cdots + a_{iM}S_i(t - M) + \varepsilon_i(t) \qquad \text{(Eq. 4)}$$

Where, S_i is the estimated brain source signal for the i^{th} channel at time step t. The a_{ij} is the corresponding autoregressive coefficient and $\varepsilon_i(t)$ is noise signals' amplitudes at time step t. This model order defines the number of previous signals' amplitudes (time steps) which estimate the current signal amplitude (time step). AR model estimates both of the autoregressive coefficients and estimated signal variance. The outputs of this model are appropriate for computing the signal to noise ratio (SNR) of the filtered signals (Tan D. S., 2010).

2.6.3 Feature Classification and Channel Selection

This part of brain signal processing is classifying the feature space or selected channels. Previous steps were an effort to extract the featured signals and to improve their signal to noise ratios. The Classifiers are used to set BCI systems' parameters from training sessions' data and to develop preliminary models for controlling BCI systems. The classifications' methods are usually selected based on the BCI systems purposes and have no notable advantages relative to each other. The typical methods for classifications are the fisher linear discriminant (FLD), support vector machine (SVM), Bayesian classifiers, Hidden Markov Model (HMM) and the Adaptive Logic Networks (ALNs). The following

paragraphs briefly describe the FLD, SVM and ALN classification methods [(Tan D. S., 2010), (Theodoridis S., 2009)].

2.6.3.1 Fisher linear discriminant (FLD)

This method transfers higher dimension featured data to lower dimension space. This method is more practical for classifying input data into two separate classes. The separability of these classes is measured by the ratio of classes' means distances and between classes' variations (J(w)). This operation maximizes the between classes scatters. This procedure is demonstrated in (Eq. 5).

$$J(w) = \frac{w^T S_B w}{w^T S_W w} \qquad \text{(Eq. 5)}$$

Where, S_w and S_B are the within and between class scatters, respectively. These parameters are as follows, respectively.

$$S_B = (m_1 - m_2)(m_1 - m_2)^T \qquad \text{(Eq. 6)}$$

$$S_W = S_1 + S_2 \qquad \text{(Eq. 7)}$$

Where, S_i and m_i are the standard deviation and average values of each class, respectively. In (Eq. 5), W is the weighting vector which diagonalizes both of within and between class scatters. This vector is calculated from the Eigen Decomposition (ED) of (Eq. 8) (Theodoridis S., 2009).

$$W = S_w^{-1}(m_1 - m_2) \quad \text{(Eq. 8)}$$

2.6.3.2 Regression methods for classifications

Typically regression methods are linear classifiers which predict the system outputs from a linear model. These methods derive the weighting matrix (W) to correlate the inputs (x) to the estimated outputs ($\hat{y}$), while involving the additional constant value (b) for the better fitting regression model. The general format is presented in (Eq. 9).

$$\hat{y} = w^T x + b \quad \text{(Eq. 9)}$$

2.6.3.3 Adaptive logistic networks (ALN)

The ALN is a more general linear regression method and consists of different linear functions to improve the capability of pattern classification. These functions (L) are presented in (Eq. 10) for the j^{th} EEG channel and i^{th} time step.

$$L_j = \sum_{i=1}^{n} w_{ij} X_j + C_j \quad \text{(Eq. 10)}$$

Where, w is the weighting vector for the input data (X) followed by the function constant (C). These sets of functions create the decision tree and their values are thresholds for true and false logical decisions. Each function could be considered as a nodal point for connecting to other nodes.

2.6.3.4 Support vector machines (SVM)

This method is similar to previous methods with respect to projecting inputs (y) to outputs space (f(y)) with linear transformation and includes the corresponding weighting (w) and dependent vectors (w_0). The general form of an SVM method is shown in (Eq. 11).

$$f(y) = w'y + w_0 \qquad \text{(Eq. 11)}$$

The SVM method results to series of functions which compute the contingency of inputs to different sets of classes. Each class has specific SVM regression function. The inputs data-sets (y) with higher function output (f(y)), probably belong to that class. This method's optimization depends on the weighting vectors or so called supporting vectors represented by $w = \sum_i c_i \alpha_i y_i$ where c and α are positive Lagrangian multiplier.

This method could be employed in nonlinear optimization and classification problem when the kernel functions replace the support vectors (Brabanter, 2011)

2.7 Summery

The methods described in this chapter are commonly used by BCI research groups to explore and extract brain signals features. The presented processing steps typically form the algorithms for generating the final desired outputs that classify a feature associated with a brain signal. However, dramatically increasing demand for more reliable and practical online BCI systems requires development and implementation of more tailored algorithms for each BCI system. Accordingly, many research studies have focused on developing

processing algorithms which consider the brain signals origins characteristics. To increase the real-time performance resolution of these systems, the analysis algorithms should adaptively calculate system parameters by employing machine learning procedures. The next chapter will focus on describing the newly modified algorithms for analyzing the SSVEP brain signals. The analysis methods are adjusted based on the SSVEP brain signals and proposed detection algorithms are feasible for implementing in future online BCI systems.

Chapter 3: Analysis Methods and Procedures

Among different brain signals, event related potentials and especially the visually evoked potentials (VEPs) are more detectable by EEG. These types of signals are less affected by artifacts and power-line noises. These signals are more stable in terms of their spatial and temporal distributions on visual cortex as well. The SSVEPs described in chapter 2, generate similar signal patterns and frequency components of visual stimulus. This characteristic is useful in estimating the original brain source signals. Overall, this characteristic has increased the variety of available SSVEPs analysis procedures to enhance the system accuracy and reliability [(Wolpaw J. R., 2007), (Alonso N., 2012), (Millán J. D. R., 2010), (Elitzur A.C., 2010), (Dobriyal M., 2011), (Bakardjiana H., 2009) (Vasquez P. M., 2008)].

An accurate analysis model can detect user intention or command for controlling the BCI system. A reliable and stable system generates faster correct commands which do not dramatically degrade the system accuracy for different subjects/test sessions.

Chapter 2 describes the traditional analysis procedures to acquire desirable outputs from brain signals. These steps similarly apply to SSVEP response detection algorithms. Figure 6 demonstrates the schematic of a typical SSVEP BCI system algorithm.

The Analysis steps which are presented schematically in figure 6 could be modified or combined in one step, according to anticipated outputs.

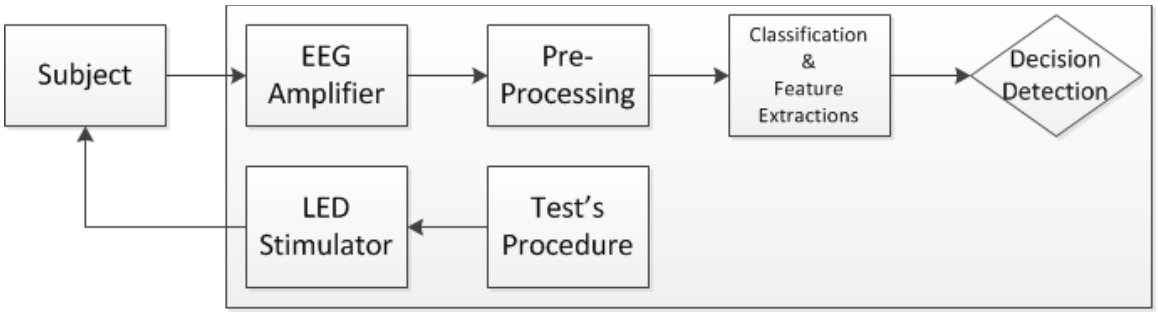

Figure 6. Schematic SSVEP BCI system algorithm

This chapter formulates and employs different modified analysis methods to detect the SSVEP brain signal responses, accurately. These presented methods are also modified to decrease the BCI systems intra/inter subjects' performance error (True Positive, TP) variations. The Formulation and organization of the analysis algorithms are presented in two sections. The first section includes the newly modified multivariate data analysis algorithms. The second section includes the employed adaptive filtering algorithms. These algorithms are developed for more accurate and reliable SSVEP response detections. These algorithms may not include all typical steps which are illustrated in figure 6. The common characteristic of these analysis algorithms is the ability to compare the correlation of the recorded brain signals with the LED stimuli signals flickering with different constant frequencies (in this research, 10, 11, 12 and 13 Hz).

The multivariate analysis methods attempt to find the underlying correlation between two sets of input data. These data-sets describe the same characteristics of a specific object. Typically, input data-sets are consisted of newly recorded and available known data to obtain more knowledge about the nature of that object. In this thesis, Canonical Correlation

Analysis (CCA) and Co-Inertia analysis are employed to evaluate the correlation between the LED stimuli and subjects' visual brain signals.

Adaptive filters are the signal processing methods in which a set of recorded signals can be filtered and denoised with the knowledge of their characteristics. These types of signal processing algorithms estimate the source signals from the recorded brain signals based on different defined criteria. These criteria commonly set to minimize the estimated source signal error value. To achieve this, the criteria define a cost function and optimized result will be obtained from minimizing the cost function value for each set of input data. Adaptive filters are specifically categorized as robust filters, if additional criteria for defining the error boundaries are considered. In this thesis, to obtain the original brain signals from the recorded EEG signals and modeled LED signal, three different adaptive filters are employed. These filters are adaptive Kalman filter, adaptive robust Gauss-Newton filter and constrained discrete DFT block adaptive filter.

Each algorithm has a decision making method which is based on either selecting the most correlated brain source signals with a LED signal (multivariate analysis methods) or selecting the brain source signals with the least noise variation (adaptive filtering methods). The obtained accuracy for each method demonstrates the number of correct user intention detections among the time-windows of a test session. The information transfer rate (ITR) is considered as criterion for evaluating these methods ability for fast response detection.

In this thesis, two sets of input signals are considered for detecting the subjects' SSVEP responses. The first set of input signals are the brain signals recorded by 8 EEG channels from visual cortex (presented in figure 3). The second set of input signals are the channels

of LED stimuli which are flickering at 10, 11, 12 and 13 Hz frequencies. The LED signals are square wave signals and their Fourier transform modeled channels consist of sine and cosine elements with different harmonics. In this thesis, each flickering LED signal (with constant frequency) is consisted of 6 channels for 3 harmonics of the signal's sine and cosine elements.

To evaluate and verify the proposed methods' accuracy, 2 different sources of recorded brain signals are employed. The first set of data provided by g.TEC CO. which were recorded from 4 healthy trained subjects. The second set of recorded brain signals are obtained from 30 healthy subjects aged between 18-65 years old participating in a SSVEP test session at the CISR laboratory. The general schema of SSVEP analysis procedures used in this thesis is presented in section 3.1.

3.1 The Brain Recorded Signals' Algorithms Schema

In this part of the thesis, schematic structure of recorded brain signals' analysis algorithms which have been used to detect user intention will be explained, briefly. Then, employed Matlab programming codes of these processing algorithms will be presented in Appendix A.

Figure 7 shows a general structure in which recorded brain signals processed with introduced analysis methods. The final outcomes of processing methods are compared to the test trials' procedure to determine the accuracy rate of each method. Figure 11 presents a schema of transformed data and their corresponding Co-Inertia axes in featured space for Co-Inertia analysis method.

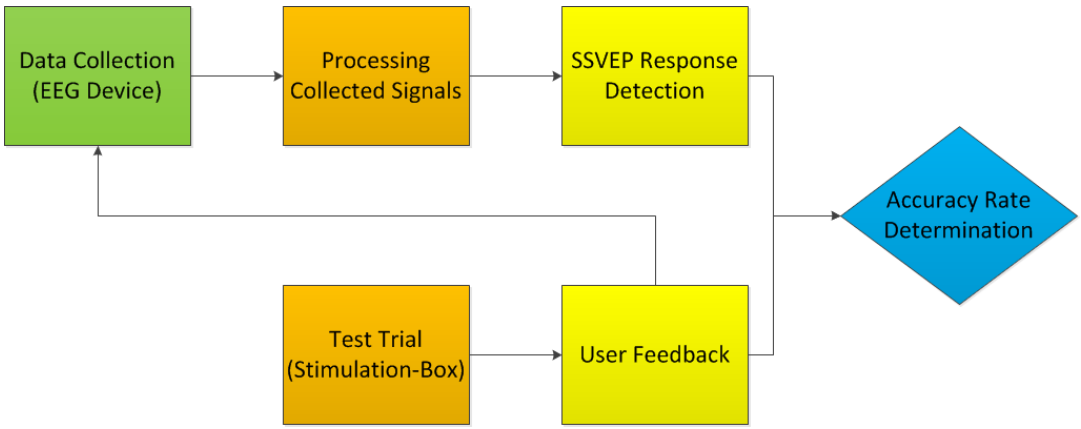

Figure 7. General flowchart representing the processing methods for recorded brain signals

Figure 8 illustrates a general schema of adaptive filters' structure. The schematic figure of CCA method is presented in figure 9.

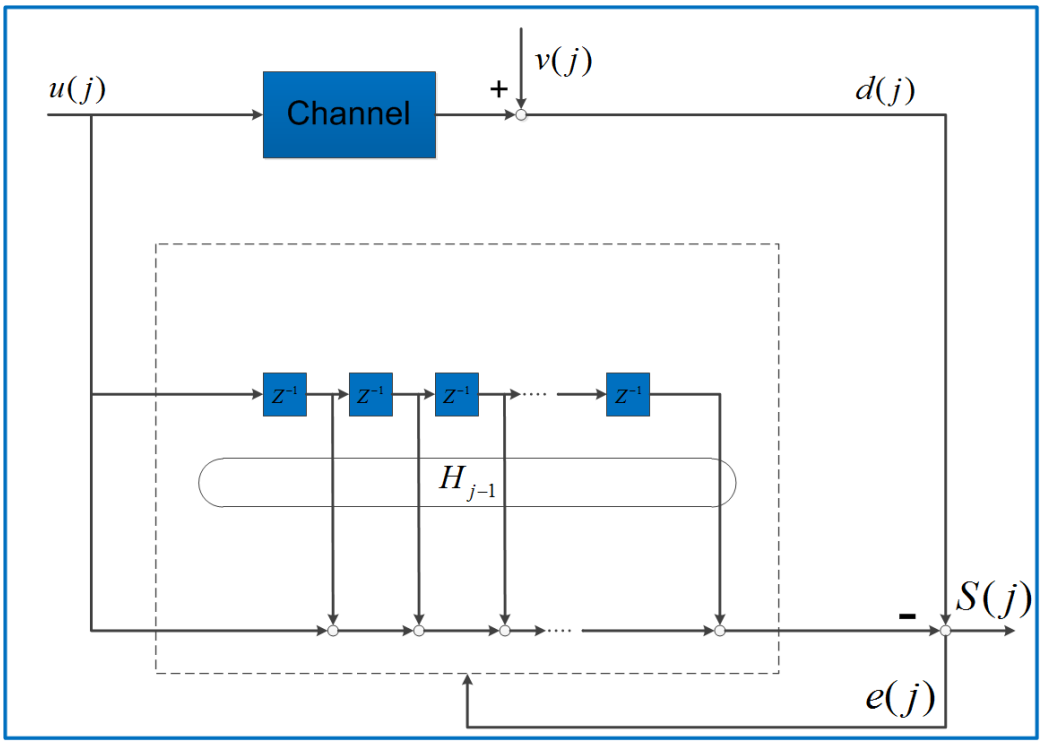

Figure 8. A schema of adaptive filters

In figure 7, Data are collected by g.USBamp with 16 electrode channels. A 0.5-30 Hz band pass filter along with 50 Hz notch filter are used to remove the artifacts and power line noises by data acquisition system. The processing part includes five aforementioned methods which are explained in this chapter. The analysis methods which are employed are as follows:

- Canonical Correlation Analysis
- Co-Inertia Analysis
- Adaptive Kalman Filter
- Adaptive Robust Gauss-Newton Filter
- Adaptive Unconstrained DFT Block Filter

The detailed explanation of each method for processing collected brain signals and estimating the original brain source signals are explained in this chapter as well (sections 3.2 and 3.3).

The SSVEP response detection of analysis methods can be categorized in two types of decision making processes. The first category of decision making methods is related to multivariate analysis methods. These methods are based on detecting the most correlated LED signal and brain recorded signal. However CCA method is enriched with additional decision making algorithms based on ARMA filter and proposed evaluation methods (statistical tests). The Second category of decision making method is based on maximum SNR method. This method selects the LED with higher SNR as user intention.

The SSVEP test session trials are explained completely in chapter 4. The test trials are consisted of 4 LEDs flickering with 10, 11, 12 and 13 Hz frequencies, simultaneously. In

each test session 5 trials of flickering LEDs are included. In each trial, LEDs are flickering for 7-seconds and subjects are asked to focus on a specific LED.

The user intentions are detected with filtering algorithms during SSVEP test trials. The results of analysis algorithms are compared with real test procedure which was planned. Then based on comparison, accuracy rate of each analysis method is acquired.

The Appendix A will provide programming codes which are used for each block in figure 7. This appendix has the programming codes aligned based on analysis steps which are presented in the schema. Initially, data collection and creating desired time-windows' Matlab codes are demonstrated. Then, each analysis method's programming code in the order that presented in this section is provided. Lastly, decision making methods' Matlab codes for both of multivariate data analysis and adaptive filtering methods are demonstrated.

3.2 The Multivariate Analyses Algorithms

3.2.1 The Canonical Correlation Analysis

The Canonical Correlation Analysis (CCA) is a multivariate analysis method which attempts to find the maximum correlation factor, ρ in (Eq. 12) between two sets of input data. Moreover, input data-sets have an underlying correlation with their obtained canonical variants (*U* and *V*) [(Lin Z., 2006), (Legendre L., 2003)].

$$\rho = \frac{E[UV]}{\sqrt{E[U^2]E[V^2]}} = \frac{E[W_x{}^T xy^T W_y]}{E[W_x{}^T xx^T W_x]E[W_y{}^T yy^T W_y]} \qquad \text{(Eq. 12)}$$

W_x and W_y are weighting matrices calculated for x (input) and y (expected values) matrices, respectively. U and V are Canonical variants. U, V and their weighting matrices could be derived with different mathematical solutions. In this section, two consecutive PCA are performed by Singular Value Decomposition (SVD) and QR decomposition on x and y matrices to solve (Eq. 12) and find the proper canonical variants and weighting matrices. This method and its solution's proof are explicated by [(Legendre L., 2003), (Bin G., 2009)] and will be reviewed in following section.

To find the weighting matrices and canonical variants, x and y matrices are decomposed for finding Q (orthogonal) and R (upper triangular) matrices, respectively. Therefore:

$$x = Q_x R_x \qquad \text{(Eq. 13)}$$

$$y = Q_y R_y \qquad \text{(Eq. 14)}$$

Next, SVD decomposition of $Q_x^T Q_y$ matrix should be obtained. The decomposition solution eigenvalues and eigenvectors are V, S and D matrices, respectively. The weighting matrices are calculated from (Eq. 15) and (Eq. 16).

$$W_x = R_x^{-1} S \qquad \text{(Eq. 15)}$$

$$W_y = R_y^{-1} D \qquad \text{(Eq. 16)}$$

QR decomposition method considers the V matrix elements as canonical correlation factors.

In this research, two sets of data from recorded brain signals (EEG signals) and LED stimuli signals are considered as inputs. The LED stimulation-box flickers with square wave signals at specific frequencies. The LED signal is considered reference signal (expected values matrix in CCA) and modeled by the sine and cosine elements of each flickering frequency. LED reference signal model is demonstrated in (Eq. 17).

$$Y(f_i) = \begin{Bmatrix} \sin(2\pi f_i t) \\ \cos(2\pi f_i t) \\ \vdots \\ \sin(2\pi h f_i t) \\ \cos(2\pi h f_i t) \end{Bmatrix} \qquad \text{(Eq. 17)}$$

Where, f_i is the LED flickering frequency and h is frequency harmonics indicator which specifies the number of the extracted brain signals' frequency components. Figure 9 demonstrates recorded brain signals and LED stimulation signal components along with their obtained canonical variants for a 1-second time-window.

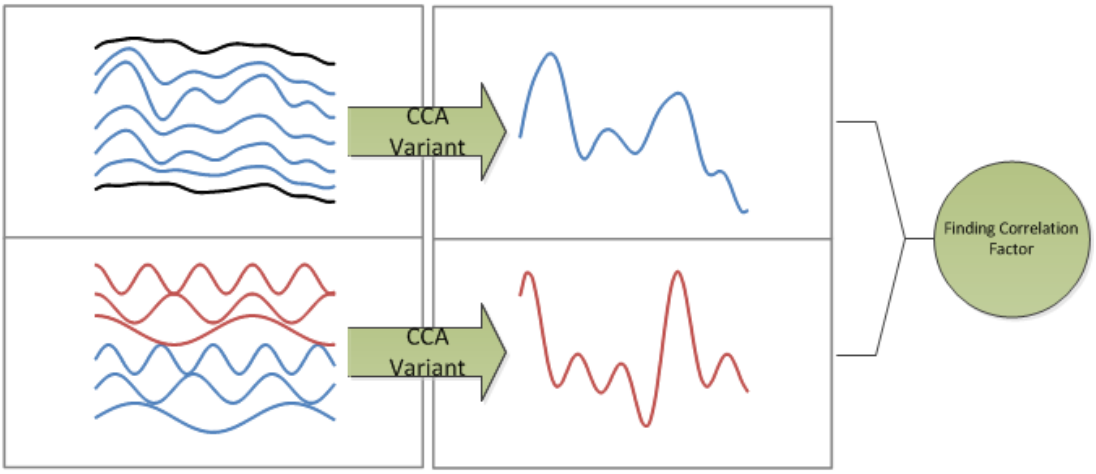

Figure 9. Canonical Correlation Analysis (CCA); Brain signals and their first canonical variant (top) & LED reference signals and their First canonical variant (bottom)

Bin et al. and Lin et al. suggested that stimulation signal with the highest correlation factor to be selected as user intention for SSVEP BCI systems with different stimulation frequencies [(Bin G., 2009), (Lin Z., 2006)]. However, in this thesis two additional decision detection (evaluation) procedures are suggested. The first procedure is based on Wilks's ratio and Bartlett's chi-square significance tests. The second procedure is based on Autoregressive Moving Average (ARMA) filtering of obtained correlation factors from inputs. The second procedure is a straightforward ARMA filtering of correlation factors and the user decision detection is based on the typical higher correlation factor rule, as explained. Hence, the following paragraphs only describe the first procedure algorithm.

3.2.1.1 Statistical significant tests algorithm

This evaluation procedure, shown in figure 10, is adjusted based on the Wilks's ratio and Bartlett's chi-square statistical tests.

It is good to mention that correct decision in figure 10 simply means that all of the statistical significant test results and typical CCA higher correlation factor selection results are equivalent. In canonical correlation analysis procedures, Wilks's ratio is interpreted similarly as in significance test in multidimensional regression models. (Eq. 18) expresses Wilks's ratio (Λ) (Lattin J. M., 2003).

$$\Lambda = \frac{|R_{yy} - R_{yx}R_{xx}^{-1}R_{xy}|}{|R_{yy}|} \qquad \text{(Eq. 18)}$$

Where, R is the covariance or cross-covariance matrix with respect to its subscripts. Wilks's ratio indicates the variance proportion in y (expected values data-set) which can be explained by the input data (x).

In other words, it clarifies the significance level of canonical variants. In this test, values near zero are representatives of the strong model.

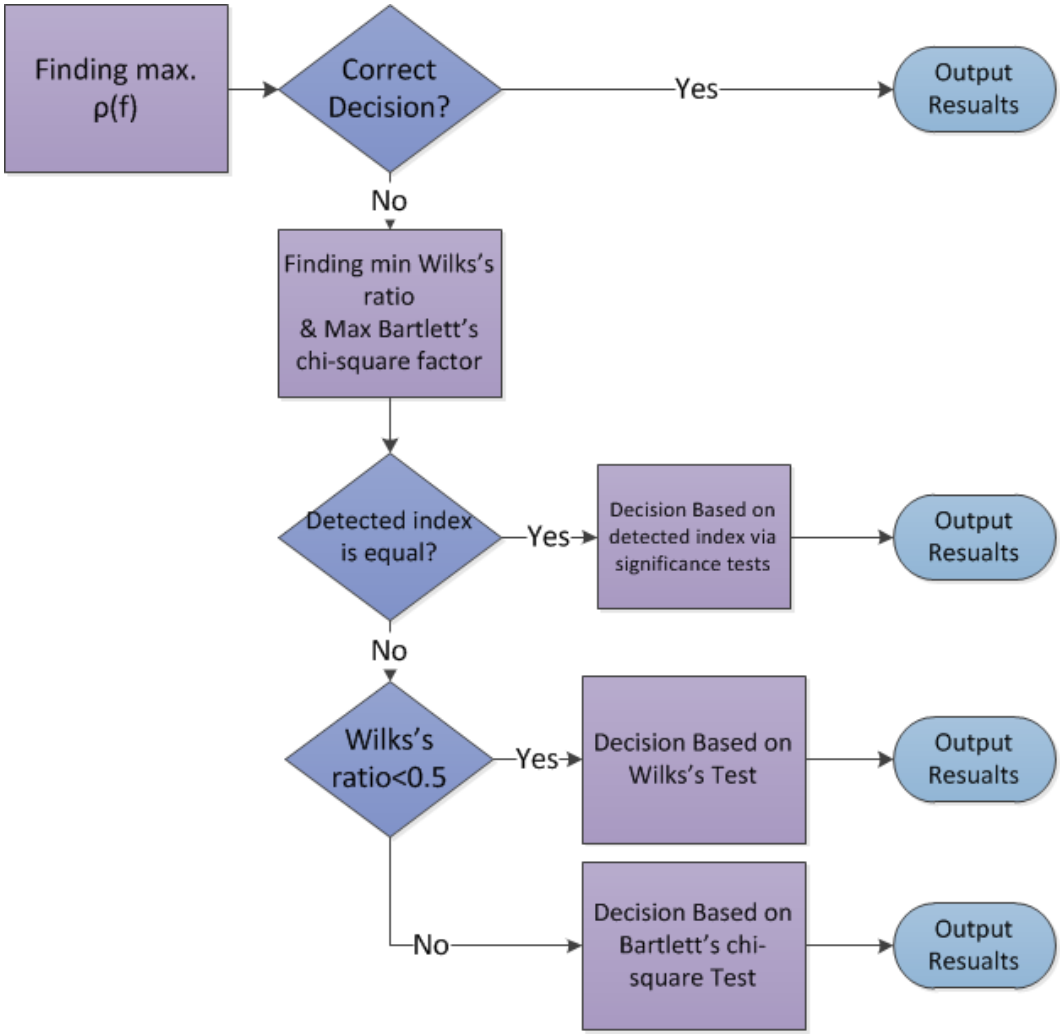

Figure 10. Statistical significant tests algorithm

Another significance test is the Bartlett's chi-square test (statistical V-test) which evaluates null hypothesis of no underlying relationship between *x* and *y*. In other words, Bartlett's chi-square factor determinates the lack of correlation between two sets of data. The higher values of v are weakening hypothesis of no correlation between the data-sets. Bartlett's chi-square approximation for Wilks's ratio is expressed in (Eq. 19).

$$V = -[(n-1) - \frac{(p+q+1)}{2}]\ln(\Lambda) \qquad \text{(Eq. 19)}$$

Where, V is the approximately χ^2 distributed with p and q degrees of freedom. n is the number of observations (data samples). p and q are the minimum ranks of x, y matrices, respectively (Lattin J. M., 2003).

This algorithm evaluates the correlation between canonical variants and their corresponding input signals (recorded brain signals and LED stimuli signals). Then, the algorithm assesses the correlation level between calculated canonical variants. In this algorithm, the priority of determining the user intention is on Wilks's ratio. The evaluation procedure substitutes its determined LED index (user intention on specific flickering LED) with the obtained LED index (user intention on flickering LED) from typical maximum correlation factor selection. This means that for the weak models obtained from input signals (the noisy signals) the CCA output index (detected LED) reflects the selected LED index based on suggested statistical significance tests.

3.2.2 The Co-Inertia Analysis

Co-Inertia analysis is a symmetric correlation analysis method which searches for the *common structures* between two data-sets. The data-sets should explain the characteristic of the same objects and could be equally interpreted in an algorithm. This method projects the data-sets onto axes of their eigen-analysis of cross-set covariance matrix (Co-Inertia axes) to detect their common characteristic. The projecting can be performed with various transformation methods. It's mentioned that input data-sets are the recorded brain signals (8 EEG channels) and LED flickering modeled signal (6 channels of sine and cosine elements of the flickering frequency). This method is not hypothesizing the directional effect and does not consider influence of data-sets on each other. The algorithm is based on SVD decomposition of centered data-sets (centered with data mean) covariance matrix and then projecting the centered data-sets onto axes of their cross-covariance matrix (Legendre L., 2003). This algorithm is briefly described herein. The cross-covariance matrix of the two centered data-sets is computed in (Eq. 20).

$$Cov_{xy} = \frac{1}{n-1} y_{cent}{}' x_{cent} \qquad \text{(Eq. 20)}$$

Where, x and y are data-sets with same number of objects (n, matrix rows) and different number of channels (N_p and N_q, EEG and LED signal channels, respectively). Cov_{xy} is cross-covariance matrix and y_{cent} and x_{cent} are the centered y and x data-sets, respectively. The Co-Inertia value is obtained from sum of squared covariances in Cov_{xy} matrix. This value is the sum of squared eigenvalues where their eigenvectors represent the Co-Inertia

axes. This partitioning is performed by SVD decomposition of the Cov_{xy} matrix as illustrated in (Eq. 21).

$$Cov_{xy}(N_p \times N_q) = V(N_p \times c)W(c \times c)U^{'}(c \times N_q) \quad \text{(Eq. 21)}$$

Where, c is the minimum rank of x and y matrices. W is the diagonal matrix of eigenvalues and U & V are the eigenvector matrices.

The projection of data-sets onto their Co-Inertia axes transfers the data to common multivariate feature space. This can be calculated with multiplying the centered data by their eigenvectors. Then, the acquired matrix is normalized with respect to its columns. The (Eq. 22) and (Eq. 23) present projection of x data-set to the feature space.

$$f_t = x_{cent} \times V \quad \text{(Eq. 22)}$$

After normalizing the columns of f_t matrix to length 1, projection process can be completed through (Eq. 23).

$$F_{t1} = \sqrt{n-1}(Wf^*) \quad \text{(Eq. 23)}$$

Where, f_t^* is the normalized f_t matrix from (Eq. 22). The projected matrix for the y data-set could be calculated with the same procedure.

In this research, LED stimulation signal and signals from EEG device are considered as two input data-sets which are describing the same concept. Therefore, Co-Inertia algorithm analysis procedure is employed to project them to same feature space for evaluation. The simpler decision detection method finds the difference between two projected data-sets. In

the case of SSVEP BCI systems with different stimulation signals, the stimulus signal with least difference from brain signals is detected as user decision or intention. Figure 11 presents a schema of the transformed data-sets into the same feature space and co-inertia axes.

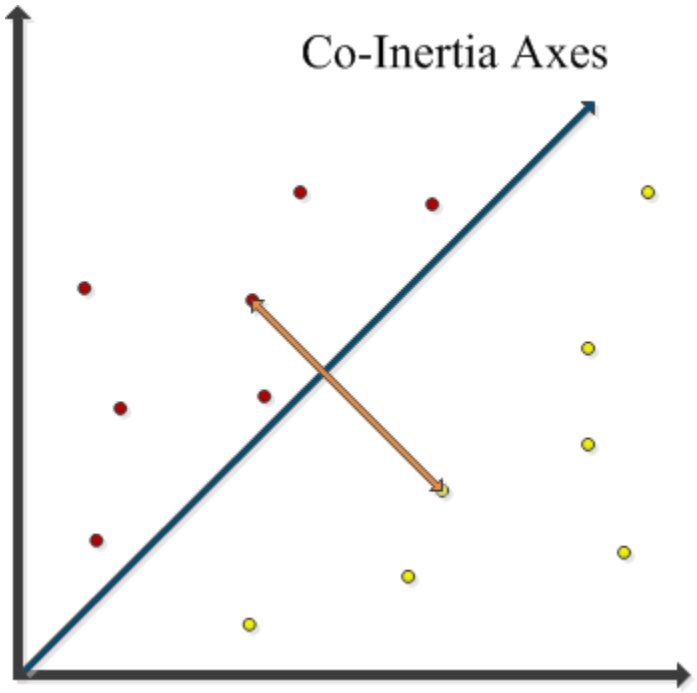

Figure 11. A schema of Co-Inertia space and Co-Inertia axes

3.3 Adaptive Filtering Algorithms

Adaptive filters have an important role in modern signal processing and control applications where processing the data without a priori knowledge is required. These algorithms have been employed for miscellaneous systems in communications, control, radar and biological engineering (Adali T., 2010). Recently, by increases in demand for more commercial BCI products, adaptive filters and machine learning algorithms are

becoming more prominent. Recent adaptive filters' implementations in SSVEP BCI systems along with the studies' promising outcomes have encouraged different research groups to improve the reliability and generalities of these algorithms [(Haufe S., 2011), (Friman O., 2007), (Vasquez P. M., 2008), (Mason S. G., 2000), (Blankertz B., 2008)]. In this thesis, some of adaptive filtering algorithms, suitable to be employed in brain signal processing and SSVEP response detection are evaluated. Prior research studies on adaptive filters with corresponding cost functions for reducing the error's rate have inspired any further research. These filters principally reduce the filter models' parameters error rate at each time step (data sample). The modifications are applied through cost functions to converge the system error boundaries.

3.3.1 The Adaptive Kalman Filter

A major assumption in modeling of SSVEP BCIs is correlation between the observed brain signals and LED stimuli signals. Accordingly, we are trying to estimate the original brain source signals from LED stimulus (6 channels of modeled LED signal) and the observed brain signals (collected by 8 EEG channels) by means of an adaptive Kalman filter. Finally, the user visual focus on LED lights will be obtained from estimated source signals Power Spectral Densities (PSDs) and maximum signal to noise ratio (SNR). The SNR is a criterion which calculates the average ratio of the signal's power amplitudes over the signal noise amplitudes.

First, Adaptive Kalman filtering of a single observed signal channel and one desired LED channel is described in the following section. Then, this filtering method is extended

to multiple numbers of EEG and LED channels to estimate brain source signals for a multiple-input multiple-output (MIMO) system. Finally, the SSVEP responses detection algorithm is presented.

3.3.1.1 Adaptive Kalman filtering model

Adaptive Kalman filter is based on a linear model between two sets of input variables which is presented in (Eq. 24) and (Eq. 25) in a state space form. For a time-invariant system, this model estimates the output x_j from measurement matrix d and input data matrix H (Sayed, 2008).

$$d = Hx_0 + v \qquad \text{(Eq. 24)}$$

$$x_j = \lambda^{-\frac{1}{2}} x_0 \qquad \text{(Eq. 25)}$$

Where, d is an N×1 matrix of LED stimulus signal for each frequency harmonic, N is the number of observations, which is set as 256 Hz; d includes sine and cosine elements of LED stimulus signal with specific frequency. x_0 is the M×1 weighting matrix and λ is a positive multiplier (forgetting factor). H is an N×M matrix of observed brain signals for an M-order adaptive filter. v is an N×1 column matrix of noise values and x_j is estimated brain source signals at j^{th} time step.

This model can be used with different state-space models. According to prior assumption, the brain source signals are evoked with similar patterns to the stimuli signals. In this research, stimuli are the LED lights. Their constant flickering frequency

could be modeled with square wave signals and presented by its Fourier Transform (FT) sine and cosine elements. This stimuli signals model is similar to the reference signal model in CCA method and demonstrated in (Eq. 17).

The matrix format of Eq. (1) for one LED stimulus signal channel and an EEG observed brain signal channel is presented in (Eq. 26).

$$\begin{bmatrix} d(0) \\ d(1) \\ \vdots \\ d(N-1) \end{bmatrix} = \begin{bmatrix} 1 & 0 & 0 & 0 \\ & \lambda^{-\frac{1}{2}} & 0 & 0 \\ & & \ddots & 0 \\ SYMM & & & \left\{\lambda^{-\frac{1}{2}}\right\}^{N-1} \end{bmatrix} \begin{bmatrix} u(0) \\ u(1) \\ \vdots \\ u(N-1) \end{bmatrix} x_0 + \begin{bmatrix} v(0) \\ v(1) \\ \vdots \\ v(N-1) \end{bmatrix} \qquad \text{(Eq. 26)}$$

In this equation, λ is called forgetting factor with a value between 0 and 1. As λ value approaches to 1, the parameters are more affected by values of previous time steps. u is an N×1 column matrix of observed brain signals. λ and u matrices, in (Eq. 26), are forming the same H matrix in (Eq. 25).

This linear model estimates x_0 (weighting) matrix by solving the exponentially-weighted recursive least square cost function formulated in (Eq. 27).

$$\min_{x_0}\left[x_0^*(\lambda\Pi)x_0 + \sum_{j=0}^{N-1} \lambda^{-j} \left| d(j) - u_j x_0 \right|^2 \right] \qquad \text{(Eq. 27)}$$

Where, Π is an arbitrary positive definite matrix which is usually selected by multiplying a small positive value (δ) by identity matrix (I). $d(j)$ and u_j are the values of d and u matrices at j[th] time step. By factoring out the constant factor λ^N from (Eq.

27), the cost function can be rewritten as (Eq. 28). This factorization is helpful for simplifying the cost function solution.

$$j(x_0) \triangleq \left[x_0^*(\lambda\Pi)x_0 + \sum_{j=0}^{N-1} \left| y(j) - u_j x_j \right|^2 \right] \quad \text{(Eq. 28)}$$

Where, *y(j)* and x_j quantities are defined in (Eq. 29) and (Eq. 30), respectively.

$$y(j) \triangleq \frac{d(j)}{(\sqrt{\lambda})^j} \quad \text{(Eq. 29)}$$

$$x_j \triangleq \frac{x_0}{(\sqrt{\lambda})^j} \quad \text{(Eq. 30)}$$

From (Eq. 26) and (Eq. 30), it is concluded that x_j satisfies the condition in (Eq. 31) which is the estimation for a brain source signal channel at the j^{th} time-step.

$$x_{j+1} = \lambda^{-\frac{1}{2}} x_j \quad \text{(Eq. 31)}$$

(Eq. 24) to (Eq. 31) define the Kalman filter parameters for estimating a brain source signal (x_j) from one LED stimulus signal channel (d) and an observed brain signal channel (u).

In this research, data was collected from 16 EEG channels (8 EEG channels from visual cortex for SSVEP response detection) and LED stimulation-box consists of 4 LED channels which result a MIMO system. Therefore, the system has 12 inputs due to

4 LED channels and 16 EEG signal channels (note: for each LED channel, 3 frequency harmonics are considered) and 24 outputs (4 LED x 6 estimated brain source signal per LED). The following section extends the adaptive Kalman filter for a MIMO system.

3.3.1.2 Adaptive Kalman MIMO filter

For a system with *Nq* channels of LED stimuli signals and *Np* channels of observed brain signals, an M-order multiple-input multiple-output (MIMO) adaptive Kalman filter model can be rewritten to calculate systems parameters at each time step. In an M-order MIMO model, *Nq* channels of LED stimuli and *Np* channels of observed brain signals are presented in vector format in (Eq. 32) and (Eq. 33), respectively.

$$d(j) = \begin{bmatrix} d_1(j) & d_2(j) & \cdots & d_{Nq}(j) \end{bmatrix} \quad \text{(Eq. 32)}$$

$$U(j) = [U_1(j) \quad U_2(j) \quad \cdots \quad U_{Np}(j)] \quad \text{(Eq. 33)}$$

Where, *d(j)* values are scalars, equal to each LED stimulus signal amplitude at j^{th} time step. Columns in *d* vector are sine and cosine elements of different stimulus signal harmonics. Each *U(j)* vector element is a channel of buffered brain signal based on the filter order which is presented in (Eq. 34).

$$U_i(j) = [u_i(j) \quad u_i(j-1) \quad \cdots \quad u_i(j-M+1)] \quad \text{(Eq. 34)}$$

From (Eq. 33) and (Eq. 34), *U* is a 1×(M×Np) vector.

Considering input vectors and initial values of $P_{0|-1} = \Pi_0$ and $\hat{x}_{0|-1} = 0$, system parameters for j≥0 are calculated from (Eq. 35) to (Eq. 39) (Sayed, 2008).

$$r_e(j) = 1 + U(j) P_{j|j-1} U^*(j) \quad \text{(Eq. 35)}$$

$$k_{Np,j} = \lambda^{\frac{-1}{2}} P_{j|j-1} U^*(j) / r_e(j) \quad \text{(Eq. 36)}$$

$$v(j) = \lambda^{\frac{-1}{2}} d(j) - U(j) \hat{x}_{j|j-1} \quad \text{(Eq. 37)}$$

$$\hat{x}_{j+1|j} = \lambda^{\frac{-1}{2}} \hat{x}_{j|j-1} + k_{Np,j} v(j) \quad \text{(Eq. 38)}$$

$$P_{j+1|j} = \lambda^{-1} \left[P_{j|j-1} - \frac{P_{j|j-1} U^*(j) U(j) P_{j|j-1}}{1 + U(j) P_{j|j-1} U^*(j)} \right] \quad \text{(Eq. 39)}$$

Where, $r_e(j)$ is called conversion factor and $k_{Np,j}$ is a 1× MP vector of Kalman filter gains at each time step. $v(j)$ is a 1× q vector, called innovation variables vector which represents the noise signals in this model. Moreover, at each iteration j, because x_j is the scaled factor of x_0 (weighing matrix), the brain source signals' estimations are obtained from (Eq. 40).

$$\hat{x}_{0|j} = \lambda^{(j+1)/2} \hat{x}_{j+1|j} \quad \text{(Eq. 40)}$$

Where, $\hat{x}_{0|j}$ is the solution of exponentially-weighted recursive least square cost function in (Eq. 41) (Sayed, 2008).

$$\min_{x_0} \left[x_0^* (\lambda \Pi) x_0 + \sum_{j=0}^{N-1} \left| y(j) - u_j x_j \right|^2 \right] \quad \text{(Eq. 41)}$$

Therefore, in summary for *Nq* channels of EEG (16 here) and *Np* channels of LED (4 here), $\hat{x}_{0|j}$ in (Eq. 40) estimates the brain source signals (6 signals for each LED, totaling 24 signals).

3.3.1.3 SSVEP response detection

The SSVEP signal patterns are ideally described by their exogenous stimulus signal. This assumption simply expresses that frequency components of SSVEP power spectrum should reach their peaks at frequency harmonics of stimulus signal. Figure 12 demonstrates the recorded brain signals (EEG measurements), measured from subject 1 for a 1-second time-window, evoked by the 10 Hz LED.

Figures 13 to 15 illustrate the estimated power spectrum of first EEG signal channel for the 1st, 2nd and 3rd harmonics of 10 Hz frequency, respectively. To detect the presence of SSVEP responses at each time-window, statistic t-test employed to calculate the SNR according to (Eq. 42) (Friman O., 2007).

$$SNR = \frac{1}{N_p N_h} \sum_{i=1}^{N_p} \sum_{j=1}^{N_h} \frac{\hat{S}(f)_{j,i}}{\hat{\sigma}^2_{j,i}} \qquad \text{(Eq. 42)}$$

Where, *Np* and N_h are the number of EEG channels and frequency harmonics, respectively. $\hat{S}(f)_{j,i}$ is the estimated power spectrum of SSVEP signal for the jth harmonic and ith brain source signal. $\hat{\sigma}^2_{j,i}$ is the estimated power of noise signal for the jth harmonic and ith brain source signal.

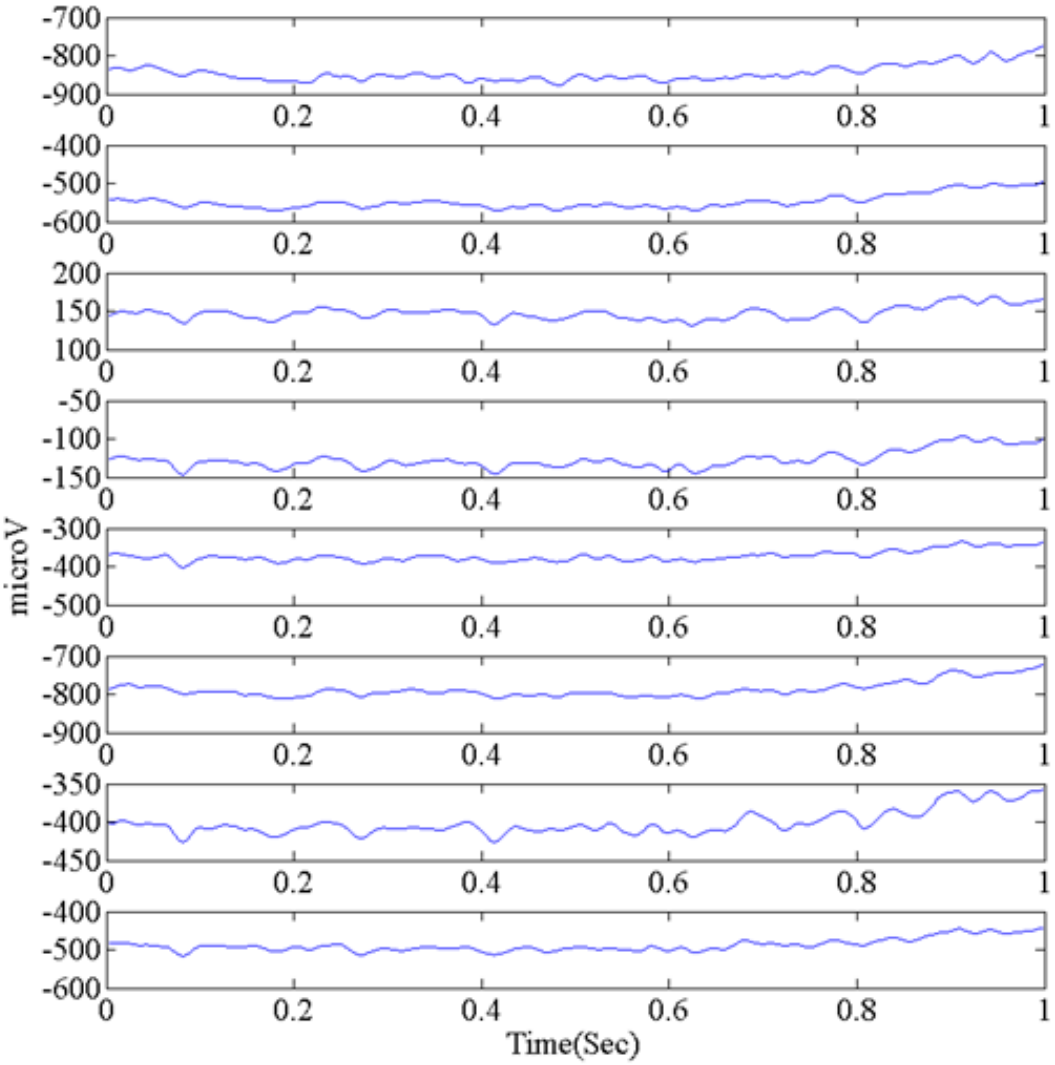

Figure 12. Measured brain signals from subject 1

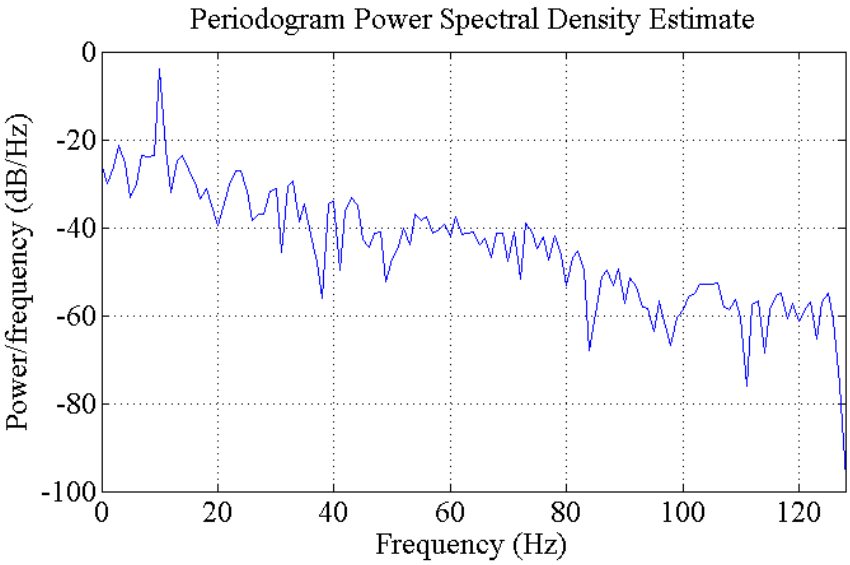

Figure 13. 1st Harmonic frequency component of the brain source signals from subject 1

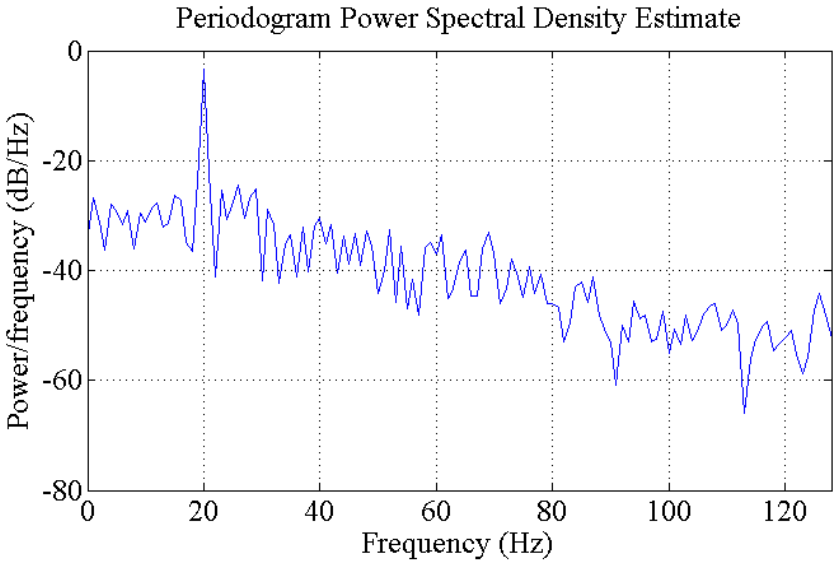

Figure 14. 2nd Harmonic frequency component of the brain source signals from subject 1

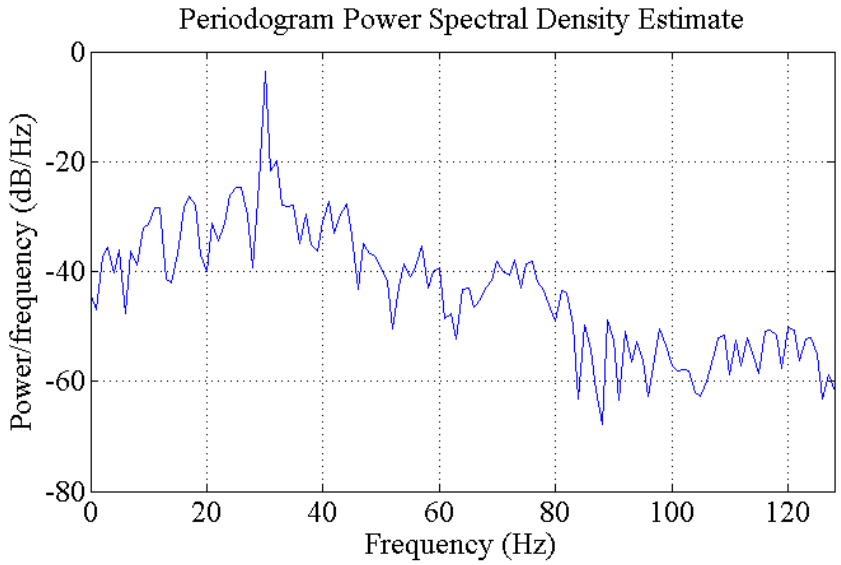

Figure 15. 3rd Harmonic frequency component of the brain source signals from subject 1

Commonly, t-test averages the signal to noise ratio (SNR) over different frequency harmonics of a brain source signal in a specific time-window. The power spectrum estimation of each brain source signal at frequency harmonic h is obtained from the squared magnitude average of Fast Fourier Transform (FFT) of each time-window. This power estimation, $\hat{S}(f)$, is presented in (Eq. 43).

$$\hat{S}(f) = \frac{1}{F_s N}\left|\sum_{n=1}^{N} x_n e^{-j(2\pi fh/F_s)n}\right|^2 \qquad \text{(Eq. 43)}$$

Where, F_s is the sampling rate and N is number of observations in sequence x_n. f is the desired frequency (Hz). The SSVEP power spectrum estimation at each harmonic is equal to the value of $\hat{S}(f)$ at that frequency. In this thesis, data sequences with 256 samples are used to estimate power spectrums.

Both of brain source signals and their noise signals are non-stationary. Therefore, to consider non-stationary property of signals in calculating SNR, both of the SSVEP response power spectrum estimation and noise variance power estimation values should be obtained from the same time step's input signals (both PSD and noise's variance should be calculated from time-windows with the same length). In this model, SNR values evaluate the level of brain signal amplitudes in comparison to the noise signal amplitudes while there is no SSVEP stimulus. To compute SNR, variance of noise signals calculated by the model indicates white noises without SSVEP responses. To estimate noise variance at each time-window, a 25-order autoregressive (AR) model is fitted on noise signals which are obtained from adaptive Kalman filter model. This value could be underestimated but it will be independent from presence of SSVEP responses. AR(p) model for an input sequence of white noise, x_n, is expressed in (Eq. 44).

$$x_n = \sum_{k=0}^{p} a_k y_{n-k} \qquad \text{(Eq. 44)}$$

Where, y_n is the estimated output value (n=1,…,p), a is the vector of autoregressive model parameters and p is the order of AR model. AR parameters are estimated by solving the Yule-Walker equations with Levinson-Durbin recursion. The estimated noise variance from Yule-Walker AR(p) model for each brain source signal and frequency harmonic, h, will be obtained from (Eq. 45) (Friman O., 2007).

$$\hat{\sigma}_{j,i}^2 = \frac{N\pi}{4} \frac{\hat{\sigma}^2}{\left| 1 + \sum_{k=1}^{p} a_k e^{-2\pi ijhf/F_s} \right|^2} \qquad \text{(Eq. 45)}$$

Where, N is the number of observations, a is the vector of AR model parameters. $\hat{\sigma}^2$ is the total noise variance estimated by AR model.

In this thesis, 4 LEDs are flickering at 10, 11, 12 and 13 Hz. To detect the user intention on stimuli LEDs, the observed brain signals are filtered via a 10-order adaptive Kalman filter with forgetting factor of 0.98 (best fitted value). Then SNR value of filtered signals is calculated at each time-window by t-test. The maximum t-test value of LEDs is considered as user intention and its stimulus signal as selected LED. The values of the filter order and forgetting factor are empirically selected based on expert decision. Generally, these values should be selected to reach the optimum system accuracy.

This model is configured for an online BCI system to calculate the brain source and noise signals in each time step. For detecting the SSVEP responses, power spectrum of brain source and noise signals are obtained at each time-window. Figure 16 shows the estimated brain source signals, which are filtered with Kalman filter for 3 frequency harmonics of 10 Hz LED stimulus signal. Signal channels in figure 16 are sine and cosine elements of the LED stimulus signal. Each element forms a channel of filtered signal for each frequency harmonic. Figure 17 demonstrates the noise signals computed from adaptive filter algorithm. The channels in this figure represent the noise signals for their corresponding estimated brain source signals. Signal's channels presented in

figure 16 and figure 17 are the results of first trial of subject 1 with user attention on 10 Hz LED. The obtained brain source signals and noise signals for subjects 22 and 7 are demonstrated in chapter 5 section 5.1.2. The subject 22 SSVEP test results were satisfactory and subject 7 showed a poor performance during the SSVEP test session. These figures present that the differences between brain sources or noise signals are not detectable without additional SSVEP response detection.

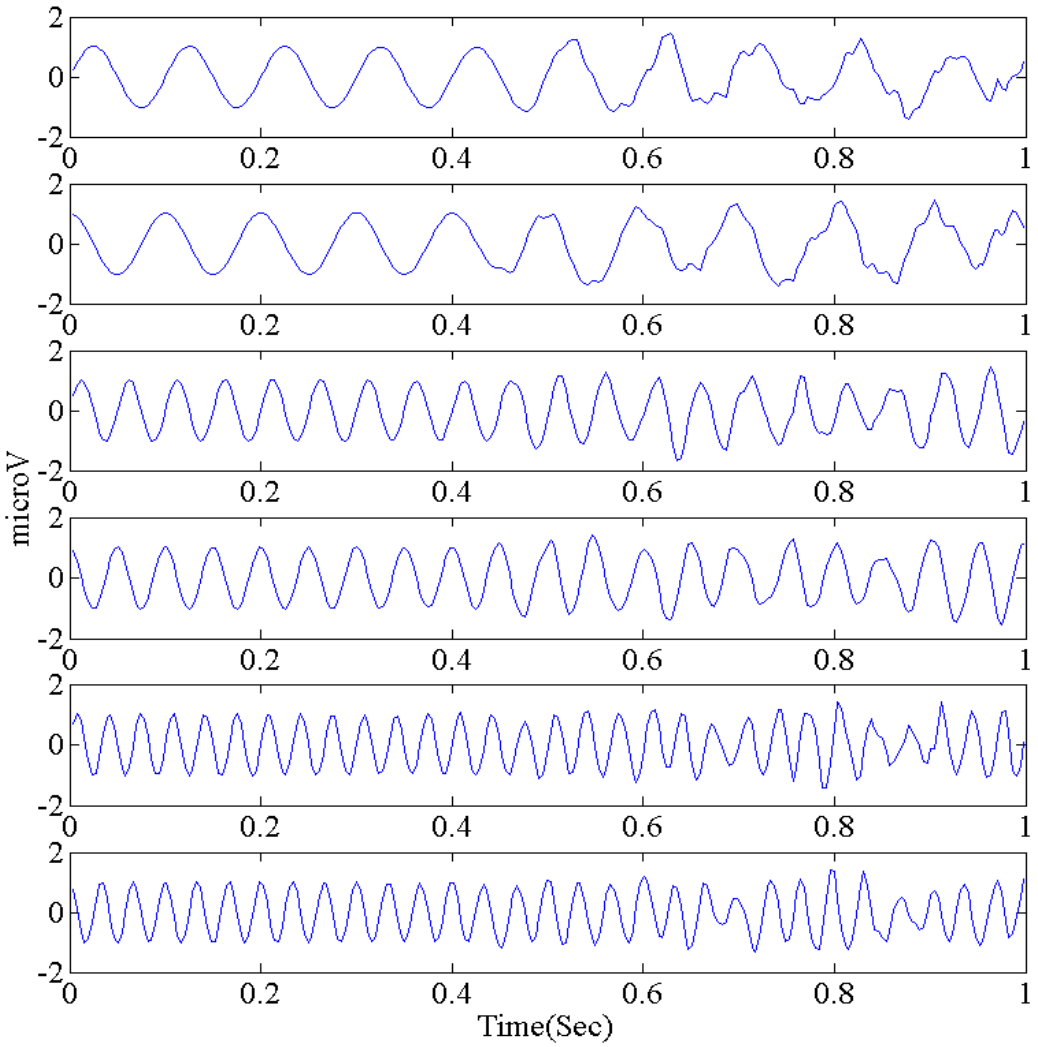

Figure 16. Various harmonics of estimated brain source signals which resulted from a 10 Hz stimulus signal, collected from subject 1

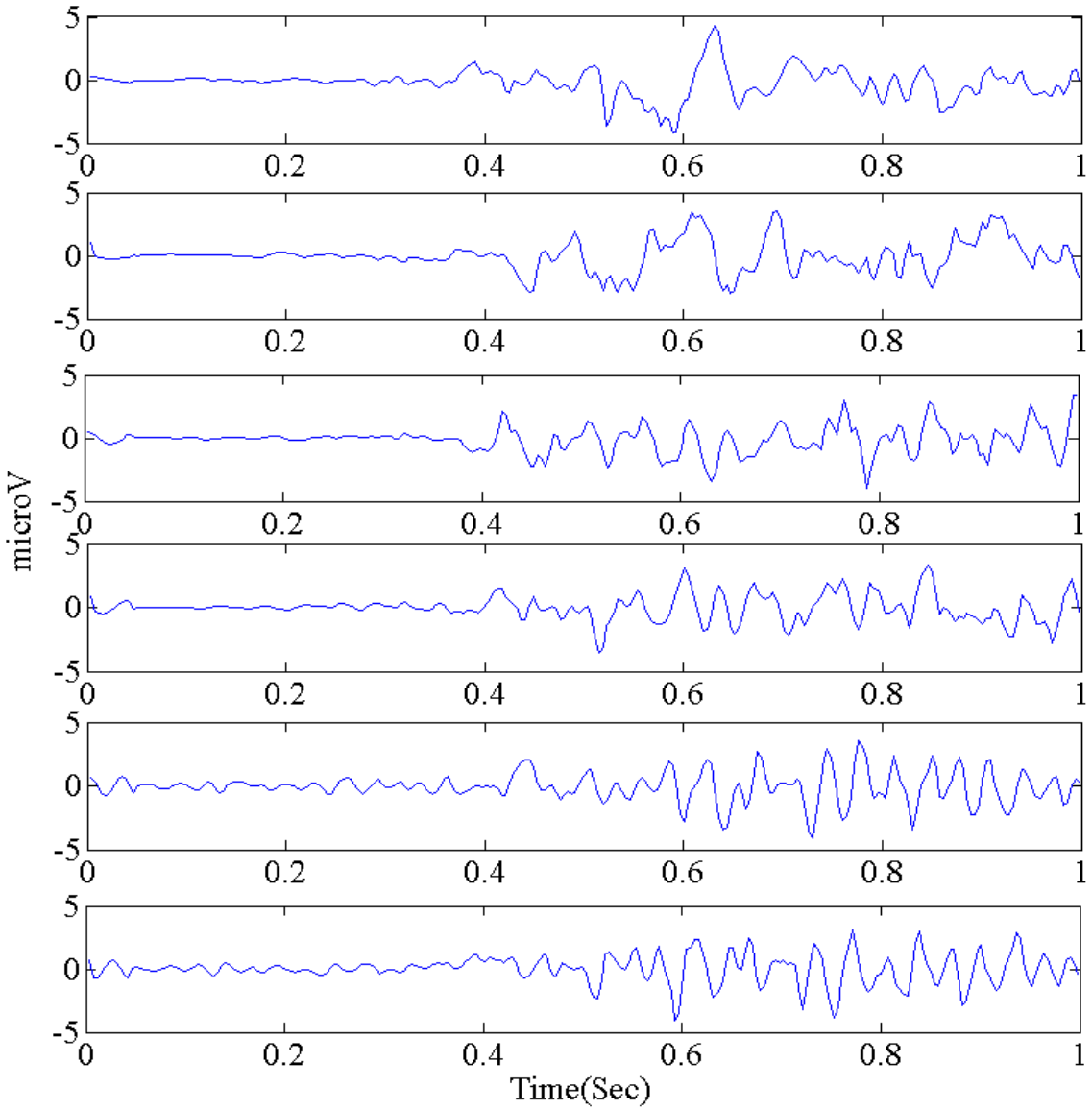

Figure 17. Obtained noise signals with 10 Hz LED stimulus from subject 1

3.3.2 The Robust Gauss-Newton Algorithm

Adaptive filters employ different design criteria to estimate the original signals from measurement signals and desired sequences. Adaptive filters are robust, when small disturbances do not degrade filter performance. In other words, small

disturbance-energy could not result in large *estimations-error* energy. The defined criteria for filtering input signals are tracking of the robustness of adaptive filters. Although, the robust filters have common characteristics with adaptive filters such as adaptive Kalman filter, these types of adaptive filters privilege from additional stability and convergence characteristic in respect to adaptive Recursive Least Square (RLS) filters. The quadratic cost functions which is employed in robust filters do not require weighting matrices to be positive definite to lead the solution into unique minimization problem. The difference between robust and RLS adaptive filters is the acquired solutions for unique output. The solution for RLS cost functions obtained from approximated minimization problem but solution in robust filters leads to the optimal minimization problem (Sayed, 2002).

3.2.2.1 Adaptive robust filter modeling

As it has been discussed before, the major assumption for analyzing SSVEPs is the presence of underlying correlations between these signals and exogenous stimulus. The SSVEP responses are detected when brain source signals are correlated to one of stimuli signal patterns. The analysis has two steps. The first step is filtering the observed brain signals to estimate original brain source signals. The second step is based on statistical t-test, which calculates the cumulative signal-to-noise ratios (SNR) of the estimated brain source signals. The SSVEP response detection is based on maximum stimuli cumulative SNR.

To model the correlation between stimuli reference signals and observed brain signals, the linear model with an N×Np reference signal matrix *d*, and an N×M

observed brain signals matrix U, is considered in (Eq. 46). M represents the filter order and Np is the number of observed brain signal channels.

$$d(i) = U(i)w^0 + v(i) \quad \text{(Eq. 46)}$$

Where, w^0 is the transformation matrix and $v(i)$ is the disturbance matrix for i=0,1,…,N-1 (i represents the time steps). The disturbance sequence is assumed to have a finite energy. Given the input signals in (Eq. 46), the estimated brain source signals at i^{th} time step, is calculated from (Eq. 47).

$$s_i \triangleq U(i)w^0 \quad \text{(Eq. 47)}$$

Where, in this equation, $U(i)$ is the vector of buffered input signals with Np signal channels. For an M-order multiple-input multiple-output (MIMO) system input signal presented in (Eq. 48).

$$U(i) = [u_1(i) \quad u_2(i) \quad \cdots \quad u_P(i)] \quad \text{(Eq. 48)}$$

Where, $U_j(i)$ (j=1:P) is the j^{th} buffered observed signal channel at time step i, which is illustrated in (Eq. 49).

$$U_j(i) = [u_j(i) \quad u_j(i-1) \quad \cdots \quad u_j(i-M+1)] \quad \text{(Eq. 49)}$$

The Transformation matrix w_0 is obtained by minimizing quadratic cost function in (Eq. 50).

$$J(w^0) \triangleq (w^0)^* \Pi w^0 + (d - uw^0)^* W (d - uw^0) \qquad \text{(Eq. 50)}$$

Where, Π and W are the Hermitian matrices ($\delta I_{P\times P}$) and play the role of weighting matrices. To achieve the filter robustness, criterion which is defined based on quadratic cost function in (Eq. 50) is demonstrated in (Eq. 51).

$$\frac{\sum_{i=0}^{N} \|s_i - d(i)\|^2}{w^{0*}\Pi w^0 + \sum_{i=0}^{N-1} |v(i)|^2} \le \gamma^2 \qquad \text{(Eq. 51)}$$

In this criterion, γ is a positive scalar and encompasses the analysis error boundaries. When the value of γ is closer to 1 the filter robustness criterion is more restrictive. The matrix, Π, can be any positive-definite matrix. In this equation, the numerator is the *estimation-error* energy. The denominator second term is the energy of disturbance and first term is the weighted energy of error in estimating the transformation matrix (Sayed, 2002). The brain source signal estimations which satisfy the robustness criterion in (Eq. 51) are calculated by equations (Eq. 52) to (Eq. 55).

$$s_i = U(i) w_{i-1} \qquad \text{(Eq. 52)}$$

$$\tilde{P}_{i-1}^{-1} = p_{i-1}^{-1} - \gamma^{-2} U(i)^* U(i) \qquad \text{(Eq. 53)}$$

$$w_i = w_{i-1} + \frac{\tilde{P}_{i-1} U(i)^*}{1 + U(i)\tilde{P}_{i-1} U(i)^*} [d(i) - U(i) w_{i-1}] \qquad \text{(Eq. 54)}$$

$$p_i = p_{i-1} + \frac{p_{i-1}U(i)^* U(i) p_{i-1}}{(1-\gamma^{-2}) + U(i)\tilde{P}_{i-1}U(i)^*} \qquad \text{(Eq. 55)}$$

These equations satisfy the robustness condition mentioned in (Eq. 51) for $i \geq 0$ and $\tilde{P}_i$ >0 (proof of the robust adaptive filtering algorithm can be found in (Sayed, 2002)). The Initial condition usually considered are $w_{-1} = 0$ and $p_{-1} = \Pi^{-1}$ (Sayed, 2002). Figure 18 illustrates the estimated brain source signals with 10 Hz LED stimulus signals for a 1-second time-window.

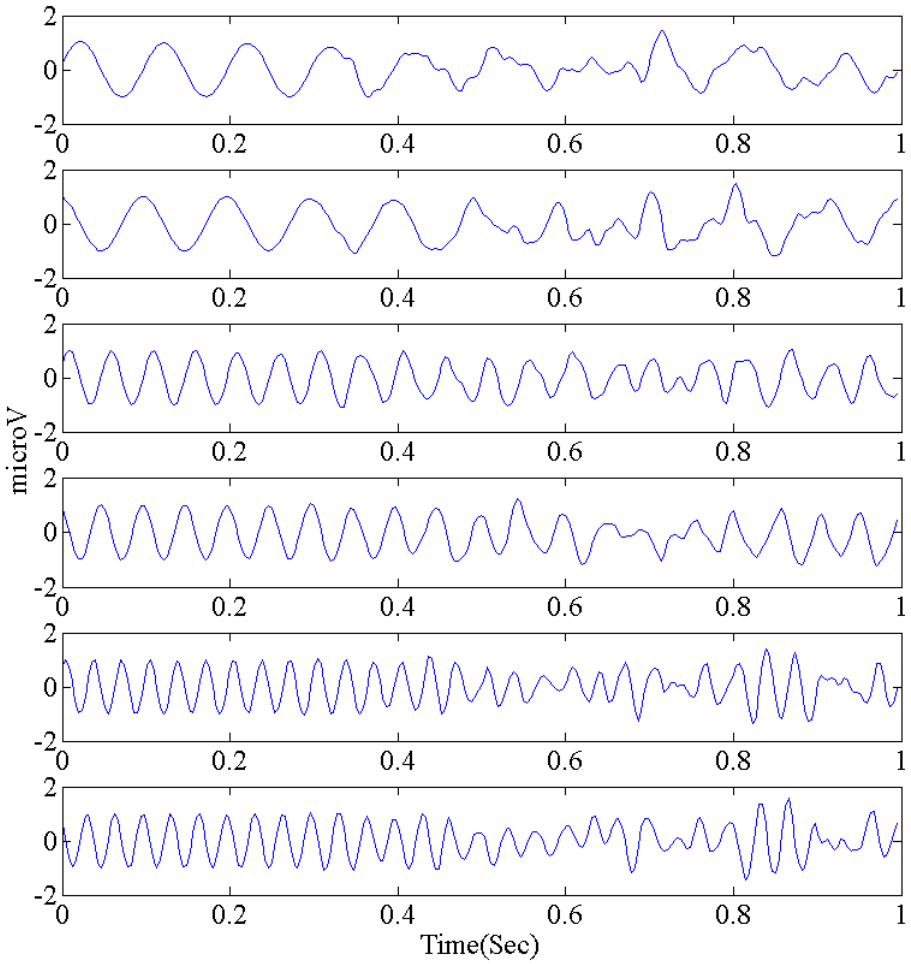

Figure 18. Estimated brain source signals for a 1-second time-window from subject 1.

3.3.2.2 SSVEP response detection

The SSVEP response detection is based on selecting the maximum estimated brain source signals SNR, which is calculated for each stimulus signal (LED signal). The statistic t-test (SNR) is calculated for each channel of estimated brain source signals. Finally t-test presented in (Eq. 56) calculates the cumulative SNR for LED stimuli different channels and harmonics. Maximum signal to noise ratio (SNR) will define the user attention on LEDs (Friman O., 2007).

$$SNR = \sum_{j=1}^{N_p} \sum_{h=1}^{N_h} \frac{\hat{S}(f)_{h,j}}{\hat{\sigma}^2_{h,j}} \qquad \text{(Eq. 56)}$$

Where, in (Eq. 56), SNR is cumulative SNR while *Np* and N_h are the number of EEG channels and stimulus frequency harmonics, respectively. $\hat{S}(f)_{h,j}$ and $\hat{\sigma}^2_{h,j}$ are the estimated power spectral density (PSD) of estimated SSVEP signals and estimated noise variations for the h^{th} harmonic and j^{th} signal channel, respectively. This value is calculated for estimated brain source signals evoked by each LED stimulus signal. The stimulus (LED) with maximum SNR value is considered as user attention. The estimated power spectral density for first frequency harmonic of 10 Hz signal channel, which is presented in figure 18, is illustrated in figure 19. In this method, estimated power spectral density is obtained for all of estimated brain source channels and harmonics with 256 Hz sampling rate. In this thesis, 4 LEDs are flickering at 10, 11, 12 and 13 Hz. To detect the user intention on stimuli LEDs, the observed brain signals are filtered through a 10-order robust adaptive filter via Gauss-Newton algorithm (step by

step formulation) with $\gamma = 4$. The filter order value and the error boundary value should be selected to acquire better optimized filer for analyzing the SSVEP brain signals.

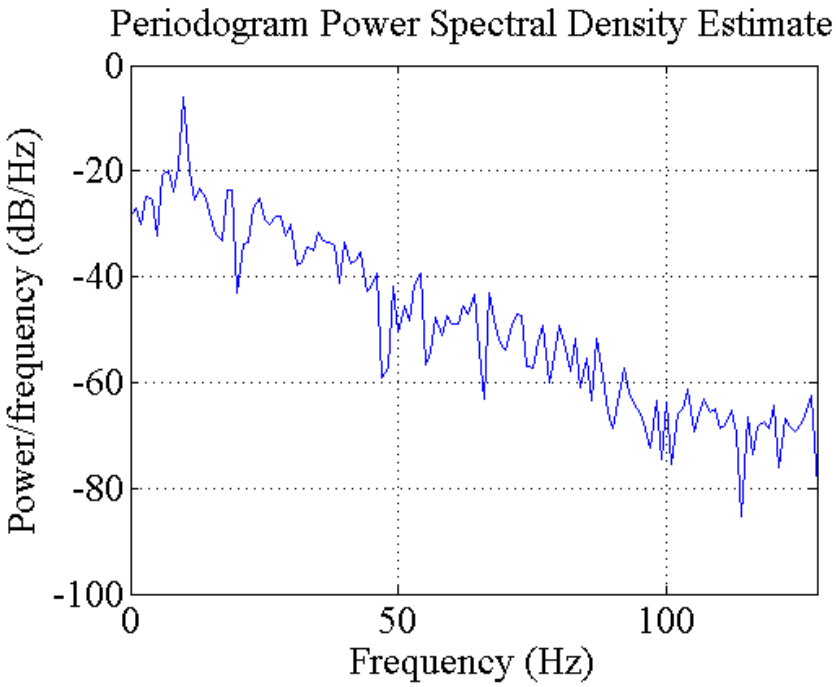

Figure 19. The Estimated Power Spectral Density (PSD) of the brain source signals for the 1st frequency harmonic of the 10 Hz LED stimulus signal.

The PSD estimation, $\hat{S}(f)_{h,j}$, of each brain source signal at frequency harmonic k is calculated from (Eq. 57).

$$\hat{S}(f)_{h,j} = \frac{1}{F_s N}\left|\sum_{n=1}^{N} x_n e^{-k(2\pi fhj/F_s)n}\right|^2 \qquad \text{(Eq. 57)}$$

Where, *Fs* is the sampling rate, *N* is the number of observations (here, 256 samples/second) and *f* is the desired frequency in Hz. To estimate noise variances $\hat{\sigma}^2_{h,j}$

for a time-window, the 25-order autoregressive Yule-Walker (AR(p=25)) model is fitted on the estimated noise signals. The $\hat{\sigma}^2_{h,j}$ for each brain source signal and frequency harmonic is obtained from (Eq. 58).

$$\hat{\sigma}^2_{h,j} = \frac{N\pi}{4} \frac{\hat{\sigma}^2}{\left| 1 + \sum_{h=1}^{p} a_h e^{-2\pi i j h f / F_s} \right|^2} \qquad \text{(Eq. 58)}$$

Where, in (Eq. 58), N is the number of data samples and a_h is the vector of AR estimated parameters. $\hat{\sigma}^2$ is the estimated noise variances by AR(p) model for the input data samples (here, 256 Hz sampling rate) (Friman O., 2007).

3.3.3 The Constrained Discrete Fourier Transform (DFT) Block Adaptive Filter

Generally, adaptive filters with recursive cost functions are problematic in convergence and computational complexity. These types of filters are mostly dependent on correlation of input data-sets and their regression functions. Meanwhile, their computational complexity is highly proportional to input buffered signals or filter order. The de-correlation properties of transfer functions such as Discrete Fourier Transform (DFT) or Discrete Cosine Transform (DCT) are exploited with adaptive transform-domain filters to pre-whiten the input data-sets. Simultaneously, to reduce the computational complexity, transform-domain filters are analyzing the data on *block-by-block* based analysis algorithms instead of *sample-by-sample* based filtering. These improvements in transform domain block adaptive filters result in improvement

of speed and reduction in computational cost. However, preparing the blocked input data for these filters originates a delay time for the system activation. This delay time is equal to the time needed for collecting samples for blocked input data (Sayed, 2002). To consider both of sine and cosine elements of the stimulus signal (as presented in (Eq. 17)), DFT block adaptive filter is employed in this thesis.

As referred in this section block adaptive filters analyze the blocks of input data-sets. The DFT block adaptive filter model is similar to adaptive recursive filter models and attempts to find brain source signals from the stimulus signal patterns and observed brain signals. This model is presented in (Eq. 59) and (Eq. 60).

$$d_{B,n} = U_n \overline{w}_n + v_{B,n}(n) \qquad \text{(Eq. 59)}$$

$$\hat{d}_{B,n} = U_n \overline{w}_{n-1} \qquad \text{(Eq. 60)}$$

Where, in these equations, $d_{B,n}$ is the block vector of the reference signals (here stimulus signals) and $v_{B,n}(n)$ is the block of the noise signals as presented in (Eq. 61) and (Eq. 62), respectively. $\overline{w}_n$ is the weighting matrix of the model in time-domain. In the following equations, n is the data blocked number and B is the number of data samples collected in each block.

$$d_{B,n} = \begin{bmatrix} d(nB+B-1) \\ \vdots \\ d(nB+1) \\ d(nB) \end{bmatrix} \qquad \text{(Eq. 61)}$$

$$v_{B,n} = \begin{bmatrix} v(nB+B-1) \\ \vdots \\ v(nB+1) \\ v(nB) \end{bmatrix} \qquad \text{(Eq. 62)}$$

In this model, U_n is the diagonal matrix of buffered input data and demonstrated in (Eq. 63).

$$U_n = \begin{bmatrix} u_{0,n} & 0 & \cdots & 0 \\ & u_{1,n} & \ddots & \vdots \\ & & \ddots & 0 \\ SYMM. & & & u_{2B-1,n} \end{bmatrix} \qquad \text{(Eq. 63)}$$

and $u_{i,n}$ is an $1 \times M/B$ buffered input data, illustrated in (Eq. 64) for an M-order adaptive filter where $i = 0,1,\cdots,2B-1$.

$$u_{i,n} = \begin{bmatrix} u_0(n) & u_1(n-1) & \cdots & u_i(n-\frac{M}{B}+1) \end{bmatrix} \qquad \text{(Eq. 64)}$$

The major difference between DFT block adaptive filter and recursive filter solutions is their pathway for calculating the weighting matrix elements. The DFT block adaptive filter transforms the data blocks by Fast Fourier Transform (FFT, here presented by F and inverse FFT is presented by F^*) to frequency-domain for computing estimated brain source signals. Then, This Filter transforms back the estimated signals to the time-domain (Sayed, 2002). Figure 20 presents the schematic algorithm of the DFT block adaptive filter.

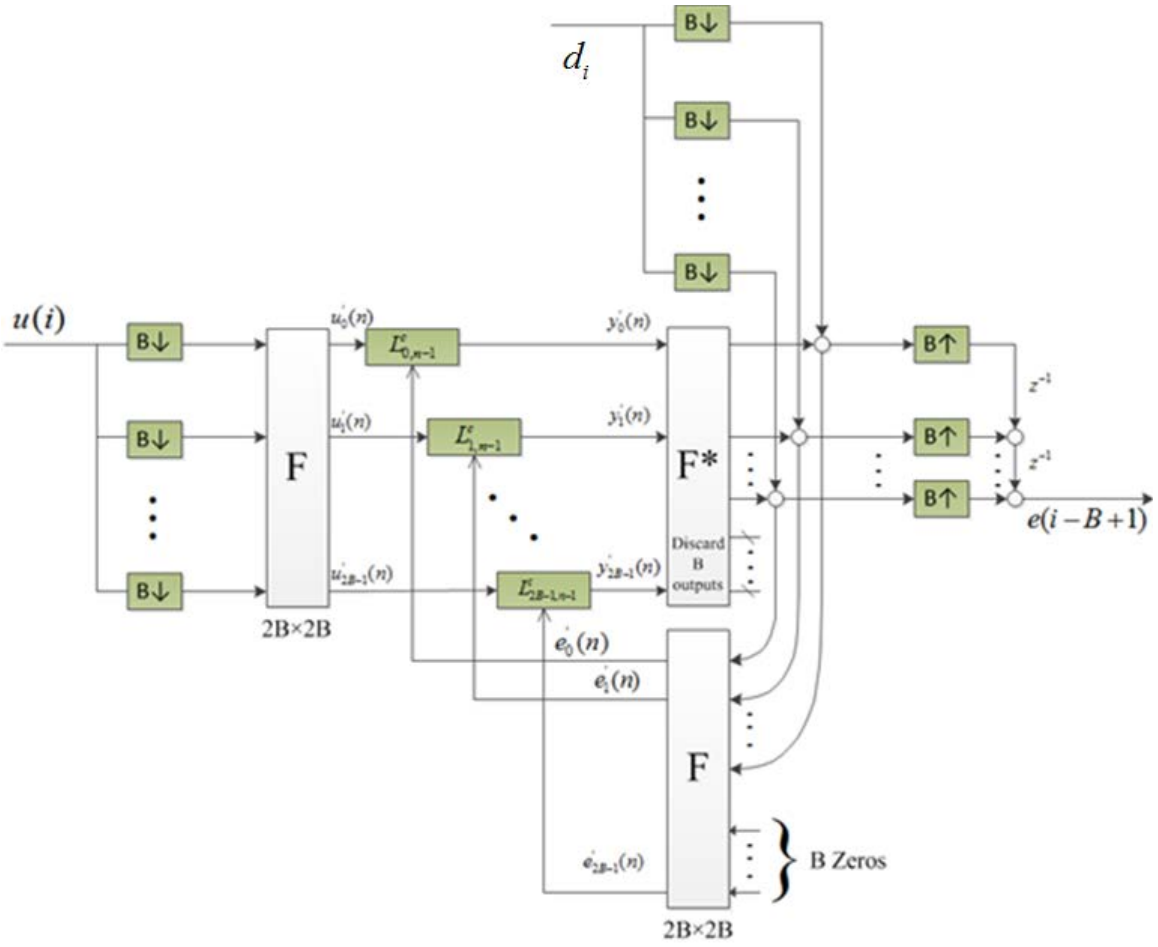

Figure 20. Schematic algorithm of the constrained DFT block adaptive filter

In this figure, $L_{i,n}^c$ is the weighting matrix corresponding coefficient in the frequency-domain. *c* denotes the constrained adaptive filter because of discarding the last B outputs of the filtered signal (difference between constrained and unconstrained filters is explained by (Sayed, 2002)). $u_i'(n)$ is the transformed matrix of the input data blocks. The weighting matrix coefficients are calculated from Normalized Least Square

(NLMS) cost function in (Eq. 65) which updates with power normalization in (Eq. 66) for each block of data.

$$l_{i,n} = l_{i,n-1} + \frac{\mu}{\lambda_i(n)} u'_{i,n} e'_i(n) \qquad \text{(Eq. 65)}$$

$$\lambda_i(n) = \beta\lambda_i(n-1) + (1-\beta)\left|u'_i(n)\right|^2 \qquad \text{(Eq. 66)}$$

Where, in these equations, $0 \leq \beta < 1$; μ is a small positive step-size parameter and should satisfy the condition in (Eq. 67) for analysis of each block. $\lambda_i(n)$ is the normalizer value for each block and $e'_i(n)$ is the model error values in the transform-domain.

$$\mu \ll \frac{1}{\lambda_i(n-1)} \qquad \text{(Eq. 67)}$$

The following steps summarize the analysis algorithm for one channel of observed brain signal collected via EEG and a single channel of LED stimulus signal. The initial conditions are defined as, $0 \leq \beta < 1$, $L^c_{i,-1} = L_{i,-1} = 0$ and $\lambda_i(-1) = 0$. The value of M / B should be an integer for blocking the buffered input data-sets properly (note (Eq. 64)). The buffered input signal $u_{B,n}$ and transformed input signal $U_{2B,n}$ are analyzed based on scheme shown in figure 20 and presented in (Eq. 68) and (Eq. 69), respectively.

$$u_{B,n} = \begin{bmatrix} u(nB+B-1) \\ \vdots \\ u(nB+1) \\ u(nB) \end{bmatrix} \quad \text{(Eq. 68)}$$

$$U_{2B,n} = F\begin{bmatrix} u_{B,n} \\ u_{B,n-1} \end{bmatrix} \triangleq col\{u'_{i,n}, i = 0:2B-1\} \quad \text{(Eq. 69)}$$

The normalizer value, $\lambda_i(n)$, for each block of data is calculated from (Eq. 70) (Sayed, 2002).

$$\lambda_i(n) = \beta\lambda_i(n-1) + (1-\beta)\left|u'_i(n)\right|^2 \;\&\; i = 0:2B-1 \quad \text{(Eq. 70)}$$

The transformed blocks of data for an M-order adaptive filter are obtained from (Eq. 71).

$$u_{i,n} = \left[u_0(n) \quad u_1(n-1) \quad \cdots \quad u_i(n-\frac{M}{B}+1)\right] \;\&\; i = 0:2B-1 \quad \text{(Eq. 71)}$$

The NLMS cost function value $L_{i,n}$, estimated brain source signals in transform-domain $y'_{i,n}$ and constrained weighting matrix coefficients $L^c_{i,n}$ are acquired from (Eq. 72) to (Eq. 77). To compute model error matrix, the estimated brain signals $\hat{d}_{B,n}$ are compared with reference signal $d_{B,n}$ in (Eq. 74) (in time-domain). Then, the error matrix is transformed into frequency-domain (here, transform-domain) to compute the constrained weighting matrix coefficients. This process scheme is shown in figure 20.

$$y_i^{'}(n) = u_{i,n}^{'} l_{i,n-1}^{c} \;\&\; i = 0:2B-1 \qquad \text{(Eq. 72)}$$

$$\hat{d}_{B,n} = [I_B \quad 0_{B\times B}] F^{*} \, col\{y_0^{'}(n), \quad \cdots \quad , y_{2B-1}^{'}(n)\} \qquad \text{(Eq. 73)}$$

$$e_{B,n} = d_{B,n} - \hat{d}_{B,n} \qquad \text{(Eq. 74)}$$

$$e_{2B,n}^{'} = F \begin{bmatrix} I_B \\ 0_{B\times B} \end{bmatrix} e_{B,n} \triangleq col\{e_i^{'}(n) \;\&\; i = 0:2B-1\} \qquad \text{(Eq. 75)}$$

$$l_{i,n} = l_{i,n-1} + \frac{\mu}{\lambda_i(n)} u_{i,n}^{'\,*} e_i^{'}(n) \;\&\; i = 0:2B-1 \qquad \text{(Eq. 76)}$$

$$\begin{bmatrix} l_{0,n}^{c\;T} \\ l_{1,n}^{c\;T} \\ \vdots \\ l_{2B-1,n}^{c\;T} \end{bmatrix} = \frac{1}{2B} F^{*} \begin{bmatrix} I_B & 0 \\ 0 & 0_{B\times B} \end{bmatrix} F \begin{bmatrix} l_{0,n}^{\;T} \\ l_{1,n}^{\;T} \\ \vdots \\ l_{2B-1,n}^{\;T} \end{bmatrix} \qquad \text{(Eq. 77)}$$

Finally, the blocks of brain source signal estimations ($\hat{d}_{B,n}$) and estimated blocks of model errors $e_{B,n}$ for one channel of EEG signal and one channel of LED stimulus signal ($d_{B,n}$) are presented in (Eq. 78) and (Eq. 79) , respectively.

$$\hat{d}_{B,n} = col\{\hat{d}(nB+B-1), \ldots, \hat{d}(nB+1), \hat{d}(nB)\} \qquad \text{(Eq. 78)}$$

$$e_{B,n} = col\{e(nB+B-1), \ldots, e(nB+1), e(nB)\} \qquad \text{(Eq. 79)}$$

To develop this algorithm for the SSVEP BCI with Multiple-Input Multiple-Output (MIMO) system, the buffered input signals in (Eq. 68) and transformed input data in (Eq. 69) should include additional columns which are representatives of the additional observed brain signal channels from EEG. As it has been discussed before, in the

sections 3.3.1 and 3.3.2, the outcome of adaptive filters (estimated brain source signals and model error matrix) should be evaluated for SSVEP response detection. The constrained DFT block adaptive filter SSVEP response detection algorithm is similar to those aforementioned adaptive recursive algorithms. The SSVEP response detection is based on calculating SNR of estimated brain source signals and selecting the maximum SNR as user attention. This process is utterly described in sections 3.3.1.3 and 3.3.2.2, therefore the repetition of similar algorithm's description is discarded for this section. This method's results show that further additional steps are required to achieve a reliable SSVEP response detection algorithm. Though, the result of this method will be used in future research by adding more elaborate signal processing steps.

Chapter 4: Experimental Protocol

This chapter starts with a brief explanation of experimental instruments' properties employed in test sessions and car driving-simulator scenarios. Then, experimental protocol of SSVEP test and detailed description of how subjects performed the car simulator tests will be explained. The SSVEP analysis algorithms and driving simulator experiments results will be discussed in the next chapter.

The SSVEP data collection and car-simulator scenarios test setup are described in two different sections and corresponding outcomes are evaluated in different sections in chapter 5. The observed brain signals during the driving simulator scenarios are recorded from visual, primary and somatosensory motor cortices. The effect of SSVEP stimulation-box activation on drivers' distraction evaluates the possibility of implementing an online SSVEP based BCI system as an in-vehicle assistive device.

The selected analysis methods described in chapter 3 have been applied to two different sets of data. First, the data-set collected by g.TEC CO. which was supplied to us by g.TEC and included 8 EEG channels brain recorded signals from visual cortex. The second data-set is an initial experiment to collect human subject data for SSVEP methods' evaluation and validations. This was a precursor subject test before the driving simulator tests, which were conducted for the second objective of this thesis, namely to explore and evaluate SSVEP as an in-vehicle driver assistance technology. Third, the CCA method was applied to collected brain signals during the driving scenarios to detect the correlation between subjects' brain signals' changes and near collision situations, as described in chapter 5.

4.1 Experimental Instruments

In this part of chapter 4, the instruments which are employed in experiments and the system properties and characteristics of each instrument are described. This section begins by introducing the car driving-simulator, then continues with explaining EEG device system properties and finally finishes by a very concise description of SSVEP stimulation-box characteristics.

4.1.1 Driving Car-Simulator

The car driving-simulator is composed of a full car base, including original controls (throttle, brake, steering wheel, blinkers…), five PCs running different parts of the simulation, a controller and three projectors. The schema of the car driving-simulator is presented in figure 21. One PC is used for inside display, speedometer, and is located near car cabin. The 2nd PC, dynamic PC, is used to run the dynamic model of vehicle. The dynamic PC is also used to access the controller and to send data to inside-display PC. It receives data from controls of the vehicle. The 3rd PC is the central controller of the system. It runs the simulation program STISIM which has access to dynamic PC and two other side-display PCs via local network. It also corresponds to central display. Two other PCs, 4th and 5th, are only used for the side displays. Three display PCs are directly connected to three projectors. The figure 22 presents the car driving-simulator which is placed in Center for intelligence systems research (CISR) laboratory at Virginia science and technology campus of the George Washington University (Soudbakhsh, 2011).

The Car dynamic movements are simulated by the VDANL program. This program uses advanced non-linear models for each vehicle's part and the car's global motion. The dynamic model uses specific files to provide parameters of the vehicle's dynamic. These files can be adjusted to define vehicle's performance during the scenarios according to the desired outputs.

It is also possible to edit dynamic model to simulate additional embedded intelligent assistive systems by creating a user-defined module. Each module is composed of two different parts, a list of break points and a list of functions. The break points specify when each function including vehicle dynamic properties must run. The desired break points of dynamic module are programmed in advance. This collected list of break points should be saved in a file. Then functions which are programmed as a library or selected from preset VDNL library run to determine the vehicle dynamic properties. List of the functions is a code written to program specific events during each scenario. The preprogrammed library of functions also modifies the desired vehicle dynamic parameters and adjusts data collection method and sampling rate of the driving-simulator. The complete collection of breaking points, functions and dynamic libraries configure the user-defined dynamic module. The configuration file should be called from central PC (STISIM program) to employ the desired dynamic system. Figure 23 shows a schema of the collocated algorithm between the dynamic and central PCs (user defined module structure).

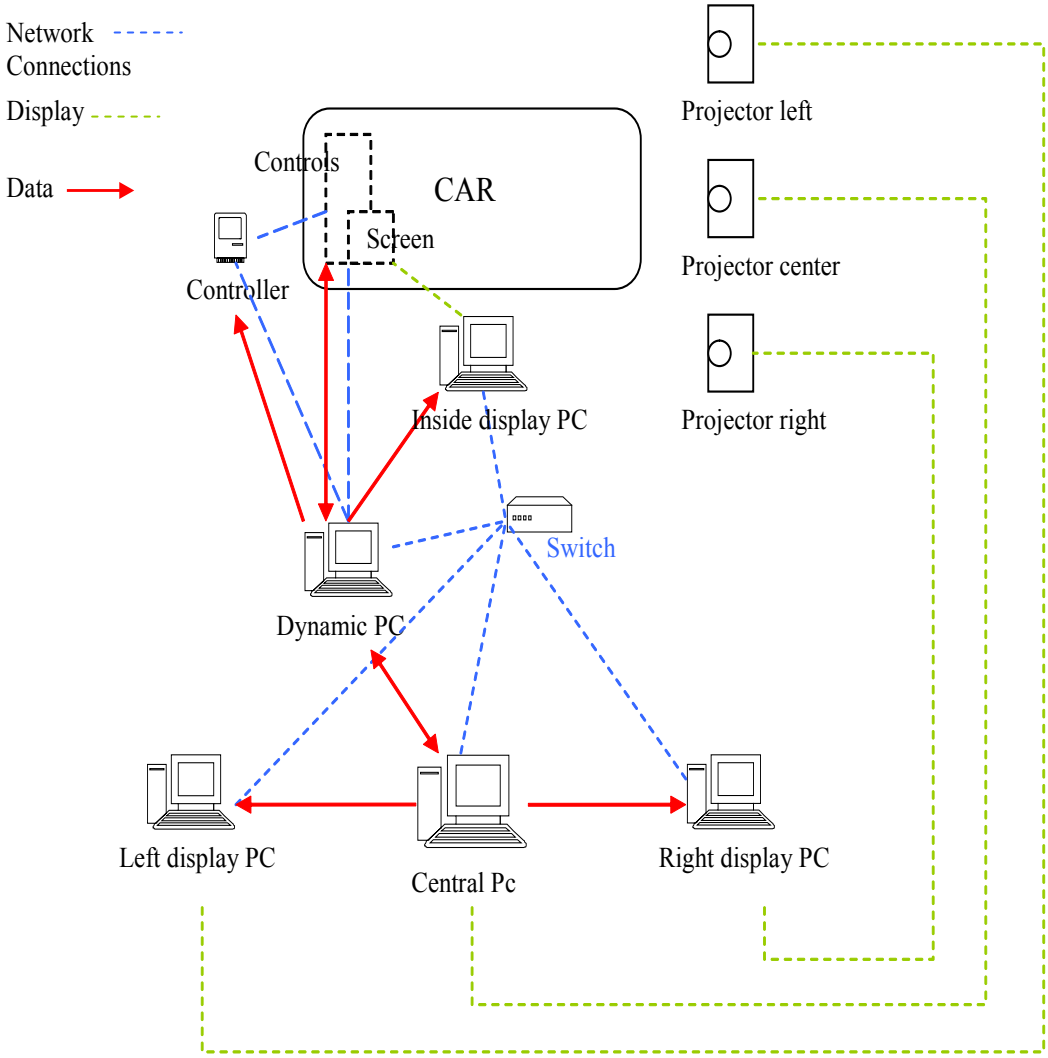

Figure 21. The schema of the car driving-simulator

Figure 22. The car driving-simulator and SSVEP setup

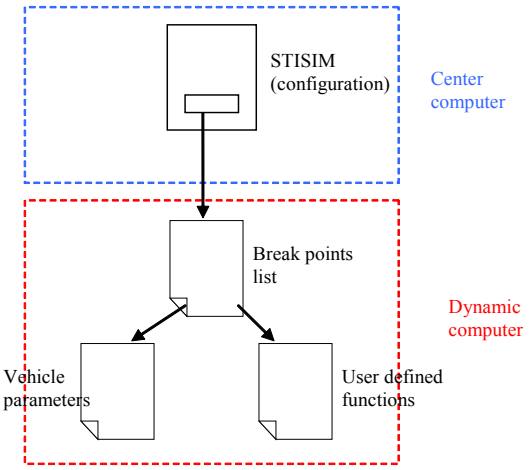

Figure 23. The user defined module structure

4.1.2 EEG System (g.USBamp)

The human brain signals are collected by a complete system of sensors (a sensor cap), amplifier, connection wires and connections, input/output to a PC and data acquisition software and processing code. The system by g.TEC (g.tec, 2013) is employed here. This is referred to as the EEG system. The three main physical components of this system are:

1. EEG amplifier
2. EEG sensor cap
3. LED stimulation-box

Each is described below.

4.1.2.1 EEG amplifier

The g.USBamp is a high accuracy biosignal data acquisition amplifier. Depending on the data collector sensor, this amplifier preprocesses brain, respiration, eye-movement,

heart and muscle activity input signals. gUSBamp is a USB 2 enabled system with more than 16 parallel signal channels which record the data with 24 bits. To prevent any interfaces between recorded data this system includes 4 ground channels. The input range of system is ± 250 mV with a resolution of < 30 nV and allows recording the Direct Current (DC) signals without any saturation. The system includes input and output channels with capability of communicating with other devices through trigger channels by synchronization. A short-cut channel connects the amplifier to the ground to prevent the system overflows. The EEG system resolution prevents any system overflow and saturation due to high electrode offset voltage which helps further artifacts treatments and corrections. Each of EEG channels analog to digital converter sample at 24576 MHz. Meanwhile, a 64-times oversampling generates an internal sampling rate of 38400 MHz. The system floating point oversamples and filters the collected data between 0 to 2400 Hz, e.g. frequency rate of 256 Hz yields to an oversampling rate of 9600 Hz. This property helps to improve the acquired signal to noise ratios. The high resolution of system is crucial for recording the evoked brain potentials when small amplitude's changes should be identified.

The g.USBamp includes a synchronization cable to interconnect with other devices, simultaneously. The amplifier system is capable of generating sinusoidal, rectangular, saw-tooth or white-noise test signals with varying amplitude and frequencies. The EEG device detects offsets and gain values of the channels to internally correct newly generated artifacts. This property is beneficial for deriving the localized brain signal sources.

4.1.2.2 EEG sensor cap

The electrodes' gel should be used to keep resistance and transition impedance rate between the skin and electrodes less than 5 KΩ. Other part of the EEG device is the cap which has to be worn on to facilitate the electrodes placement (g.tec, 2013). Placing the EEG electrode at their predefined location according to the 10-20 system or other developed systems is crucial for recording signals with better quality. 10-20 EEG electrodes placement is shown in figure 24 and figure 1 (Elitzur A.C., 2010).

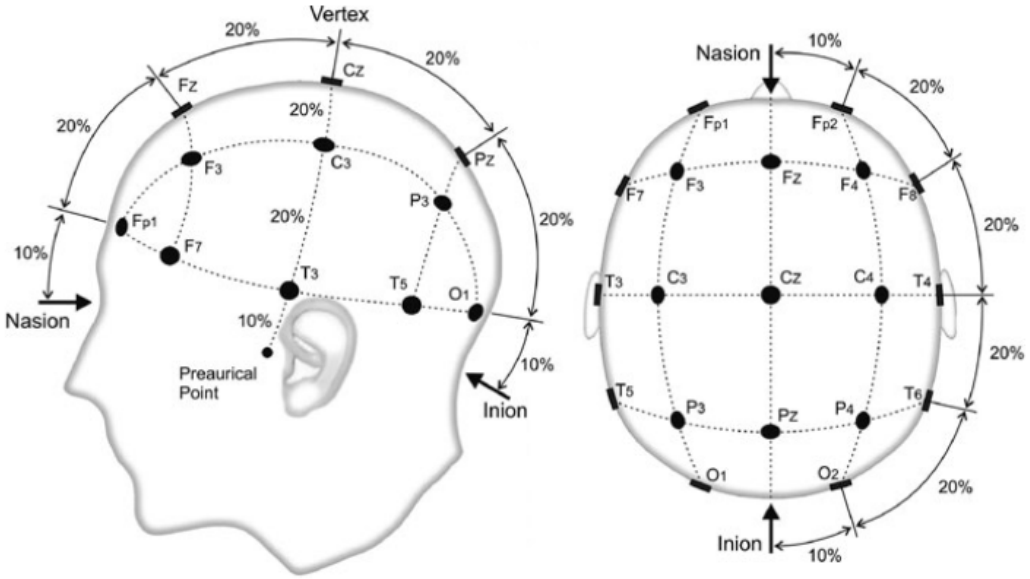

Figure 24. 10-20 international electrodes placement (Elitzur A.C., 2010)

The employed EEG device in this research study is g.GAMMAcap which, is presented in figure 25. This cap is configured with active or passive electrodes which are easily placed inside the cap based on 70 location electrode placement system.

Figure 25. The g.GAMMAcap (g.tec, 2013).

4.1.2.3 EEG stimulation-box

g.STIMbox (LED stimulation-box) is a stimulator with digital I/O which has 14 digital inputs and 16 digital outputs. The system supports USB 2. The stimulation-box I/O is connected by two 26 pin Sub-D connectors. Top of the box includes 8 digital I/O connectors which can be used by clinch connectors. The system power can be supplied by USB connector without any external power supplier. Figure 26 demonstrates the complete package of gSTIMbox and LED stimulators (g.tec, 2013).

Figure 26. The SSVEP stimulation-box (g.tec, 2013).

4.2 Experimental Protocols

This section addresses the experimental protocols to collect the data for single SSVEP test session and driving car-simulator experiments.

First, two sets of data are applied to evaluate and verify the accuracy and ITR of introduced methods in chapter 3. The first set of data was provided by g.TEC CO. collected from visual cortex by 8 EEG channels. The second set of data was collected from 30 healthy subjects aged between 18-65 years old at the CISR laboratory. This data was collected as preliminary test session (SSVEP experiment) before car driving-simulator experiments which will be explained later in this section. Both of data-sets were recorded from visual cortex by 8 EEG channels and the same experimental protocol.

Second, three car driving simulator scenarios were developed to collect the drivers' behaviors confronting near collision situations (3 near collision situations in each driving scenario). For the subjects who had never participated in a car driving-simulator test, a preliminary 8 minutes scenario was additionally designed. This scenario's longitudinal distance or timing is based on previous studies (Soudbakhsh, 2011). These driving

scenarios are described later in this chapter. The subjects had valid US driving license and they were briefed with consent Institute Research board (IRB) form before taking the tests. The study was approved by IRB which is an independent committee established to review, control and approve the experiments that involve human subjects.

- First driving scenario collects drivers' normal behavior
- Second scenario collects the drivers' behaviors with a short LED warning before the near collision situation
- Third scenario collects the drivers' behavior with a longer period of LED warning before the near collision situations

4.2.1 SSVEP Data Collection Experiments

The purpose of this data collection experiment was to evaluate the SSVEP analysis methods explained in chapter 3. Two sets of data were collected by g.TEC CO. and CISR laboratories with a same test protocol. The test protocol is explained in the following paragraphs.

Data was collected from 30 healthy subjects from 8 EEG electrodes with acquisition rate of 256 Hz. The electrode placement is pictured in figure 27 for evaluating the SSVEP response detections. Ground electrode was placed at electrode location called Fpz with a reference electrode over right earlobe. Electrode gel was used to keep the resistance level below 5 kΩ.

Recorded data were band-passed from 0.5 to 30 Hz for removing the undesired artifacts (included in data acquisition software). Notch filter at 50 Hz was employed to diminish the

power line noises by the data acquisition system. Figure 28 represents a subject performing the SSVEP test while LED stimulation-box is activated.

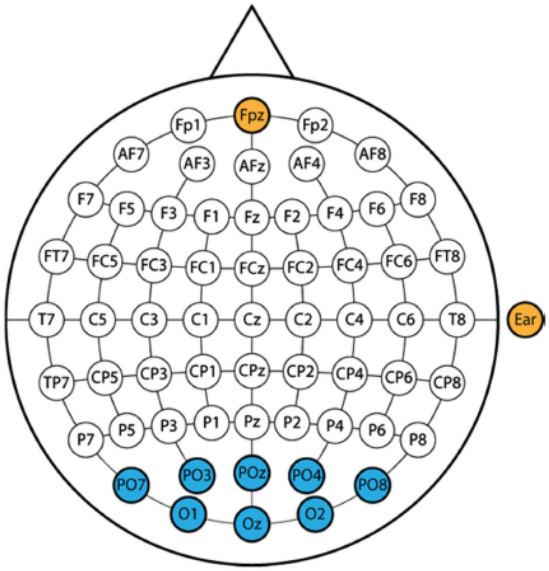

Figure 27. Electrode placement (Guger C., 2012)

Test protocol was based on 4 LEDs flickering with different frequency rates. In each trial, user was asked to focus on one LED for 7-seconds which was followed by 3-seconds of no flickering LED (resting time). Test trial included focusing on 10, 11, 12 and 13 Hz frequencies, respectively. Then, this trial was repeated 5 times during a test (Guger C., 2012). Test protocol and LED stimulation-box scheme are illustrated in figure 29. Subjects participated in one SSVEP test session before performing the car driving-simulator tests. Each SSVEP test session began after 10-seconds of delay (preparation time).

The LED stimulation-box, which is presented in figure 28 and figure 29, has four LED lights. The LED which is positioned on top of the box was set to flicker at 10 Hz during the

SSVEP test sessions. Other LEDs from right to left were flickering at 11, 12 and 13 Hz, respectively.

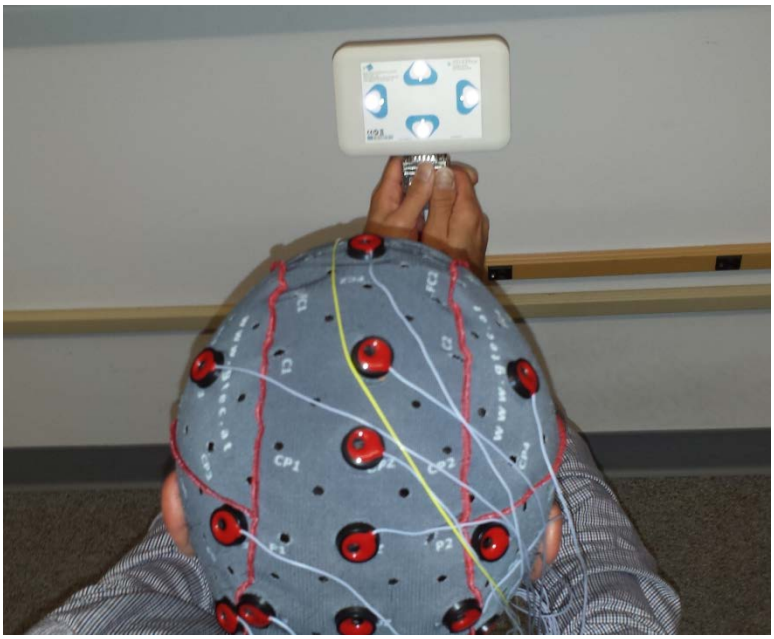

Figure 28. The LED stimulation-box

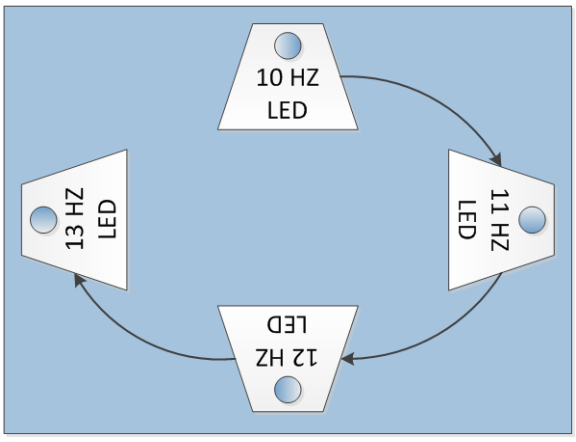

Figure 29. The LED stimulation-box and trials' schema

4.2.2 Car Simulator Driving scenarios

The purpose of car-simulator driving experiments were to collect the drivers' behavior and reactions while they were facing a near collision situations.

The speed, braking pedal pressure, longitudinal distance and time were collected to evaluate the drivers' behavior. Based on collected data, Time to Collisions (TTC) and braking (or reaction) distances of each driver was calculated (explained in the next chapter). Three sessions have been tested with drivers (subjects) wearing EEG sensors cap while driving. All sessions include three near collision situations in which subjects are faced with suddenly appearing obstacles.

1. The first test scenario contained normative driving with the presented possible near collision scenario and without any LED stimulus as in-vehicle warning device (car, pedestrians and parked taxi).
2. The second test scenario contained a similar scenario to the first session, but with a LED warning given 3-second before a possible crash with an appearing object (police car, truck and ambulance truck).
3. The third scenario contained of suburban and urban areas and LED warning is given 5-seconds before a possible crash in a near collision situation. The obstacles are car, a truck and pedestrians.

The subjects who participated in this study had valid US driving license and aged from 18-65. All of the subjects were healthy and briefed by IRB consent form before taking the test. The subjects were allowed to participate in experiments only if they never had experienced nausea during their previous ground, aerial or maritime transportations. After

SSVEP and driving-simulator experiments, subjects were asked to fill a questionnaire for evaluating their experiments during the test. The questionnaire form is provided in appendix C. For Those subjects who never participated in a car driving-simulator study a preliminary scenario was designed. This scenario includes urban, residential, highway and rural areas to help the subjects to be more familiar with driving-simulator. The preliminary scenario was 37000 ft long or 500-seconds based on previous studies suggestions (Soudbakhsh, 2011).

The first scenario was 15000 ft including rural and suburban areas. This scenario was planned to collect the normal drivers' behavior confronting a near collision situations. This scenario had three obstacles which appeared on the road (in front of the subjects' vehicle) 2-seconds before the collision. The obstacles were a car appearing in front of the vehicle, pedestrians crossing the street, and an ambulance driving out of parking lot. Figure 30 presents the first scenario obstacles.

The second scenario was 15000 ft with almost the same nature as the first scenario. In this scenario, a 3-seconds LED warning was given to the drivers before each near collision situation. The subjects were not informed that warning system will be activated during their driving task. This short LED warning period was considered to detect the effect of LED stimulation-box activation on drivers' brain signals. Moreover, LED warning was employed to evaluate the effect of warning LEDs on drivers' behavior. Figure 31 presents the obstacles of this scenario.

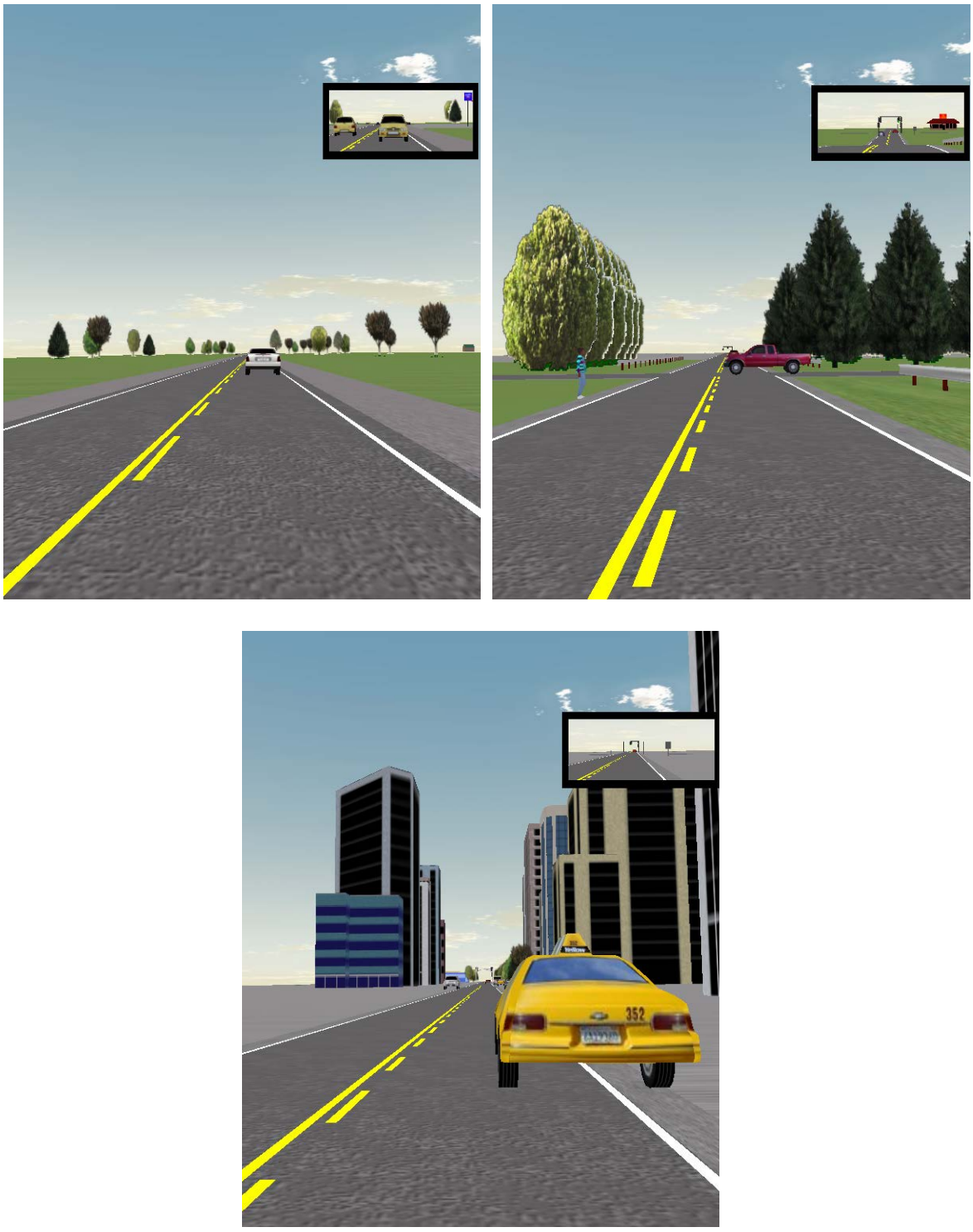

Figure 30. The first scenario (normal driving) near collision situations

The third scenario was 31000 ft including suburban and urban areas. The LED warning system was activated 5-seconds before the near collision situations. The subjects were informed of the LED warning activation before each crash. This scenario was planned to measure the effect of an active SSVEP based BCI warning system presence on drivers' behavior and brain signals confronting the near collision situations. This scenario had three obstacles which are presented in figure 32.

The longer period of LED warning was considered to determine whether a SSVEP based BCI in-vehicle assistive system could be helpful or distractive comparing to the normal situation. To prevent any biased data collection, the second and third scenarios were driven randomly. The random performance of the warning scenarios moderates the subjects' learning processes which could be resulted from recurrence of LED warning activations. The results of the driving simulator experiments are described in section 5.2 of the next chapter.

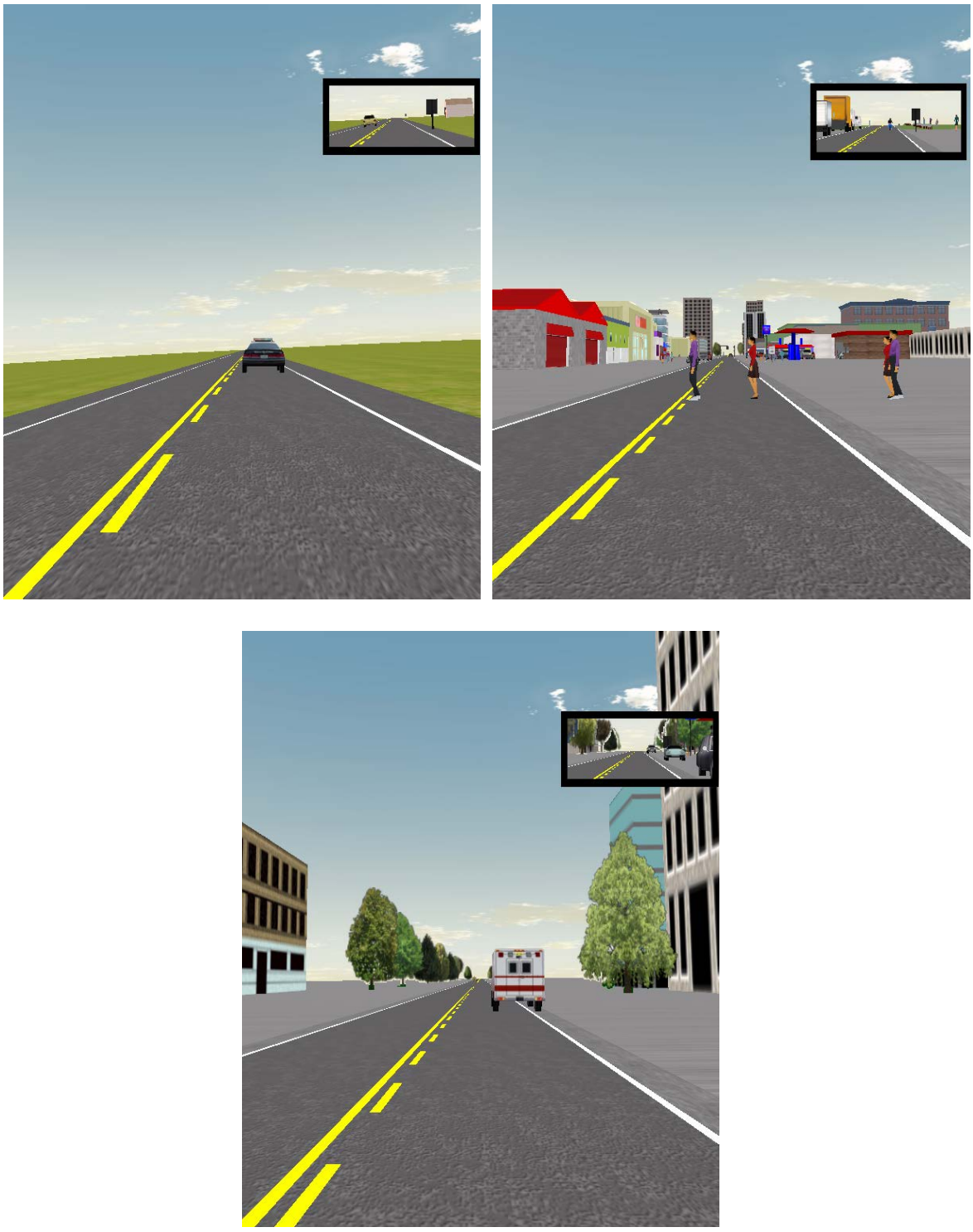

Figure 31. The second scenario (short LED warning) near collision situations

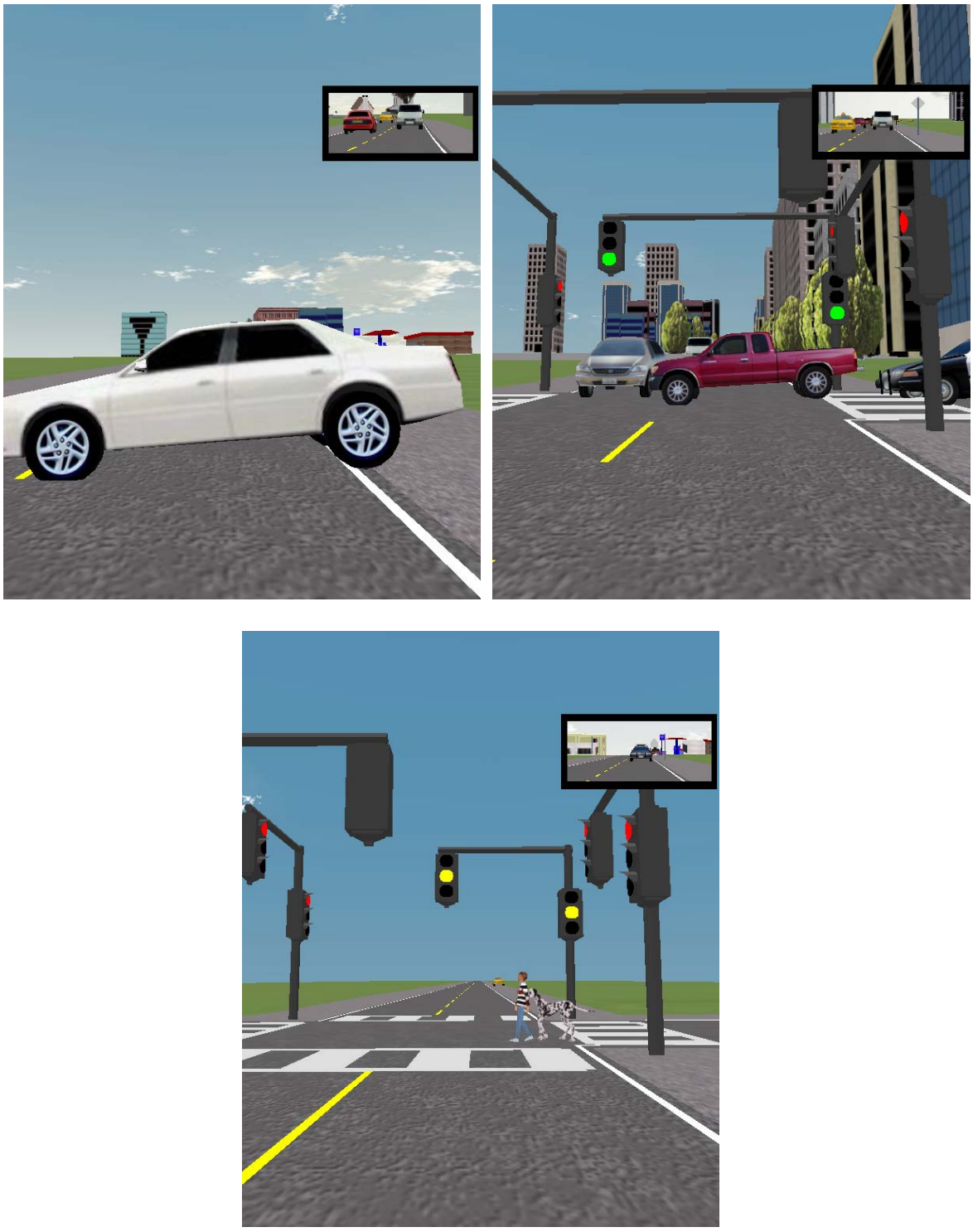

Figure 32. The third scenario (long LED warning) near collision situations

Chapter 5: Results and Discussions

The first part of this chapter, as discussed, will reveal the results of analyses algorithms described in chapter 3. The SSVEP response detection algorithms' accuracy rate and their corresponding Information Transfer Rate (ITR) are calculated. All of these analyses are computed based on overlapping 224 samples in each time-window of 256 samples (256 Hz sampling rate), to acquire an outcome every 1/16 of second. The accuracy rate is the number of correct detected subjects' SSVEP responses (in each time-window) during a test session. The ITR is a factor for measuring the system capability of real-time performances. This factor formula is described later in this chapter. Then, 4 successful methods evaluations' results are presented. These methods are, CCA, CCA with statistical significant tests' evaluation, adaptive Kalman filter and adaptive Gauss-Newton filter. The SSVEP response detections' evaluation results of the described methods are included in different sections as listed below.

- Analysis methods evaluation with g.TEC data-sets (section 5.1).
- Analysis methods evaluation with collected data-sets in CISR (section 5.2).

To evaluate these methods, collected brain signals are recorded via 8 EEG channels from visual cortex (figure 27) during a SSVEP test session as described in chapter 4.

In the second part, time to collisions and reaction distances before an emergency situation are considered as drivers' performances evaluation factor. Meanwhile, it shows the distraction or vigilance level due to the LED stimulation-box activation [(Lin C. T., 2005), (Lin C. T., 2005), (Rimini-Doering M., 2001), (Haufe S., 2011)].

The car driving-simulator scenarios' collect the drivers' performances and brain signals in three scenarios which are listed below (details are described in chapter 4) (section 5.2).

- Scenario without a LED stimuli collision warning.
- Scenario with a LED stimuli collision warning with a short obstacle detection period of 3-seconds.
- Scenario with a LED stimuli collision warning with a longer obstacle detection period of 5-seconds.

Henceforth, the SSVEP stimulation-box activation as a warning system during the driving task will be evaluated. The reaction distance and time to collision of each driver in scenarios with short and long warning periods are compared with their performance during the normal scenario. The short warning period evaluates the SSVEP based warning stimuli as a driving assistant system. The longer period of LED stimuli determines the effect of long-term presence of an active SSVEP based BCI as an in-vehicle device.

The last part is an attempt to correlate the brain signals in normal and short warning scenarios with LED stimulus signal (10 Hz flickering frequency as a warning signal). This part attempts to detect any underlying meaningful correlation between subjects' brains activities and LED signal before a near collision situation for future in-vehicle systems.

5.1 SSVEP Response Detection Results

This part of thesis will present the SSVEP response detection analysis methods' results. Moreover, it attempts to evaluate each method capability for employing in an online BCI system by calculating the Information Transfer Rate (ITR). ITR (Bits/Trial) presents the

information bits which are obtained in each test trial. Therefore this feature introduces the capacity of analysis algorithm for providing information during a trial. In each trial, certain amount of information is required for reliable online BCI systems performance (Obermaier B., 2001). This part of thesis presents the analysis results of the *Canonical Correlation Analysis*, *Adaptive Kalman Filter* method and *Adaptive Robust Gauss–Newton* Algorithms. These methods resulted in accurate and reliable SSVEP brain signals response detections. The results of these methods evaluations obtained from, first g.TEC data and second our human subjects' study are presented.

5.1.1 SSVEP Analysis Results of g.TEC Data

The analyses methods are evaluated with data provided (4 subject's test sessions) by g.TEC medical and biomedical company which has been used for their SSVEP response detection analysis. The average accuracy rates and ITRs for each method and all of 4 subjects are compared with each other. Meanwhile their level of accuracy and ITR for online performances is discussed.

The major challenge of SSVEP BCIs is to find the frequency components of brain signals and extract proper information in order to later classify and detect user commands. The introduced methods in this thesis were first employed to analyze provided data by g.TEC (as an external data source) since different data analysis methods (modified by g.TEC research group) reached to certain level of accuracy with these data-sets (Guger C., 2012).

The SSVEP test sessions consisted of 4 LEDs flickering with 10, 11, 12 and 13 Hz frequencies. LEDs were flickering for 7 seconds in a cycle and this cycle was repeated 5 times for each subject. The data sampling rate was 256 Hz, meaning that each 1-second time-window had 256 samples. By overlapping 224 samples in time-windows, the SSVEP responses will be detected every 1/16 of second. The accuracy of SSVEP response detections for the test session and different subjects are provided. The accuracy rate presents the average percentage of the correct user intention detection in each trial. The ITR (Bits/Trial) is obtained from the following (Eq. 80) (Vasquez P. M., 2008).

$$ITR(Bits/Trial) = \log_2 N + P\log_2 P + (1-P)\log_2(\frac{1-P}{N-1}) \qquad \text{(Eq. 80)}$$

Where, N is the number of LED stimuli signals and P is the system average accuracy rate. This formula uses the average accuracy rate of each subject's SSVEP test session to calculate the ITR of each subject/test. Then, based on this equation, higher system average accuracy increases the ITR (second and third terms of the equation). Moreover, the higher number of SSVEP stimuli increases the ITR based on the first and third terms of the equation (Obermaier B., 2001).

Figure 33 and figure 34 show the analysis results of 4 subjects' SSVEP test sessions obtained from introduced algorithms in chapter 3. Figure 33 shows the accuracy rate in percentage and figure 34 shows the ITR in bits/trial.

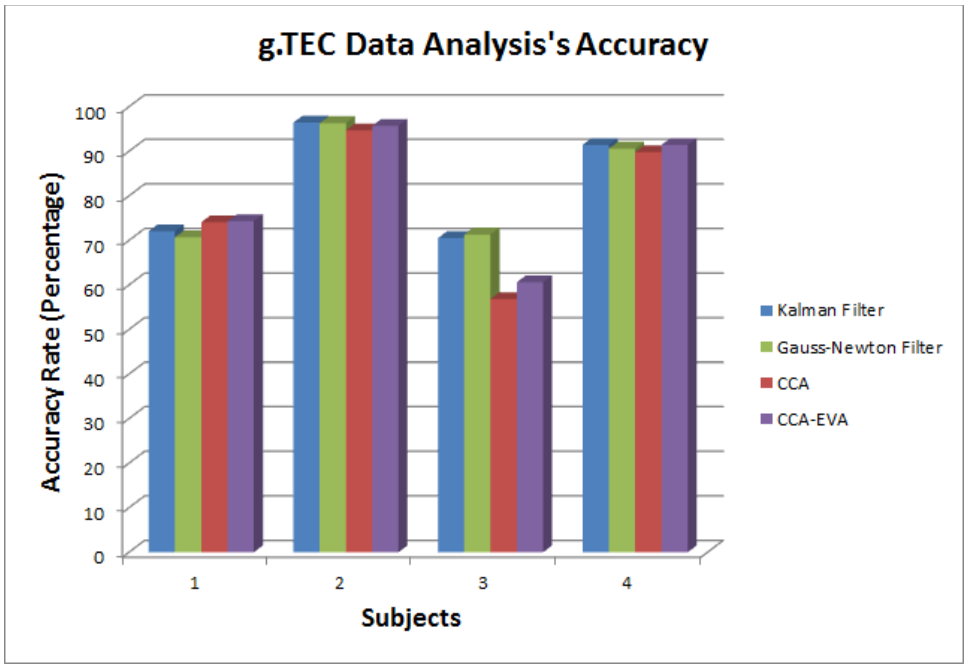

Figure 33. Average accuracy rate for subjects/algorithms

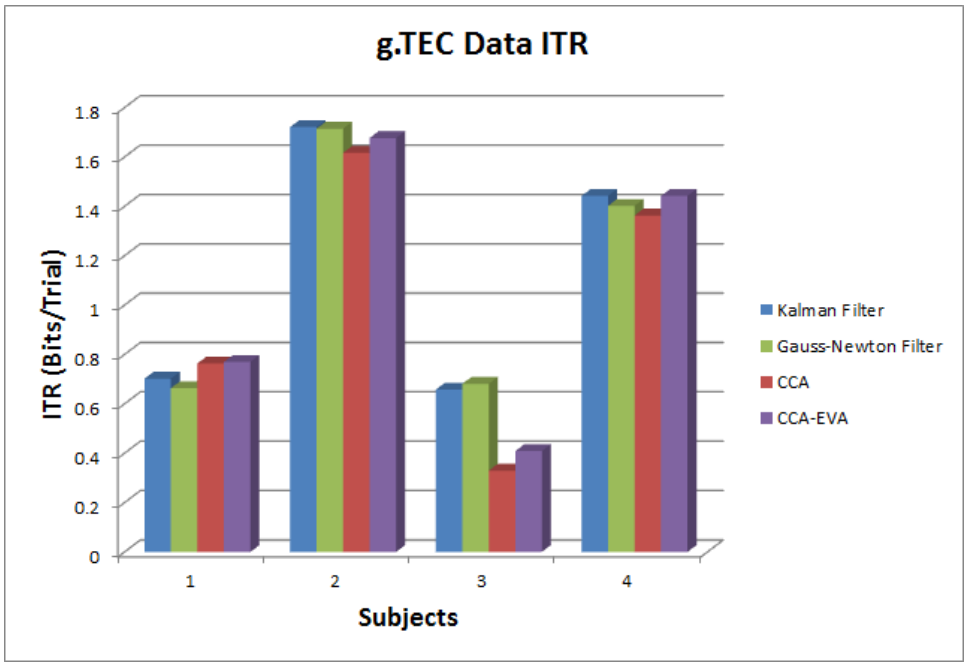

Figure 34. ITR for aubjects/algorithms

As it can be seen in these figures, the average accuracy rates are adequately ranged between 60 to 90 %. Subject 3 shows poor performance with SSVEP BCI which can be caused by distraction or subject's brain physiological structure, which generates electromagnetic fields that are not detectable by EEG. Usually, for subjects who use the BCI systems for the first time their focus on LEDs are not quite enough to provoke detectable visual potentials for EEG. The ITR for all subjects except subject 3 are higher than the range of 0.6 to 0.8 (Bits/Trial). This represents feasible SSVEP response detection algorithms for online BCI systems (Obermaier B., 2001).

5.1.2 SSVEP Response Detection Analysis

This section provides the results of the SSVEP response data collected for 30 subjects and the performance of the four selected analysis methods. One of the major challenges of SSVEP BCIs is to find frequency components of brain signals and extract proper information in order to later classify and detect user commands. Canonical correlation analysis has been offered for analyzing SSVEPs by (Bin G., 2009) and later was evaluated by many different research groups to obtain its level of average accuracy for different tests/subjects [(Bin G., 2009), (Lin Z., 2006), (Bin G., 2009)].

Despite the many advantages of CCA method, such as less computational time and higher accuracy with efficient ITR (as indicated in early papers' results), there is a prevalent issue of decreasing average accuracy with fewer number of samples. The smaller time-windows that are required for real-time processing decrease the CCA accuracy rate. The other important CCA issue which may be considered for real-time processing

algorithms is that it configures an open loop control system where there is no regulation for error rate. Recent attempts for developing online BCI systems resulted in introducing complex signal filtering, closed loop control systems, machine learning methods and different transforms for detecting the user intention without training sessions and acceptable accuracy rate [(Friman O., 2007), (Chang H. C., 2010), (Lee P. L., 2011), (Zhao L., 2010), (Kimura Y., 2013), (Wang H., 2010)]. As it has been discussed in chapter 3, adaptive and robust filters have the advantage of controlling the error boundaries with different cost functions and criteria. Our modified adaptive algorithms are limited to time-windows with specific length of data samples to estimate the PSD of each LED. However, this is more dominant for CCA method since with smaller time-windows the accuracy of estimating correlation factors decreases and system deficiency increases. Nevertheless, overlapping data samples helps to create larger time-windows for CCA and PSD estimations. The preliminary results obtained from g.TEC data confirm independence of accuracy from overlapping the samples in time-windows. Hence, overlapping samples in a time-window improves the system capability for generating outputs every few hundreds of milliseconds, e.g. in our test, the model finds the user command, every 62.5 milliseconds.

Figures 35 and 36 show the obtained correlation factors for subject 22 test session via CCA and Modified CCA-Evaluation methods, respectively (overlapped time-windows). Each LED and observed brain signals result in a correlation signal. In this research, subjects are tested with 4 flickering LEDs with frequency rates of 10, 11, 12 and 13 Hz. The LEDs were flickering for 7-seconds and this cycle was repeated 5 times during a test session. These two figures clearly present the increase in brain signals' correlations with

flickering LED signals. As it can be seen, correlation increased for the 10, 11, 12 and 13 Hz LEDs, respectively. This pattern repeated 5 times during a test session. Comparing the correlation factors of different LEDs at each time step and selecting the maximum correlation value detects the user intention.

Figures 37 and 38 present the estimated original brain source signals and estimated noise signals recorded from subject 22 for the first second of his test session (10 Hz LED). These two figures demonstrate the obtained results from adaptive Kalman filter algorithm. These two figures are the calculated brain source and noise signals for subject 22 who satisfactorily performed during the SSVEP test session. Moreover, Figure 39 and figure 40 present the obtained brain source and noise signals from subject 7 for the first second of the SSVEP test session. The subject 7 had a poor performance during SSVEP test session and acquired system accuracy is correspondingly low. These two figures are provided to demonstrate that obtained brain source and noise signals from the filtering algorithms show no difference between the subjects with detectable (DSR) and non-detectable SSVEP responses (NSR). Hence, as mentioned in chapter 3, SSVEP response detection requires additional steps to calculate the PSD and accordingly SNR of the brain source and noise signals. The user intention detections via adaptive filters depend on maximum obtained SNR for different LED stimuli.

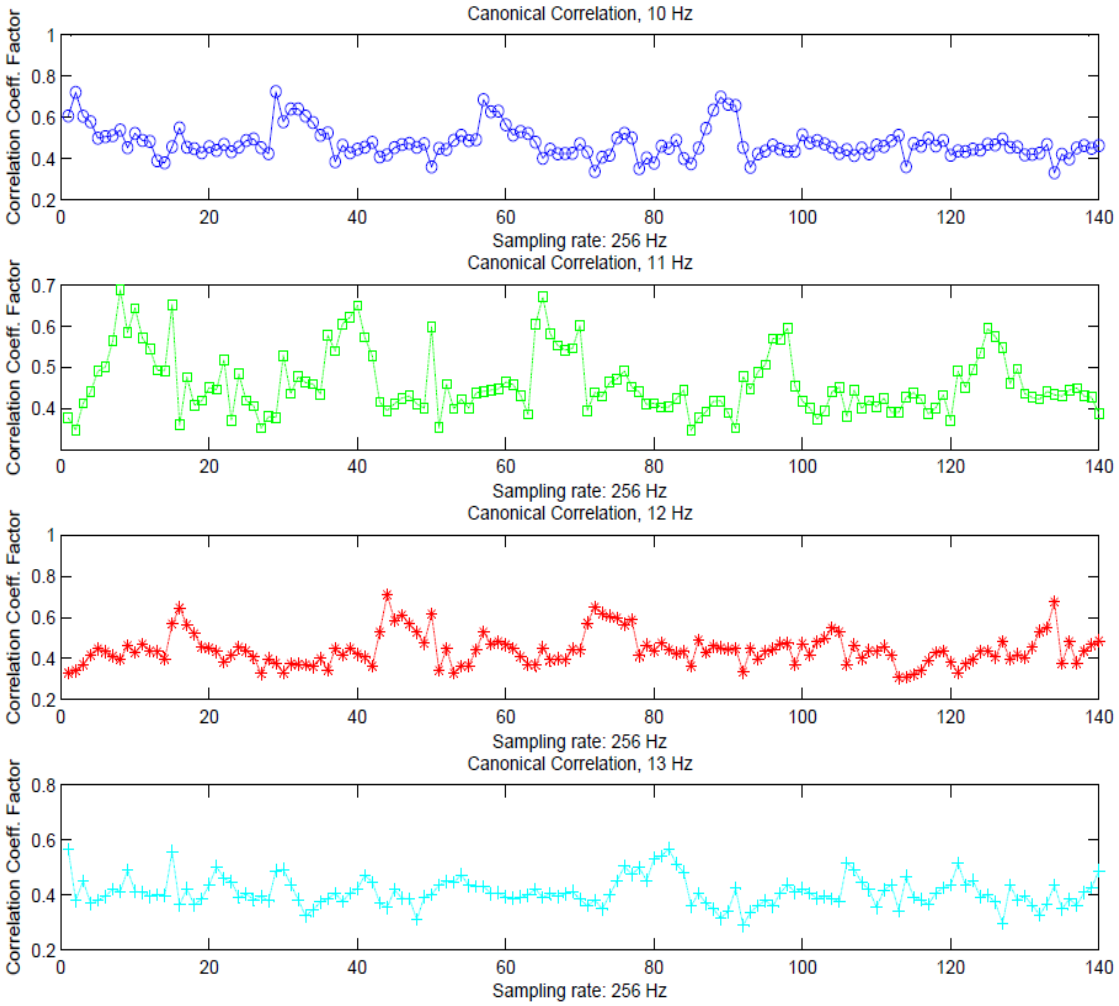

Figure 35. Correlation factors obtained via modified CCA-evaluation method

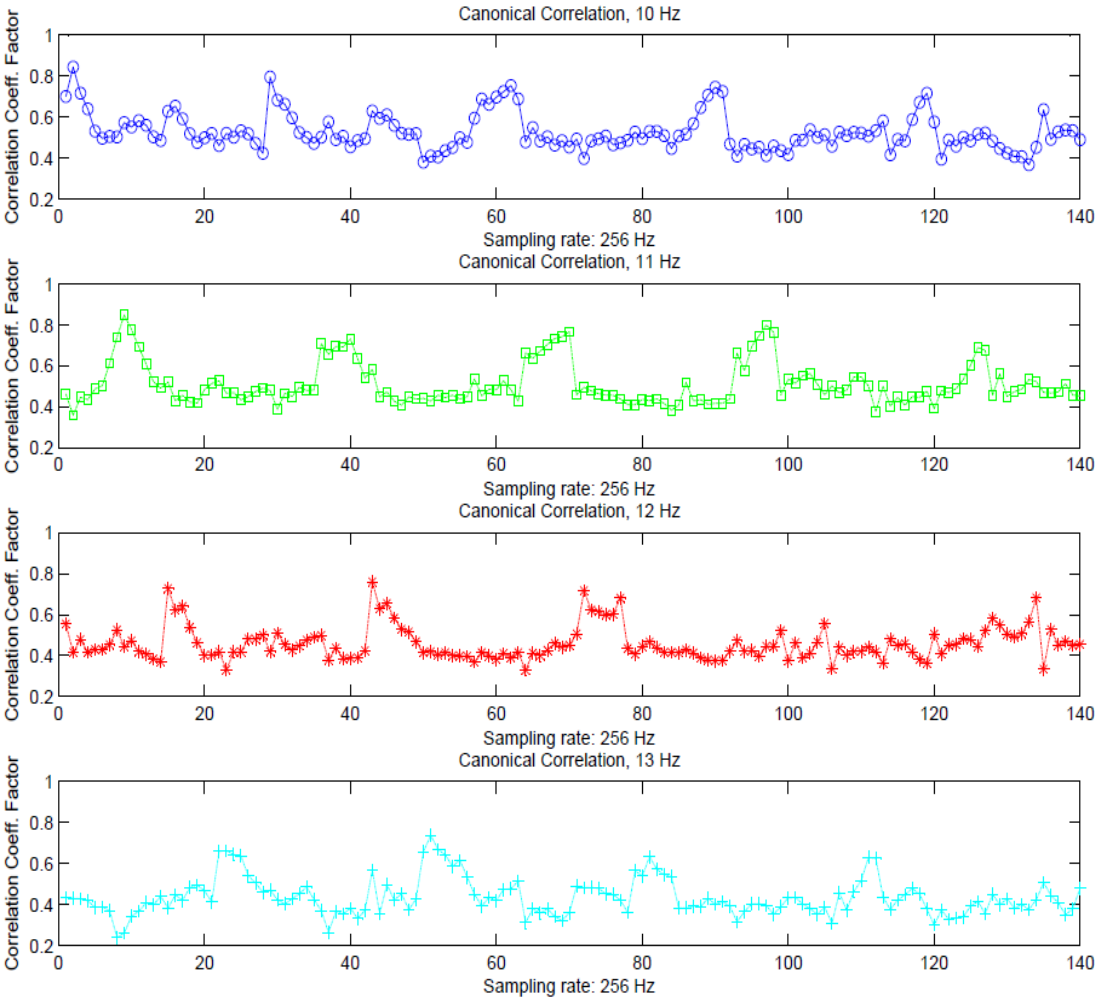

Figure 36. Correlation factors obtained via CCA method

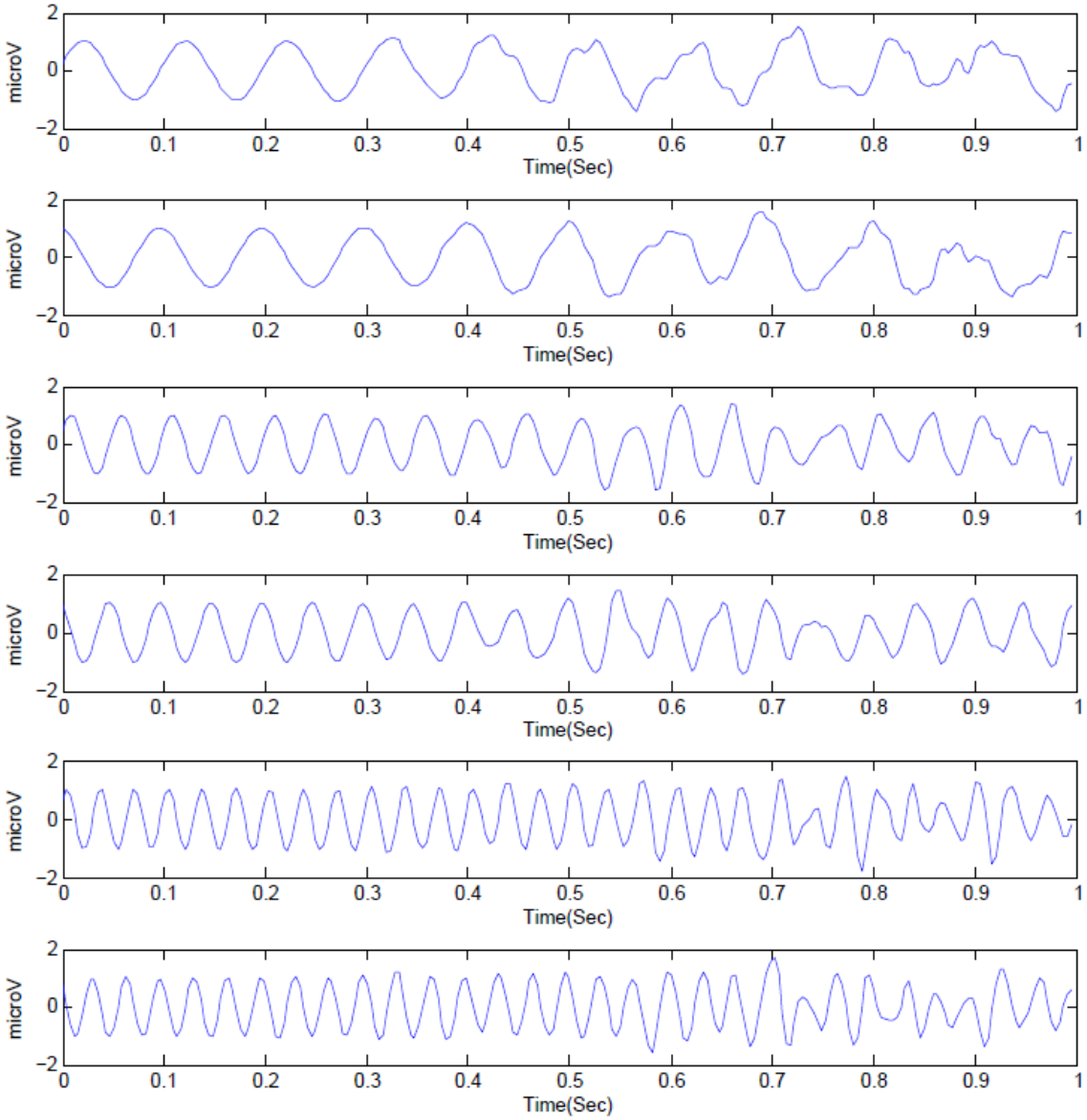

Figure 37. Estimated brain source signals via adaptive Kalman filter recorded from subject 22

These two figures consisted of 6 signal channels of sine and cosine elements of brain source signals and their corresponding noises for 3 frequency harmonics (section 3.3).

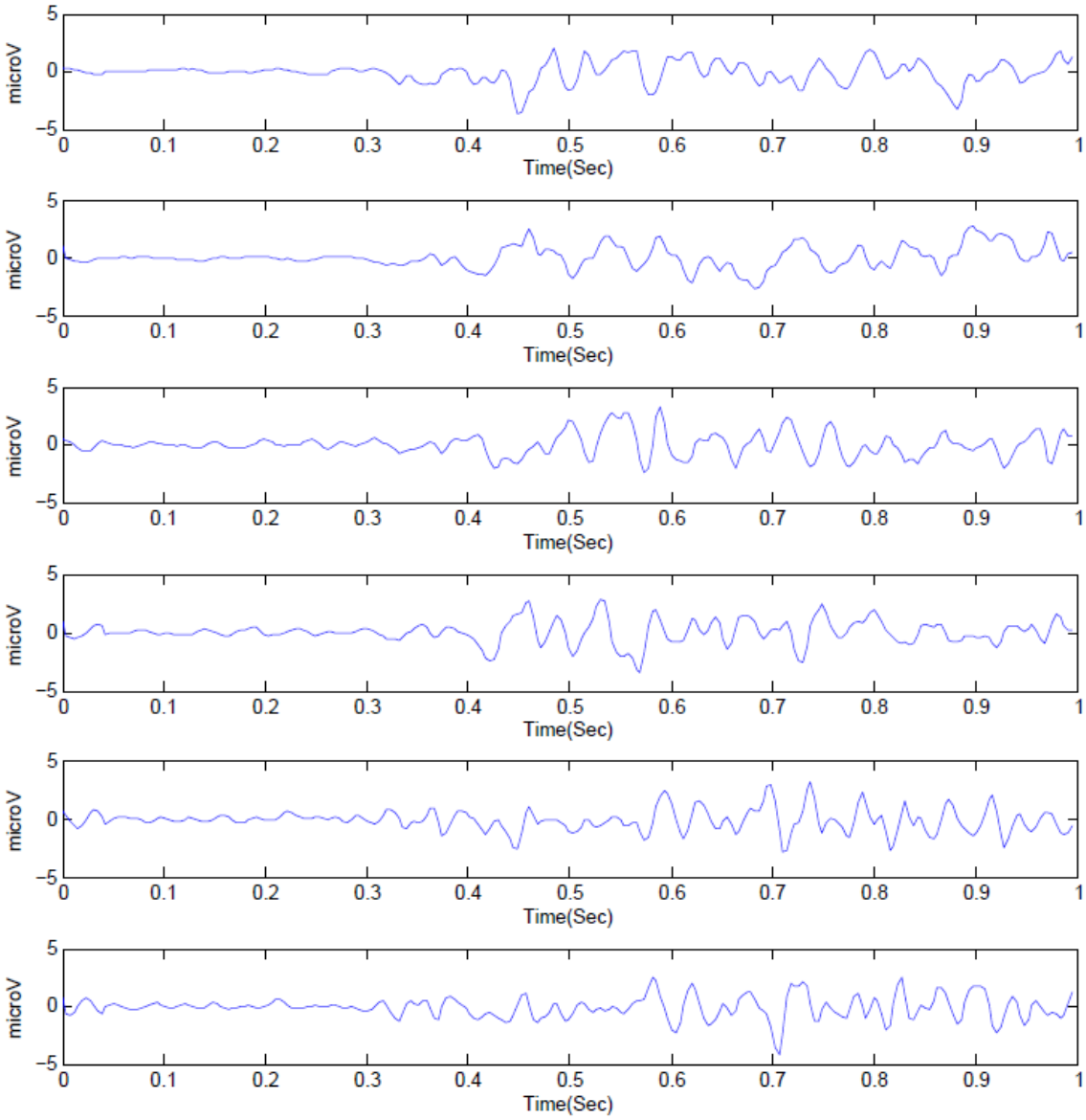

Figure 38. Estimated noise signals via adaptive Kalman filter recorded from subject 22

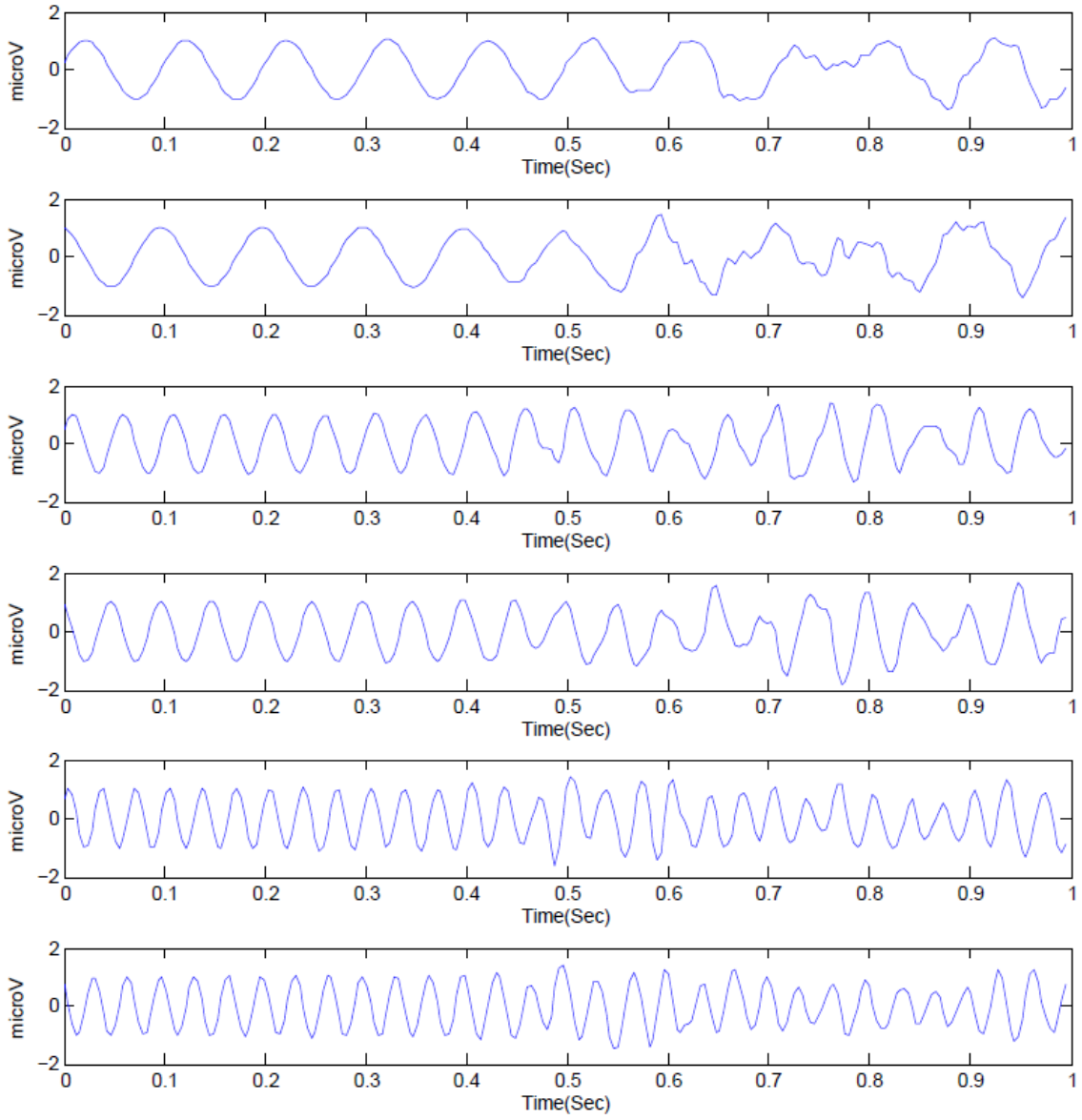

Figure 39. Estimated brain source signals via adaptive Kalman filter recorded from subject 7

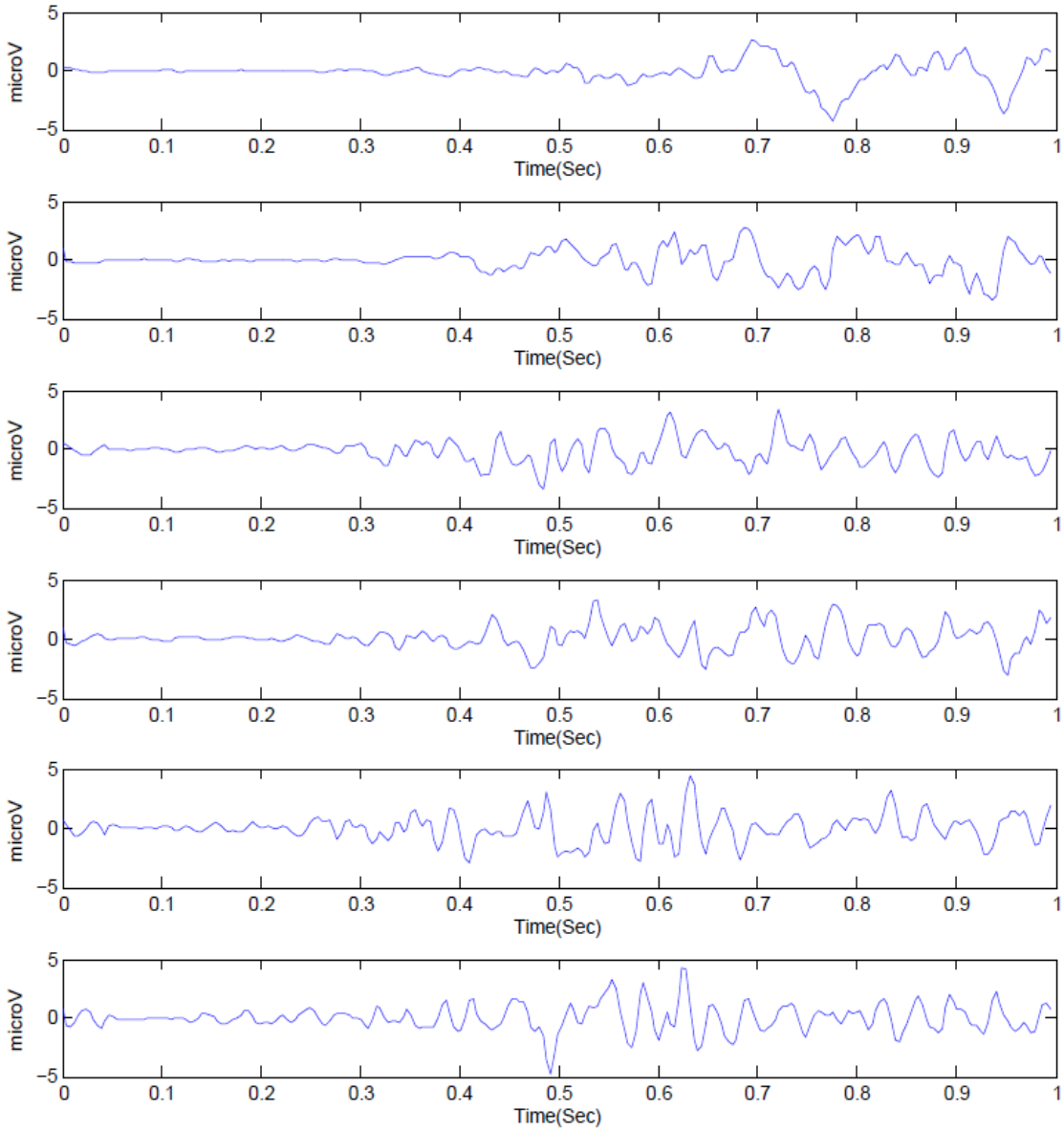

Figure 40. Estimated noise signals via adaptive Kalman filter recorded from subject 7

Figures 41 and 42 demonstrate the estimated brain source signals and corresponding noise signals for subject 22 during the same time-window for 10 Hz LED using adaptive robust Gauss-Newton algorithm. These figures also consisted of 6 channels based on LED

stimulus signal. Stimulus signal includes 6 channels of sine and cosine elements of LED signal and 3 corresponding harmonics (section 3.2.2.1).

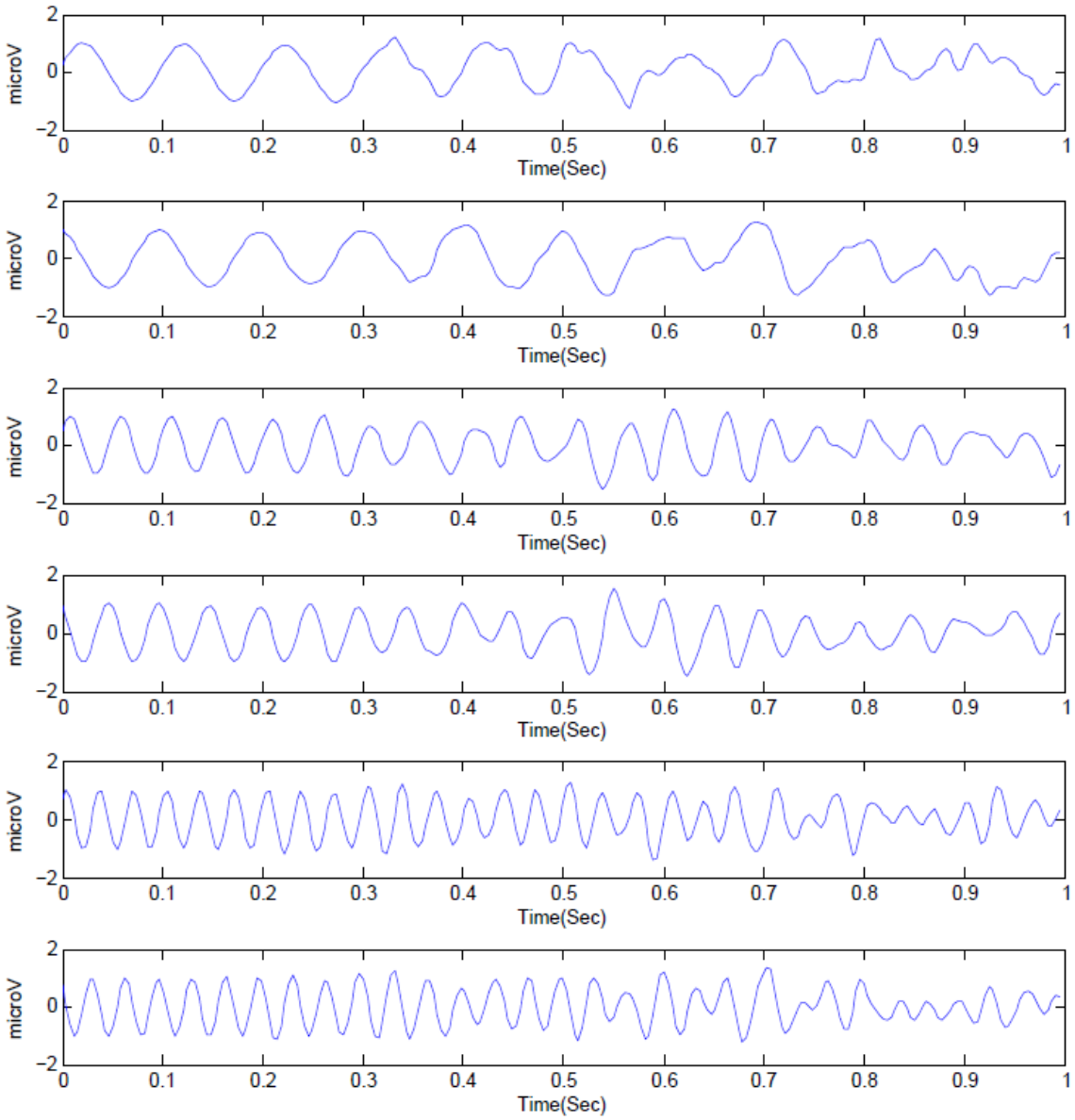

Figure 41. Estimated brain source signals via adaptive robust Gauss-Newton filter recorded from subject 22

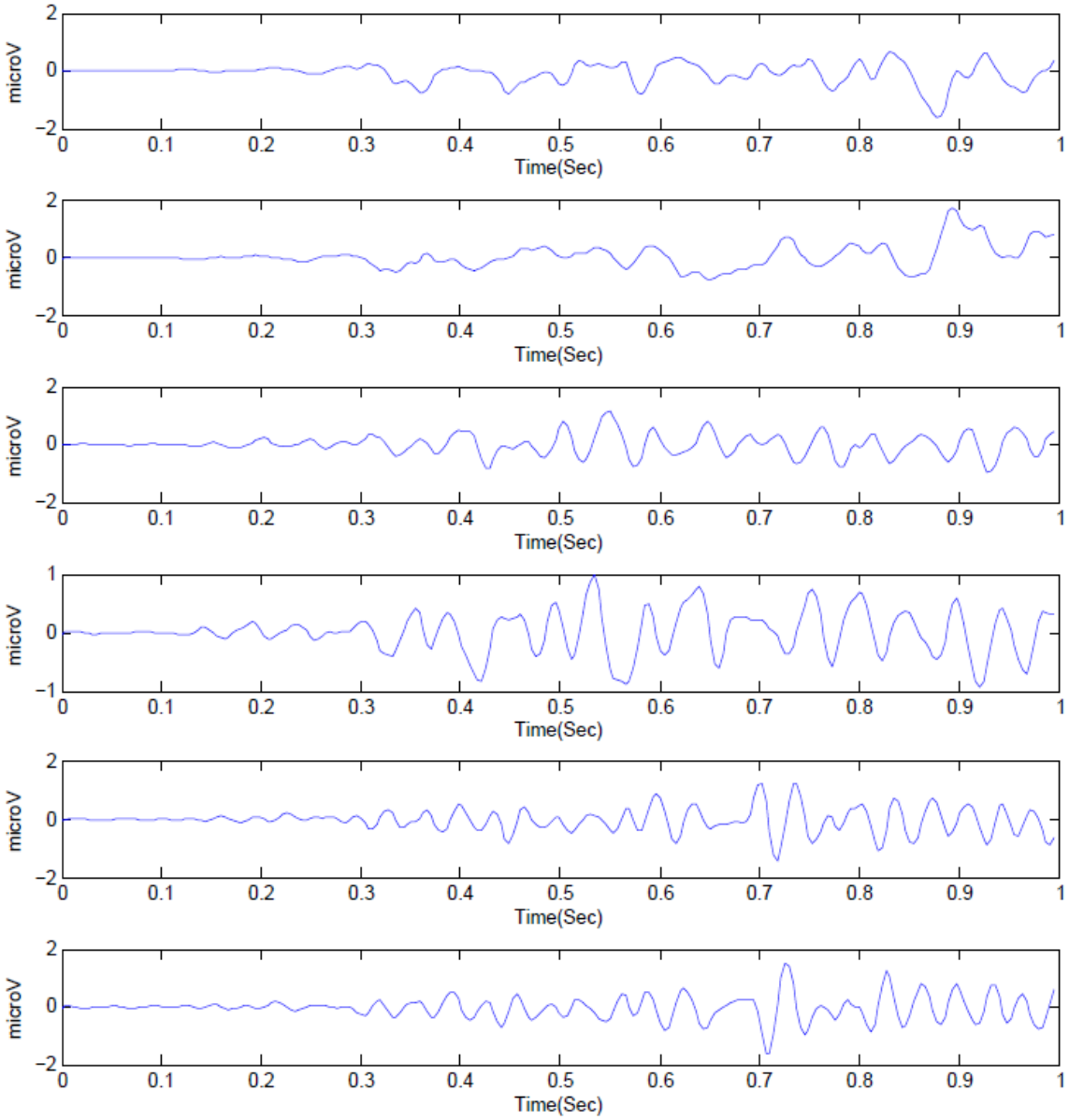

Figure 42. Estimated noise signals via adaptive robust Gauss-Newton filter recorded from subject 22

Figures 43 and 44 present the obtained brain source and noise signals from subject 7 via Gauss-Newton filter. The figures presented for subject 22 (with detectable SSVEP

responses) and subject 7 (with non-detectable SSVEP responses) show no noticeable difference between obtained brain source and noise signals. Hence, additional SSVEP response detection step is needed.

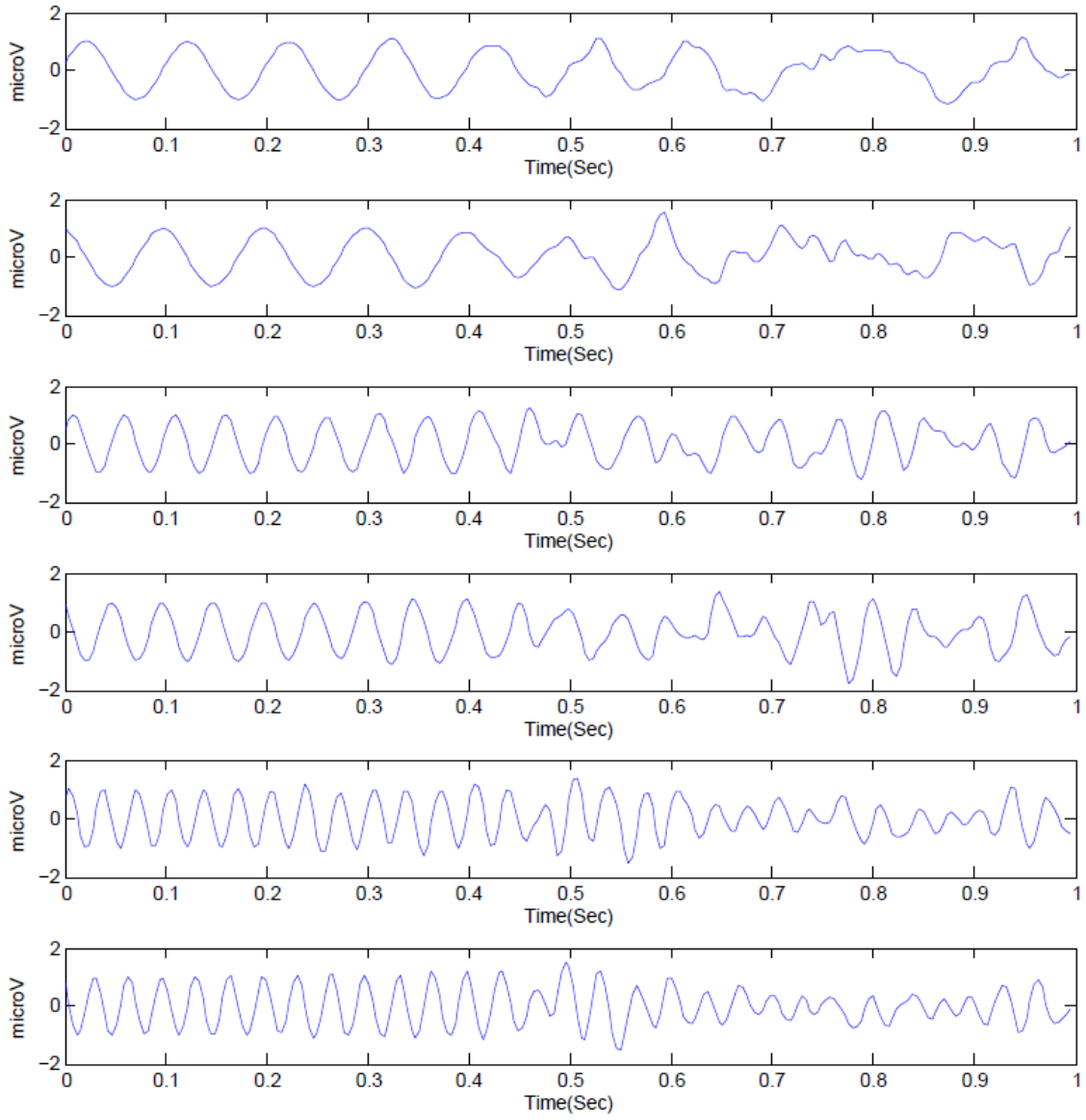

Figure 43. Estimated brain source signals via adaptive robust Gauss-Newton filter recorded from subject 7

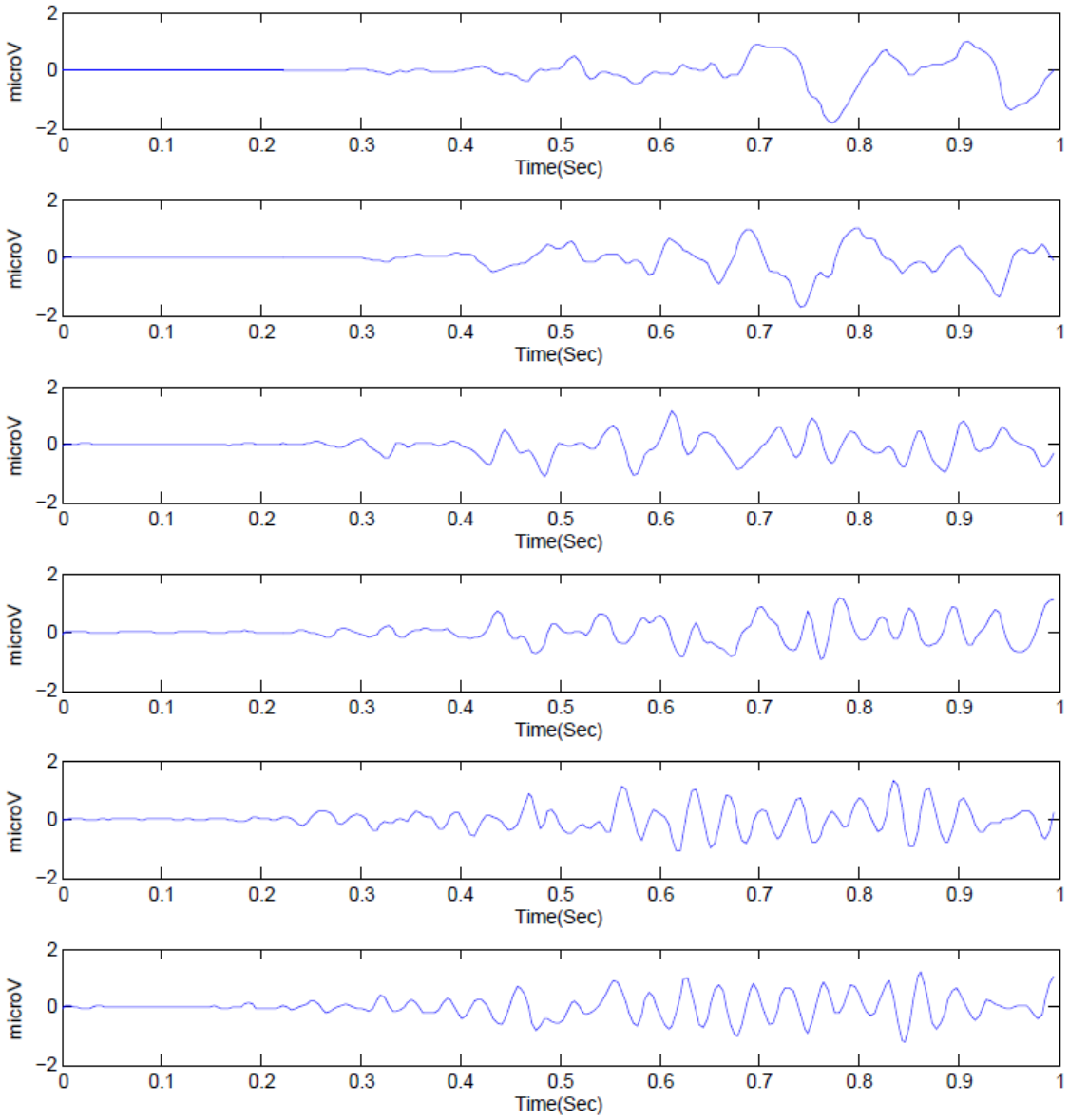

Figure 44. Estimated noise signals via adaptive robust Gauss-Newton filter recorded from subject 7

After estimating the brain source signals and noise signals for each LED frequency, the SNR value of estimated brain source signals for all LEDs are obtained according to chapter 3 methods. Finally, the maximum SNR values between different LEDs indicate the selected

LED by subject. Figure 45 shows the calculated average accuracy rate during the SSVEP test session for subjects via different proposed methods in this thesis. The subjects who reached the accuracy rate of 50-60 % have a satisfactory BCI performance. However, for the BCI systems with real-time performance, accuracy range of 60-80 % is anticipated according to the earlier studies [(Elitzur A.C., 2010), (Blankertz B., 2010), (Guger C., 2012), (Obermaier B., 2001)]. The results of analysis models in figure 45 confirm the models capability of detecting SSVEP responses. In our research, some subjects couldn't perform satisfactorily during SSVEP test and reached the lower accuracy rate. As suggested by earlier studies, this mostly happens when the subjects never participated in SSVEP test before.

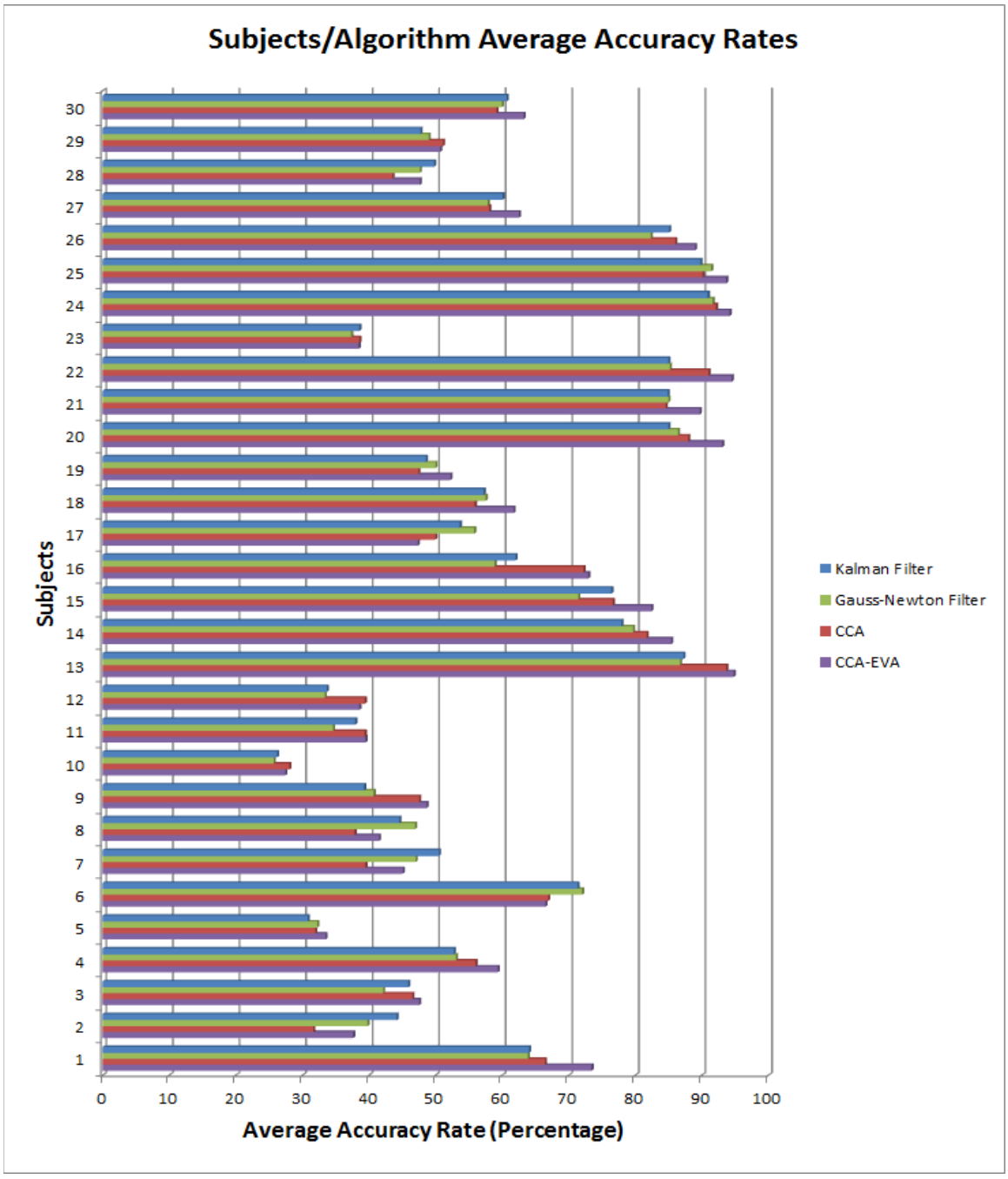

Figure 45. Average accuracy rate for subjects/algorithm

To compare all of the proposed methods with each other more precisely, subjects' accuracy rates quartiles are calculated (box-plot). Each quartile presents the range of accuracy in which 25 % of the study's population distributed. Figure 46 presents the Box-Plot of all methods analysis results. In this figure, the worst and best accuracies and the distribution of subjects' performances for each method are demonstrated in quartiles. This figure shows that all of the methods introduced in this thesis are comparable which means their performance as an online SSVEP based BCI is almost similar. Figure 33 also shows that the SSVEP response detections obtained from g.TEC data are comparable.

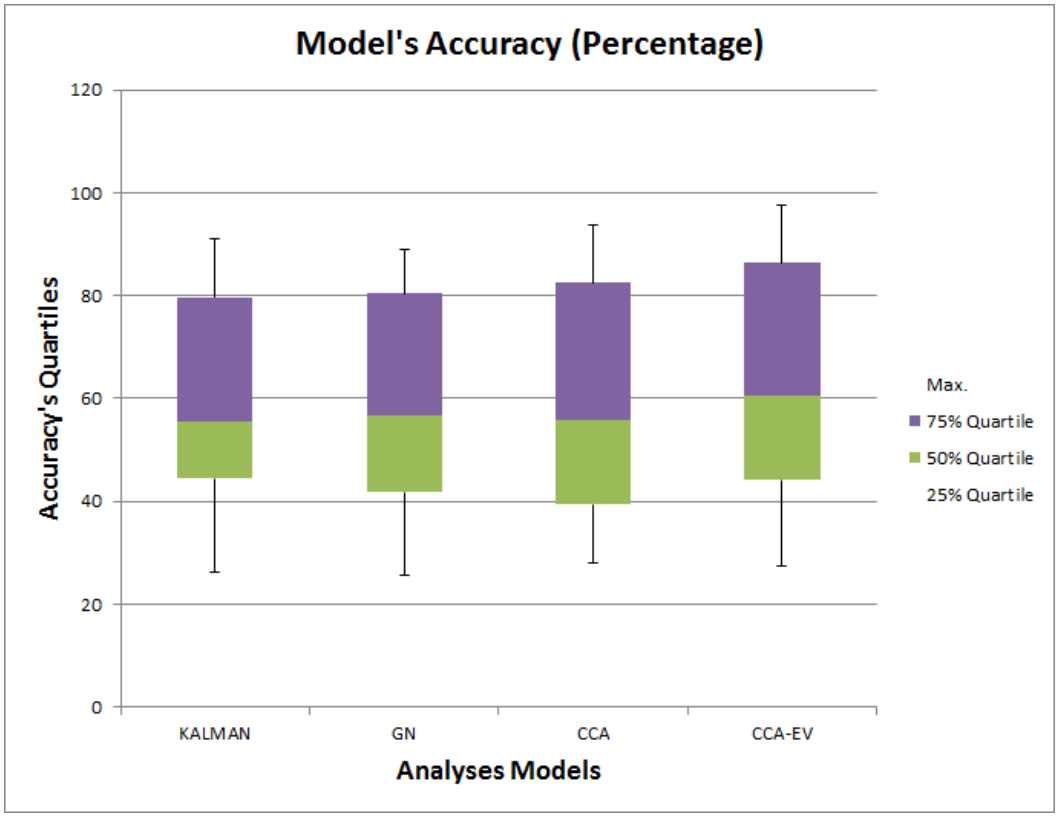

Figure 46. The box-plot of all models analysis results

Figure 47 is used to better indicate how the data analysis results of proposed methods are distributed in 25 percentiles. The important part of figure 46 and figure 47 is the middle 50 percentiles that present the average performance of subjects with SSVEP BCIs.

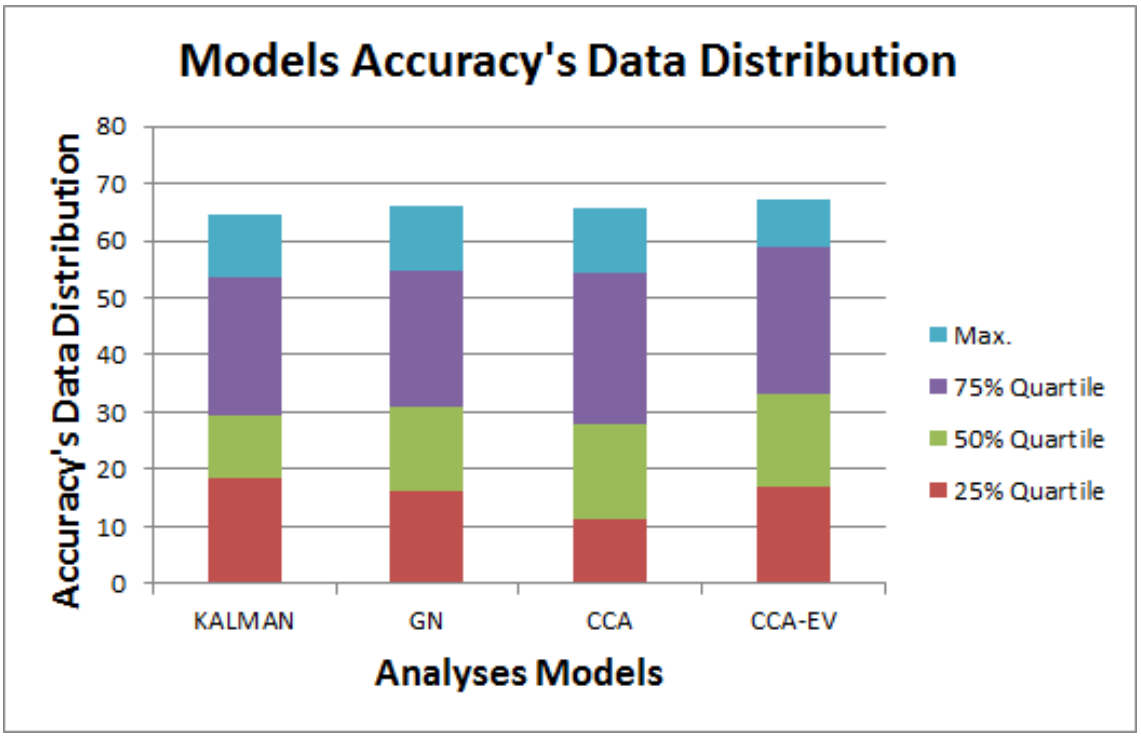

Figure 47. The percentile distribution-plot of all models analysis results

Figure 48 shows subjects' ITRs for the four selected analysis models. In this figure, the amounts of ITR for different subjects are comparable with their corresponding accuracy rate in figure 45. In section 5.1.1, it's explained that according to (Eq. 80), the amount of ITR is dependent on subjects' accuracy rate.

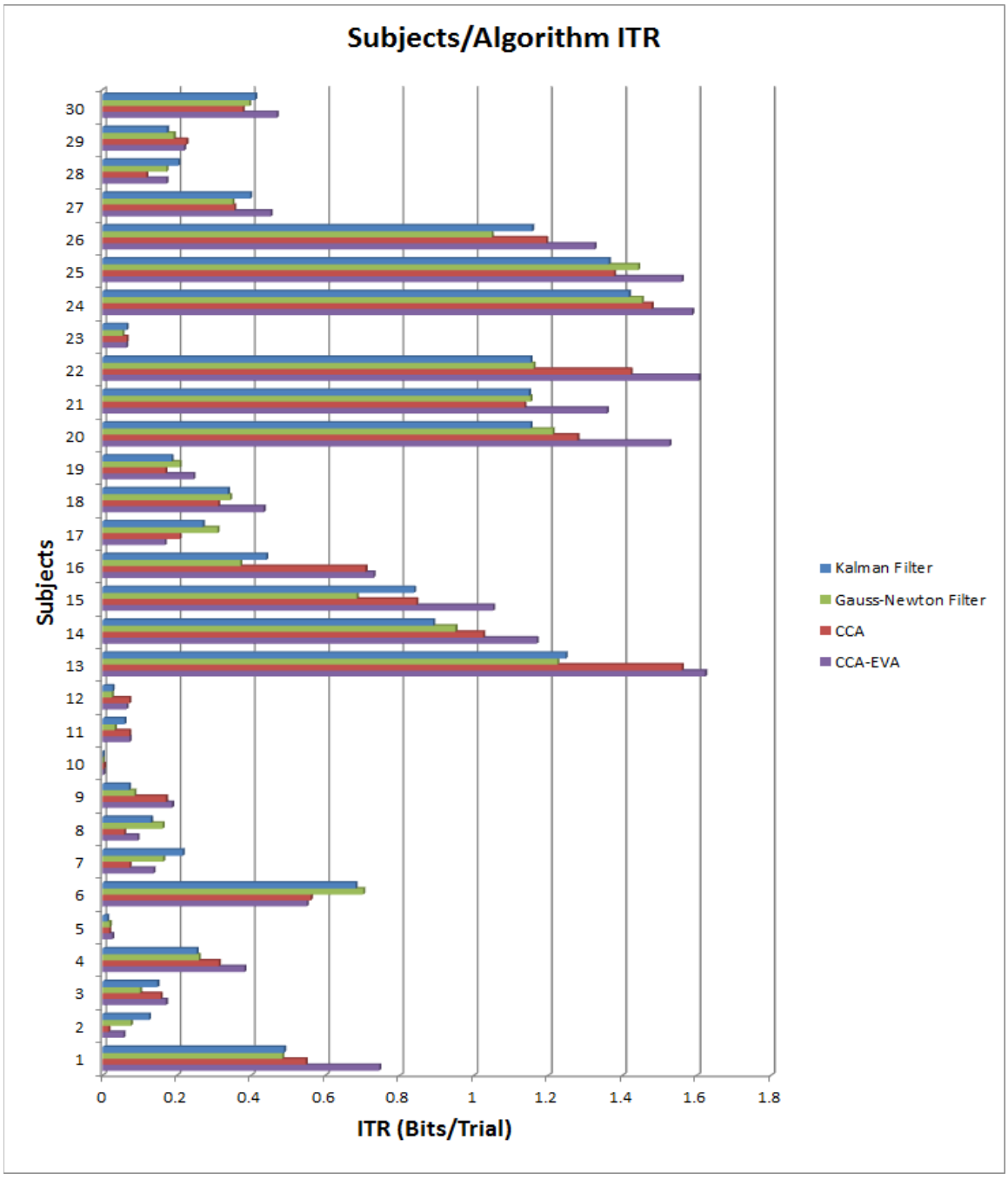

Figure 48. subjects' ITR/algorithm

The ITR for different models are also calculated from (Eq. 80) to compare the capability of transferring bits of information during the test session. Figure 49 and figure 50 show the same data distribution aspect as was explained for accuracy rate quartiles and percentiles, respectively. A Satisfactory ITR rate for online performances is considered higher than 0.6 per trial. The ITR range of more than 0.8-1 bits/trial satisfies the SSVEP based BCI real-time performances (Obermaier B., 2001).

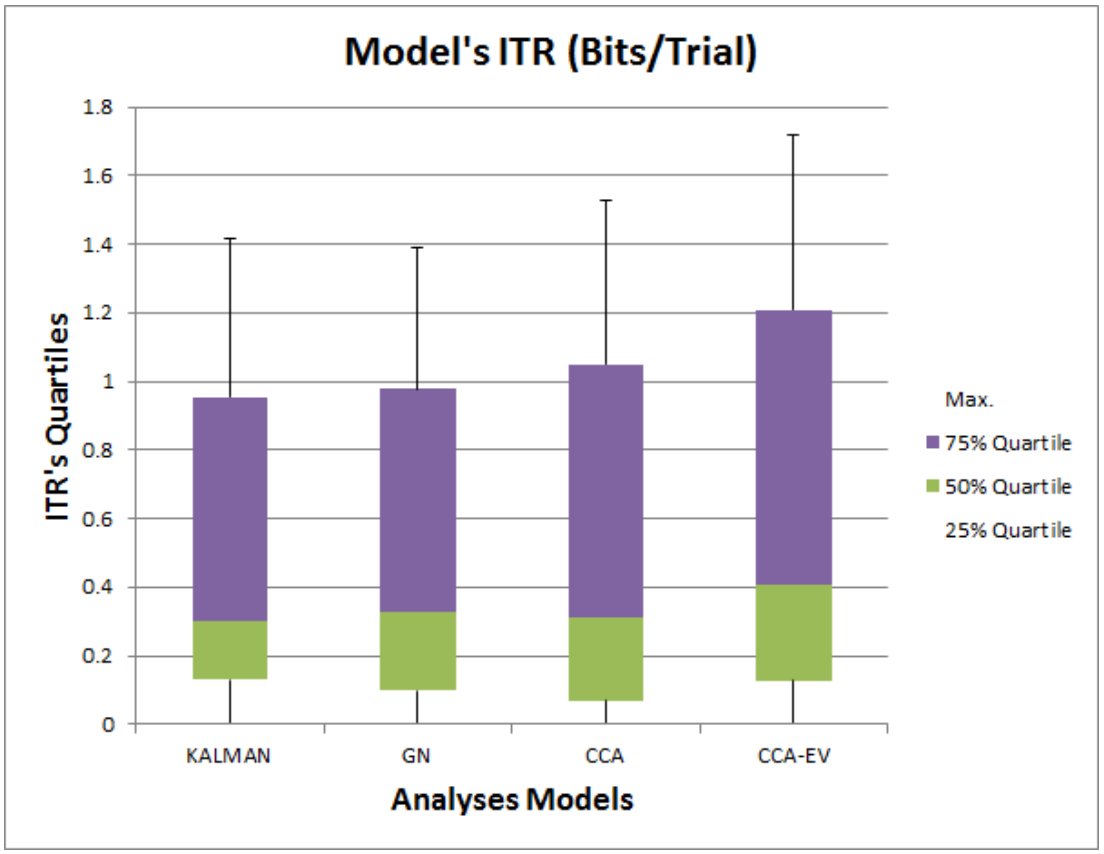

Figure 49. The box-plot of all models ITR results

Based on accuracy results almost half of the subjects performed satisfactorily during the SSVEP test session since the average accuracy rate changes between 40 to 80 %. This was observed even though none of the subjects had ever participated in a SSVEP test session. This is presented in figure 46 and figure 47 where middle 50 % of the subjects' analysis results are approximately similar for different methods. However, ITR results obtained for 50 % of the subjects with NSRs are not satisfactory for online BCI purposes, regardless of analysis model. Referring to (Eq. 80) ITR is affected by both the accuracy rate and total number of SSVEP triggers.

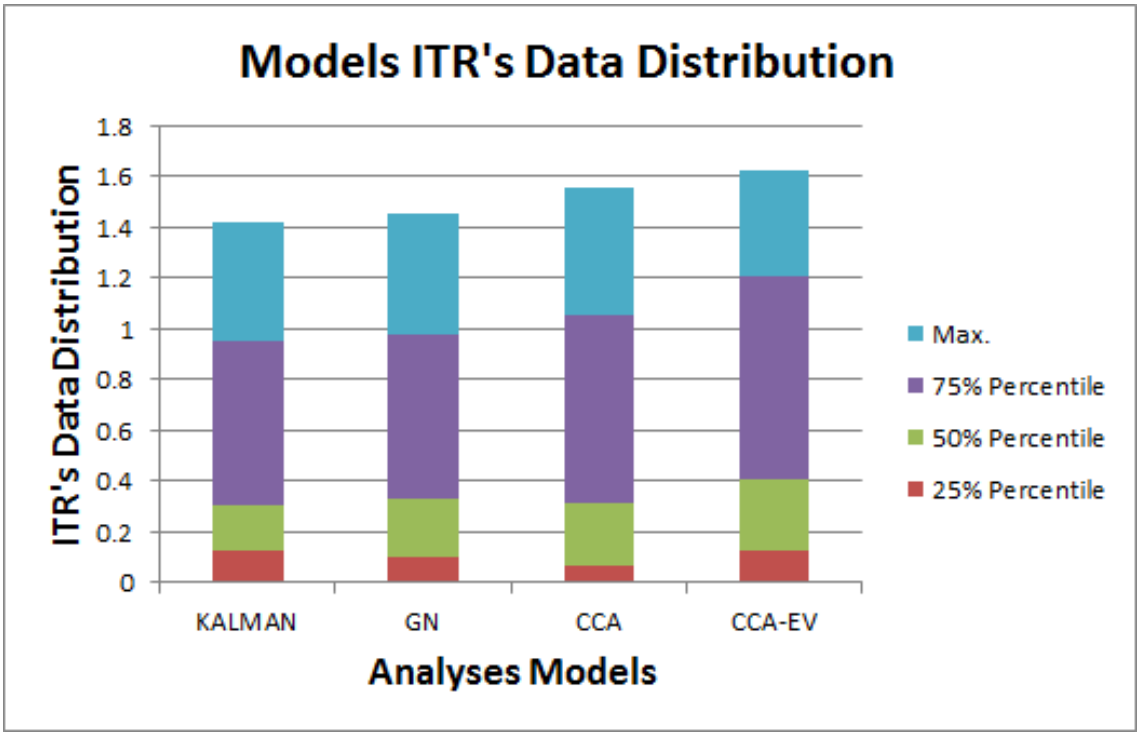

Figure 50. The percentile distribution-plot of all models ITR results

The first and second 25 % of subjects' ITRs (dissatisfactory ITRs from subjects with NSR) con density of distribution between 0-0.3 bits/trials can be observed in figure 50. This is an indication for why the ITRs are unacceptable for employing in online BCIs. Then, as shown in figure 49 the higher 50 % of the subjects' ITR is ranged between 0.4-1.4. This can be considered as a good performance and represents the adequacy of analysis models for real-time BCI systems, especially for ITRs higher than 0.8.

The four selected analysis methods introduced in chapter 3 are evaluated in this section. The analysis results were described in two sections. First section was based on the data provided by g.TEC. The results of the g.TEC data show an acceptable accuracy rate and ITR for real-time BCI systems. The high level of accuracy which is reached by g.TEC data verifies the validity of these methods' assumptions for filtering the SSVEP signals. The accuracy rate for all of the methods are comparable and within the range of 70-90 %. This shows that these methods had no privilege over each other. However, the adaptive filtering methods are closed loop systems which decrease and stabilize the system error at each time step. The second data-sets were collected from subjects at CISR. The SSVEP test protocol in which these subjects participated was the same as g.TEC SSVEP experiments. The subjects who participated in CISR SSVEP test session were never performed a SSVEP based BCI system. This affected their focus on LED stimuli and also affected the acquired analysis results. However, many subjects' analysis results reached a satisfactory accuracy rate of more than 50 %.

5.2 Car Driving-Simulator Scenarios' Results

In this thesis, three driving scenarios were designed for testing volunteer subjects. In each scenario, the drivers' time to collision (TTC) and reaction distances (RD) were measured to determine the drivers' reaction to a near collision situation. These two factors are presented in (Eq. 81) and (Eq. 82).

$$TTC = T_c - T_r \qquad \text{(Eq. 81)}$$

Where, T_c and T_r are the time of crash and time of first driver's reaction, respectively. In this thesis, driver's reaction is detected either with braking pedal pressure or steering wheel angel. The steering wheel angel of more than 1 rad/sec and braking pedal pressure of more than 0 is considered as driver's reaction based on previous studies (Soudbakhsh, 2011). The braking pedal pressure is measured with the range of 0 (no pedal pressure) to 100 (full pedal pressure). The time of first driver's reaction is the time before the accident when one of the above conditions is met. The reaction distance is calculated from (Eq. 82).

$$RD = L_c - L_r \qquad \text{(Eq. 82)}$$

Where, L_c and L_r are the longitudinal distances of the crash and first driver's reaction, respectively.

First scenario was based on driving on rural and suburban area which included three near collision events. In this scenario, drivers' reaction distances and Time to Collision (TTC) were recorded to measure their normal performances confronting a near collision situation. The short and long (2^{nd} and 3^{rd} scenarios) warning period scenarios' orders were

changing randomly to prevent any biased data collection. As mentioned before, during the short warning scenario drivers were not informed that LEDs will warn them just before emergency situation. Before the long warning scenario, they were informed that LEDs will be activated like a warning system before an emergency situation. The logic behind this driving scenario is to show how drivers will perform in presence of an active SSVEP stimulation LEDs warning system (scenario 3). The second scenario is designed to measure how a SSVEP based BCI short warning period will affect drivers' performances in case that emergency condition is detected just before it happens. The other important aspect of short warning period is that nowadays' real sensors have a short detection range. The drivers' brain signals correlation during the normal and short warning scenarios are compared with 10 Hz LED signal (the activated frequency during warning sessions) to determine the subjects' brain activities and SSVEP response detection.

Figure 51 shows the box-plot of all 30 subjects/scenarios. The middle 50 % of the subjects show a better performance in short warning scenario with respect to their normal reaction distances. Although, the middle 50 % of subjects in long warning scenario have a wider range of reaction distances, they mostly have longer (improved) reaction distances. The results are even far better than their normal performances if we consider the top 25 % of the drivers. Generally, figure 51 shows that the drivers' performances during the long warning and short warning scenarios satisfactorily improve with respect to the normal driving. It can be seen that some subjects performed far better during the short warning scenario which could have happened because of learning process after they participated in

the long warning scenario. The learning process also helped the subjects who participated in the long warning scenario before the short warning scenario.

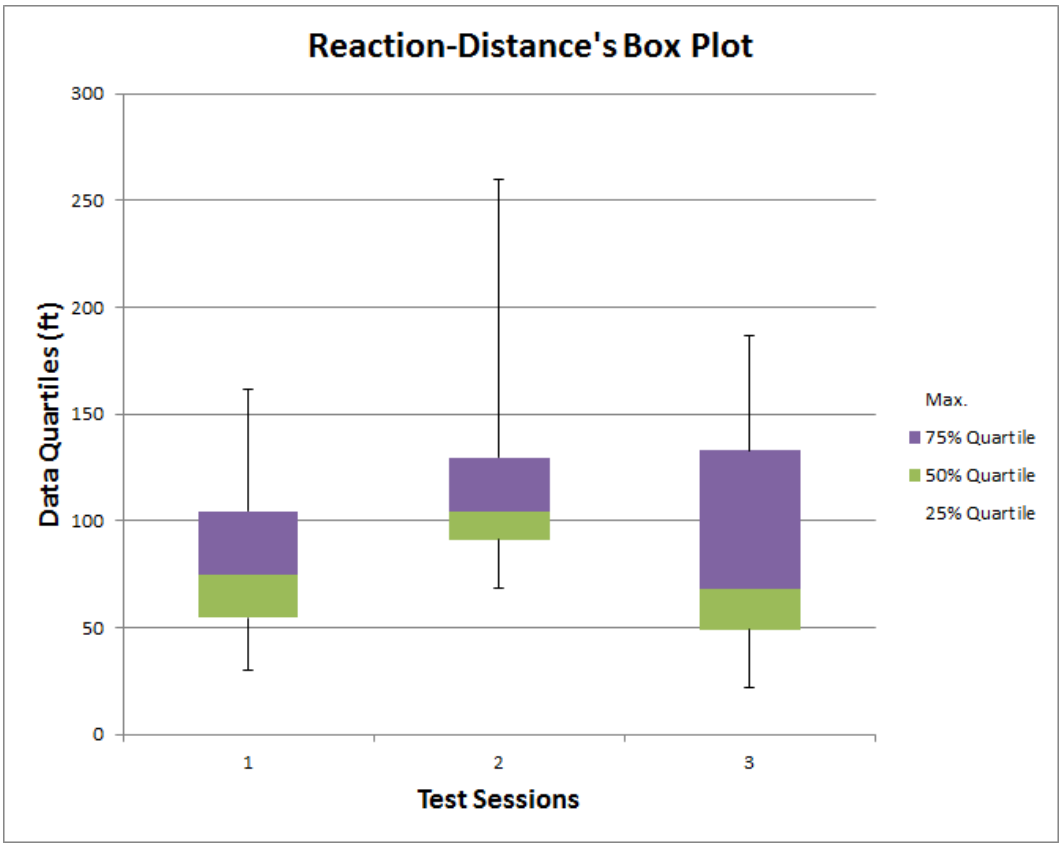

Figure 51. box plot for scenarios/subjects

Figure 52 illustrates how the collected reaction distances are distributed in each test session. This figure is not meant to compare data distribution of scenarios with each other. Nonetheless, its purpose is to better demonstrate the diversity of subjects' performances in each scenario. It determines the difference between worst and best subjects' performances. For example, figure 52 shows that in 1st and 2nd scenarios 75 % of the subjects almost performed similarly and their reaction distances' range differ from 52 to 70 ft, respectively.

Figure 51 and figure 52 together interpret collected reaction distances by comparing the data between different scenarios and determining their distribution in one scenario, respectively. The same logic is used to interpret the drivers' performances by collecting TTC. The final results are presented in figure 53 and figure 54, respectively.

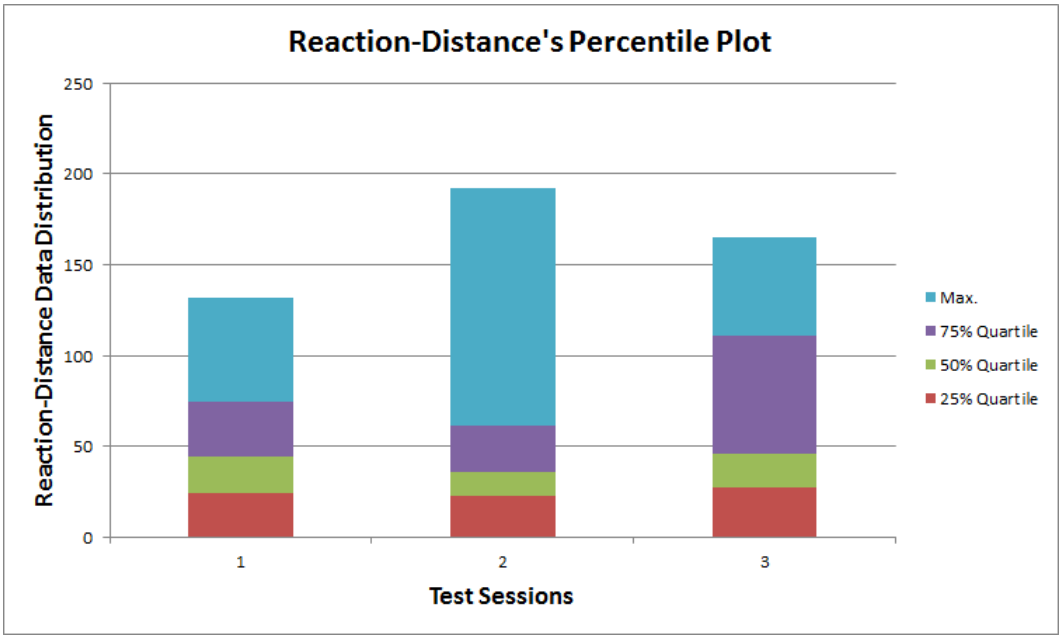

Figure 52. Reaction distances' data distributions

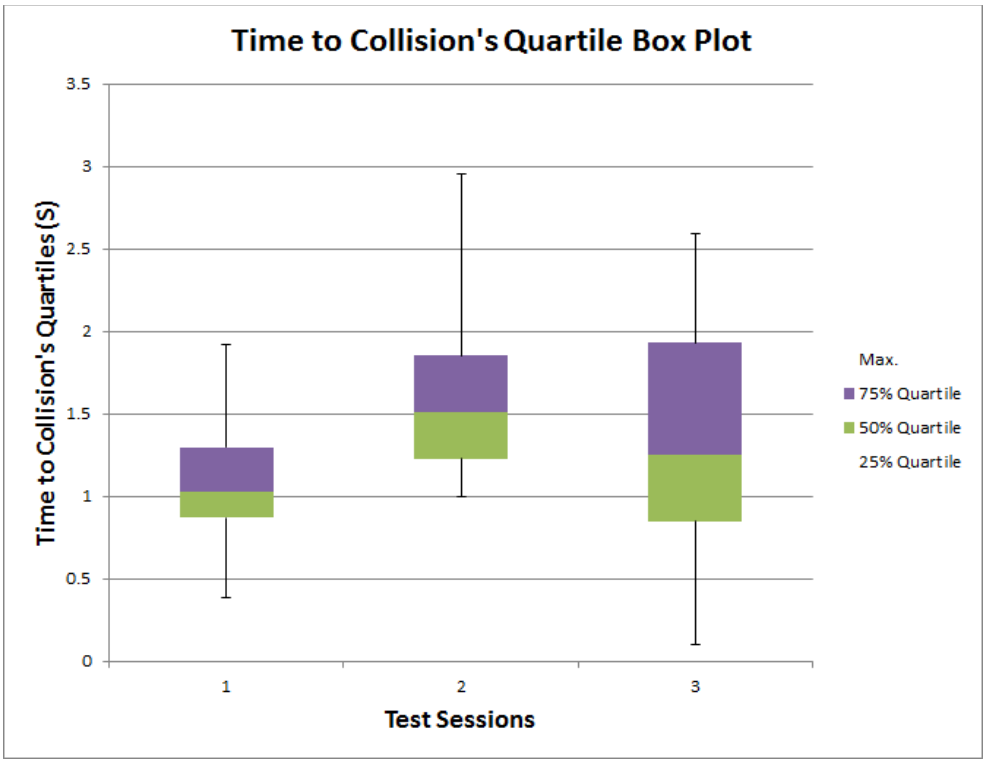

Figure 53. TTC box plot for subjects/scenarios

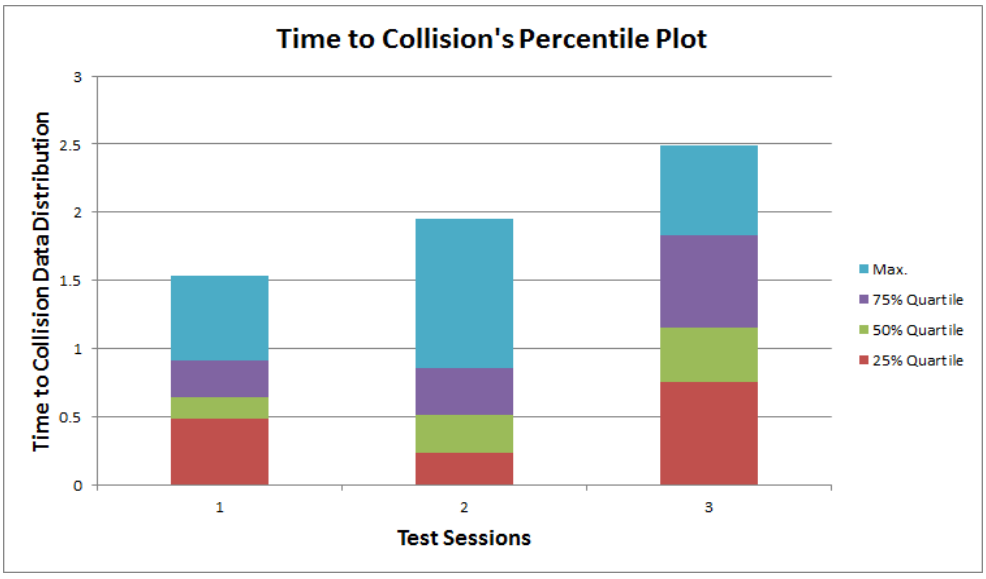

Figure 54. TTC data distribution

Interestingly, the same conclusion resulted from collecting drivers' TTC. Their TTC for short warning scenario is more than other scenarios which means that they reacted faster to near collision situation with respect to other scenarios. It's worth mentioning that drivers were given 2-seconds to react before an accident happened during the normal driving scenario. In short warning scenario, this time increased to 3 seconds by considering the LEDs activation and for long-warning scenario, this period was 5 seconds. The 5 seconds LED warning activation in the long warning scenario was designed to evaluate the drivers' performances in the presence of an active SSVEP based BCI system. The 3 seconds of warning (even without informing the subjects of LEDs' activation) helped them to react better. As mentioned before, the effect of learning process for subjects should be considered. The subjects with worst performances may be the ones who become distracted or failed to fully focus on the warnings during the scenarios. Figure 55 demonstrates all of the subjects' calculated reaction distances. This figure shows that for most of the subjects, reaction distances are higher in the warning scenarios. This means that the LED warning was helping the subjects to react faster. It's possible that for those subjects who have less reaction distances in warning scenarios, the LED warning causes distraction. However, another aspect that should be considered for drivers with a very short reaction distances in long warning scenario is that they started to decrease their speed long before the emergency situation and therefore they needed less stopping distance. In many test sessions, warning systems prevented the collision which is presented in table 1, table 2 and table 3 for the 1st, 2nd and 3rd test sessions, respectively. In the following tables Y means that subjects failed to

react fast enough and crash happened (rare-end collision) and N means that no crash happened.

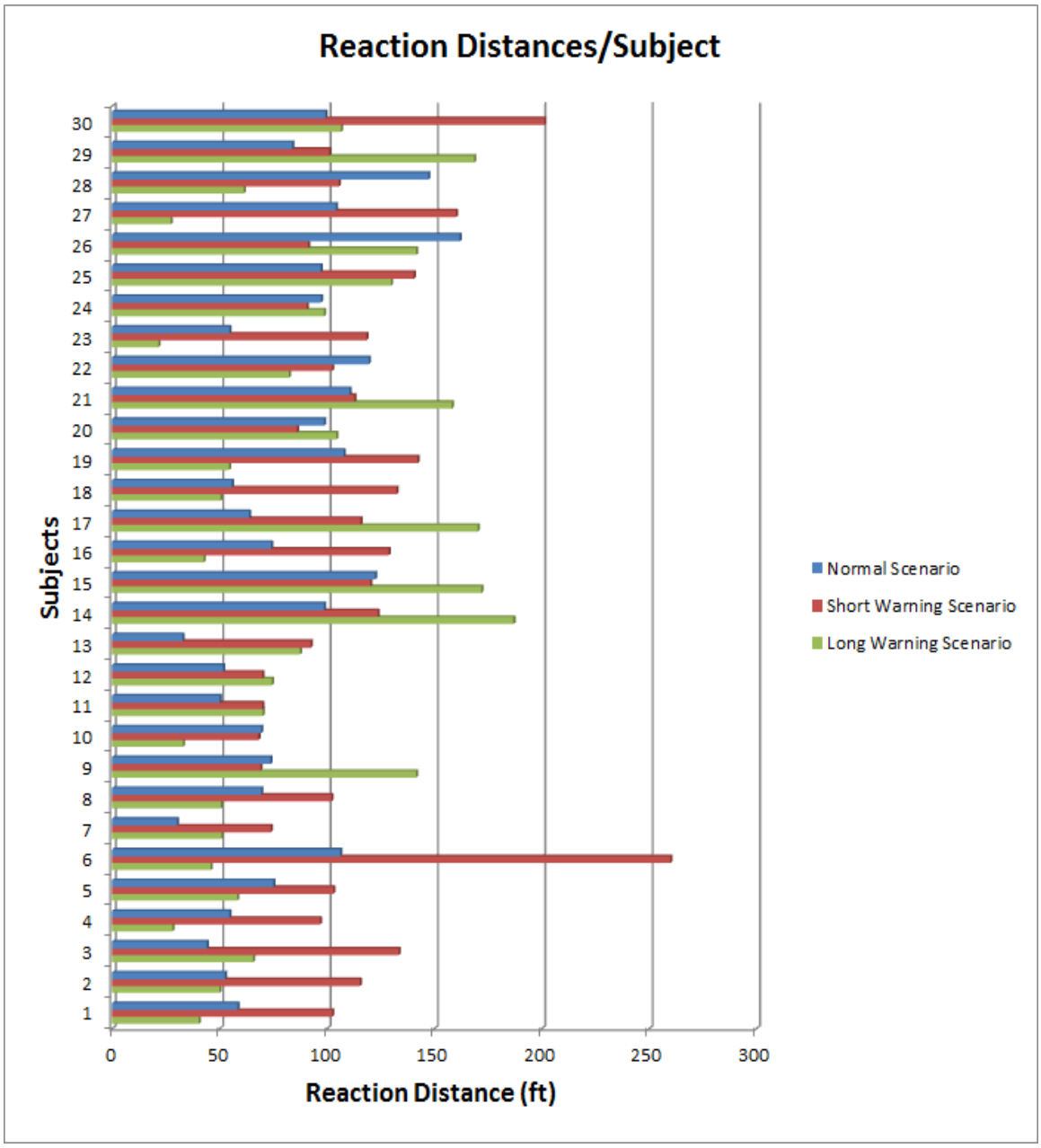

Figure 55. Subjects/scenario reaction distances (ft)

Table 1. Subjects' crashes during normal driving scenario

Normal Driving Scenario			
subjects/events	1	2	3
1	Y	Y	Y
2	Y	Y	Y
3	Y	Y	Y
4	Y	Y	Y
5	Y	Y	Y
6	Y	Y	Y
7	Y	Y	Y
8	Y	Y	Y
9	Y	Y	Y
10	Y	Y	Y
11	Y	Y	Y
12	Y	Y	Y
13	Y	Y	Y
14	Y	Y	Y
15	Y	Y	Y
16	Y	Y	Y
17	Y	Y	Y
18	Y	Y	Y
19	Y	N	Y
20	Y	Y	Y
21	Y	Y	Y
22	Y	Y	Y
23	Y	Y	Y
24	Y	Y	Y
25	Y	Y	Y
26	Y	Y	Y
27	Y	Y	Y
28	N	N	N
29	Y	Y	Y
30	Y	Y	Y
Total Percentage of the crashes	96.66	93.33	96.66

Table 2. Subjects' crashes during short warning driving scenario

Short Warning Driving Scenario			
subjects/events	1	2	3
1	Y	N	N
2	Y	N	Y
3	N	N	N
4	Y	Y	Y
5	Y	Y	N
6	Y	N	Y
7	Y	N	Y
8	Y	Y	Y
9	Y	Y	Y
10	Y	Y	Y
11	Y	N	Y
12	Y	N	Y
13	Y	Y	Y
14	Y	Y	Y
15	Y	Y	Y
16	Y	N	Y
17	Y	N	N
18	N	Y	N
19	Y	N	Y
20	Y	N	Y
21	Y	Y	Y
22	Y	Y	Y
23	Y	Y	N
24	N	N	N
25	Y	Y	N
26	Y	Y	y
27	Y	Y	N
28	N	N	Y
29	Y	Y	Y
30	N	Y	N
Total Percentage of the crashes	83.33	56.66	66.67

Table 3. Subjects' crashes during short warning driving scenario

Long Warning Driving Scenario			
subjects/events	1	2	3
1	Y	N	N
2	Y	Y	Y
3	N	N	N
4	Y	N	Y
5	Y	Y	Y
6	Y	Y	Y
7	Y	N	N
8	Y	Y	Y
9	Y	Y	Y
10	Y	Y	Y
11	Y	N	N
12	Y	N	Y
13	Y	Y	N
14	Y	N	N
15	Y	N	N
16	Y	N	Y
17	Y	N	Y
18	Y	Y	N
19	Y	N	Y
20	N	Y	N
21	N	N	N
22	Y	Y	Y
23	Y	N	N
24	N	N	N
25	N	Y	N
26	Y	Y	N
27	Y	N	Y
28	N	N	Y
29	N	N	N
30	Y	N	Y
Total Percentage of the crashes	76.66	40	50

As it can be observed from table 2 and table 3, the total percentage of crashes in short and long warning scenarios adequately decreased with respect to the normal driving scenario. This shows that without considering worst subject performances, in general, LED warning flashes are helpful for improving drivers' vigilance in near collision situations and they don't have distractive effect. In this section, tables 1 to 3 demonstrate a decrease in the total number of crashes. Meanwhile, figure 51 and 53 show higher TTC and longer RD in warning scenarios. In these box-plots the results are presented in quartiles which show the subjects' reactions distribution. Statistical significance tests are needed to compare the difference between the car-simulator scenarios. The Analysis of Variance (ANOVA) is used to test the difference between each scenario's mean across groups. ANOVA evaluates the null hypothesis of no difference across groups by comparing the different estimates of the groups' variances. This method considers F-distribution in each group and compares the difference between variances by calculating the within and across groups sum of squares. The null hypothesis will be rejected as the value of F-test increases and wilks's ratio decreases below 0.05 (Lattin J. M., 2003). Table 4 shows the obtained RD mean and standard deviation for each scenario while table 5 presents the ANOVA test results.

As it can be seen in these tables, standard deviation is different among groups and the ANOVA test shows the F-value of 461.7 (Intercept) and wilks's ratio (sig.) of less than 0.0001. This result illustrates a very significant change between car-simulator scenarios. ANOVA test and the quartiles box-plots results show that drivers' behaviors significantly improved in warning scenarios comparing to their normal driving behavior.

Table 4. Scenarios' mean and standard deviations

Descriptive Statistics			
Dependent Variable=RD			
Test ID	Mean	Std. Deviation	N
Normal	82.236	32.405	30
Short Warning	114.375	40.085	30
Long Warning	84.85	50.267	30
Total	94.153	43.566	90

Table 5. ANOVA test results

Test of Between-Subjects Effects						
Dependent Variable=RD						
Source	Sum of Squares	df	Mean Square	F	Sig.	Partial Eta Squared
Corrected Model	18596.74 (a)	2	9298.37	5.38	0.006	0.11
Intercept	797831.1	1	797831.1	461.73	0	0.84
TestsID	18596.74	2	9298.37	5.38	0.006	0.11
Error	150329.074	87	1727.92			
Total	966756.92	90				
Corrected Total	168925.81	89				
a. R Squared=0.11 (Adjusted R Squared=0.90)						

The partial eta squared (η^2) value for test IDs (table 5) show that car-simulator experiments' participants (30 subjects) represent 11 % of total drivers' behaviors variation.

5.3 Brain Signals Correlation Detection

In this part, the underlying correlation between the brain signals and the activated LED signal (10 Hz frequency) is evaluated. These signals are collected during normal driving scenario and short warning scenarios. The purpose is to find out and determine the existence of a noticeable or detectable correlation between the warning LED signal and the

driver's brain signals (SSVEP). Likewise, brain signals collected from normal driving session with no LED activation are expected to show less increase in correlation factors' amplitudes. The evaluated brain signals are collected from samples of 3 seconds before and 1 second after the near collision situation. The correlation between the brain signals collected from scenario 1 (with no LED activation) and scenario 2 (with short LED warning period) is obtained from CCA analysis method. The data acquisition system employed 0.5-30 Hz band-pass filter and 50 Hz notch filter to record the signals. The obtained correlation factors and SNRs are compared to detect the noticeable differences between the recorded brain signals' activities during these two scenarios. The procedure to calculate the correlation factors and SNRs is described as follows:

- Collecting the recorded brain signals from samples of 3 seconds before and 1 second after each crash/scenario.
- Calculating the correlation factors and canonical variants of the recorded brain signals (for both scenarios) and LED warning signal via CCA method (chapter 3, section 3.2.1).
- Comparing the obtained canonical factors of the first and second scenarios with each other to detect the differences in correlation patterns.
- Calculating the SNRs of the obtained canonical variants based on chapter 3, section 3.3.1.3).
- Comparing the obtained SNRs of the first and second scenarios with each other to detect the underlying correlations variants' differences.

The recorded brain signals (recorded from each subject) and LED signals' correlation factors are obtained from (Eq. 12) for each scenario/crash. Figure 56 and figure 57 show the obtained correlation factors of subject 22 driving experiments. These figures present the correlation factors obtained for the first near collision situation of the first and second scenarios, respectively. The subject 22 SSVEP signals were detectable (DSR). The brain signals were collected with 256 Hz sampling rate and time-windows were overlapped every 0.0625 second. Therefore, for a 4-second time-window (3-seconds before and 1 second after each crash), 65 correlation factors were obtained. For each subject, near collision situation happens on time step 48. These figures show increases in correlation factors amplitudes before each crash. However, this pattern (increases in correlation factors' amplitudes) occurs for both of the normal and short warning scenarios. This means that subject brains' activities before each near collision situation was not just affected by LED warning signal. The correlation factors' amplitudes are higher for the second scenario (with warning LED). It's worth mentioning, that the correlation factor of less than 0.5 shows statistically insignificant correlation (Lattin J. M., 2003).

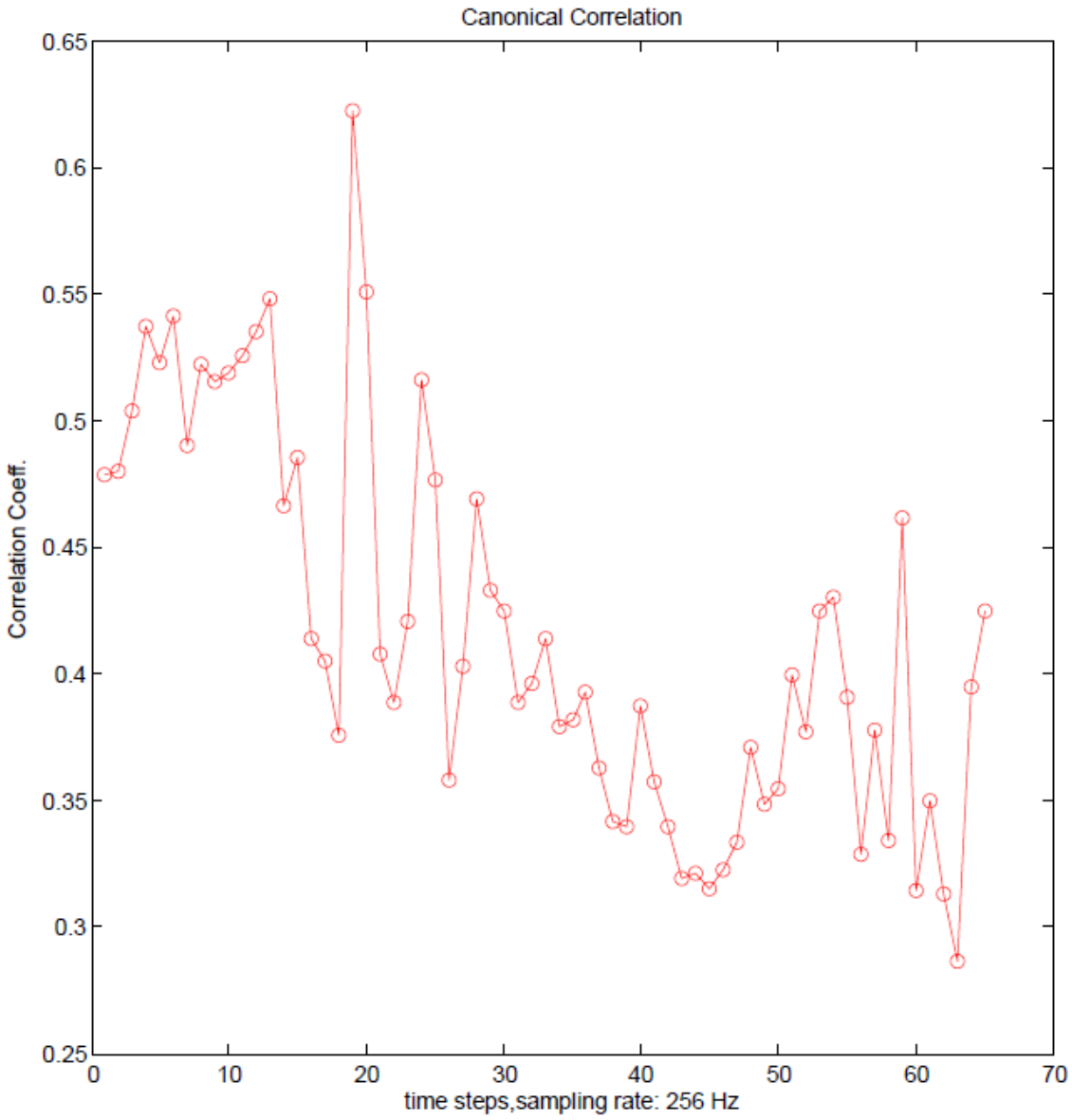

Figure 56. Correlation factors obtained from subject 22 driving experiment during the first scenario and first near collision situation

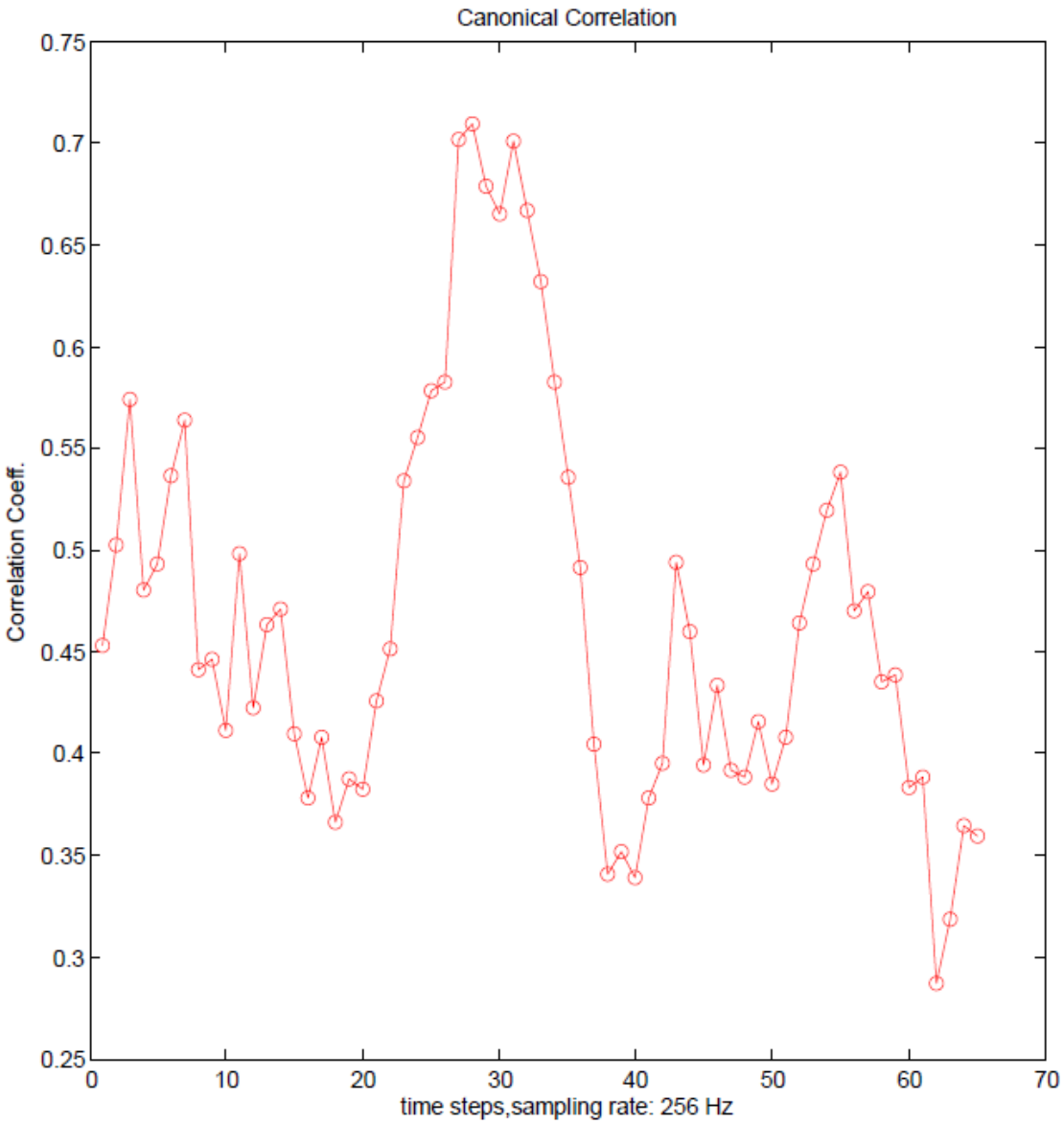

Figure 57. Correlation factors obtained from subject 22 driving experiment during the second scenario and first near collision situation

Figure 58 and figure 59 show the obtained correlation factors of the first near collision situation for subject 7 driving experiments (this subject had NSR). These figures also show increase in correlation factors' amplitudes before the near collision situation.

The obtained correlation factors' amplitudes are higher for subjects' second scenarios' compared to the first scenarios (before near collision situations).

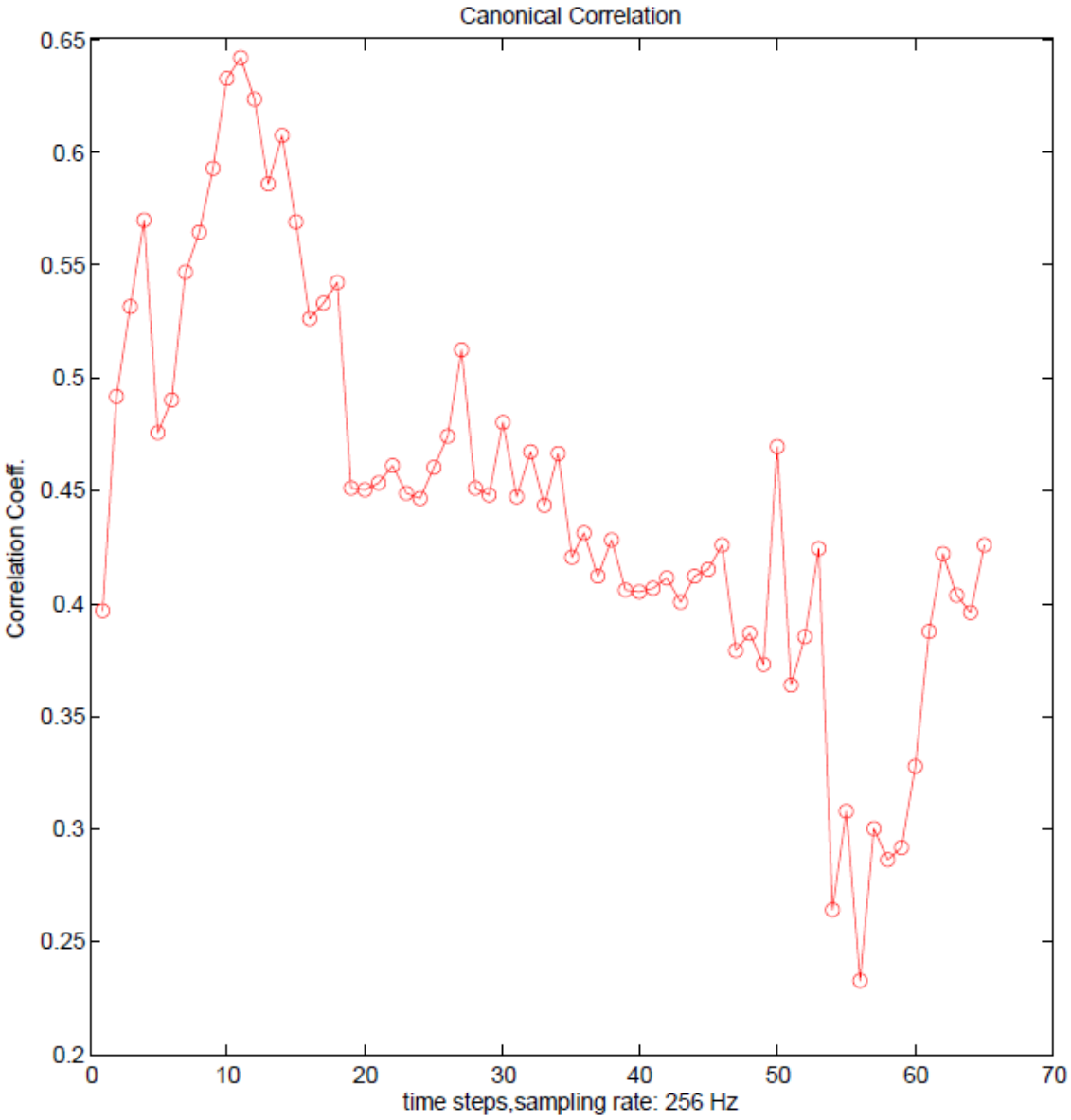

Figure 58. Correlation factors obtained from subject 7 driving experiment during the first scenario and first near collision situation

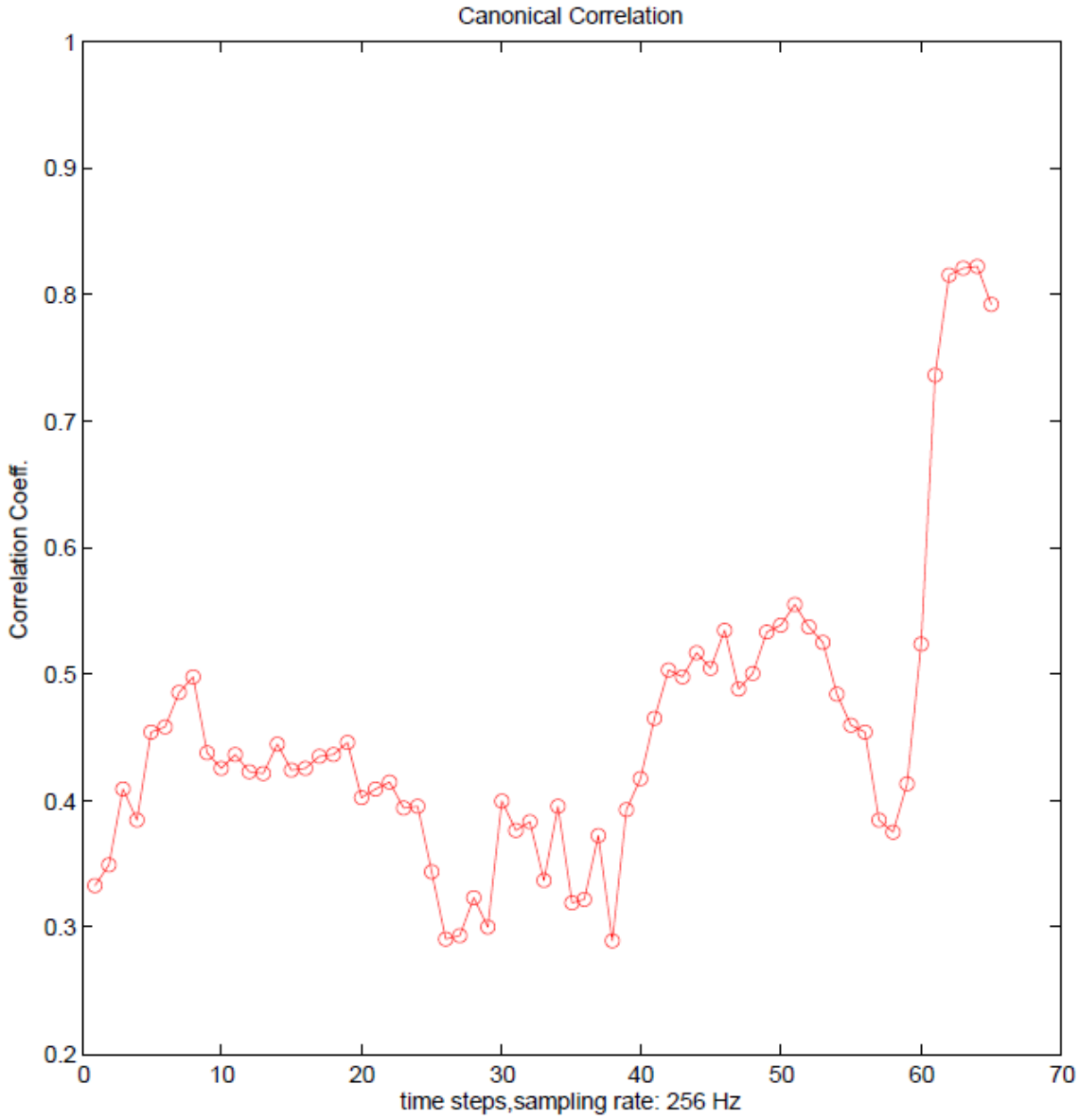

Figure 59. Correlation factors obtained from subject 7 driving experiment during the second scenario and first near collision situation

These two subjects canonical factors' patterns for the 2nd and 3rd near collision situations are presented in appendix B; along with, 6 other subjects' canonical factors for the first near collision situations of the 1st and 2nd scenarios.

The canonical variants obtained from recorded brain signals and LED warning signal via CCA was used to calculate SNRs. The SNR for each near collision situation and subject/scenario is obtained according to (Eq. 42). This equation calculates the SNR by averaging the ratio of the source signals' PSD from (Eq. 43) and noise signals' variance from (Eq. 44). The obtained canonical variants' matrices from the recorded brain signals during the normal and short warning scenarios calculated from (Eq. 12) to (Eq. 16) are considered as source signals. The LED signal is considered as the noise signal. Hence, the ratio of estimated canonical variants' powers and LED signal variance are comparable. This helps to compare the brain activities' patterns (SNRs) in both scenarios. Figure 60 presents the obtained SNRs in 4-seconds time-window of the first near collision situation during the subject 22 driving-simulator experiments. Figure 61 similarly shows the obtained SNRs from the first near collision situation of the subject 7 driving simulator experiments. The subject 22 had DSR and subject 7 had NSR. These figures show the detectable SNR peaks before near collision situation for both subjects. It's noticeable that SNR peaks' occurrences before the near collision situations are not completely affected by subjects' performances or LED warning activations.

Figures 56 to 61 show the increase in the level of drivers' brain activities (correlation factors and SNRs) before the near collision situations. This means that the LED warning effect on brain signals was not drastic. In other words, the major factor which affected the subjects' brain activities was confronting an emergency situation. The near collision situations in each scenario caused increases in subjects' motor and sensory motor neurons firing rates. The increase in neurons' firing rate appeared as SNR peaks and canonical

correlation factor amplitudes' increases. Another factor which probably affected the SSVEP response detections is the drivers' full attention on activated LED warnings. The LED stimulation-box was placed on steering wheel as presented in figure 22.

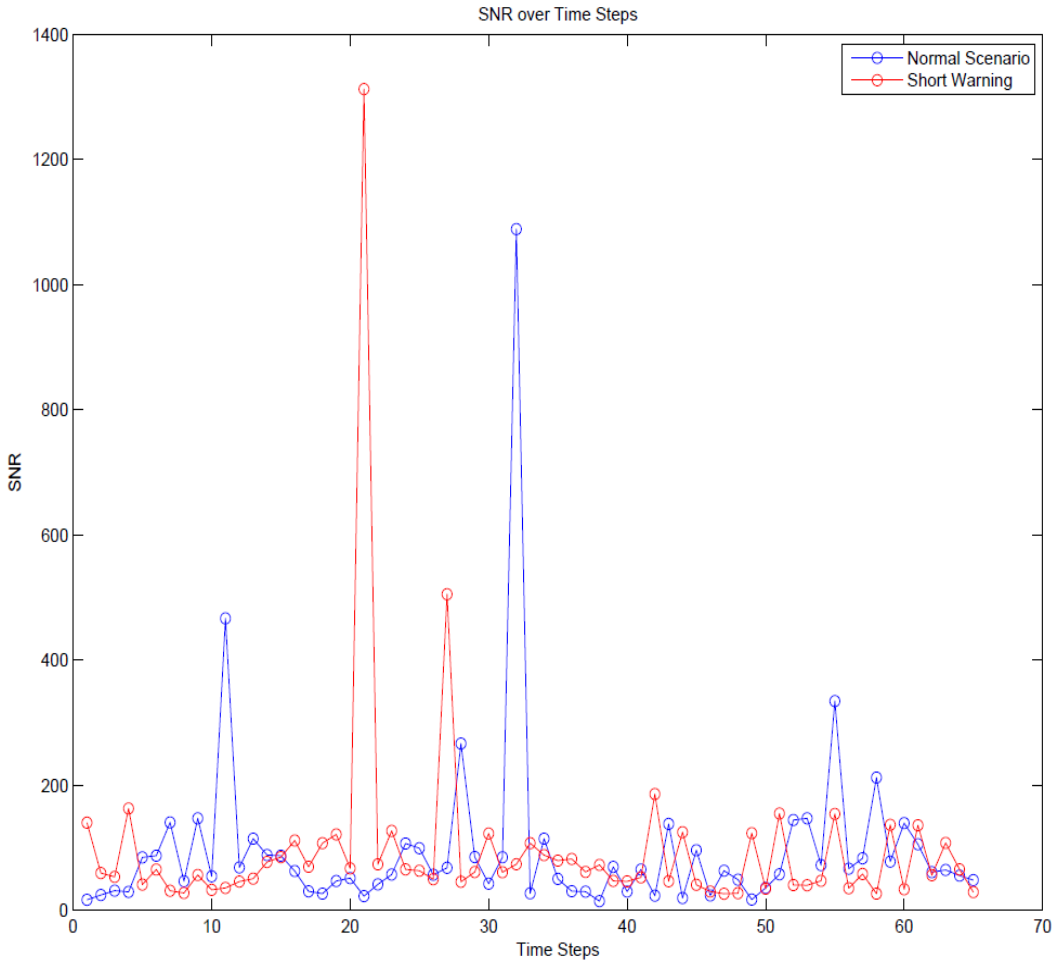

Figure 60. The obtained SNR from the first near collision situation of the subject 22 driving-simulator experiments

The subjects were asked to focus on their driving task during the scenario. Hence, they might not had focused or looked at the LED stimulation-box. Thus, the SSVEP response

(from visual cortex) patterns (the obtained correlation factors and SNRs) are affected by the brain activities in different cortices.

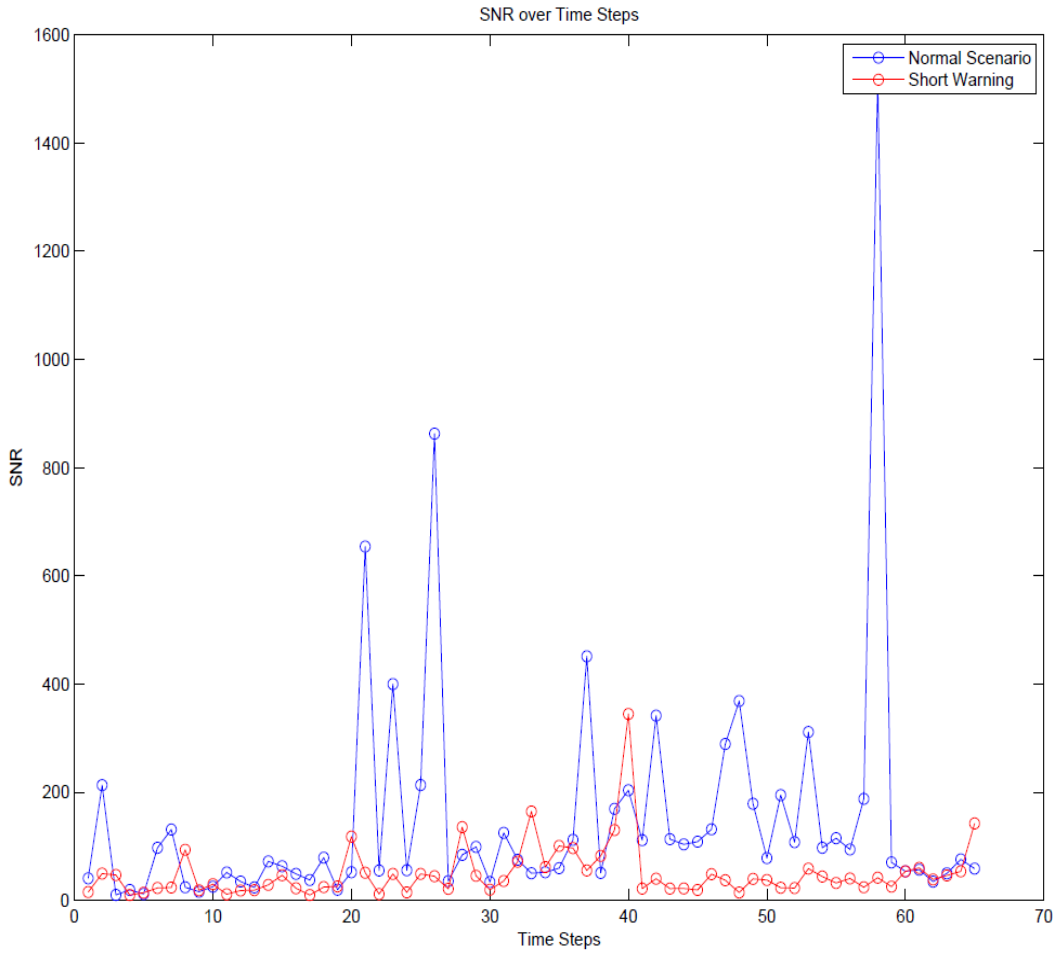

Figure 61. The obtained SNR from the first near collision situation of the subject 22 driving-simulator experiments

However, in this research the final conclusion shouldn't be based on these results because of some drawbacks during the data collections. One major drawback of the experiments is that the EEG recordings and SSVEP stimuli were not internally synched

with car driving-simulator data collector. Although both systems were set to collect samples with 256 Hz rate, but during the analysis procedure data samples from EEG recordings and car driving-simulator were not coinciding with each other. For instance, in some cases, data matrices which were collected from EEG and car-simulator did not have the same number of samples (number of arrays in matrices' rows indicating the total number of collected samples were not equal).

Another major issue of this analysis is caused by corrupted brain signals with artifacts from driving task, limb movements, and measurement noises. Therefore, it should be considered that any conclusion on this matter for determining the SSVEP responses' patterns lay on future and more reliable analysis procedures.

Chapter 6: Conclusions and Future Developments

The research was based on first modifying and modeling analysis algorithms which are independent of training sessions with capability of being employed in future online BCI assistive devices (chapter 3). These methods are evaluated with two data-sets. First data-set was provided by g.TEC which was recorded by 8 EEG channels from visual cortex (figure 27). The second data-set was recorded from 30 healthy subjects aged between 18-65 years old at CISR (chapter 4, section 4.2.1). The analysis methods' evaluation results are presented in chapter 5, section 5.1. The analysis methods are evaluated by average accuracy and ITR as different factors as described in chapter 3 and section 5.1. The outcomes of single SSVEP test sessions which were held before driving scenarios are presented in figure 45. Despite of some subjects' poor performances, many participants reached 50-60 % accuracy rate and ITR of more than 0.6-0.8 bits/trial. This shows promising analysis algorithms for detecting the SSVEP brain signals of subjects who never used a BCI system (subjects were never participated in SSVEP experiments). The analysis methods' evaluation results from g.TEC data-sets show reliability of the introduced methods for employing in online BCIs (subjects were participated in other BCI tests before collecting the g.TEC SSVEP data-sets).

The second purpose was to evaluate drivers' behaviors in presence of SSVEP warning system and to detect the SSVEP responses' patterns (described in chapter 5, sections 5.2 and 5.3). Three different driving scenarios were designed to collect the driving-simulator's data as described in chapter 4, section 4.2.2. The TTC and RD of each driver were

considered (refer to (Eq. 81) and (Eq. 82)) as factors for evaluating the drivers' behaviors. The obtained results show that activating a LED warning system before each near collision situation improves the drivers' reactions. The long warning scenario was designed to evaluate the effect of long-term presence of activated SSVEP stimulus on drivers' behavior. The final results as presented in table 3 and table 2 demonstrate the decrease in total number of crashes for each subject.

Among all of this research purposes, the later was uniquely studied for future online in-vehicle assistant systems. It determined whether we are capable of detecting brain signals patterns' before emergency situations. This can be helpful in cases where activating a BCI system saves critical time needed for drivers to react and prevent crashes. However current results are not completely support the capability of claiming that brain signals activities and SSVEP patterns are detected satisfactorily (near 100 %) as an in-vehicle assistive system.

The higher TTC and longer reaction distances are observed in warning scenarios (figure 51 and figure 53). However, the reaction distances' minimum value in figure 51 for long warning scenario is less than normal driving scenario. This shows that some drivers were probably distracted by long duration of flickering LED stimuli and partially lost their attention. Nevertheless, during the car driving-simulator test sessions many drivers learned that long warning stimuli indicate an upcoming emergency situation. So, they decreased their speed long before (within 5-seconds of warning) near collision situation and their recorded reaction distances and TTCs are less than their normal behavior (figure 53). Since the drivers never had enough time to decrease their speed during the short warning scenario, this conclusion is not completely valid for the short warning scenario. These two

conclusions interpret both figure 51 and figure 53 and demonstrate that having shorter reaction distances and TTCs in long warning scenario is not necessarily caused by drivers' distraction.

6.1 Future Research

The purpose of this research was to detect SSVEP responses with newly modified analysis algorithms. These algorithms are designed with capability of being employed in real-time performances without previous training sessions. Meanwhile, the results which are presented in the last chapter still show that analysis algorithms should be improved for real-time and emergency situations. Likewise, results of fast SSVEP response detection show the necessity for better and more complicated algorithms for determining the visual signals' patterns and detecting the brain activities.

Regardless of far ahead achievements which are still necessary for employing a SSVEP based BCI in vehicles, outcomes of this research show that SSVEP LED stimuli is helpful. The drivers' performances are improved as measured by reaction distances and TTC in both short and long warning scenarios. The analysis algorithms detected the users' intentions on LED stimuli satisfactorily in many cases.

This study experiments and data collection flaws can be improved in the future research. These drawbacks and suggestions for future experiments are listed below:

- LED stimulation-box location was set on steering wheel. The drivers' attention on warning LEDs decreased because of the location and resulted on less accurate SSVEP response detections. For future studies, the LED stimulation-

box should be placed in a suitable location which can be seen completely by the drivers.

- The subjects' age and gender was not considered prior to the experiments. Hence, the effect of these two factors was not evaluated on drivers' behaviors during the car-simulator test sessions.
- The obstacles were not changing randomly during the different scenarios and test sessions. This issue increased the learning process effect on drivers' behaviors which should be resolved for the future studies.
- The data collection devices, car-simulator and EEG, collected the data with 256 Hz sampling rate. However, the car-simulator network was not internally synched with the EEG device. This issue caused an unsynchronized data collection in which both devices' data samples were not coincided. In future research, this problem should be resolved by internally synchronizing the data collection devices.
- The SSVEP response detections algorithms show satisfactory accuracy rates and ITRs. However, the obtained accuracy and ITR results can be improved by more elaborate processing algorithms.

Bibliography

Aapo H. Juha K.,Erkki O. Independent component analysis [Book]. - New York City : J. Wiley, 2001.

Adali T. Haykin S. S. Adaptive Signal Processing: Next Generation Solutions [Book]. - New York City : J. Wiley IEEE Press, 2010.

Allison B. Z. Brunner C.,Kaiser V.,Muller-Putz G. R.,Neuper C.,Pfurtscheller G. Toward a hybrid brain–computer interface based on imagined movement and visual attention [Journal] // J. of Neural Eng.. - 2010. - pp. 1-9.

Alonso N. Fernando L.,Gomez-Gil J. Brain Computer Interfaces, a Review [Journal] // Sensors. - 2012. - pp. 1211-1279.

Bakardjiana H. Tanakaa T.,Cichockia A. Optimization of SSVEP brain responses with application to eight-command Brain–Computer Interface [Journal] // Elsevier. - 2009. - pp. 34-38.

Bell C. J. Shenoy P.,Chalodhorn R.,Rao R. P. N. Control of a humanoid robot by a noninvasive brain–computer interface in humans [Journal] // J. of Neural Eng.. - 2008. - pp. 214-220.

Bießmann V. V. F. Data-driven analysis for multimodal neuroimaging // Thesis. - Berlin : Technischen Universität Berlin, Dec. 7, 2012.

Bin G. Gao X.,Yan Z.,Hong B.,Gao S. An online multi-channel SSVEP-based brain–computer interface using a canonical correlation analysis method [Journal] // J. Neural Eng.. - 2009. - pp. 1-6.

Bin G. Gao X.,Yan Z.,Hong B.,Gao S. An online multi-channel SSVEP-based brain–computer interface using a canonical correlation analysis method [Journal] // J. Neural Eng.. - 2009. - pp. 1-6.

Birbaumer N. Breaking the silence: Brain–computer interfaces (BCI) for communication and motor control [Journal] // Psychophysiology. - 2006. - pp. 517-532.

Blankertz B. Dornhege G.,Krauledat M.,Müller K. R.,Curio G. The non-invasive Berlin Brain–Computer Interface: Fast acquisition of effective performance in untrained subjects [Journal] // Elsevier NeuroImage. - 2007. - pp. 539-550.

Blankertz B. Lemm S.,Kawanabe M.,Müller K. R.,Tomioka R. Optimizing Spatial Filters for Robust EEG Single-Trial Analysis [Journal] // IEEE Signal Processing Magazine. - 2008. - pp. 41-56.

Blankertz B. Tangermann M.,Vidaurre C.,Fazli S.,Sannelli C.,Haufe S.,Maeder C.,Ramsey L.,Sturm I.,Curio G.,Müller K. R. The Berlin brain–computer interface: non-medical uses of BCI technology [Journal] // Frontiers in Neuroscience. - 2010. - pp. 1-17.

Brabanter K. D. Least Squares Support Vector Regression with Applications to Large-Scale Data: a Statistical Approach // Thesis. - Leuven : Katholieke Universiteit Leuven, April 2011.

Brouwer A. M. van Erp J. B. F. A tactile P300 brain-computer interface [Journal] // Frontiers in Neuroscience. - 2010. - pp. 1-11.

Chang C. W. Ko L. W.,Lin F. C.,Su T. P.,Jung T. P.,Lin C. T.,Chiou J. C. Drowsiness Monitoring with EEG-Based MEMS Biosensing Technologies [Journal] // GeroPsych. - 2010. - pp. 107-113.

Chang H. C. Deng H. T., Lee P. L.,Wu C. H.,Shyu K. K. Real-Time Control of an SSVEP-Actuated Remote-Controlled Car [Conference] // SICE Annual Conference. - Taipei, Taiwan : SICE, 2010. - pp. 1884-1887.

Dobriyal M. Brain-Computer Interfaces using SSVEPs // Thesis. - Kingsville : Texas A&M University, May 2011.

Donchin E. Spencer K. M.,R. Wijesinghe The Mental Prosthesis: Assessing the Speed of a P300-Based Brain–Computer Interface [Journal] // IEEE Transactions on Rehabilitation Eng.. - 2000. - pp. 174-179.

DOT Driver Distraction Guidelines US Visual-Manual NHTSA Driver Distraction Guidelines [Report]. - Washington, D.C. : NHTSA, 2010.

DOT Safety Facts US Traffic Safety Facts [Report]. - Washington, D.C. : NHTSA, 2011.

Elitzur A.C. Mersini-Houghton L.,Schlosshauer M.A.,Silverman M.P. Brain-Computer Interfaces: Revolutionizing Human–Computer Interaction [Book]. - Berlin : Springer, 2010.

Friman O. Volosyak I.,Gräser A. Multiple Channel Detection of Steady-State Visual Evoked Potentials for Brain-Computer Interfaces [Journal] // IEEE Transactions on Biomedical Eng.. - 2007. - pp. 742-750.

g.tec Medical and Biomedical company [Online] // g.tec Medical Engineering. - 2013. - 2012. - http://www.gtec.at.

Galan F. Nuttin M.,Lew E.,Ferrez P.W.,Vanacker G.,Philips J.,Millan J. d. R. A brain-actuated wheelchair: Asynchronous and non-invasive Brain–computer interfaces for continuous control of robots [Journal] // Elsevier Clinical NeuroPhysiology. - 2008. - pp. 2159-2169.

Guger C. Allison B. Z.,Großwindhager B.,Prückl R.,Hintermüller C.,Kapeller C.,Bruckner M.,Krausz G.,Edlinger G. How many people could use an SSVEP BCI? [Journal] // Frontiers in Neuroscience. - 2012. - pp. 1-6.

Haufe S. Treder M. S.,Gugler M. F.,Sagebaum M., Curio G.,Blankertz B. EEG potentials predict upcoming emergency brakings during simulated driving [Journal] // J. Neural Eng.. - 2011. - pp. 1-11.

Kimura Y. Tanaka T.,Higashi H.,Morikawa N. SSVEP-Based Brain–Computer Interfaces Using FSK-Modulated Visual Stimuli [Journal] // IEEE Transactions on Biomedical Eng.. - 2013. - pp. 2831-2838.

Lal S. K. L. Craig A. Driver fatigue: Electroencephalography and psychological assessment [Journal] // Psychophysiology. - 2002. - pp. 313-321.

Lattin J. M. Carroll J. D.,Green P. E. Analyzing Multivariate Data [Book]. - Pacific Grove, CA : Thomson Brooks/Cole, 2003.

Lee P. L. Yeh C. L.,Cheng J. Y. S.,Yang C. Y.,Lan G. Y. An SSVEP-Based BCI Using High Duty-Cycle Visual Flicker [Journal] // IEEE Transactions on Biomedical Eng.. - 2011. - pp. 3350-3359.

Legendre L. Legendre P. Numerical Ecology [Book]. - New York City : Elsevier Scientific Pub. Co., 2003.

Liang S. F. Lin C. T.,Wu R. C.,Chen Y. C.,Huang T. Y.,Jung T. P. Monitoring Driver's Alertness Based on the Driving Performance Estimation and the EEG Power Spectrum Analysis [Conference] // Engineering in Medicine and Biology 27th Annual Conference. - Shanghai, China : [s.n.], 2005.

Lin C. T. Wu R. C,Jung T. P.,Liang S. F.,Huang T. Y. Estimating Driving Performance Based on EEG Spectrum Analysis [Journal] // EURASIP Journal on Applied Signal Processing. - 2005. - pp. 3165–3174.

Lin C. T. Wu R. C.,Liang S. F.,Chao W. H.,Chen Y. J.,Jung T. P. EEG-Based Drowsiness Estimation for Safety Driving Using Independent Component Analysis [Journal] // IEEE Transactions on Circuts and Systems. - 2005. - pp. 2726-2738.

Lin Z. Zhang C.,Wu W.,Gao X. Frequency Recognition Based on Canonical Correlation Analysis for SSVEP-Based BCIs [Journal] // IEEE Transactions on Biomedical Eng.. - 2006. - pp. 2610-2614.

Lotze M. Halsband U. Motor imagery [Journal] // Elsevier J. of Physiology. - 2006. - pp. 386-395.

Martinez P. Bakardjian H.,Cichocki A. Fully OnlineMulticommand Brain-Computer Interface with Visual Neurofeedback Using SSVEP Paradigm [Journal] // Hindawi Publishing Corporation Computational Intelligence and Neuroscience. - 2007. - pp. 1-9.

Mason S. G. Birch G. E. A Brain-Controlled Switch for Asynchronous Control Applications [Journal] // IEEE Transactions on Biomedical Eng.. - 2000. - pp. 1297-1307.

Matousek M. Petersen I. A Method for Assessing Alertness Fluctuations from EEG Spectra [Journal] // Electroencephalography and clinical Neurophysiology. - 1983. - pp. 108-113.

Matousek M. Petersen I. A Method for Assessing Alertness Fluctuations from EEG Spectra [Journal] // Elsevier Scientific. - 1983. - pp. 108-113.

Millán J. D. R. Rupp R.,Müller-Putz G. R.,Murray-Smith R.,Giugliemma C.,Tangermann M.,Vidaurre C., Combining brain–computer interfaces and assistive

technologies: state-of-the-art and challenges [Journal] // Frontiers in Neuroscience. - 2010. - pp. 1-15.

Miyajima C. Nishiwaki Y.,Ozawa K.,Wakita T.,Itakura F. Driver Modeling Based on Driving Behavior and Its Evaluation in Driver Identification [Conference] // Proceeding of IEEE. - [s.l.] : IEEE, 2007. - pp. 427-737.

Mulder M. Mulder M., Passen M.,Kitazaki M. V.,Hijikata S. S.,Boer E. R. Reaction-Time Task During Car-Following with an Active Gas Pedal [Conference] // IEEE International Conference on Systems, Man and Cybemetics. - Hague, Netherlands : IEEE, 2004. - pp. 2465-2470.

Müller G. R. Pfurtscheller G. Control of an Electrical Prosthesis With an SSVEP-Based BCI [Journal] // IEEE Transactions on Biomedical Eng.. - 2008. - pp. 361-364.

Nudo R. J. Mechanisms for recovery of motor function following cortical damage [Journal] // Elsevier NeuroBiology. - 2006. - pp. 638-644.

Nunez P. L. Srinivasan R. Electric Fields of the Brain: The Neurophysics of EEG [Book]. - Oxford : Oxford University Press, 2006.

Nunez P.,Srinivasan R. Electric Fields of the Brain: The Neurophysics of EEG [Book]. - Oxford, U.K. : Oxford University Press, 2006.

Obermaier B. Neuper C.,Guger C.,Pfurtscheller G. Information Transfer Rate in a Five-Classes Brain–Computer Interface [Journal] // IEEE Transactions on Neural Systems and Rehabilitation Eng.. - 2001. - pp. 283-288.

Parikh P. Tzanakou E. M. Detecting Drowsiness While Driving Using Wavelet Transform [Journal] // IEEE. - 2004. - pp. 79-80.

Pfurtscheller G. Muller G. R.,Pfurtscheller J.,Gernerd H. J.,Rupp R. 'Thought' – control of functional electrical stimulation to restore hand grasp in a patient with tetraplegia [Journal] // Elsevier Neuroscience Letters. - 2003. - pp. 33-36.

Polich J. Updating P300: An Integrative Theory of P3a and P3b [Journal] // Clin. Neurophysiol.. - 2007. - pp. 2128-2148.

Rau P. S. Drowsy Driver Detection and Warning System for Commercial Vehicle Drivers: Operational Test Design, Data Analysis and Progress [Report]. - Washington, D.C. : NHTSA, 2005.

Rimini-Doering M. Manstetten D.,Altmueller T.,Ladstaetter U.,Mahler M. Monitoring Driver Drowsiness and Stress in a Driving Simulator [Conference] // PROCEEDINGS of the First International Driving Symposium on Human Factors in Driver Assessment, Training and Vehicle Design. - Snowmass Village at Aspen, Colorado, USA : [s.n.], 2001. - pp. 58-63.

Sayed A. H. Adaptive Filters [Book]. - Hoboken, NJ : J. Wiley, 2008.

Sayed A. H. Fundamentals of Adaptive Filtering [Book]. - Hoboken, NJ : J. Wiley, 2002.

Schmidt E. A. et. al Assessing Drivers' Vigilance State during Monotonous Driving [Conference] // Fourth International Driving Symposium on Human Factors in Driver Assessment, Training and Vehicle Design. - Stevenson, Washington : TRB, 2007. - pp. 138-145.

Soudbakhsh D. Development of a Novel Steering Control Collision Avoidance System // Dissertation. - Washington : The George Washington University, March 23, 2011.

Tan D. S. Nijholt A. (Editors) Brain-Computer Interfaces: Applying our Minds to Human-Computer Interaction [Book]. - London, U.K. : Springer, 2010.

Tangermann M. W. Krauledat M.,Grzeska K.,Sagebaum M.,Vidaurre C.,Blankertz B.,Muller K. R. Playing Pinball with non-invasive BCI [Journal] // Neural Information Processing Systems. - Berlin : [s.n.], 2008. - pp. 1-8.

Tavella M. Leeb R.,Rupp R.,Millan J. R. Towards Natural Non-Invasive Hand Neuroprostheses for Daily Living [Conference] // 32nd Annual International Conference of the IEEE EMBS. - Buenos Aires : IEEE EMBS, 2010. - pp. 126-129.

Theodoridis S. Koutroumbas K. Pattern Recognition [Book]. - London, U.K. : Elsevier, 2009.

Vasquez P. M. Bakardjian H.,Vallverdu M.,Cichocki A. Fast Multi-command SSVEP Brain Machine Interface without Training [Journal] // Springer-Artificial Neural Networks. - 2008. - pp. 300-307.

Vural E. Cetin M.,Ercil A.,Littlewort G.,Bartlett M.,Movellan J. Drowsy Driver Detection Through Facial Movement Analysis [Conference] // Proceedings of the 2007 IEEE international conference on Human-computer interaction. - [s.l.] : Springer-Verlag, 2007. - pp. 6-18.

Wang H. Li T,Huang Z. Remote Control of an Electrical Car with SSVEP-Based BCI [Journal] // IEEE. - 2010. - pp. 837-840.

Ward N. S. Cohen L. G. Mechanisms Underlying Recovery of Motor Function After Stroke [Journal] // Arch. Neurological. - 2004. - pp. 1844-1848.

Wolpaw J. R. Jonathan J. R. Brain–computer interfaces as new brain output pathways [Journal] // J. Physiology. - 2007. - pp. 613-619.

Wolpaw J. R. McFarland D. J. Control of a two-dimensional movement signal by a noninvasive brain–computer interface in humans [Journal] // Proceedings of National Academy of Science. - 2004. - pp. 17849–17854.

Wu Y. Yuan H.,Chen H.,Li J. A Study on reaction time Distribution of group drivers at car-following [Conference] // Second International Conference on Intelligent Computation Technology and Automation. - Washington, D.C. : IEEE Computer Society Washington, DC, USA, 2009. - pp. 452-455.

Zhao L. et al. Research on SSVEP Feature Extraction Based on HHT [Conference] // Seventh International Conference on Fuzzy Systems and Knowledge Discovery. - Yantai, China : FSKD, 2010. - pp. 2220-2223.

Appendix A

Data collection and data splitter Matlab code:

Removing outlier digits ±100 μV, (brain signals from evoked potentials have the range of ±70 μV

```
function X=replace(x,k)
%% this replacement function is just being made to remove the EEG
channels recorded the sensory data if it's needed and to replace the
numbers in the last row which are showing the
% SSVEP LED stimulator signal performances to just 0 and 1 values for
% performing or not performing status.....................k=0 means no
change for the sensory channels,k=1 means remove the sensory channels
%% this part is just replacing

[n,m]=size(x);

for j=1:m
    if x(n,j)==0
        x(n,j)=0;
    else
        x(n,j)=1;
    end
end
if k==0
    X=x;
elseif k==1
    X=[x(1:9,:);x(n,:)];
end
```

Selecting the desired time windows

```
function [Xout,IDout]=split4kalman(x,not,npacking,noverlap)
% no overlap needs noverlap=0, other wise percentage of cover
xa=x(2:9,:);
trg=x(10,:);
id=x(11,:)+1;
M=length(trg);
indf=find(trg,1,'first');

trgn=trg(:,indf:M);
Xa=xa(:,indf:M);
id=id(:,indf:M);
%% First Step of separating valuable recorded data from rest times

ri=0;
fi=0;
```

```
ff=0;
rr=0;
for i=0:not-1

j=0;
jj=0;
k=0;
kk=0;
while jj<(j+1)
    if trgn(rr+jj+1)==1
        j=j+1;
        jj=jj+1;
    else
        j=j-1;
        jj=jj;
    end
end

while (kk<(k+1)) && (rr+jj+kk<M-1)
    if   ((rr+jj+kk+1)<54001) && (trgn(rr+jj+kk+1)==0)
        k=k+1;
        kk=kk+1;
    else
        k=k-1;
        kk=kk;
    end
end

if i<not-1
   fi=ri+1;
   ff=(fi-1)+(jj);
   ri=ff+kk;
else
   fi=ri+1;
   ff=(fi-1)+(jj);
end

X=Xa(:,fi:ff);
IND=id(:,fi:ff);
idout1(i+1).id=IND;
Xout1(i+1).X=X;
rr=ff+kk;

end

%% spliting data with decided time-windows
for i=1:not
    xa=Xout1(i).X;
    id=idout1(i).id;
    [m n]=size(xa);
    nn=floor(n/npacking); % by this approximation we are discarding the
rest of trial data from following analysis procedure
```

```
    nloop=((nn-1)*(1/(1-noverlap))+1);
    fi=0;
    ff=0;
  for j=1:nloop
      % for now overlapping is discarded
      fi=npacking*(1-noverlap)*(j-1)+1;
      ff=fi-1+npacking;
      Xout(i,j).X=xa(:,fi:ff);
      IDout(i,j).ID=id(:,fi:ff);
  end

end
```

CCA Matlab code:

```
function
[Xccaout,Aout,Bout,rout,Uout,Vout,statsout,RR,C,I,RRol,Col,Iol,Erate,Er
ateni,Erateol,xtl,wilks,chisq,Ini]=cca4ssvep2(X,ntest,not,npacking,S,no
verlapped)
% cca4ssvep2 is for our data and 1 is for gtec
nn=npacking;
h=npacking/256;
%Xa=X(2:9,1:56320);
[m n]=size(X);
fe=0;
fi=0;
ri=1281; % means that first 10 s was base line activity and
useless0+nn*trest/h+
%% Spliter Call
[Xccaout]=split4kalman(X,not,npacking,noverlapped);


%% Data Analysis for CCA, test Run confirmation


% Creation of STIMULATION Frequencies, first run with 3 harmonics,
stimulus
% are 10, 11, 12, 13 Hz, respectively
t=0.0039*(0:1:(npacking-1));
Yref1=[sin(20*pi*t);cos(20*pi*t);sin(40*pi*t);cos(40*pi*t);sin(60*pi*t)
;cos(60*pi*t)];
%;sin(40*pi*t);cos(40*pi*t);sin(60*pi*t);cos(60*pi*t)
Yref2=[sin(22*pi*t);cos(22*pi*t);sin(44*pi*t);cos(44*pi*t);sin(66*pi*t)
;cos(66*pi*t)];
%;sin(44*pi*t);cos(44*pi*t);sin(66*pi*t);cos(66*pi*t)
Yref3=[sin(24*pi*t);cos(24*pi*t);sin(48*pi*t);cos(48*pi*t);sin(72*pi*t)
;cos(72*pi*t)];
%;sin(48*pi*t);cos(48*pi*t);sin(72*pi*t);cos(72*pi*t)
Yref4=[sin(26*pi*t);cos(26*pi*t);sin(52*pi*t);cos(52*pi*t);sin(78*pi*t)
;cos(78*pi*t)];
%;sin(52*pi*t);cos(52*pi*t);sin(78*pi*t);cos(78*pi*t)
Yref(1).Yref=Yref1;
Yref(2).Yref=Yref2;
Yref(3).Yref=Yref3;
Yref(4).Yref=Yref4;


if S==1
    nloop=ntest;
elseif S==2
    nloop=((ntest-1)*(1/(1-noverlapped))+1);
end
[nnn,Wn]=cheb1ord([9.9 13.1]/256,[9.5 13.5]/256,1,60);
```

```
[b,a] = cheby1(nnn,1,Wn);

for i=1:20
    for j=1:nloop
        Xccain1=Xccaout(i,j).X;
      %  Xccain2=amuse(Xccain1);
       % Xccain21=sgolayfilt(Xccain2',ntest-2,npacking-1)';
        Xcca = filter(b,a,Xccain1);
        for k=1:4
[AA,BB,rr,UU,VV,statss]=canoncorr(Xcca',Yref(k).Yref');

        A(k).A=AA;
        B(k).B=BB;
        r(k).r=rr;
        U(k).U=UU;
        V(k).V=VV;
        stats(k).stats=statss;

        end
        Aout(i,j).A=A;
        Bout(i,j).B=B;
        rout(i,j).r=r;
        Uout(i,j).U=U;
        Vout(i,j).V=V;
        statsout(i,j).stats=stats;
    end
end

%% Printing r of 4 stimulus
RR=zeros(4,(20*nloop));  %number of total tests
for i=1:20
    for j=1:nloop
        for k=1:4
            RR(k,((i-1)*nloop+j))=max(abs(rout(i,j).r(1,k).r));
        end
    end
end
Xaxis=[1:1:length(RR)];
%************************************************************************
************************************************************************
*************************
nw=num2str(npacking); %?????????????????????????????????? plot 1
canonical correlation coeff.
subplot(4,1,1), plot(Xaxis,RR(1,:),'-ob')
ylabel('Correlation Coeff.')
xlabel('time steps,sampling rate: 256 Hz')
title('Canonical Correlation, 10 Hz')
subplot(4,1,2), plot(Xaxis,RR(2,:),'--sg')
ylabel('Correlation Coeff.')
xlabel('time steps,sampling rate: 256 Hz')
title('Canonical Correlation, 11 Hz')
subplot(4,1,3), plot(Xaxis,RR(3,:),'--*r')
```

```
ylabel('Correlation Coeff.')
xlabel('time steps,sampling rate: 256 Hz')
title('Canonical Correlation, 12 Hz')
subplot(4,1,4), plot(Xaxis,RR(4,:),'-.+c')
ylabel('Correlation Coeff.')
xlabel('time steps,sampling rate: 256 Hz')
title('Canonical Correlation, 13 Hz')

%% Detection of Intention, Error Rate computation
% process is simple and has no statistical test
% I vector indicates which row or here which frequency has the max
% correlation.
%************************************************************************
************************************************************************
*************************
% this means I vector pointing at user intention
[C,I]=max(RR,[],1);
%figure
%plot(Xaxis,I)
%ylabel('Max Index NO.')
%xlabel('Test set')
%title('Cmd evaluation')

%************************************************************************
************************************************************************
*************************
% calculating overlapped RR matrix (RRol is smoothed Covariance matrix
for
% every signal and test set)

RRol=zeros(4,(20*nloop));  %number of total tests
for i=1:20
    for j=1:2
    for k=1:4
    RRol(k,((i-1)*nloop+j))=RR(k,((i-1)*nloop+j));
    end
    end
end
for i=1:20
    for j=3:nloop
        for k=1:4
            RRol(k,((i-1)*nloop+j))=mean(RR(k,((i-1)*nloop+j-2):((i-
1)*nloop+j)));
        end
    end
end
%************************************************************************
************************************************************************
*************************
%%%%%%%%%%%%%%%%%%%%%%%%%%%%%%%%%%%%%%%%%%%%%%%%%%%%%%%%%%%%%%%%%%%%%%%
% plot 2 smoothed correlation coeff.
figure
subplot(4,1,1), plot(Xaxis,RRol(1,:),'-ob')
```

```
ylabel('Correlation Coeff. Factor')
xlabel('Sampling rate: 256 Hz')
title('Canonical Correlation, 10 Hz')
subplot(4,1,2), plot(Xaxis,RRol(2,:),'--sg')
ylabel('Correlation Coeff. Factor')
xlabel('Sampling rate: 256 Hz')
title('Canonical Correlation, 11 Hz')
subplot(4,1,3), plot(Xaxis,RRol(3,:),'--*r')
ylabel('Correlation Coeff. Factor')
xlabel('Sampling rate: 256 Hz')
title('Canonical Correlation, 12 Hz')
subplot(4,1,4), plot(Xaxis,RRol(4,:),'-.+c')
ylabel('Correlation Coeff. Factor')
xlabel('Sampling rate: 256 Hz')
title('Canonical Correlation, 13 Hz')
%**************************************************************************
**************************************************************************
**************************
% printing user intention based on overlapped RR (smoothed correlation
% coeff.
[Col,Iol]=max(RRol,[],1);
%figure
%plot(Xaxis,Iol)
%ylabel('Max Index NO. with smth Corr. Coeff.')
%xlabel('Test set')
%title('Cmd evaluation by MA filter RR')
%% Finding every test trial error rate

% flickering test protocol based on gSTIMbox
xtl=zeros(1,length(I));
ffi=0;
ffe=0;
for i=1:5
for k=1:4
   ffi=((k-1)+4*(i-1))*(nloop)+1;
   ffe=(ffi-1)+(nloop);
   xtl(1,ffi:ffe)=k*ones(1,nloop);
end
end
%xtl(1,1:125)=ones(1,125);
%xtl(1,126:250)=2*ones(1,125);
%xtl(1,251:375)=3*ones(1,125);
%xtl(1,376:500)=4*ones(1,125);

E=zeros(1,length(I));
Eol=zeros(1,length(Iol));

for j=1:20*nloop
    E(1,j)=isequal(I(1,j),xtl(1,j));
end

for j=1:20*nloop
```

```
    Eol(1,j)=isequal(Iol(1,j),xtl(1,j));
end


ffi=0;
ffe=0;
Erate=zeros(1,20);
for i=1:20
    ffi=(i-1)*nloop+1;
    ffe=ffi-1+nloop;
    Erate(i)=((sum(E(ffi:ffe))/nloop)*100);
end

ffii=0;
ffee=0;
Erateol=zeros(1,20);
for i=1:20
    ffii=(i-1)*nloop+1;
    ffee=ffii-1+nloop;
    Erateol(i)=((sum(Eol(ffii:ffee))/nloop)*100);
end


Xaxis=[1:1:length(Erate)];
%%%%%%%%%%%%%%%plot 3 Error rate without considering smoothed Canonical
%%%%%%%%%%%%%%%correlation coeff.
figure
plot(Xaxis,Erate)
ylabel('AVERAGE ACCURACY RATE %')
xlabel('Test set')
title('accuracy evaluation of each trial')
%%%%%%%%%%%%%%%plot 4 Error rate with considering smoothed Canonical
%%%%%%%%%%%%%%%correlation coeff.
Xaxis=[1:1:length(Erateol)];
figure
plot(Xaxis,Erateol)
ylabel('ERAVERAGE ACCURACY RATE %')
xlabel('Test set')
title('accuracy evaluation of each trial with smoothed Canonical
Correlation Coeff.')

%% evaluation test by wilks and chisq criteria
% finding wilks criteria for each test run and min value
wilks=zeros(4,(20*nloop));  %number of total tests
for i=1:20
    for j=1:nloop
        for k=1:4
            wilks(k,((i-
1)*nloop+j))=min(abs(statsout(i,j).stats(1,k).stats.Wilks));
        end
    end
end
```

```
% finding chisq criteria for each test run and max value
chisq=zeros(4,(20*nloop));  %number of total tests
for i=1:20
    for j=1:nloop
        for k=1:4
            chisq(k,((i-
1)*nloop+j))=max(abs(statsout(i,j).stats(1,k).stats.chisq));
        end
    end
end

% finding the index of mostly correlated data by statistic test
[Cwilks,Iwilks]=min(wilks,[],1);
[Cchisq,Ichisq]=max(chisq,[],1);

% new indexing criteria by test confirmation

Ini=zeros(1,length(Iol));
for i=1:20*nloop
    if isequal(Iwilks(i),Ichisq(i))==1
        Ini(i)=Iwilks(i);
    elseif isequal(Iwilks(i),Ichisq(i))==0
        if Cwilks<0.2
         Ini(i)=Iwilks(i);
        elseif Cwilks>=0.2
            Ini(i)=Ichisq(i);
        end
    end
end

for i=1:20*nloop
    if isequal(Iol(i),Ini(i))==1
        Ini(i)=Iol(i);
    else
        Ini(i)=Ini(i);
    end
end

eni=zeros(1,length(Ini));

for j=1:20*nloop
    eni(1,j)=isequal(Ini(1,j),xtl(1,j));
end
Erateni=zeros(1,20);

ffni=0;
ffne=0;
for i=1:20
    ffni=(i-1)*nloop+1;
    ffne=ffni-1+nloop;
    Erateni(i)=((sum(eni(ffni:ffne))/nloop)*100);
```

```
end

%plot 5 the Error rate under consideration of evaluation test
Xaxis=[1:1:length(Erateni)];
figure
plot(Xaxis,Erateni)
ylabel('AVERAGE ACCURACY RATE %')
xlabel('Test set')
title('accuracy evaluation of each trial with considering evaluation
test')
% for later Excel use
Erate=Erate';
Erateni=Erateni';
Erateol=Erateol';
RR=RR';
RRol=RRol';

%% calculating ITR
% B=log2(N)+plog2(p)+(1-p)*log2((1-p)/(N-1)), B=bits/trial and for each
% in each test npacking/256*60*1/(1-noverlap) multiple by B results in
% bits/min ITR
% ITR for each method calculated
```

Co-Inertia Matlab code:

```
function [Fx,Fy,c,d]=Xcoinertia2(X,Y)
% this m file operates the coinertia analysis on every two data
matrices
% that recieves.
% X(n*p1) and Y(n*p2) are two datasets, n is observation no. and p1 &
p2
% are no. of variants for each matrix respectively,
%
%%Coinertia analysis preparation
if nargin < 2
    disp('message:(stats:canoncorr:TooFewInputs)');
end

[n,p1] = size(X);
if size(Y,1) ~= n
    disp('message:(stats:canoncorr:InputSizeMismatch');
elseif n == 1
    disp('message:(stats:canoncorr:NotEnoughData)');
end
p2 = size(Y,2);
% performing FIR1 bandpass filter with Savitzky-Golay window function




% calculating centred matrices,

xc = X - repmat(mean(X,1), n, 1);
yc = Y - repmat(mean(Y,1), n, 1);
% finding the max no. of co-inertia axes that data should be objected
on

cov12=(1/(n-1))*xc'*yc;
cc=min(rank(xc),rank(yc));
covv=cov12'*cov12;
[V U]=eig(covv);
crank=nnz(diag(U));

if cc<=crank
    c=cc;
else
    c=crank;
end
% computing the objected matrices

[L,W,M] = svds(cov12,c);
% diag. matrix of eigenvalues
```

```
D=W^2;

F1=normc(xc*L);
Fx=(sqrt(n-1)*F1)*D^(1/2);
F2=normc(yc*M);
Fy=(sqrt(n-1)*F2)*D^(1/2);
% calculating the objected distances based on mahalanobis distance
dd=pdist2(Fy,Fx);
d=diag(dd);
```

Adaptive Kalman filter

```
function [cfout,Sout,Vout]=kal4ssvep2(Xout,L,lamda,npack)
% performing Kalman filter modified for Exponentially weighted RLS
filter
% of order L, forgetting factor lamda less than 1, npack is the time
steps
% in each data pack, not is the total number of trial for each EEG test
% matrix x


[m n]=size(Xout);
%%
%%
            t=0.0039*(1:1:npack);

xref1=[sin(20*pi*t);cos(20*pi*t);sin(40*pi*t);cos(40*pi*t);sin(60*pi*t)
;cos(60*pi*t)]';
            %;sin(40*pi*t);cos(40*pi*t);sin(60*pi*t);cos(60*pi*t)

xref2=[sin(22*pi*t);cos(22*pi*t);sin(44*pi*t);cos(44*pi*t);sin(66*pi*t)
;cos(66*pi*t)]';
            %;sin(44*pi*t);cos(44*pi*t);sin(66*pi*t);cos(66*pi*t)

xref3=[sin(24*pi*t);cos(24*pi*t);sin(48*pi*t);cos(48*pi*t);sin(72*pi*t)
;cos(72*pi*t)]';
            %;sin(48*pi*t);cos(48*pi*t);sin(72*pi*t);cos(72*pi*t)

xref4=[sin(26*pi*t);cos(26*pi*t);sin(52*pi*t);cos(52*pi*t);sin(78*pi*t)
;cos(78*pi*t)]';
            %;sin(52*pi*t);cos(52*pi*t);sin(78*pi*t);cos(78*pi*t)
            xref(1).xref=xref1;
            xref(2).xref=xref2;
            xref(3).xref=xref3;
            xref(4).xref=xref4;
%%
%%
%[nnn,Wn]=cheb1ord([9.9 13.1]/256,[9.5 13.5]/256,1,60);
%[b,a] = cheby1(nnn,1,Wn);
for i=1:m
    for j=1:n
        for jj=1:4
            hs=Xout(i,j).X';
            %hs=amuse(hhs')';
            %hs = filter(b,a,hhs)';
            [mmm nnn]=size(hs);
            % setting up the initial values
            cf=0;
            re=0;
            Kp=zeros(nnn*L,1);
            v=zeros(1,6);
```

```
            % mmm time steps of each channel nnn
            p=(lamda^-1)*eye(nnn*L,nnn*L);
            x=zeros(nnn*L,6);
            x0=zeros(nnn*L,6);
            U=zeros(mmm,nnn*L);
            for ii=1:mmm
                 % creating input matrix U 1*(nnn*L) at each time frame
with p
                 % channels data of L overlap of time
                %%%%%%%%%%%%%%%%%%%%%%%%%%%%%%%%%%%%%%%%%%%%%%%%
                for k=1:nnn
                for kk=1:L
                    if ii-kk>=0
                    U(ii,(k-1)*L+kk)=hs((ii-kk+1),k);
                    else
                        U(ii,(k-1)*kk+kk)=0;
                    end
                end
                end
                %%%%%%%%%%%%%%%%%%%%%%%%%%%%%%%%%%%%%%%%%%%%%%%%
                re=1+U(ii,:)*p*U(ii,:)';
                Kp=(lamda^-0.5)*p*U(ii,:)'/re;
                v=(lamda^-1)*xref(jj).xref(ii,:)-(U(ii,:)*x);
                x=(lamda^-0.5)*x+Kp*v;
                p=(lamda^-1)*(p-
((p*U(ii,:)'*U(ii,:)*p)/(1+U(ii,:)*p*U(ii,:)')));
                x0=(lamda^(0.5*(ii+1)))*x;
                cf=lamda*cf+(v*v')/re;
                cfout(i,j).cf(ii,jj)=cf;
                Sout(i,j).Sf(1,jj).Sf(ii,:)=U(ii,:)*x0*(lamda^(-
0.5*(ii+1)));
                Vout(i,j).Vf(1,jj).Vf(ii,:)=v;

            end
        end
    end
end
```

Adaptive robust Gauss-Newton filter

```
function [Sout,Vout]=gn4ssvep(Xout,L,gamma,npack)
% performing Kalman filter modified for Exponentially weighted RLS
filter
% of order L, forgetting factor lamda less than 1, npack is the time
steps
% in each data pack, not is the total number of trial for each EEG test
% matrix x


[m n]=size(Xout);
%%
%%
            t=0.0039*(1:1:npack);

xref1=[sin(20*pi*t);cos(20*pi*t);sin(40*pi*t);cos(40*pi*t);sin(60*pi*t)
;cos(60*pi*t)]';
            %;sin(40*pi*t);cos(40*pi*t);sin(60*pi*t);cos(60*pi*t)

xref2=[sin(22*pi*t);cos(22*pi*t);sin(44*pi*t);cos(44*pi*t);sin(66*pi*t)
;cos(66*pi*t)]';
            %;sin(44*pi*t);cos(44*pi*t);sin(66*pi*t);cos(66*pi*t)

xref3=[sin(24*pi*t);cos(24*pi*t);sin(48*pi*t);cos(48*pi*t);sin(72*pi*t)
;cos(72*pi*t)]';
            %;sin(48*pi*t);cos(48*pi*t);sin(72*pi*t);cos(72*pi*t)

xref4=[sin(26*pi*t);cos(26*pi*t);sin(52*pi*t);cos(52*pi*t);sin(78*pi*t)
;cos(78*pi*t)]';
            %;sin(52*pi*t);cos(52*pi*t);sin(78*pi*t);cos(78*pi*t)
            xref(1).xref=xref1;
            xref(2).xref=xref2;
            xref(3).xref=xref3;
            xref(4).xref=xref4;
%%
%%
%[nnn,Wn]=cheb1ord([9.9 13.1]/256,[9.5 13.5]/256,1,60);
%[b,a] = cheby1(nnn,1,Wn);
for i=1:m
    for j=1:n
        for jj=1:4
            hs=Xout(i,j).X';
            %hs=amuse(hhs')';
            %hs = filter(b,a,hhs)';
            [mmm nnn]=size(hs);
            % setting up the initial values
            % mmm time steps of each channel nnn
            p=(gamma^-1)*eye(nnn*L,nnn*L);
            w=zeros(nnn*L,6);
            pbar=zeros(nnn*L,nnn*L);
```

```
            Pb=zeros(nnn*L,nnn*L);
            U=zeros(mmm,nnn*L);
            for ii=1:mmm
                 % creating input matrix U 1*(nnn*L) at each time frame
with p
                 % channels data of L overlap of time
                %%%%%%%%%%%%%%%%%%%%%%%%%%%%%%%%%%%%%%%%%%%%%%%%
                for k=1:nnn
                for kk=1:L
                    if ii-kk>=0
                    U(ii,(k-1)*L+kk)=hs((ii-kk+1),k);
                    else
                        U(ii,(k-1)*kk+kk)=0;
                    end
                end
                end
                %%%%%%%%%%%%%%%%%%%%%%%%%%%%%%%%%%%%%%%%%%%%%%%%
                Pb=inv(p)-(gamma)^(-2)*U(ii,:)'*U(ii,:);
                pbar=inv(Pb);

w=w+((pbar*U(ii,:)')/(1+(U(ii,:)*pbar*U(ii,:)')))*(xref(jj).xref(ii,:)-
(U(ii,:)*w));
                p=p-((p*U(ii,:)'*U(ii,:)*p)/((1-gamma^-2)^-
1+(U(ii,:)*p*U(ii,:)')));
                Sout(i,j).Sf(1,jj).Sf(ii,:)=U(ii,:)*w;
                Vout(i,j).Vf(1,jj).Vf(ii,:)=(xref(jj).xref(ii,:)-
(U(ii,:)*w));

            end
        end
    end
end
```

Adaptive unconstrained DFT filter

```
function
[Xout1,U2bnout,lamdaout,Dbar,Ebar]=dftblock4ssvep(Xout,B,M,beta,mu,nove
rlap)
%% spliting data with decided time-windows
[m n]=size(Xout);
R=(M/B);
for I=1:n
    xa=Xout(I).X;
    [mm nn]=size(xa);
    N=floor(nn/B); % by this approximation we are discarding the rest
of trial data from following analysis procedure
    nloop=((N-1)*(1/(1-noverlap))+1);
    fi=0;
    ff=0;
  for J=1:nloop
      % for now overlapping is discarded
      fi=B*(1-noverlap)*(J-1)+1;
      ff=fi-1+B;
      Xout1(I,J).X=xa(:,fi:ff)';
  end
end
%% Creating the F transform matrix
F=dftmtx(2*B);
% F=zeros(2*B,2*B);
% for ii=1:(2*B)
%     for jj=1:(2*B)
%         F(ii,jj)=exp((-1i*2*pi*((ii-1)*(jj-1)))/(2*B));
%     end
% end

%% creating the U'2B,N and computing lamda matrix
for ii=1:n
    for jj=1:nloop
        for jjj=1:mm
            for iii=1:2*B
                lamdaout(ii,jj).lamda(iii,jjj)=0;
            end
        end
    end
    for jj=2:nloop
        X0=Xout1(ii,jj-1).X;
        X1=Xout1(ii,jj).X;
        %U2bn=F*[X1;X0];
        U2bn=fft([X1;X0]);
        [k,p]=size(U2bn);
        for jjj=1:p
            for iii=1:k
                lamda(iii,jjj)=(beta*(lamdaout(ii,jj-
1).lamda(iii,jjj)))+((1-beta)*(abs(U2bn(iii,jjj))^2));
```

```
            end
        end
        U2bnout(ii,jj-1).U2bn=U2bn;
        lamdaout(ii,jj).lamda=lamda;
    end
end

%% Creating the LED signals
            t=0.0039*(1:1:B);

xref1=[sin(20*pi*t);cos(20*pi*t);sin(40*pi*t);cos(40*pi*t);sin(60*pi*t)
;cos(60*pi*t)]';
            %;sin(40*pi*t);cos(40*pi*t);sin(60*pi*t);cos(60*pi*t)

xref2=[sin(22*pi*t);cos(22*pi*t);sin(44*pi*t);cos(44*pi*t);sin(66*pi*t)
;cos(66*pi*t)]';
            %;sin(44*pi*t);cos(44*pi*t);sin(66*pi*t);cos(66*pi*t)

xref3=[sin(24*pi*t);cos(24*pi*t);sin(48*pi*t);cos(48*pi*t);sin(72*pi*t)
;cos(72*pi*t)]';
            %;sin(48*pi*t);cos(48*pi*t);sin(72*pi*t);cos(72*pi*t)

xref4=[sin(26*pi*t);cos(26*pi*t);sin(52*pi*t);cos(52*pi*t);sin(78*pi*t)
;cos(78*pi*t)]';
            %;sin(52*pi*t);cos(52*pi*t);sin(78*pi*t);cos(78*pi*t)
            xref(1).xref=xref1;
            xref(2).xref=xref2;
            xref(3).xref=xref3;
            xref(4).xref=xref4;
%%       after computing the lamda matrix we are preparing the buffered
        % data
        % M is the filter order and R=M/B is the size of buffered
vector
        % for each element
        % configuring the buffered matrix of U'k,n
     % null assumption on Lckn matrix
     for ll=1:2*B
        Lckn(ll).Lckn=zeros((R*p),6);
        %Lkn1(ll).Lkn1=zeros((R*p),6);
        Lkn(ll).Lkn=zeros((R*p),6);
     end


 for ii=1:n

     for jj=1:nloop-1
         for K=1:4

         Ukn=zeros((2*B),(R*p));
         for iii=1:R
             if (jj-iii+1)>0
                 U(iii).U=U2bnout(ii,(jj-iii+1)).U2bn;
```

```
            else
                U(iii).U=zeros((2*B),(p));
            end
        end
        for iii=1:p
            for jjj=1:R
                Ukn(:,(jjj+(iii-1)*R))=U(jjj).U(:,iii);
            end
        end

        % finding the y'k,n matrix of 2B*q
        for k=1:(2*B)
        Ykn(k,:)=Ukn(k,:)*Lckn(k).Lckn;
        % Ykn(k,:)=Ykn1;
        end
        %Dbarbn=[eye(B),zeros(B)]*inv(F)*Ykn;
        Dbarbn=[eye(B),zeros(B)]*ifft(Ykn);
        Ebn=xref(K).xref-Dbarbn;
        %E2bn=F*[eye(B);zeros(B)]*Ebn;
        E2bn=fft([eye(B);zeros(B)]*Ebn);

        % configuring the Lkn matrix for each EEG and LED
        % channel

        % for each of p channels:
        for kk=1:(2*B)
            %Lkn=0;
            % for each time step of 2B in a block
            for k=1:p
                %Lkn1=0;
                for hh=1:R
                    if ((jj+1)-(hh-1))>1
                        Lkn(kk).Lkn((((k-
1)*R)+hh),:)=Lkn(kk).Lkn((((k-1)*R)+hh),:)+((mu/(lamdaout(ii,((jj+1)-
(hh-1))).lamda(kk,k)))*(Ukn(kk,(((k-1)*R)+hh)))'*E2bn(kk,:));
                        %Lkn(kk).Lkn(((k-
1)*R+1):(k*R),:)=Lkn(kk).Lkn(((k-
1)*R+1):(k*R),:)+((mu/(lamdaout(ii,jj+1).lamda(kk,k)))*(Ukn(kk,((k-
1)*R+1):(k*R)))'*E2bn(kk,:));
                    else
                        Lkn(kk).Lkn((((k-
1)*R)+hh),:)=Lkn(kk).Lkn((((k-1)*R)+hh),:);
                    end

                end
                %Lkn(kk).Lkn()=Lkn1(kk).Lkn1;
            end

        end

        % configuring the Lckn matrix for each channel of EEG and LED
        % for each of q channels, q=6
```

```
            for k=1:6
                LKN=zeros((2*B),(R*p));
                LCKN=zeros((2*B),(R*p));
                for kk=1:2*B
                    LKN(kk,:)=Lkn(kk).Lkn(:,k)';
                end
                %LCKN=inv(F)*[eye(B),zeros(B);zeros(B),zeros(B)]*F*LKN;
                LCKN=ifft([eye(B),zeros(B);zeros(B),zeros(B)]*fft(LKN));
                for kk=1:2*B
                    Lckn(kk).Lckn(:,k)=LCKN(kk,:)';
                end
            end
            % configureing the final Dbar and Error Matrices for each LED
frequency

            %Dbar=zeors(n,nloop-1);
            %Ebar=zeors(n,nloop-1);
            Dbar(ii).Dbar(K).Dbar(:,((jj-1)*B+1):jj*B)=Dbarbn';
            Ebar(ii).Ebar(K).Ebar(:,((jj-1)*B+1):jj*B)=Ebn';
            end
        end
    end
```

Decision making methods:

SSVEP response detection for Kalman filter:

```
function
[Xout1,U2bnout,lamdaout,Dbar,Ebar]=dftblock4ssvep(Xout,B,M,beta,mu,nove
rlap)
%% spliting data with decided time-windows
[m n]=size(Xout);
R=(M/B);
for I=1:n
    xa=Xout(I).X;
    [mm nn]=size(xa);
    N=floor(nn/B); % by this approximation we are discarding the rest
of trial data from following analysis procedure
    nloop=((N-1)*(1/(1-noverlap))+1);
    fi=0;
    ff=0;
  for J=1:nloop
      % for now overlapping is discarded
      fi=B*(1-noverlap)*(J-1)+1;
      ff=fi-1+B;
      Xout1(I,J).X=xa(:,fi:ff)';
  end
end
%% Creating the F transform matrix
F=dftmtx(2*B);
% F=zeros(2*B,2*B);
% for ii=1:(2*B)
%     for jj=1:(2*B)
%         F(ii,jj)=exp((-1i*2*pi*((ii-1)*(jj-1)))/(2*B));
%     end
% end

%% creating the U'2B,N and computing lamda matrix
for ii=1:n
    for jj=1:nloop
        for jjj=1:mm
            for iii=1:2*B
                lamdaout(ii,jj).lamda(iii,jjj)=0;
            end
        end
    end
    for jj=2:nloop
        X0=Xout1(ii,jj-1).X;
        X1=Xout1(ii,jj).X;
        %U2bn=F*[X1;X0];
        U2bn=fft([X1;X0]);
        [k,p]=size(U2bn);
        for jjj=1:p
```

```
            for iii=1:k
                lamda(iii,jjj)=(beta*(lamdaout(ii,jj-
1).lamda(iii,jjj)))+((1-beta)*(abs(U2bn(iii,jjj))^2));
            end
        end
        U2bnout(ii,jj-1).U2bn=U2bn;
        lamdaout(ii,jj).lamda=lamda;
    end
end

%% Creating the LED signals
            t=0.0039*(1:1:B);

xref1=[sin(20*pi*t);cos(20*pi*t);sin(40*pi*t);cos(40*pi*t);sin(60*pi*t)
;cos(60*pi*t)]';
            %;sin(40*pi*t);cos(40*pi*t);sin(60*pi*t);cos(60*pi*t)

xref2=[sin(22*pi*t);cos(22*pi*t);sin(44*pi*t);cos(44*pi*t);sin(66*pi*t)
;cos(66*pi*t)]';
            %;sin(44*pi*t);cos(44*pi*t);sin(66*pi*t);cos(66*pi*t)

xref3=[sin(24*pi*t);cos(24*pi*t);sin(48*pi*t);cos(48*pi*t);sin(72*pi*t)
;cos(72*pi*t)]';
            %;sin(48*pi*t);cos(48*pi*t);sin(72*pi*t);cos(72*pi*t)

xref4=[sin(26*pi*t);cos(26*pi*t);sin(52*pi*t);cos(52*pi*t);sin(78*pi*t)
;cos(78*pi*t)]';
            %;sin(52*pi*t);cos(52*pi*t);sin(78*pi*t);cos(78*pi*t)
            xref(1).xref=xref1;
            xref(2).xref=xref2;
            xref(3).xref=xref3;
            xref(4).xref=xref4;
%%       after computing the lamda matrix we are preparing the buffered
        % data
        % M is the filter order and R=M/B is the size of buffered
vector
        % for each element
        % configuring the buffered matrix of U'k,n
     % null assumption on Lckn matrix
     for ll=1:2*B
        Lckn(ll).Lckn=zeros((R*p),6);
        %Lkn1(ll).Lkn1=zeros((R*p),6);
        Lkn(ll).Lkn=zeros((R*p),6);
     end


 for ii=1:n

     for jj=1:nloop-1
         for K=1:4

         Ukn=zeros((2*B),(R*p));
```

```
            for iii=1:R
                if (jj-iii+1)>0
                    U(iii).U=U2bnout(ii,(jj-iii+1)).U2bn;
                else
                    U(iii).U=zeros((2*B),(p));
                end
            end
            for iii=1:p
                for jjj=1:R
                    Ukn(:,(jjj+(iii-1)*R))=U(jjj).U(:,iii);
                end
            end

            % finding the y'k,n matrix of 2B*q
            for k=1:(2*B)
            Ykn(k,:)=Ukn(k,:)*Lckn(k).Lckn;
            % Ykn(k,:)=Ykn1;
            end
            %Dbarbn=[eye(B),zeros(B)]*inv(F)*Ykn;
            Dbarbn=[eye(B),zeros(B)]*ifft(Ykn);
            Ebn=xref(K).xref-Dbarbn;
            %E2bn=F*[eye(B);zeros(B)]*Ebn;
            E2bn=fft([eye(B);zeros(B)]*Ebn);

            % configuring the Lkn matrix for each EEG and LED
            % channel

            % for each of p channels:
            for kk=1:(2*B)
                %Lkn=0;
                % for each time step of 2B in a block
                for k=1:p
                    %Lkn1=0;
                    for hh=1:R
                        if ((jj+1)-(hh-1))>1
                            Lkn(kk).Lkn((((k-
1)*R)+hh),:)=Lkn(kk).Lkn((((k-1)*R)+hh),:)+((mu/(lamdaout(ii,((jj+1)-
(hh-1))).lamda(kk,k)))*(Ukn(kk,(((k-1)*R)+hh)))'*E2bn(kk,:));
                            %Lkn(kk).Lkn(((k-
1)*R+1):(k*R),:)=Lkn(kk).Lkn(((k-
1)*R+1):(k*R),:)+((mu/(lamdaout(ii,jj+1).lamda(kk,k)))*(Ukn(kk,((k-
1)*R+1):(k*R)))'*E2bn(kk,:));
                        else
                            Lkn(kk).Lkn((((k-
1)*R)+hh),:)=Lkn(kk).Lkn((((k-1)*R)+hh),:);
                        end

                    end
                    %Lkn(kk).Lkn()=Lkn1(kk).Lkn1;
                end

            end
```

```
        % configuring the Lckn matrix for each channel of EEG and LED
        % for each of q channels, q=6
        for k=1:6
            LKN=zeros((2*B),(R*p));
            LCKN=zeros((2*B),(R*p));
            for kk=1:2*B
                LKN(kk,:)=Lkn(kk).Lkn(:,k)';
            end
            %LCKN=inv(F)*[eye(B),zeros(B);zeros(B),zeros(B)]*F*LKN;
            LCKN=ifft([eye(B),zeros(B);zeros(B),zeros(B)]*fft(LKN));
            for kk=1:2*B
                Lckn(kk).Lckn(:,k)=LCKN(kk,:)';
            end
        end
        % configureing the final Dbar and Error Matrices for each LED
frequency

        %Dbar=zeors(n,nloop-1);
        %Ebar=zeors(n,nloop-1);
        Dbar(ii).Dbar(K).Dbar(:,((jj-1)*B+1):jj*B)=Dbarbn';
        Ebar(ii).Ebar(K).Ebar(:,((jj-1)*B+1):jj*B)=Ebn';
        end
    end
 end
```

SSVEP response detection for Gauss-Newton filter

```
function [Psout,Pvout,f,ind,SNR,Arate]=psd4gn(Sout,Vout)

% assuming LED stimulation box flickers at 10 11 12 13 Hz for channels
1 to
% 4 of l channels of input structures
[m n]=size(Sout);
for i=1:m
    for j=1:n
        [k l]=size(Sout(i,j).Sf);
        for ii=1:l
            [mm nn]=size(Sout(i,j).Sf(k,ii).Sf);
            PS=zeros(1,nn);
            for jj=1:nn
            [pxx
f]=periodogram(Sout(i,j).Sf(k,ii).Sf(:,jj)',[]','onesided',mm,256);
            Pxx=max(pxx);
         %   Pxxout(i,j).Pxx(k,ii).pxx(:,jj)=Pxx;
            PS(1,jj)=Pxx;
            end
            Psout(i,j).Ps(:,ii).Ps=PS;
        end
    end
end

for i=1:m
    for j=1:n
        [k l]=size(Vout(i,j).Vf);
        for ii=1:l
            [mm nn]=size(Vout(i,j).Vf(k,ii).Vf);
            SIGMA2=zeros(1,nn);
            for jj=1:nn
           % [pxxv
f]=periodogram(Vout(i,j).Vf(k,ii).Vf(:,jj)',[]','onesided',mm,256);
            [ar_coeffs,NoiseVariance] =
aryule(Vout(i,j).Vf(k,ii).Vf(:,jj)',25);

          % Pxxvout(i,j).Pxxv(k,ii).pxxv(:,jj)=Pxxv;
            SIGMA2(1,jj)=NoiseVariance;
            end
            Pvout(i,j).Pv(:,ii).Pv=SIGMA2;
        end
    end
end

for i=1:m
     for j=1:n
          for ii=1:l
                SnR=0;
             for jj=1:nn
```

```
snr=Psout(i,j).Ps(ii).Ps(1,jj)^2/Pvout(i,j).Pv(ii).Pv(1,jj);
                SnR=snr+SnR;
              end
                SNR(i,j).SNR(1,ii)=SnR;
          end
            [C I]=max(SNR(i,j).SNR,[],2);
            ind(i,j)=I;
     end
end

%% creating test set up indexing matrix
ti=ones(m,n);
for i=1:m
    ti(i,:)=(i-(4*(ceil(i/4)-1)))*ones(1,n);
end

%% Accuracy rate calculations
rate=zeros(m,n);
for i=1:m
    for j=1:n
        rate(i,j)=isequal(ti(i,j),ind(i,j));
    end
end

Arate=zeros(1,m);
for i=1:m
    Arate(1,i)=(sum(rate(i,:))/n)*100;
end

Xaxis=[1:1:length(Arate)];
figure
plot(Xaxis,Arate)
ylabel('AVERAGE ACCURACY RATE %')
xlabel('Test set')
title('accuracy evaluation of each trial')
Arate=Arate';
```

Printing signal plots code:

```
function []=plotsig(t,varargin)
% t is our time vector, varargin is from workspace and are the signals
user
% intends to plot
n=nargin;

for i=1:n
hold on
Z=varargin{i};
[m k]=size(Z);
for j=1:m
   figure(i);
   set(figure(i),'Position',[250+(i-1)*100 0 900 900]);
   subplot(m,1,j), plot(t,Z(j,:))
   xlabel('Time(Sec)')
   ylabel('microV')
end
hold off
end
```

Power Spectral Density (PSD) Matlab code for detecting SSVEP response peaks (Matlab 2011b,copy-right reserved for Mathworks CO.):

```
function [Px,w,units,Sxx] = periodogram(x,win,varargin)
%PERIODOGRAM  Power Spectral Density (PSD) estimate via periodogram
method.
%   Pxx = PERIODOGRAM(X) returns the PSD estimate of the signal
specified
%   by vector X in the vector Pxx.  By default, the signal X is
windowed
%   with a rectangular window of the same length as X. The PSD estimate
is
%   computed using an FFT of length given by the larger of 256 and the
next
%   power of 2 greater than the length of X.
%
%   Note that the default window (rectangular) has a 13.3 dB sidelobe
%   attenuation. This may mask spectral content below this value
(relative
%   to the peak spectral content). Choosing different windows will
enable
%   you to make tradeoffs between resolution (e.g., using a rectangular
%   window) and sidelobe attenuation (e.g., using a Hann window). See
%   WinTool for more details.
%
%   Pxx is the distribution of power per unit frequency. For real
signals,
%   PERIODOGRAM returns the one-sided PSD by default; for complex
signals,
%   it returns the two-sided PSD.  Note that a one-sided PSD contains
the
%   total power of the input signal.
%
%   Pxx = PERIODOGRAM(X,WINDOW) specifies a window to be applied to X.
%   WINDOW must be a vector of the same length as X.  If WINDOW is a
window
%   other than a rectangular, the resulting estimate is a modified
%   periodogram.  If WINDOW is specified as empty, the default window
is
%   used.
%
%   [Pxx,W] = PERIODOGRAM(X,WINDOW,NFFT) specifies the number of FFT
points
%   used to calculate the PSD estimate.  For real X, Pxx has length
%   (NFFT/2+1) if NFFT is even, and (NFFT+1)/2 if NFFT is odd.  For
complex
%   X, Pxx always has length NFFT.  If NFFT is specified as empty, the
%   default NFFT is used.
%
%   Note that if NFFT is greater than the segment the data is zero-
padded.
```

```
%   If NFFT is less than the segment, the segment is "wrapped" (using
%   DATAWRAP) to make the length equal to NFFT. This produces the
correct
%   FFT when NFFT < L, L being signal or segment length.
%
%   W is the vector of normalized frequencies at which the PSD is
%   estimated.  W has units of rad/sample.  For real signals, W spans
the
%   interval [0,Pi] when NFFT is even and [0,Pi) when NFFT is odd.  For
%   complex signals, W always spans the interval [0,2*Pi).
%
%   [Pxx,W] = PERIODOGRAM(X,WINDOW,W) where W is a vector of
%   normalized frequencies (with 2 or more elements) computes the
%   periodogram at those frequencies using the Goertzel algorithm. In
this
%   case a two sided PSD is returned. The specified frequencies in W
are
%   rounded to the nearest DFT bin commensurate with the signal's
%   resolution.
%
%   [Pxx,F] = PERIODOGRAM(X,WINDOW,NFFT,Fs) returns a PSD computed as a
%   function of physical frequency (Hz).  Fs is the sampling frequency
%   specified in Hz. If Fs is empty, it defaults to 1 Hz.
%
%   F is the vector of frequencies at which the PSD is estimated and
has
%   units of Hz.  For real signals, F spans the interval [0,Fs/2] when
NFFT
%   is even and [0,Fs/2) when NFFT is odd.  For complex signals, F
always
%   spans the interval [0,Fs).
%
%   [Pxx,F] = PERIODOGRAM(X,WINDOW,F,Fs) where F is a vector of
%   frequencies in Hz (with 2 or more elements) computes the
periodogram at
%   those frequencies using the Goertzel algorithm. In this case a two
%   sided PSD is returned. The specified frequencies in F are rounded
to
%   the nearest DFT bin commensurate with the signal's resolution.
%
%   [...] = PERIODOGRAM(...,'twosided') returns a two-sided PSD of a
real
%   signal X. In this case, Pxx will have length NFFT and will be
computed
%   over the interval [0,2*Pi) if Fs is not specified and over the
interval
%   [0,Fs) if Fs is specified.  Alternatively, the string 'twosided'
can be
%   replaced with the string 'onesided' for a real signal X.  This
would
%   result in the default behavior.  The string 'twosided' or
'onesided'
```

```
%   may be placed in any position in the input argument list after
WINDOW.
%
%   PERIODOGRAM(...) with no output arguments by default plots the PSD
%   estimate in dB per unit frequency in the current figure window.
%
%   EXAMPLE:
%      Fs = 1000;    t = 0:1/Fs:.3;
%      x = cos(2*pi*t*200)+randn(size(t));  % A cosine of 200Hz plus
noise
%      periodogram(x,[],'twosided',512,Fs); % The default window is
used
%
%   See also PWELCH, PBURG, PCOV, PYULEAR, PMTM, PMUSIC, PMCOV, PEIG,
%   SPECTRUM, DSPDATA.

%   Author(s): R. Losada
%   Copyright 1988-2011 The MathWorks, Inc.
%

error(nargchk(1,6,nargin,'struct'));

% Look for undocumented (unsupported) window compensation flag.
if nargin>2 & any(strcmpi(varargin{end},{'ms','psd'})), %#ok
    esttype = varargin{end};  % Can only be specified as last input
arg.
    varargin(end) = [];       % remove from input arg list.
else
    esttype = 'psd';     % default
end

N = length(x); % Record the length of the data

% Generate a default window if needed
winName = 'User Defined';
winParam = '';
if (nargin == 1) || isempty(win),
   win = rectwin(N);
   winName = 'Rectangular';
   winParam = N;
end

[options,msg,msgobj] = periodogram_options(isreal(x),N,varargin{:});
if ~isempty(msg), error(msgobj); end

Fs    = options.Fs;
nfft  = options.nfft;

% Compute the PS using periodogram over the whole nyquist range.
[Sxx,w] = computeperiodogram(x,win,nfft,esttype,Fs);
```

```
nrow = 1;
% If frequency vector was specified, return and plot two-sided PSD
% The computepsd function expects NFFT to be a scalar
if (length(nfft) > 1),
    [ncol,nrow] = size(nfft);
    nfft = max(ncol,nrow);
    if (length(options.nfft)>1 && strcmpi(options.range,'onesided'))
        warning(message('signal:periodogram:InconsistentRangeOption'));
        options.range = 'twosided';
    end
end

% Compute the 1-sided or 2-sided PSD [Power/freq] or mean-square
[Power].
% Also, compute the corresponding freq vector & freq units.
[Pxx,w,units] = computepsd(Sxx,w,options.range,nfft,Fs,esttype);

if nargout==0, % Plot when no output arguments are specified
   w = {w};
   if strcmpi(units,'Hz'), w = {w{:},'Fs',options.Fs}; end
   hpsd = dspdata.psd(Pxx,w{:},'SpectrumType',options.range);

   % Create a spectrum object to store in the PSD object's metadata.
   hspec = spectrum.periodogram({winName,winParam});
   hpsd.Metadata.setsourcespectrum(hspec);

   plot(hpsd);

else
   Px = Pxx;
   % If the frequency vector was specified as a row vector, return
outputs
   % the correct dimensions
   if nrow > 1,
       Px = Px.'; w = w.'; Sxx = Sxx.';
   end
end

%-------------------------------------------------------------------------
--------
function [options,msg,msgobj] =
periodogram_options(isreal_x,N,varargin)
%PERIODOGRAM_OPTIONS   Parse the optional inputs to the PERIODOGRAM
function.
%   PERIODOGRAM_OPTIONS returns a structure, OPTIONS, with following
fields:
%
%   options.nfft         - number of freq. points at which the psd is
estimated
%   options.Fs           - sampling freq. if any
%   options.range        - 'onesided' or 'twosided' psd
```

```
% Generate defaults
options.nfft = max(256, 2^nextpow2(N));
options.Fs = []; % Work in rad/sample

% Determine if frequency vector specified
freqVecSpec = false;
if (~isempty(varargin) && length(varargin{1}) > 1)
    freqVecSpec = true;
end

if isreal_x && ~freqVecSpec,
   options.range = 'onesided';
else
   options.range = 'twosided';
end

if any(strcmp(varargin, 'whole'))
    warning(message('signal:periodogram:invalidRange', 'whole',
'twosided'));
elseif any(strcmp(varargin, 'half'))
    warning(message('signal:periodogram:invalidRange', 'half',
'onesided'));
end

[options,msg,msgobj] = psdoptions(isreal_x,options,varargin{:});

% [EOF] periodogram.m
```

Appendix B

1. Correlation factors for 2nd and 3rd near collision situations of subjects 22 and 7.
2. The SNRs for 6 other subjects 1st near collision situations (other than presented subjects 22 and 7). These subjects had DSR and NSR for correlation analysis.

For all of the following figures near collision situation happens on time step 48 and time steps axes configure a 4-seconds time window.

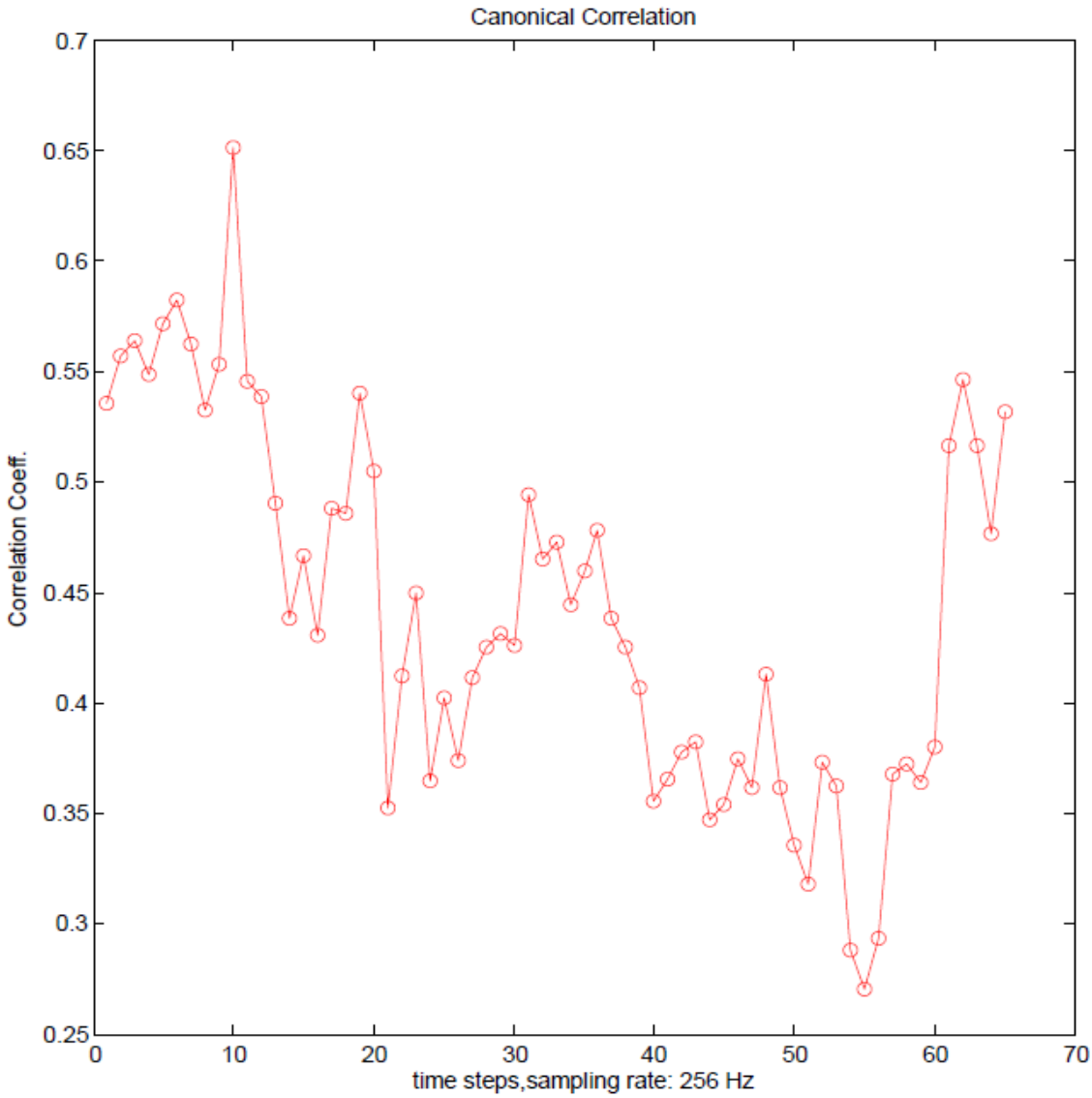

Figure 62. Correlation factors obtained from subject 7 driving experiment during the first scenario and 2nd near collision situation

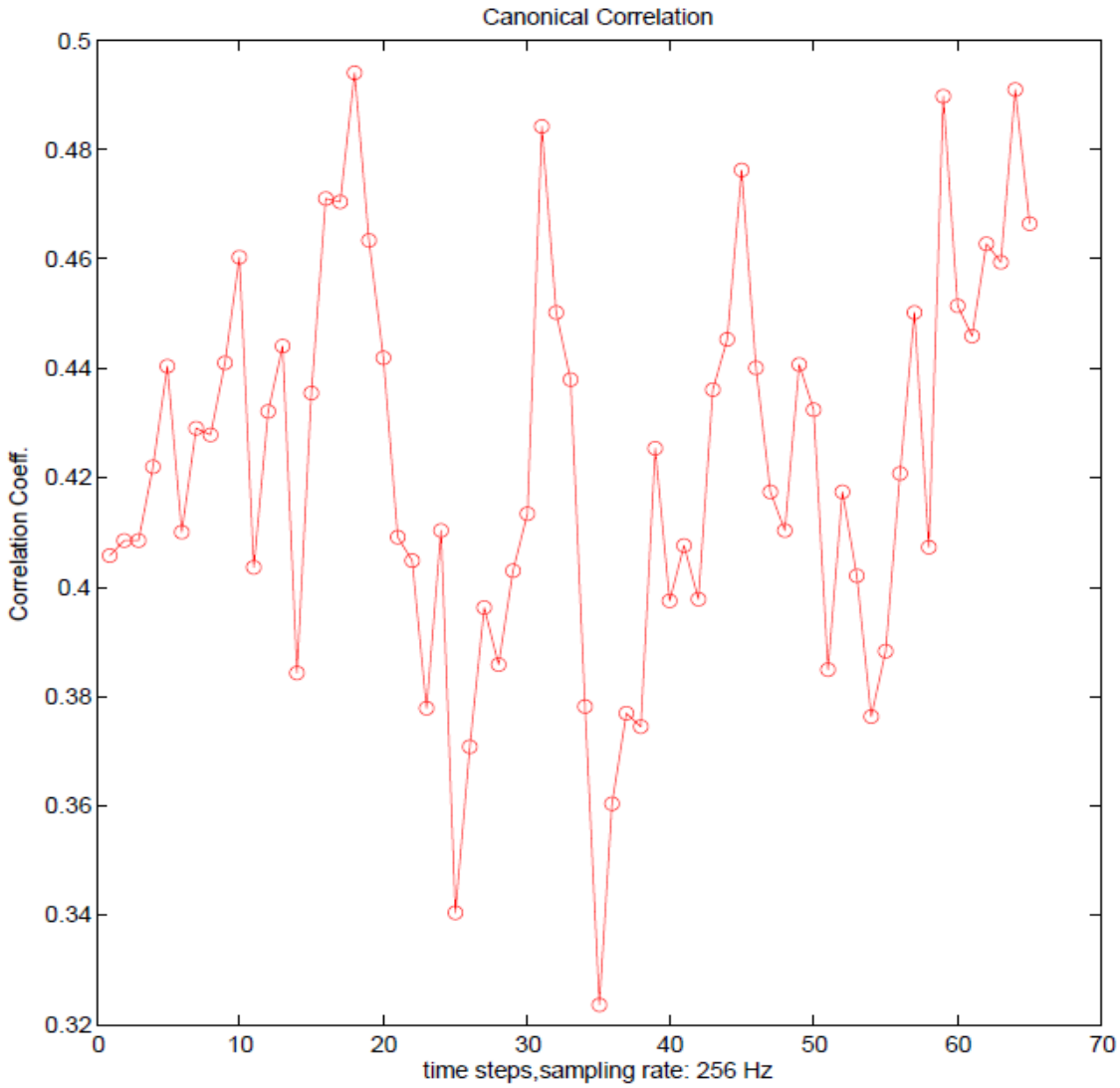

Figure 63. Correlation factors obtained from subject 7 driving experiment during the second scenario and 2nd near collision situation

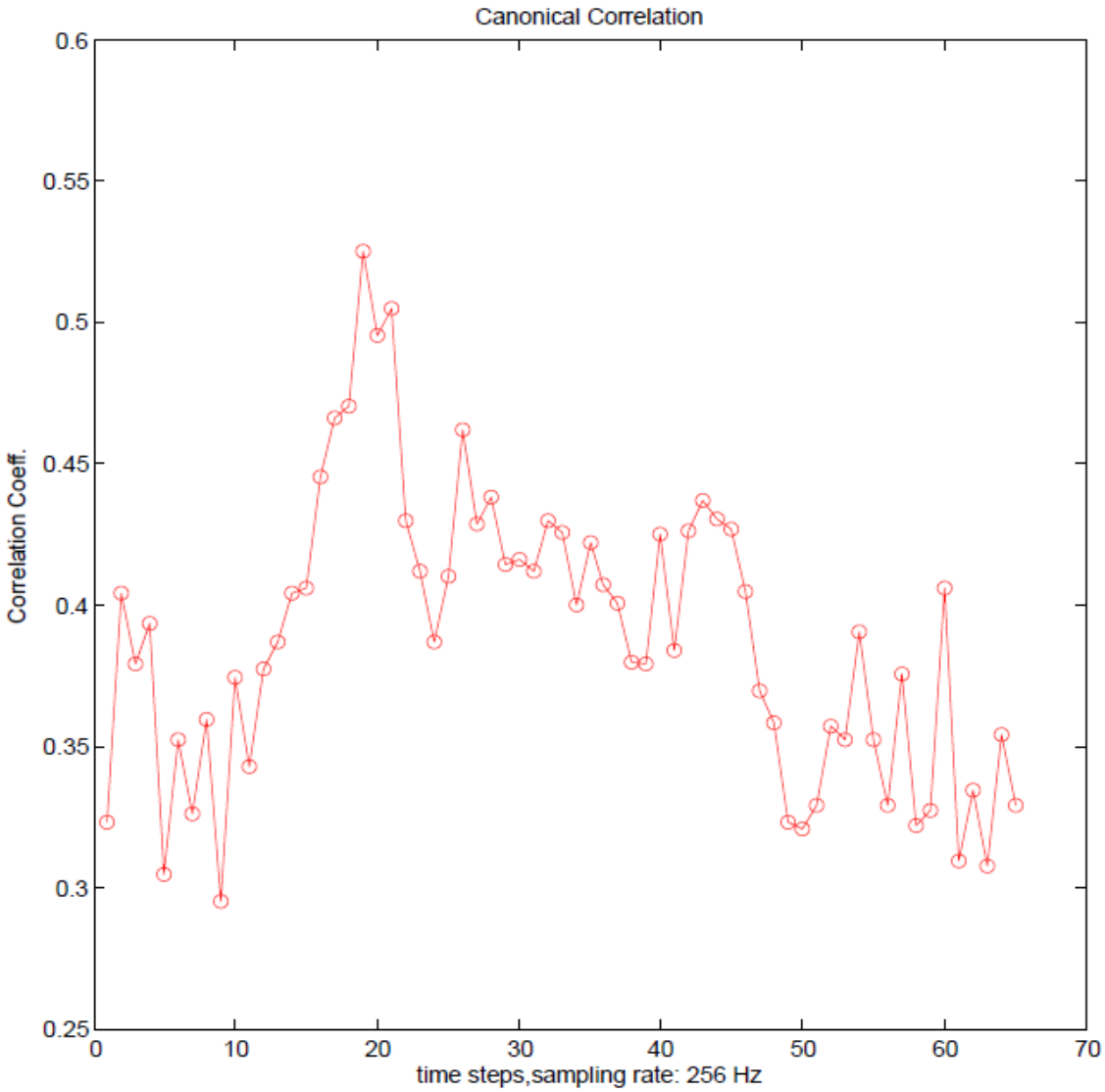

Figure 64. Correlation factors obtained from subject 7 driving experiment during the first scenario and 3rd near collision situation

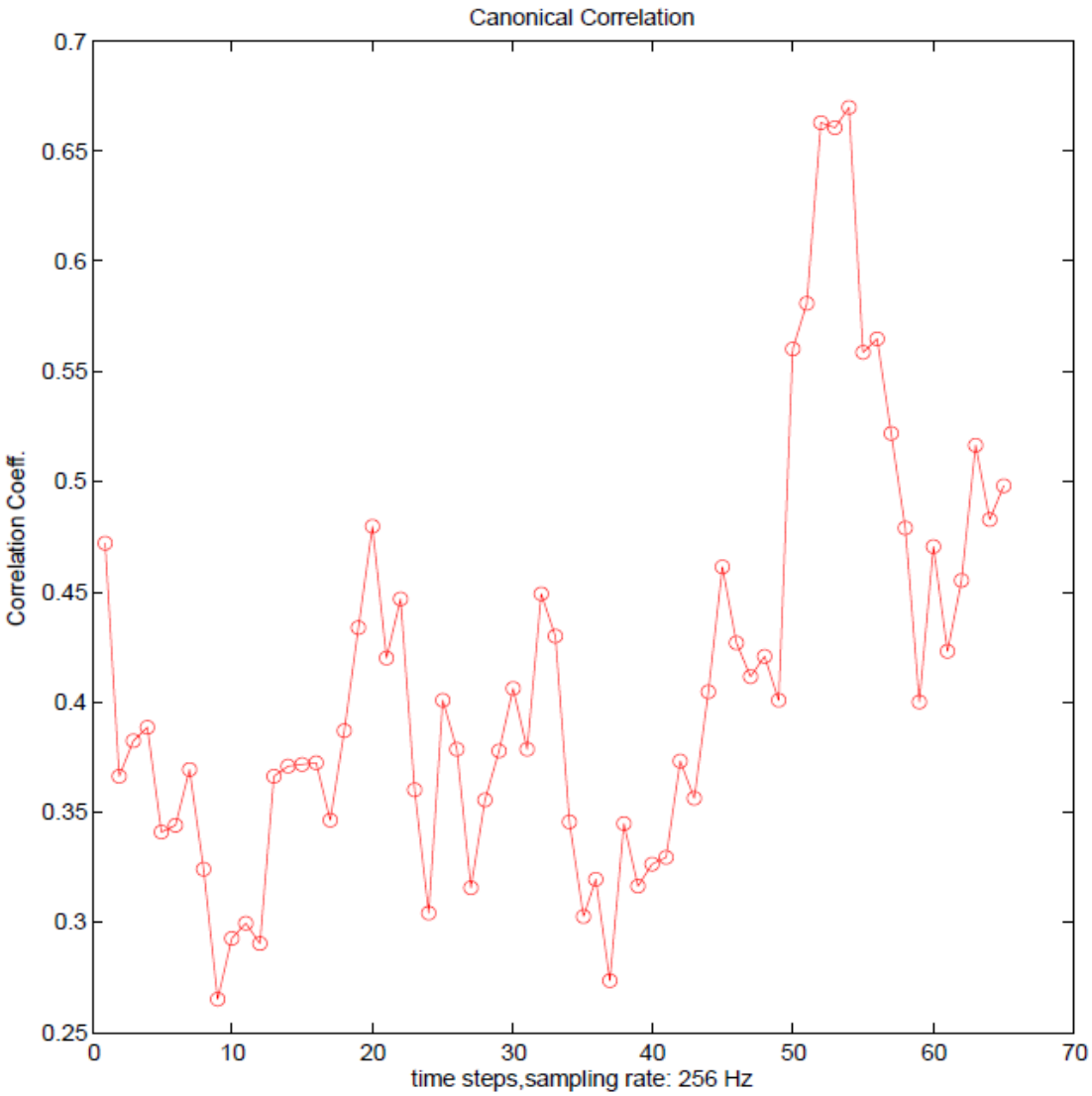

Figure 65. Correlation factors obtained from subject 7 driving experiment during the second scenario and 3rd near collision situation

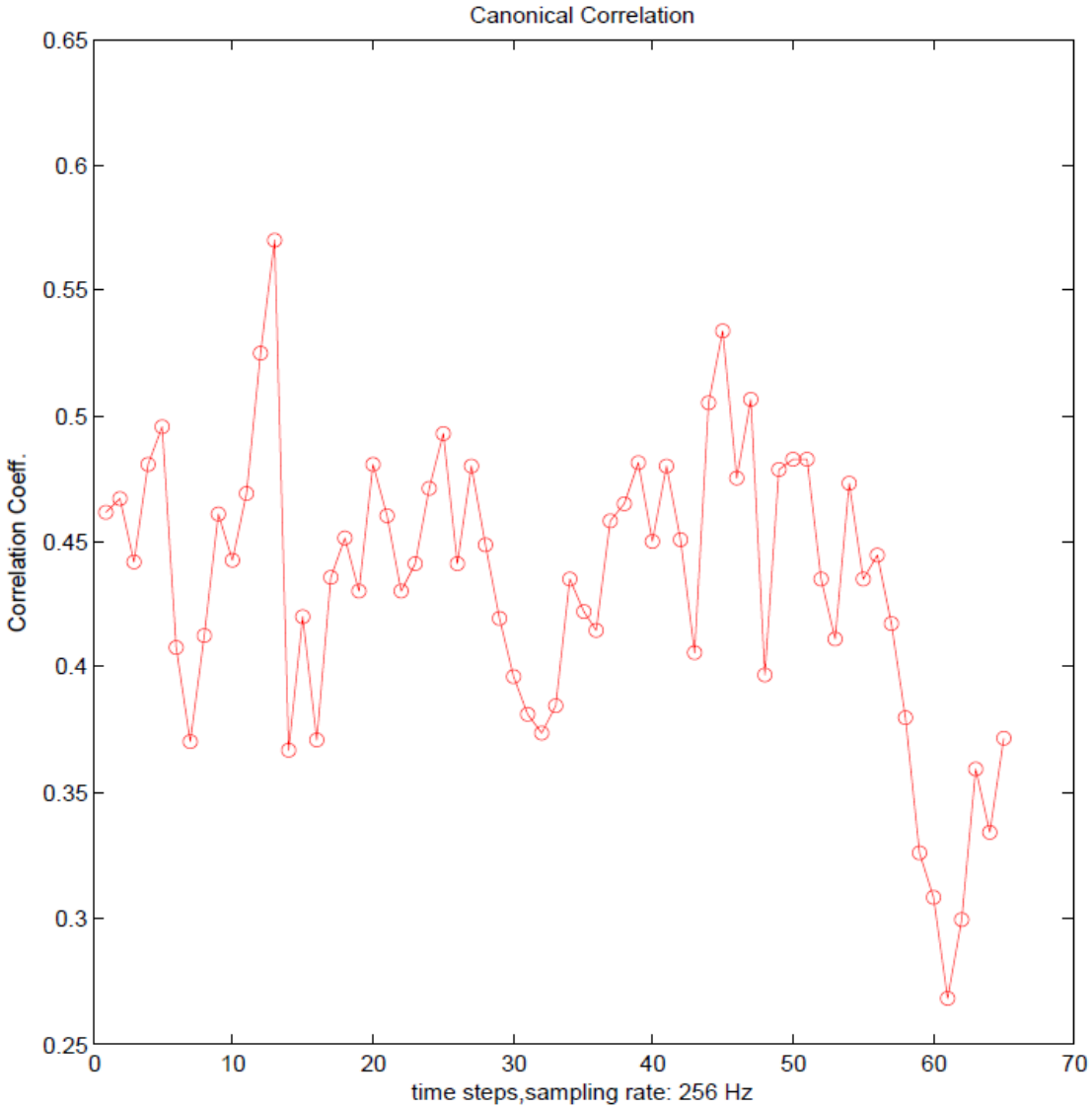

Figure 66. Correlation factors obtained from subject 22 driving experiment during the first scenario and 2nd near collision situation

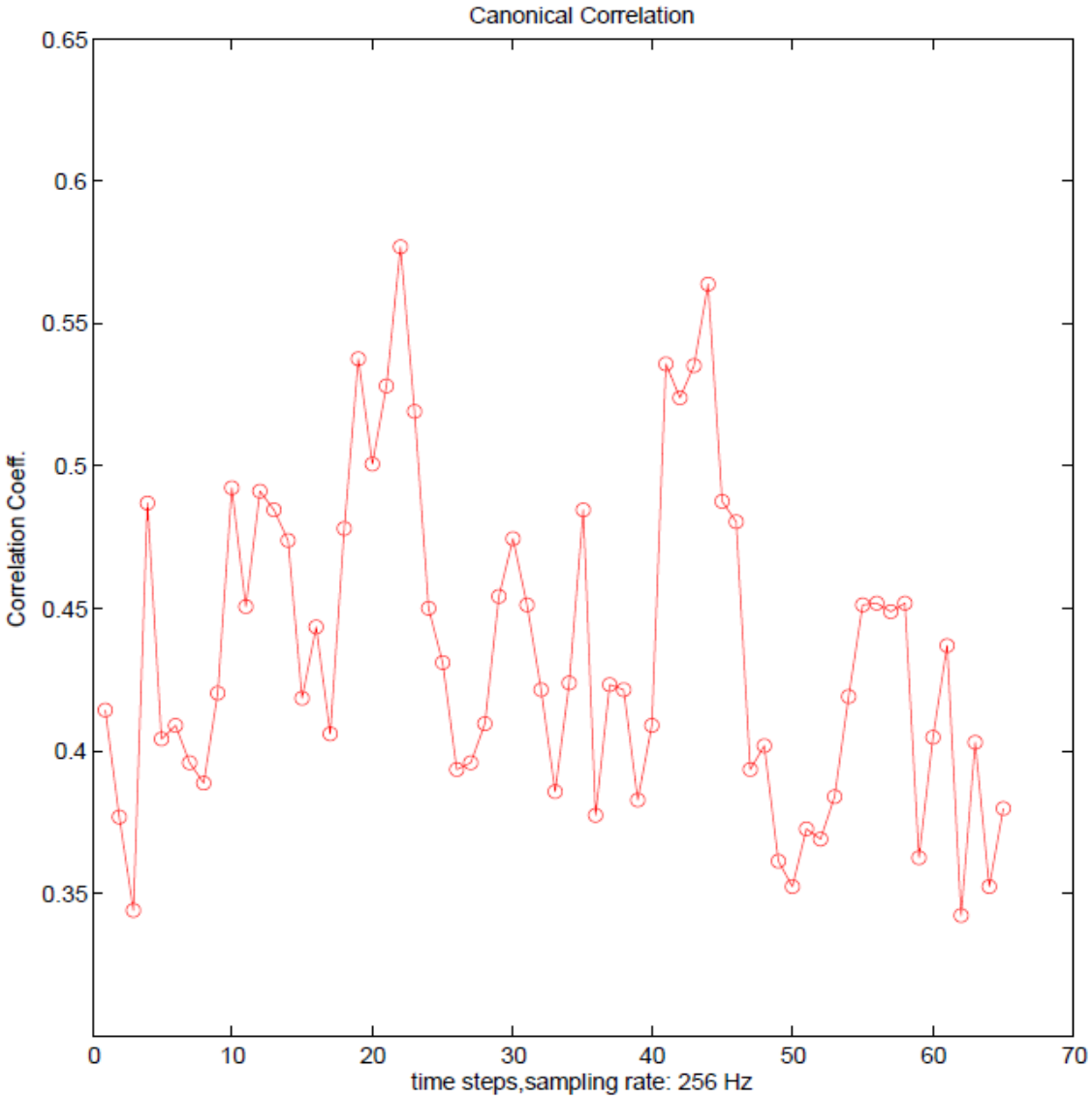

Figure 67. Correlation factors obtained from subject 22 driving experiment during the second scenario and 2nd near collision situation

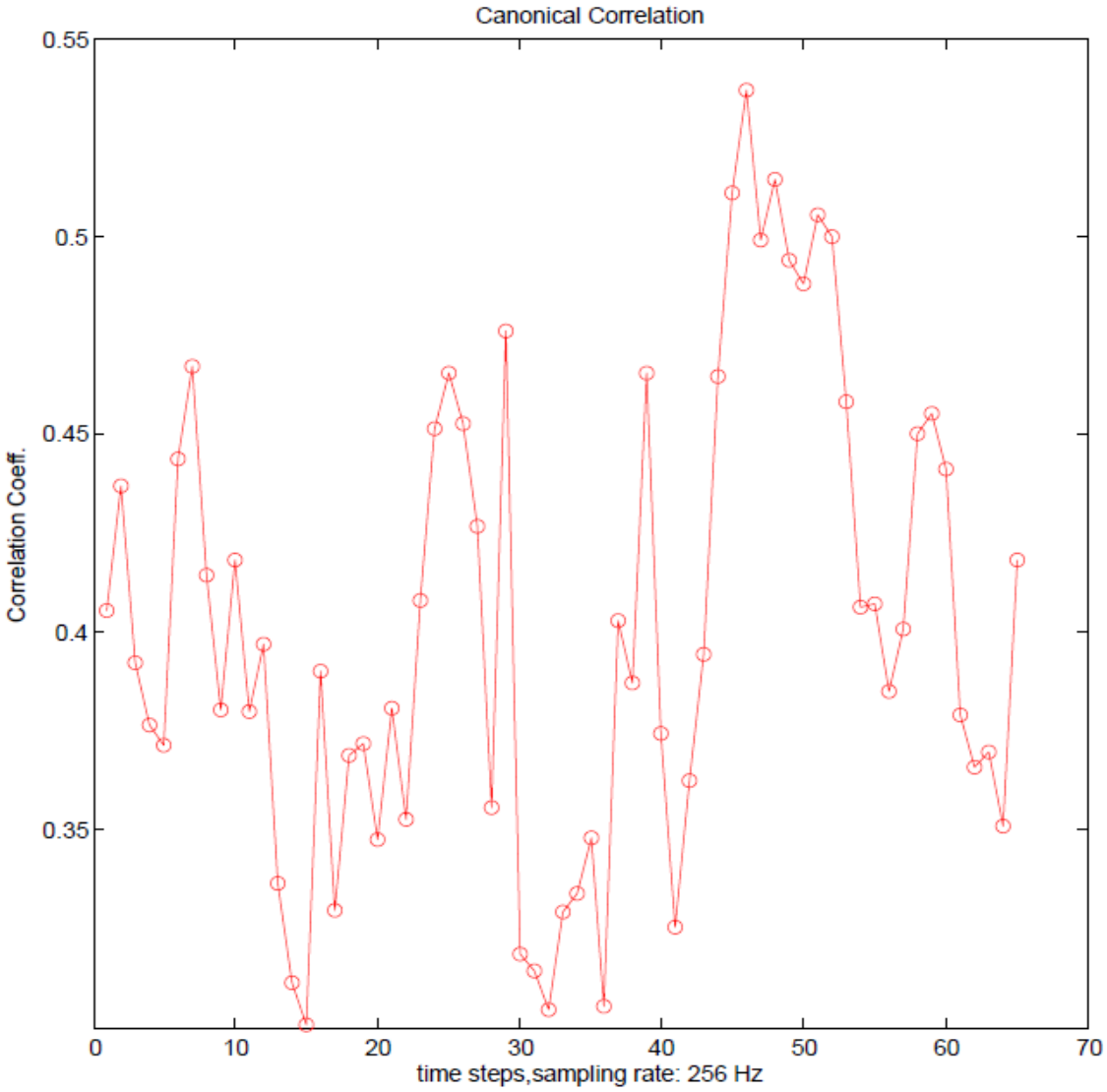

Figure 68. Correlation factors obtained from subject 22 driving experiment during the first scenario and 3rd near collision situation

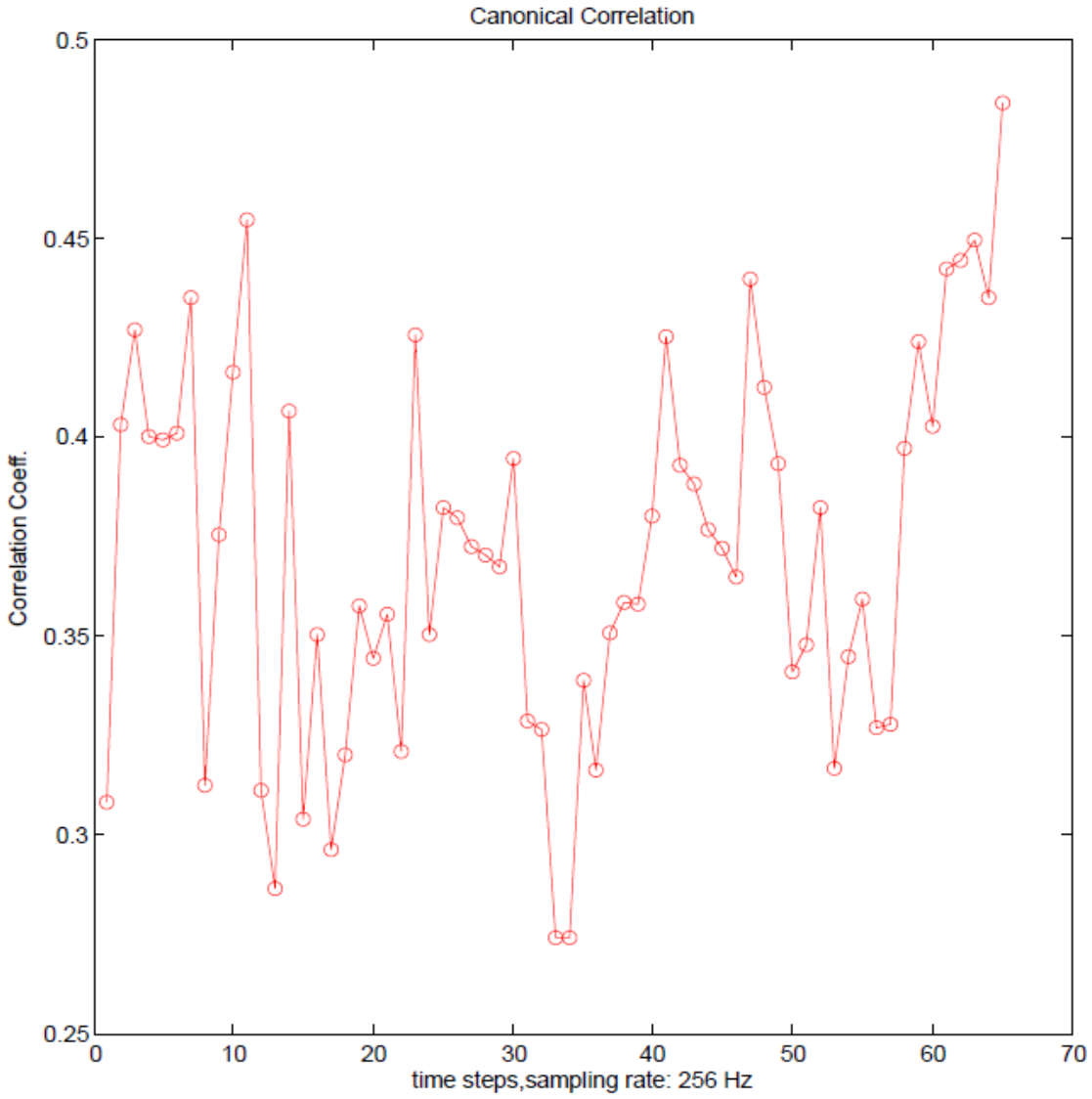

Figure 69. Correlation factors obtained from subject 22 driving experiment during the second scenario and 3rd near collision situation

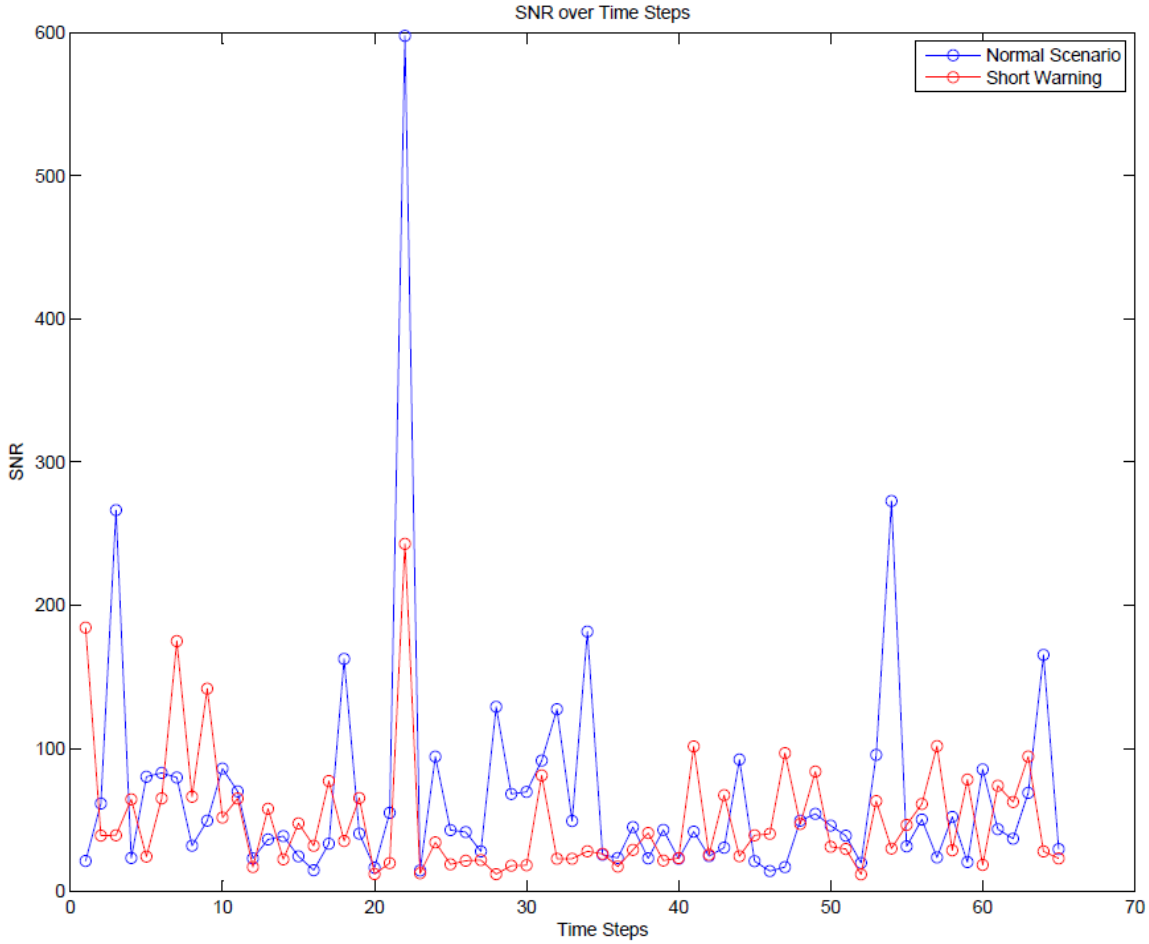

Figure 70. The obtained SNR from the first near collision situation of the subject 6 driving-simulator experiments

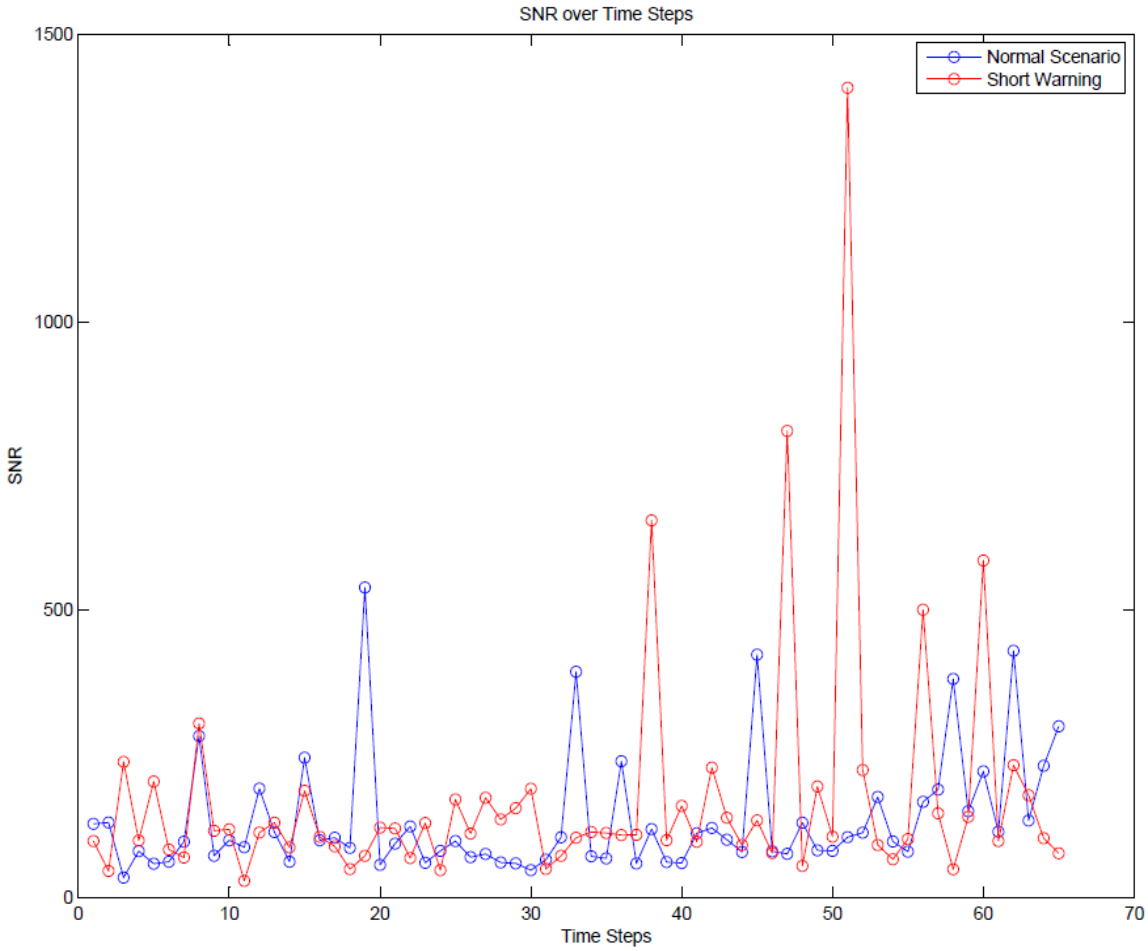

Figure 71. The obtained SNR from the first near collision situation of the subject 10 driving-simulator experiments

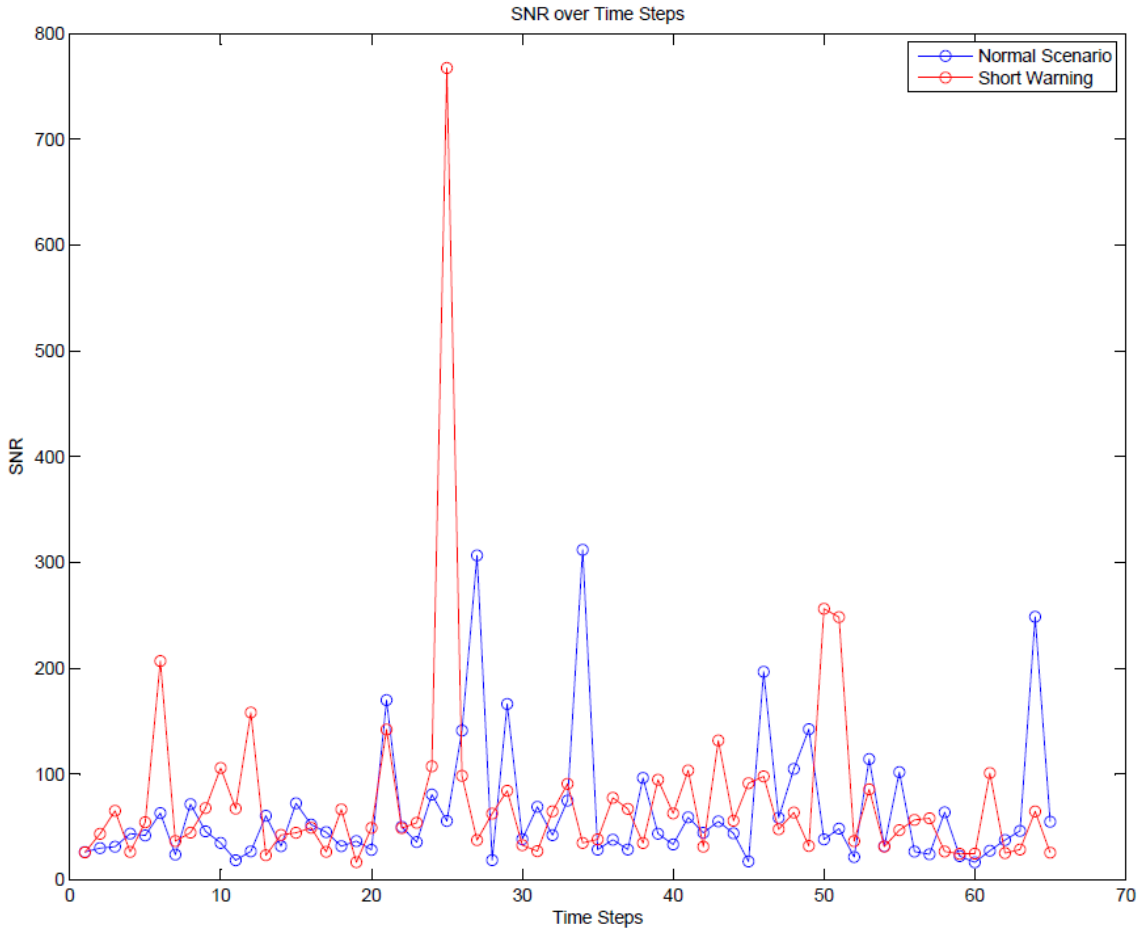

Figure 72. The obtained SNR from the first near collision situation of the subject 13 driving-simulator experiments

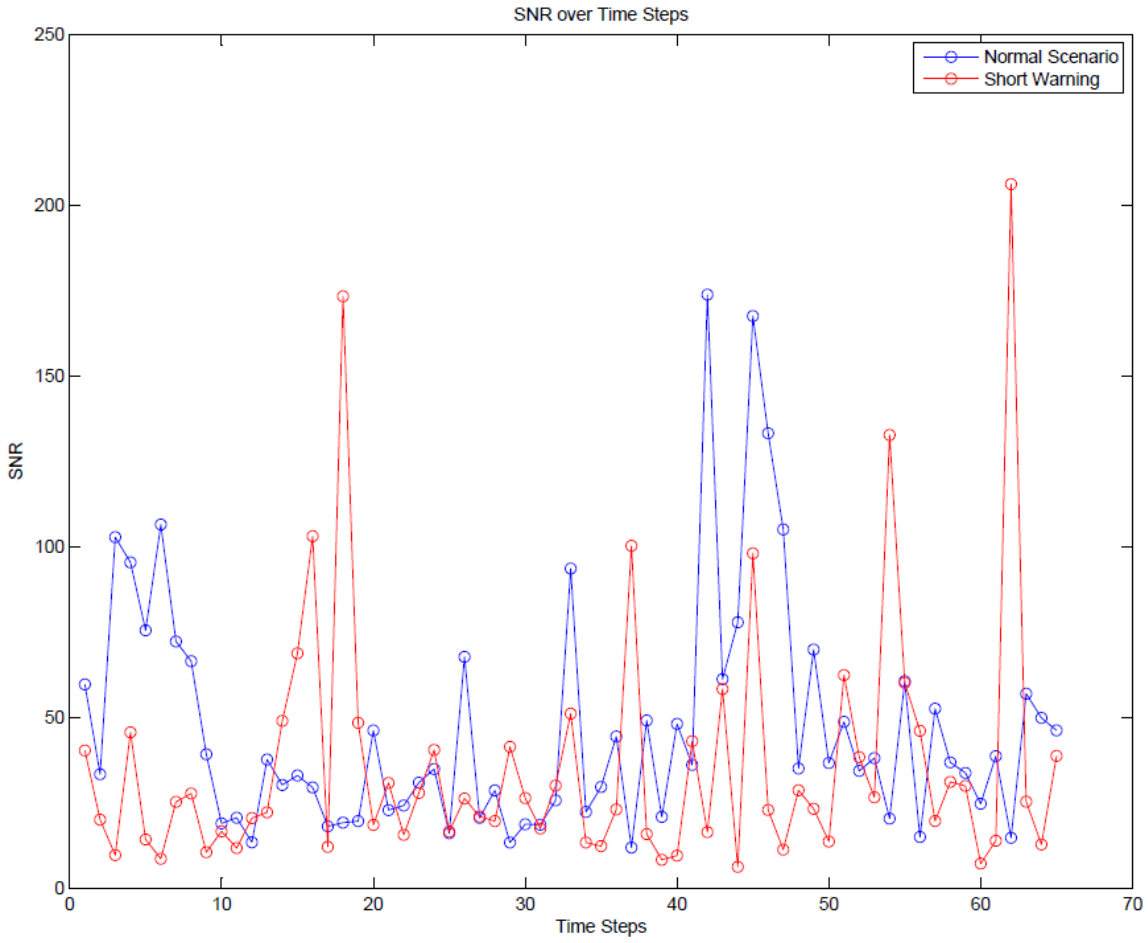

Figure 73. The obtained SNR from the first near collision situation of the subject 18 driving-simulator experiments

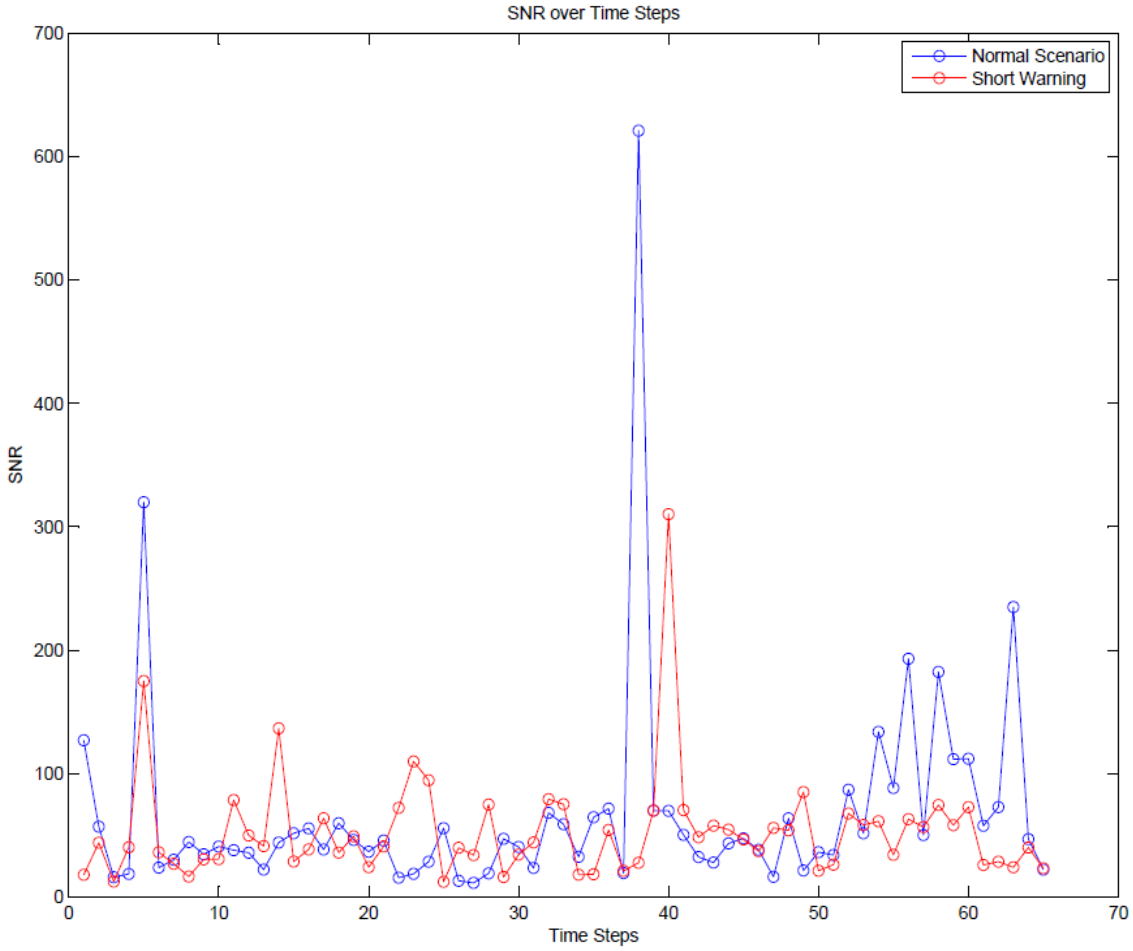

Figure 74. The obtained SNR from the first near collision situation of the subject 27 driving-simulator experiments

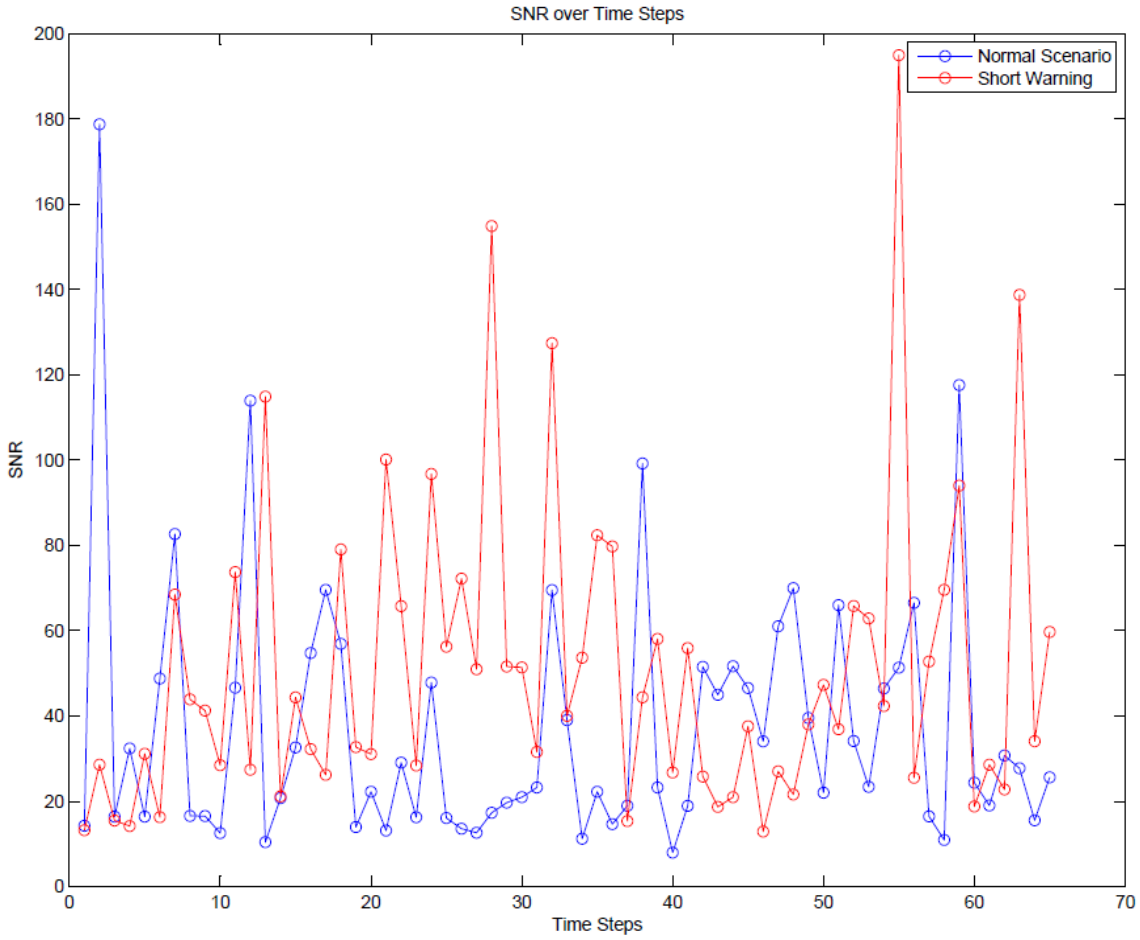

Figure 75. The obtained SNR from the first near collision situation of the subject 30 driving-simulator experiments

Appendix C

Questionnaire

Driver Evaluation of the Car Simulator

Driver No._____ Date:_____

(This information as well as all other information will be kept confidential)

Question 1: Please rate your experience with the car-simulator:

1	2	3	4	5	6	7	8	9
Not Realistic at All			Fairly Realistic					Very Realistic

Question 2: Were you able to estimate the distance with the objects in front of you correctly?

1	2	3	4	5	6	7	8	9
Too Close				Correct				Too Far

Question 3: How do you rate steering wheel stiffness compared to your vehicle (or what you are used to)?

1	2	3	4	5	6	7	8	9
Very Loose				Normal				Very Stiff

Question 4: How do you rate the braking system of the car simulator in comparison to your vehicle (or what you are used to)?

1	2	3	4	5	6	7	8	9
Stopped Too Late			Stopped Normally					Stopped Sooner

Question 5: How do you rate the overall handling of the car in comparison to your vehicle (or what you are used to)?

1	2	3	4	5	6	7	8	9
Much Harder				Same				Much Easier

Comments:_____

_____

_____

_____

_____

_____

_____

_____

_____

_____

Driver Evaluation of the LED's Stimulator Test

Driver No._____ Date:_____

(This information as well as all other information will be kept confidential.)

Question 1: Have you ever participated in an experiment in which your brain signals recorded with an EEG device?

Yes No

Question 2: Please rate from 1 to 9, your level of comfort when you were wearing the EEG-Cap:

1 2 3 4 5 6 7 8 9

Uncomfortable Somehow Uncomfortable Comfortable

Question 3: Did you have any preliminary knowledge (or ever have heard about) Brain-Computer Interface systems (BCIs) before participating in this experiment?

Yes No

If yes: Have you ever participated in an experiment in which a Brain-Computer Interface (BCI) system being tested?

Yes No

Question 4: Was the flickering LED's Stimulator box experiment irritating your eyes?

1 2 3 4 5 6 7 8 9

Too Much Somehow Not at ALL

Question 5: Do you think that you would use any kind of system with the visual stimulator, as you experienced, if it was available as an assistive product?

1 2 3 4 5 6 7 8 9

Not at ALL Somehow Acceptable

Comments:_____

_____

_____

_____

_____

_____

_____

_____

_____

Driver Evaluation of the car simulator experiments

Driver No._____ Date:_____

(This information as well as all other information will be kept confidential.)

Question 1: Please rate from 1 to 9, how the flickering LED's distracted you during the driving scenarios?

1 2 3 4 5 6 7 8 9

Very Much — Somehow — Not at all

Question 2: Please rate from 1 to 9, was the short flickering LED's warning period helpful to improve your reaction to the emergency situation?

1 2 3 4 5 6 7 8 9

Worsened — Not Helpful — Improved

Question 3: Please rate from 1 to 9, was the longer period of LEDs flickering increased the time you normally need to react to the emergency situations, during these driving scenarios?

1 2 3 4 5 6 7 8 9

Increased — Didn't Change — Decreased

Question 4: Please rate from 1 to 9, how wearing the EEG-Cap affected you and your driving skill during these tests?

1 2 3 4 5 6 7 8 9

Worsen my driving skill — Somehow — didn't affect me

Question 5: Do you think that such a warning system will help you to avoid/mitigate any accident(s)?

1 2 3 4 5 6 7 8 9

No (Not Helpful) — Somehow — Yes (Helpful)

Question 6: Do you think that you would use such a system if it was available in your car?

1 2 3 4 5 6 7 8 9

No — maybe — Yes

Question 7: Have you used any kind of intelligent driving assistant system such as cruise control? Yes/ No

Please rate the level of your satisfaction with intelligent driving assistant systems that you have used before:

1 2 3 4 5 6 7 8 9

I didn't like it — somehow liked it — I use it whenever I can

Comments:_____

_____

_____

_____

_____

_____

_____

Driver's self-evaluation

Have you even taken a safety driving course? Yes No

How many accidents have you been involved in within the past five years? _____
If so, what type of accidents? (Circle one)
Rear-end Intersection Head-on Other (please describe) _____

How many miles do you drive annually?
Less than 2000mi 2000-7500mi More than 7500mi

How do you characterize your skill of driving?

1	2	3	4	5	6	7	8	9
Not good				Average				Expert

Please describe your own reaction to avoid near collision (emergency) situations of these experiments:

1. I was surprise and couldn't react
2. Later than my normal reaction time
3. I reacted just like my normal driving
4. Better than normally

Please rate the difficulty level of the near collision (emergency) situations in these tests?

1	2	3	4	5	6	7	8	9
Impossible to avoid				Difficult				Very Easy

Which one of the following best describes your estimation of distance to the cars on the road?

1. They were Located where I estimated them
2. They were closer than I estimated
3. They were farther than I estimated
4. Others (Please describe):_____

Comments:_____
_____
_____
_____
_____
_____
_____